Une approche neuro-computationnelle de la prise de décision et de sa régulation contextuelle

Philippe Domenech

THESE DE L'UNIVERSITE DE LYON

Ecole doctorale *Neurosciences et Cognition*

Présentée par : *Philippe DOMENECH*

Pour l'obtention du DIPLOME DE DOCTORAT (arrêté du 7 août 2006)

Une approche neuro-computationnelle de la prise de décision et de sa régulation contextuelle

---

Soutenue publiquement le vendredi 16 septembre 2011

JURY:
Dr. Jean-Claude DREHER- Directeur de thèse
Pr. Franck DURIFF - Rapporteur
Pr Philippe FOSSATI - Examinateur
Pr Etienne KOECHLIN - Examinateur
Dr Mathias PESSIGLIONE- Rapporteur
Dr. Emmanuel PROCYK - Examinateur
Pr. Christian SCHEIBER - Examinateur

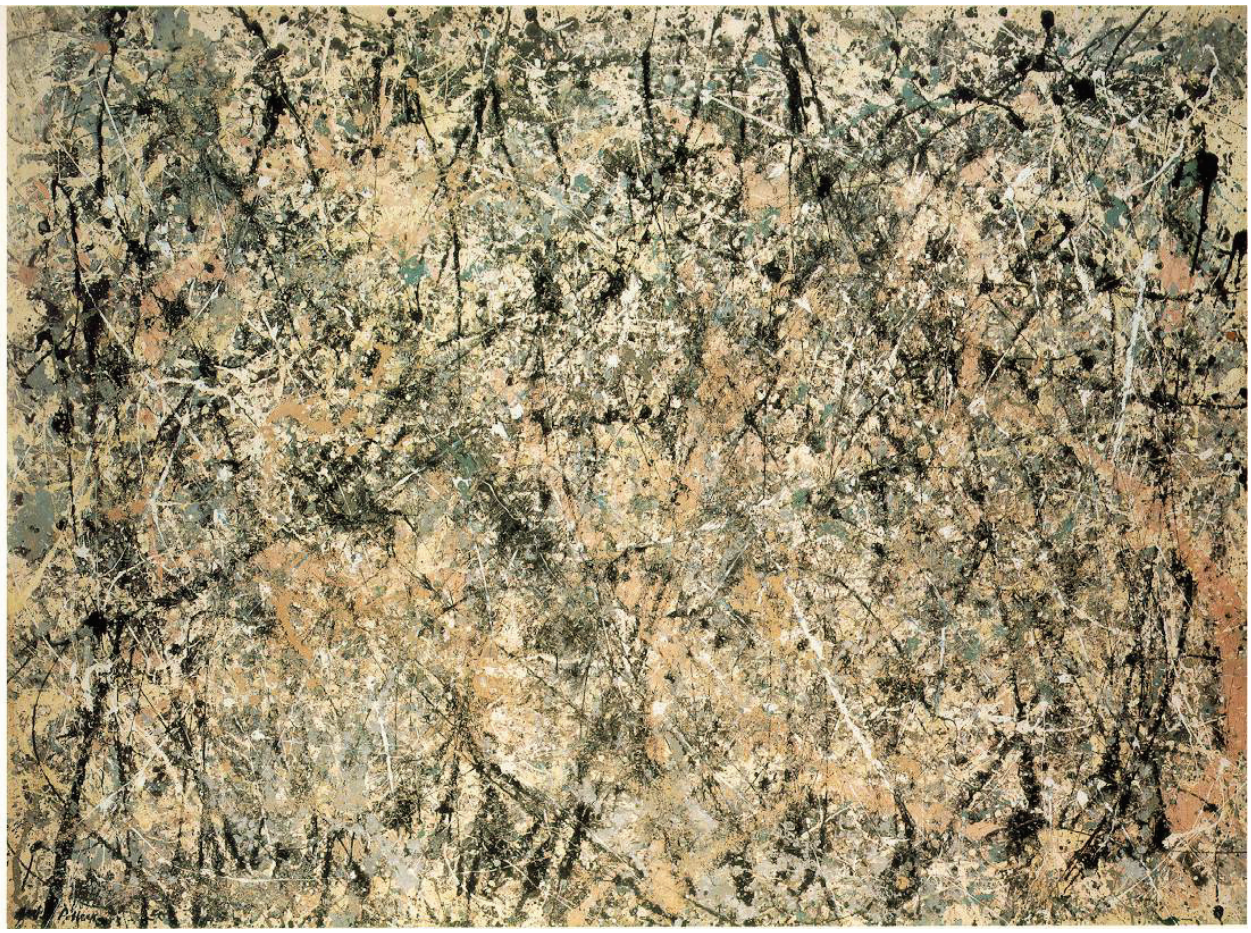

Jackson Pollock – Lavender Mist

« Il ne faut donc pas se demander si nous percevons vraiment un monde, il faut dire au contraire : le monde est cela que nous percevons. »

Maurice Merleau-Ponty

Remerciements :

Je tiens ici à témoigner ma reconnaissance à tous ceux qui ont été à mes cotés durant ces années où se sont entremêlées activité hospitalière et recherche.

Mes remerciements vont avant tout à Carine qui m'accompagne depuis 10 ans – déjà – le long d'un chemin jalonné d'épreuves, à ma famille et à mes amis.

Je tiens également à remercier les rapporteurs et examinateurs de mon jury, qui ont accepté d'évaluer mon travail : Dr M. Pessiglione, Pr F. Durif, Pr E. Koechlin, Pr P Fossati, Dr E. Procyk, Pr C. Scheiber, ainsi que mon directeur de thèse, Dr JC Dreher.

Je remercie les membres du Centre de Neuroscience Cognitive. Ma pensée va plus particulièrement à mes compagnons de thèse et amis : Guillaume Barbalat, Valérian Chambon, Elise Métereau et Guillaume Sescousse.

Pour finir, je remercie mes confrères et consœurs médecins, mes collègues infirmiers, avec qui nous nous essayons, jour après jour, d'aider au mieux nos patients.

Résumé :

Décider, c'est sélectionner une alternative parmi l'ensemble des options possibles en accord avec nos buts. Les décisions perceptuelles, correspondant à la sélection d'une action sur la base d'une perception, résultent de l'accumulation progressive d'information sensorielle jusqu'à un seuil de décision. Aux niveaux comportemental et cérébral, ce processus est bien capturé par les modèles de décision par échantillonnage séquentiel. L'étude neurobiologique des processus de décision, guidée par l'usage de modèles computationnels, a permis d'établir un lien clair entre cette accumulation d'information sensorielle et un réseau cortical incluant le sillon intra-pariétal et le cortex dorso-latéral préfrontal. L'architecture des réseaux biologiques impliqués dans la prise de décision, la nature des algorithmes qu'ils implémentent et surtout, l'étude des relations entre structure biologique et computation est au cœur des questionnements actuels en neurosciences cognitives et constitue le fil conducteur de cette thèse.

Dans un premier temps, nous nous sommes intéressés aux mécanismes neuraux et computationnels permettant l'ajustement du processus de décision perceptuelle à son contexte. Nous avons montré que l'information *a priori* disponible pour prédire nos choix diminue la distance au seuil de décision, régulant ainsi dynamiquement la quantité d'information sensorielle nécessaire pour sélectionner une action. Pendant la prise de décision perceptuelle, le cortex cingulaire antérieur ajuste le seuil de décision proportionnellement à la quantité d'information prédictive disponible et le cortex dorso-latéral préfrontal implémente l'accumulation progressive d'information sensorielle.

Dans un deuxième temps, nous avons abordé la question de l'unicité, au travers des domaines cognitifs, des mécanismes neuro-computationnels implémentant la prise de décision. Nous avons montré qu'un modèle de décision par échantillonnage séquentiel utilisant la valeur subjective espérée de chaque option prédisait avec précision le comportement de sujets lors de choix économiques risqués. Pendant la décision, la portion médiale du cortex orbito-frontal code la différence entre les valeurs subjectives des options considérées, exprimées sur une échelle de valeur commune. Ce signal orbito-frontal médian sert d'entrée à un processus de décision par échantillonnage séquentiel implémenté dans le cortex dorso-latéral préfrontal.

Pris ensemble, nos travaux précisent les contours d'une architecture fonctionnelle de la prise de décision dans le cortex préfrontal humain en établissant une cartographie des modules computationnels qu'il implémente, mais aussi en caractérisant la façon dont l'intégration fonctionnelle de ces régions cérébrales permet l'émergence de la capacité à prendre des décisions.

MOTS-CLES : Décision, IRM fonctionnelle, Diffusion, Bayesien, Information, Valeur subjective, Contexte

DISCIPLINE : Neurosciences Cognitives

INTITULE ET ADRESSE DU LABORATOIRE :
Centre de Neuroscience Cognitive – UMR 5229 67 Bd Pinel 69675 Bron Cedex France

Abstract :

Decision-making is the selection of an alternative according to our inner goals. Perceptual decisions, the selection of an action based on our perceptions, are made when sensory evidence accumulated over time reaches a decision threshold. This cognitive process is well accounted for by sequential sampling models of decision-making. Moreover, the model-driven neurobiological study of the decision-making process has linked the accumulation of sensory information with a parieto-prefrontal cortical network. The architecture of these cortical networks, the algorithms implemented and the mapping of elementary computations onto biological structures are the questions at the core of this thesis.

First, we investigated the neural mechanisms underlying the contextual modulation of the decision-making process. We showed that predictive information on the forthcoming stimuli decreased the distance to the decision threshold, adjusting dynamically the amount of sensory information required to commit to a choice. In our study, the anterior cingulate cortex modulated the decision threshold in proportion to the amount of predictive information and the dorso-lateral prefrontal cortex accumulated sensory information. Then, we addressed the question of the unicity across cognitive domains of the neuro-computational mechanisms of decision-making. We showed that a sequential sampling model of decision-making using subjective values as its inputs precisely predicted Human economic decision-making behavior. Moreover, we showed that the medial part of the orbito-frontal cortex coded the difference between the subjective values of the options under scrutiny on a common scale. This orbito-frontal decision-related value signal drove the sequential sampling decision-making process implemented in the dorso-lateral prefrontal cortex.

Taken together, our work delineates a functional architecture of Human decision-making by mapping elementary computations onto the human prefrontal cortex and by characterizing how the functional integration between these brain regions subserves the ability to make choices.

Key words: Decision-making, fMRI, Drift-diffusion model, Bayesian Inference, Information theory, Subjective Value, Contextual regulation

LISTE DES ABREVIATIONS

Les abréviations sont définies en français ou en *anglais*

<u>Régions cérébrales :</u>

- **ACC :** *Anterior Cingulate Cortex* (cortex cingulaire antérieur)
- **FEF :** *Frontal Eye Field*
- **FRR :** *Frontal Reaching Region*
- **IPS :** *Intra-Parietal sulcus* (ou Sillon intra-parietal)
- **MT :** Aire temporale moyenne ou V5
- **OFC :** *Orbito-Frontal Cortex* (cortex orbito-frontal)
    - lOFC : *lateral Orbito-Frontal Cortex*
    - mOFC ou vmPFC : *medial Orbito-Frontal Cortex* ou *ventro-medial prefrontal cortex*
- **PFC :** *Prefrontal Cortex* (ou cortex préfrontal)
    - MPFC : *Medial Prefrontal Cortex* (cortex préfrontal médian)
    - DLPFC : *Dorso-Lateral Prefrontal Cortex* (cortex dorso-latéral préfrontal)
- **Pre-SMA** : *Supplementary pre-motor area* (ou Aire pré-motrice supplémentaire)
- **PRR :** *Parietal Reaching Region*
- **SNpc :** *Substantia Nigra pars compacta*
- **SNpr :** *Substantia Nigra pars reticulata*
- **STN :** *Sub-thalamic Nucleus* (ou Noyau sous-thalamique)
- **S1 :** Aire somesthésique primaire
- **VTA :** *Ventral Tegmental Area* (aire tégmentale ventrale)
- **V1 :** Aire 17 de Brodmann ou Aire visuelle primaire

Autres Abréviations :

- **BOLD :** *Blood Oxygen Level Dependent*
- **DDM :** *Drift-diffusion model*
- **EEG :** Electroencéphalographie
- **ERP :** *Event-related potential*
- **fMRI (ou IRMf) :** *functional Magnetic Resonance Imaging* (Imagerie par Résonance Magnétique fonctionnelle)
- **LATER :** *Linear Approach to Threshold with Ergodic Rate*
- **LBA :** *Linear Ballistic Accumulator* (ou Accumulateur Linéaire Balistique)
- **LCA :** *Leaky Competition Accumulation model*
- **ROI :** *Region of Interest*
- **RT :** *Reaction Time* (ou temps de réaction)
- **rTMS :** Stimulation Magnétique Répétitive transcranienne
- **SAT :** Dilemme entre vitesse et performance ou *« speed-accuracy tradeoff »*
- **SPRT :** *Sequential Probability Ratio Test* (ou test séquentiel du ratio de probabilité)
- **SSM :** *Sequential Sampling Model of decision-making* (ou modèle de décision par échantillonnage séquentiel)

Table des matières

1. PREAMBULE

Décider, c'est sélectionner une alternative parmi l'ensemble des options possibles en accord avec nos buts : A droite ou à gauche ? Vanille ou chocolat ? Dois-je saluer cette personne ? Me battre ou m'enfuir ? Risquer une perte dans l'espoir d'un gain ? Du plus critique au plus trivial, nous résolvons continuellement de tels problèmes. La capacité à prendre des décisions occupe donc une position cardinale parmi les cognitions Humaines. La survie dans un environnement incertain nécessite de s'adapter avec flexibilité à l'ensemble des situations auxquelles nous sommes susceptibles d'être confrontés. Cette pression évolutive nous pousse à être des décideurs efficaces, capables de choisir en un minimum de temps l'alternative maximisant les chances d'atteindre notre but[1]. Etant le fruit de millions d'années d'évolution, le cerveau Humain est donc capable de décider avec efficacité dans des domaines cognitifs très différents, contrôlant un vaste répertoire comportemental sur la base de sources d'information diverses et hétérogènes[2]. Pour se faire, il doit pouvoir tirer parti de l'ensemble des informations à sa disposition afin de comparer les multiples buts qu'il poursuit à l'aune de leurs valeurs subjectives et de leurs vraisemblances[3,4]. L'architecture des réseaux biologiques impliqués dans la prise de décision, la nature des algorithmes qu'ils implémentent et surtout, l'étude des relations entre structure biologique et computation est au cœur des questionnements actuels en Neuroscience Cognitive[3,5,6]. Ce souci d'élucider les mécanismes neuro-computationnels de la prise de décision constitue le point de départ de ce travail de thèse.

Adoptant une perspective Bayesienne, nous nous sommes d'abord intéressé aux mécanismes neurobiologiques et computationnels par lesquels le cerveau humain élabore un modèle interne de son environnement, i.e. un système de croyance, afin d'établir des prédictions quant à l'issue de ses choix et guider le processus de prise de décision. En effet, collecter de l'information en faveur des différentes alternatives prend du temps, et l'injection d'information *a priori* - prédictive de l'option la plus susceptible d'être choisie au vu des expériences passées - dans le processus de décision, réduit potentiellement la quantité d'information à collecter et donc, à performance constante, le temps de décision. Dans un deuxième temps, nous avons abordé la question de l'unicité des mécanismes neuro-computationnels implémentant la décision Humaine à

travers les différents domaines cognitifs. En effet, il est frappant de constater à quel point les situations décisionnelles auxquelles nous sommes confrontés peuvent varier, reposant tantôt sur l'analyse perceptuelle de l'environnement, tantôt sur l'analyse économique de la valeur subjective des options considérées, ou même sur le rappel d'expériences passées. Nous avons donc testé l'hypothèse que les modèles neuro-computationnels décrivant les choix basés sur l'information sensorielle - i.e. les mêmes algorithmes de choix dans les mêmes régions cérébrales - puissent être pareillement impliqués dans la prise de décision basée sur les valeurs, et plus particulièrement les valeurs subjectives, jetant ainsi un pont entre deux domaines cognitifs distincts et articulant les approches neuroéconomique, neurobiologique et computationnelle du choix.

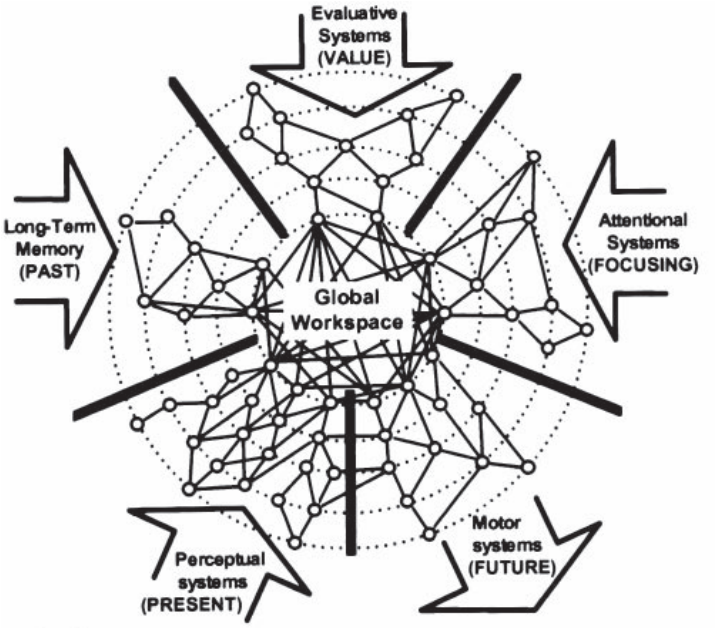

Figure 1 : Ce schéma illustre le concept d'un module de décision unique, connecté à ses 3 systèmes d'entrés principaux que sont les modules cognitifs traitant l'information sensorielle (« *perceptual systems* »), la capacité d'accéder à son expérience passée sous forme de souvenirs (« *long-term memory* ») et finalement, le système de valuation (« *evaluative system* ») au cœur des théories économiques du choix. On notera que cette représentation n'individualise pas explicitement le processus de prise de décision et son système de régulation contextuelle. D'après Dehaene *et al.*[7]

Dans une première partie, nous introduisons succinctement le cadre théorique de l'analyse séquentielle et ses rapports à l'inférence Bayesienne. Puis, nous abordons la notion de prise de décision en évoquant son émergence progressive à l'intersection

travers les différents domaines cognitifs. En effet, il est frappant de constater à quel point les situations décisionnelles auxquelles nous sommes confrontés peuvent varier, reposant tantôt sur l'analyse perceptuelle de l'environnement, tantôt sur l'analyse économique de la valeur subjective des options considérées, ou même sur le rappel d'expériences passées. Nous avons donc testé l'hypothèse que les modèles neuro-computationnels décrivant les choix basés sur l'information sensorielle - i.e. les mêmes algorithmes de choix dans les mêmes régions cérébrales - puissent être pareillement impliqués dans la prise de décision basée sur les valeurs, et plus particulièrement les valeurs subjectives, jetant ainsi un pont entre deux domaines cognitifs distincts et articulant les approches neuroéconomique, neurobiologique et computationnelle du choix.

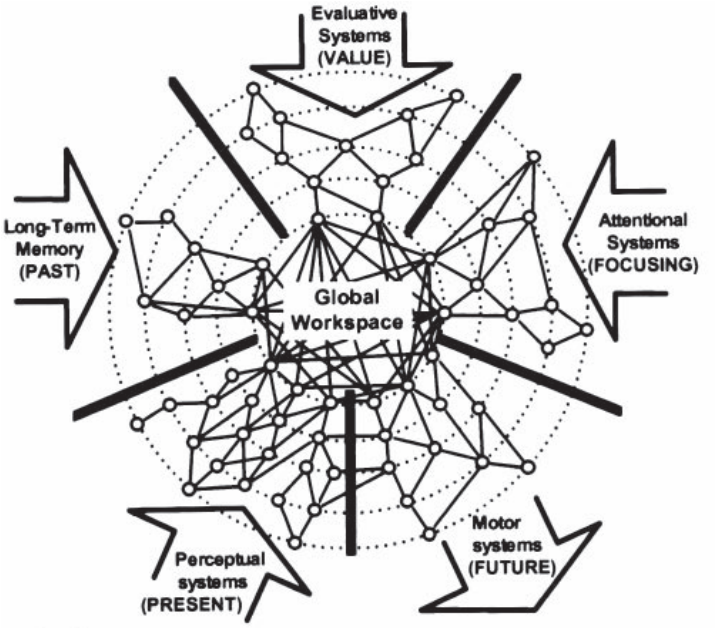

Figure 1 : Ce schéma illustre le concept d'un module de décision unique, connecté à ses 3 systèmes d'entrés principaux que sont les modules cognitifs traitant l'information sensorielle (« *perceptual systems* »), la capacité d'accéder à son expérience passée sous forme de souvenirs (« *long-term memory* ») et finalement, le système de valuation (« *evaluative system* ») au cœur des théories économiques du choix. On notera que cette représentation n'individualise pas explicitement le processus de prise de décision et son système de régulation contextuelle. D'après Dehaene *et al.*[7]

Dans une première partie, nous introduisons succinctement le cadre théorique de l'analyse séquentielle et ses rapports à l'inférence Bayesienne. Puis, nous abordons la notion de prise de décision en évoquant son émergence progressive à l'intersection

entre neuroscience, psychophysique et psychologie, au travers d'une revue des modèles mathématiques de décision simple, suivie d'une revue de la littérature neurobiologique illustrant la convergence progressive entre notre connaissance des réseaux neuraux implémentant la sélection de l'action sur la base d'information sensorielle et les concepts issus de ces travaux de modélisation, jusqu'à la formalisation de modèles neuro-computationnels de la décision perceptuelle. Finalement, nous introduisons les théories économiques du choix dans une perspective historique avant de faire l'état de l'art en neuroéconomie de la décision, discipline visant à évaluer la validité neurobiologique des théories économiques. Nous clôturons cette section en introduisant la théorie des champs décisionnels et en discutant les arguments en faveur d'un cadre neuro-computationnel commun aux décisions simples. Dans la partie expérimentale, nous présentons les résultats de deux études d'imagerie par résonance magnétique fonctionnelle (IRMf) visant à préciser les mécanismes neuro-computationnels de la décision humaine. La première étude pose la question des mécanismes d'ajustement du processus de décision perceptuelle à son contexte grâce à un paradigme manipulant systématiquement l'information prédictive et l'incertitude (au sens de Shannon[8]) de séquences de décisions perceptuelles. Dans la deuxième étude, nous abordons la question de l'unicité des mécanismes neuro-computationnels implémentant la prise de décision au travers des domaines cognitifs grâce à un paradigme de prise de décision économique risquée, c'est-à-dire basée sur les valeurs subjectives espérées attribuées à chaque option. Enfin, nous terminerons par une discussion générale replaçant nos résultats dans une architecture fonctionnelle du cortex préfrontal Humain vue sous l'angle des Neurosciences Computationnelles.

2. INTRODUCTION

a. Banburismus et analyse séquentielle

Traversant Hyde Park un jour de brouillard, j'aperçois la silhouette d'un chien : Dois-je faire marche arrière ou continuer à avancer en ne tenant pas compte d'un danger potentiel ? Prenant le temps de la réflexion, je distingue finalement un labrador à l'air avenant, une balle en mousse dans la gueule… Il est donc probable que ce chien soit domestiqué et que son maitre ne soit pas très éloigné ! Je décide donc de continuer mon chemin. Repensant à cet épisode, je réalise que, le brouillard étant particulièrement épais ce matin là, faire ce choix m'a pris un certain temps. Peut-être aurais-je dû me rappeler qu'à cette heure, de nombreux londoniens sortent leurs chiens pour leur promenade quotidienne, ce qui m'aurait probablement permis d'arriver plus rapidement à la même conclusion…

On appelle décision perceptuelle la sélection d'un comportement sur la base d'une perception. Formellement, une décision perceptuelle peut donc être vue comme un test d'hypothèse sur l'état du monde réel à partir des informations collectées par les organes sensoriels. En effet, dans une situation décisionnelle donnée, sélectionner le comportement adéquat nécessite d'évaluer l'adéquation entre perception - i.e. une représentation catégorielle interne des éléments présents dans notre environnement - et le monde réel (voir Fig. 2). La tâche est difficile car l'information sensorielle n'est disponible que sous la forme d'un code neural abstrait et intrinsèquement bruité du fait des étapes successives de traitement qui lui sont appliquées au sein des portions sensorielles du néocortex[5,9,10].

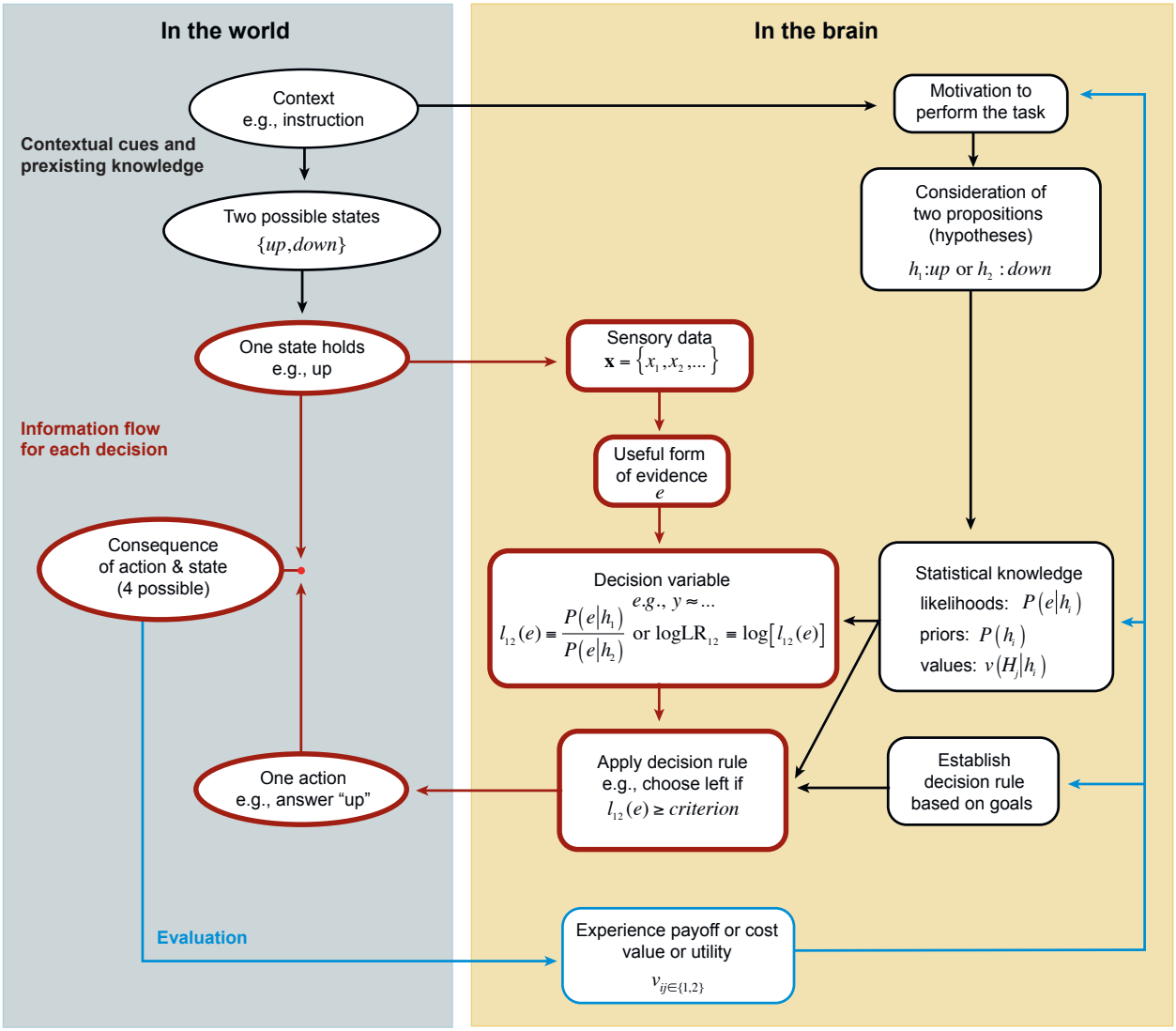

Figure 2 : Algorithme implémentant une décision perceptuelle entre deux alternatives (encadrés rouges). La section à gauche représente le monde réel (fond gris) et la partie droite les computations effectuées par le cerveau pour sélectionner l'action appropriée (fond jaune). L'information contextuelle *a priori* permet de guider le processus de prise de décision (encadrés noirs). Cette information *a priori* est mise à jour après chaque choix en fonction de ses conséquences (encadré bleu). D'après Gold[5].

Dans cette situation, le cerveau fait donc face à un problème proche de celui rencontré par les cryptanalystes de l'armée anglaise durant la seconde guerre mondiale[11]. En effet, l'armée allemande cryptait ses communications grâce à une machine électromécanique, appelée Enigma (voir Fig. 3), appliquant une substitution de caractères polyalphabétique grâce à des rotors mobiles montés en série. Le décryptage du message était ensuite obtenu en tapant à nouveau le texte crypté sur une machine Enigma initialisée dans la même position que durant l'étape de cryptage. Dans sa version

à trois rotors, il y avait 17576 positions initiales, ou clefs de cryptage, possibles. La procédure d'encryption utilisée par l'armée allemande utilisait une clef principale, identique pour l'ensemble des messages transmis un jour donné. Tout message encodé débutait par la répétition d'un code de trois lettres représentant une clef de cryptage secondaire choisie librement par l'opérateur pour chaque nouveau message. Cette dernière était utilisée pour coder le reste du message. Il va sans dire que le problème cryptographique posé par le décodage de ces messages était épineux au vu des moyens de calcul de l'époque.

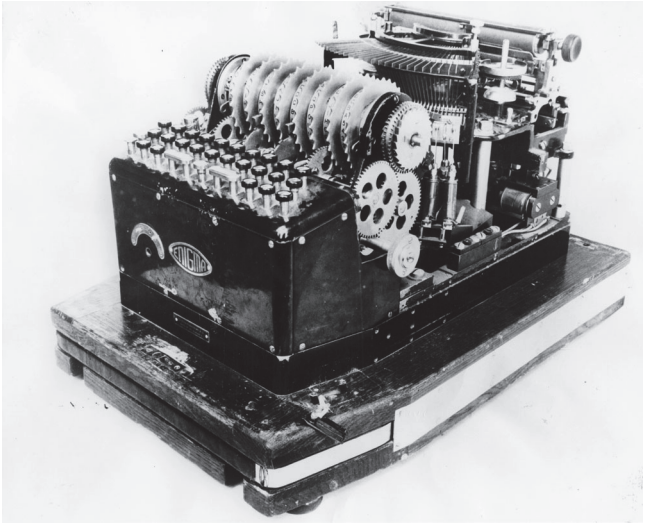

Figure 3 : Enigma est une machine permettant de crypter de textes grâce à un système électromécanique composé de rotors multiples montés en série implémentant une substitution polyalphabétique. Enigma fut massivement utilisée durant la seconde guerre mondiale par l'armée allemande afin de protéger ses transmissions.

L'originalité de l'approche de Turing, ou Banburismus, est sa capacité à exploiter ce dernier point de la procédure de cryptage afin d'inférer le troisième composant de la clef principale. Pour ce faire Turing développa un cadre théorique original qui allait jeter les bases d'une théorie plus générale de la décision par échantillonnage séquentiel[12]. Le point clef de sa méthode consistait à examiner des paires de messages encodés un même jour et dont les deux premières lettres étaient identiques, puis d'identifier si un décalage de cadre de lecture des messages permettait de remettre en phase les clefs secondaires, i.e. de faire comme si la même clef secondaire avait été utilisée pour coder les deux messages. Cette méthode repose donc sur 3 étapes critiques permettant de minimiser le temps de décision à un niveau de performance donné : (1) une méthode de quantification des preuves en faveur de l'hypothèse testée, (2) Une méthode de mise à jour de cette quantité au fur et à mesure que des nouvelles données sont examinées et (3) une règle de décision permettant de terminer le processus de décision. Cette

problématique rappelle donc celle à laquelle fait face le cerveau lorsqu'il doit décider si un percept correspond effectivement à un objet existant dans le monde réel.

Pour décider si deux messages avaient été encodés avec la même clef secondaire, Alan Turing comptait le nombre de caractères identiques à une même position entre les messages (*match*). En effet, deux messages encodés avec des clefs différentes (*h0* dans Eq. 1-3) produiraient un résultat proche du hasard (p=1/26 lettres possibles), alors que deux messages encodés avec les même clefs (*h1* dans Eq. 1-3) reflèteraient les propriétés statistiques de la langue dans laquelle les messages originaux étaient écrits, s'écartant ainsi du hasard. En inspectant successivement chaque paire de caractère des messages testés, on peut donc recalculer après chaque nouvelle observation la quantité d'évidence (« *weight of evidence* », *woe* dans Eq. 1) comme le rapport de la probabilité d'observer un nombre donné de *match* entre les deux messages à ce point de la chaine de caractères sous l'hypothèse que les clefs de cryptages soient identiques ($\Pr(m/h1)$) ou pas ($\Pr(m/h0)$).

$$woe = \log\left(\frac{\Pr(m/h1)}{\Pr(m/h0)}\right) \qquad \text{(Eq. 1)}$$

Utiliser le logarithme de cette quantité permet simplement de pouvoir additionner, et donc d'accumuler, l'évidence supplémentaire apportée par l'observation d'une nouvelle paire de caractères en faveur de l'une ou l'autre des hypothèses (voir Fig. 2). Cette façon de calculer l'évidence produit une quantité positive quand les observations sont en faveur de *h1* et une quantité négative quand elles sont en faveur de *h0*. Une autre propriété intéressante de cette mesure est que la réversibilité entre probabilités des causes et des effets permise par le théorème de Bayes permet de calculer le niveau relatif de croyance dans les hypothèses testées, i.e. un log-ratio de probabilités *a posteriori* ($\Pr(h0/m)$ et $\Pr(h1/m)$ dans Eq. 2). Il est intéressant de noter que ce renversement fait naturellement émerger la participation de nos croyances *a priori* (avant toute collecte de données) sur l'issue de la décision dans le calcul du rapport des probabilités *a postériori* de chaque hypothèse ($\Pr(h0)$ et $\Pr(h1)$ dans Eq. 2). De ce point de vue, croyances *a priori* et vraisemblance d'une hypothèse à la vue des observations faites sont simplement additionnées lors de la décision, une source d'information pouvant se substituer à l'autre (voir Fig. 2).

$$\log\left(\frac{\Pr(h1/m)}{\Pr(h0/m)}\right) = \log\left(\frac{\Pr(h1)}{\Pr(h0)}\right) + woe \qquad \text{(Eq. 2)}$$

Finalement, si l'on considère le cas d'une décision binaire (ex : même clefs de cryptage ou non ?) et qu'on définit *B* comme étant la quantité d'évidence au moment de l'arrêt du processus de délibération, alors *B* peut-être utilisé pour fixer une règle de terminaison du processus de décision. L'équation 2 peut être réarrangée illustrant ainsi comment *B* se comporte alors comme un seuil de décision permettant de déterminer *a priori* la précision de l'inférence (Eq. 3). Le mécanisme de décision proposé par A. Turing permet donc une inférence contrôlant la probabilité d'erreur et limitant le temps passé à accumuler de l'information, définissant ainsi un compromis entre durée et performance du processus de décision. De plus, si l'accumulation d'évidence est linéaire, alors cette stratégie de décision est optimale dans le sens où elle minimise le temps de décision pour une probabilité d'erreur donnée[9].

$$\Pr(h1/m) = \frac{1}{1+10^{-B}} \qquad \text{(Eq. 3)}$$

Après la guerre, les travaux de Wald sur l'analyse séquentielle montreront que cette approche est généralisable à l'ensemble des décisions par échantillonnage séquentiel, c'est-à-dire à toutes les situations où l'inférence implique une évaluation dynamique des données collectées jusqu'à ce qu'un critère de décision défini *a priori* soit remplit. L'analyse séquentielle est donc définie par opposition au test d'hypothèse classique où un échantillon de taille prédéterminé est constitué avant toute inférence. Cette analyse permet donc de diminuer les coûts liés à la décision. Plus spécifiquement, le processus décrit dans ce chapitre correspond à un test d'inférence Bayesien appelé test séquentiel du ratio de probabilité (SPRT)[12]. Une propriété importante de ce test est que le risque de première espèce dépend de la distance au seuil supérieur de décision et sa puissance de la distance au seuil inférieur, établissant ainsi une relation directe entre quantité d'évidence nécessaire pour prendre une décision et les caractéristiques de l'inférence[5,10,12].

b. Modélisation des processus décisionnels simples

Depuis plus d'un siècle, l'étude expérimentale des processus cognitifs sous-tendant nos décisions anime les champs de la psychologie expérimentale et mathématique, conduisant ainsi au développement de modèles quantitatifs du comportement humain en situation de décision. L'émergence récente des neurosciences cognitives computationnelles a contribué à un regain d'intérêt pour ces disciplines. Une revue exhaustive de ces travaux dépassant le cadre de cette thèse, je me limiterai ici à une présentation des modèles de décision les plus influents du point de vue de la neurobiologie cognitive[5,13-16].

Ces modèles ont été développés dans le but de rendre compte du comportement des primates lors de décisions simples, i.e. lorsqu'un sujet, placé dans un environnement stable, sélectionne une action selon une règle d'association entre stimulus et réponse prédéfinie (voir Fig. 1). Ces modèles mathématiques de décision ont été utilisés avec succès dans de nombreux types de tâches[17-25] ; tâches de décisions « lexicales » : une chaine de caractère correspond-elle à un mot ou non ?, une lettre est-elle une consonne ou une voyelle ?; tâches de « numérosité » : un chiffre est-il plus grand ou plus petit qu'un autre ?; tâches de « récupération mnésique » à court et à long terme : ai-je déjà vu ce stimulus ? Mais aussi dans des tâches de décision perceptuelle[5,22,25-29] consistant à sélectionner une action sur la base d'une perception : un trait est-il plus grand ou plus petit qu'une référence ?, un flash lumineux est-il plus intense ou pas ?, suis-je en train de regarder un visage ou une maison ?, dans quelle direction un nuage de points se déplace-t-il ? (Voir Fig. 10A)… Plus récemment, il a été proposé d'appliquer ces modèles théoriques à l'étude de décisions plus complexes, basées sur la valeur subjective des différentes alternatives considérées[30-32].

Probabilité de choix et distribution des temps de réaction

L'analyse des données recueillies pendant les tâches de choix s'est longtemps limitée au traitement statistique séparé des taux d'erreurs et des temps moyens de réaction, le plus souvent par des analyses de variance. Or, même dans le cas de décisions binaires, il existe des interactions complexes entre les moments des distributions de temps de réaction et la proportion d'erreur qui sont inaccessibles à ce type d'analyse statistique. Ces effets robustes témoignent pourtant des mécanismes élémentaires constituant le processus de prise de décision[33].

C'est ce constat qui a motivé le développement de modèles mathématiques capables de prédire conjointement les distributions de temps de réaction et les proportions de choix dans une situation expérimentale donnée. Leur intérêt est double puisque confronter les prédictions de ces modèles aux données expérimentales permet de tester les hypothèses computationnelles sur lesquelles ils sont construits, et que la mesure des variations de leurs paramètres en fonction des situations expérimentales permet l'exploration raisonnée et computationnellement définie des processus cognitifs qui les sous-tendent.

Un model mécanistique du processus de prise de décision doit donc rendre compte des phénomènes suivant (voir Fig. 4) : (1) La variance des temps de réaction est proportionnelle à sa moyenne[34-36], (2) La distribution de temps de réaction présente une asymétrie positive (voir Fig. 10B) (3) Le modèle doit pouvoir produire des erreurs, (4) Il existe un compromis entre vitesse de décision et performance tel que les temps de réaction tendent à être plus long lorsque les taux d'erreurs diminuent[22,27,28] (5) La moyenne des temps de réaction des choix corrects est inférieure à celle des choix erronés lorsque les conditions de décision aboutissent à un taux d'erreur faible et inversement lorsque le taux d'erreur est important[23,33].

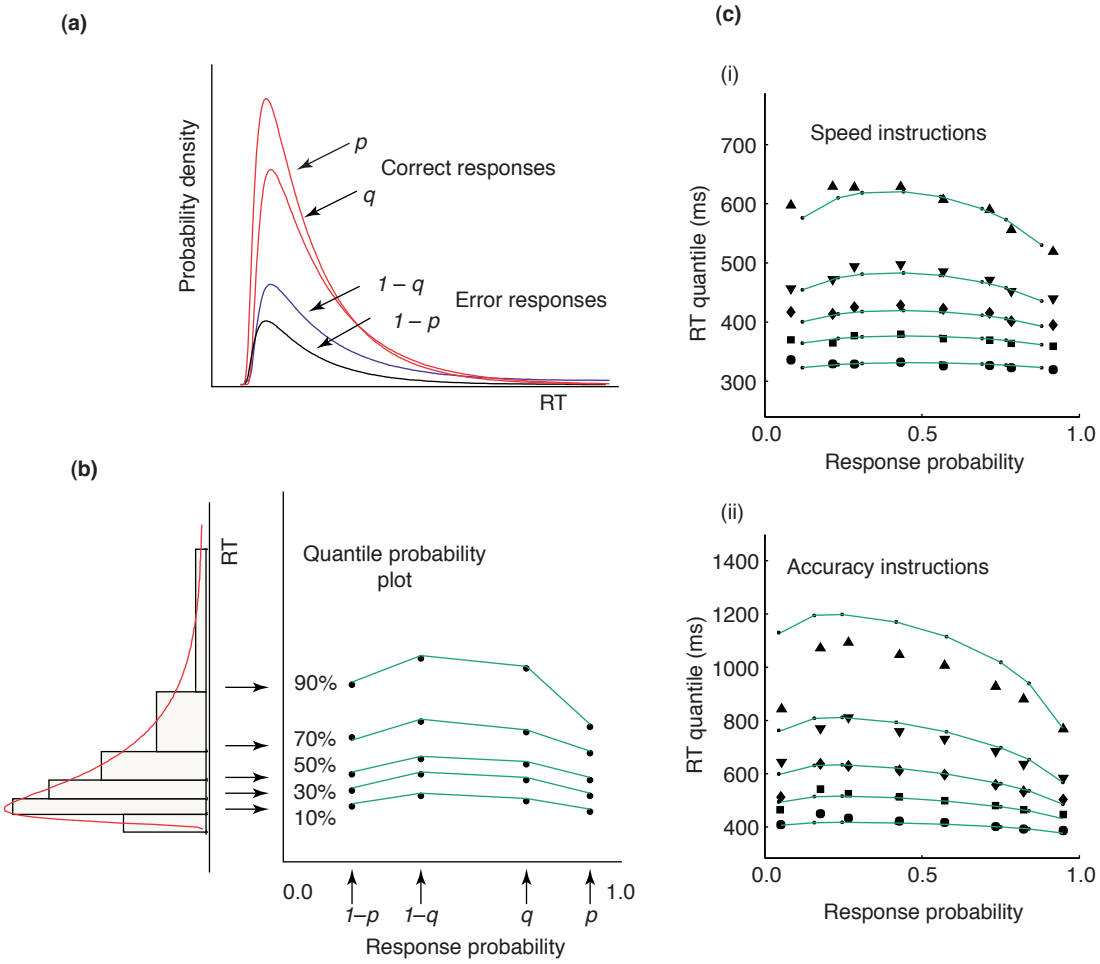

Figure 4 : (A) Relations entre distribution de temps de réaction typiquement observées lors de choix binaires simples dans une condition où la décision est facile et une condition où la décision est difficile. Les distributions pour les choix corrects sont représentées en rouge, celles pour les erreurs en noir. Soit p, la proportion de réponse correcte dans la condition facile et q, la proportion de réponses correctes dans la condition difficile. **(B)** Quantile de la distribution des temps de réaction pour les quatre conditions représentées en A (correct/erreur*facile/difficile). **(C-D)** même graphe que B présentant les données issues d'une tâche de décision perceptuelle (formes géométriques noires) et les prédictions d'un modèle de diffusion ajusté à ces données (lignes vertes) dans une condition demandant au sujet de privilégier la vitesse de réponse **(C)** ou de minimiser les erreurs **(D)**. Un modèle LCA fournissait des prédictions quasi identiques. D'après Smith et Ratcliff[14].

Prise de décisions par accumulation d'évidence vers un seuil de décision

- **Principes communs à l'ensemble des modèles par échantillonnage séquentiel**

Depuis 50 ans, le cadre théorique dominant pour expliquer les données issues des tâches de choix simple est celui de l'analyse par échantillonnage séquentiel (voir paragraphe 1b). Dans ce cadre théorique, la prise de décision est un phénomène progressif comprenant une période de « délibération » durant laquelle les évidences en faveur de chaque alternative sont accumulées par sommations itératives au sein de « variables de décision ». Ce processus d'accumulation d'évidence se poursuit jusqu'à ce qu'une variable de décision atteigne une quantité critique appelée « seuil de décision ». Atteindre le seuil de décision déclenche la sélection du comportement correspondant selon un mécanisme « winner-takes-all ». La variable de décision agrège donc les évidences produites par des modules cognitifs qui transforment, en amont du processus d'accumulation, les différents types d'informations disponibles en évidence en faveur de chaque alternative. Dans le cas des décisions perceptuelles, la conversion de l'information sensorielle en évidence est assurée par la chaine de traitement comprise entre l'organe sensoriel et les cortex sensoriels associatifs[5,37]. Du fait des multiples sources de bruit intrinsèques au traitement et à l'encodage de cette information sensorielle, le code neural représentant le niveau d'évidence est lui-même bruité, c'est à dire entaché d'incertitude. Il fluctue donc d'instant en instant même lorsque le niveau d'information est stable. Il est intéressant de noter qu'une propriété importante du processus d'accumulation est de débruiter ces signaux d'entrée du processus décisionnel afin de réaliser une inférence Bayesienne contrôlant les risques de première et de deuxième espèce.

De nombreux modèles de décision par échantillonnage séquentiel ont été développés autour de cette architecture globale, représentant autant de variations autour d'un thème principal, et essayant ainsi d'élargir progressivement le champ des comportements expliqués. Ces modèles se répartissent en deux familles selon le mécanisme modélisant l'accumulation d'évidence pendant la période de délibération : les modèles implémentant une marche aléatoire vers le seuil de décision (« random walk ») et les modèles modélisant l'accumulation comme une distribution de droite menant au seuil (« random ray »).

- **Modélisation d'accumulation d'évidence par une marche aléatoire vers le seuil de décision**

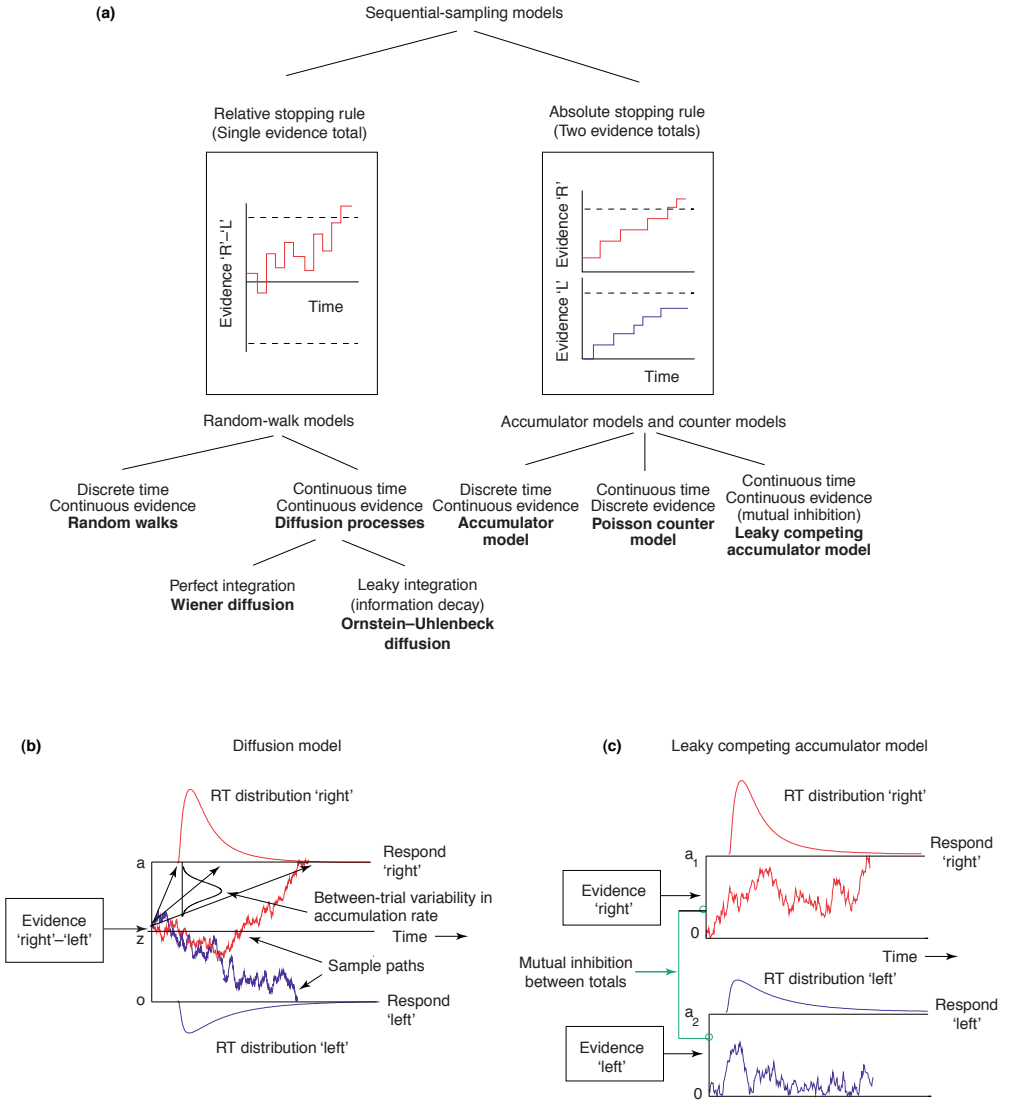

Figure 5 : Modèles de décision par échantillonnage séquentiel pour des choix binaires. **(A) Taxonomie de cette famille de modèle.** La distinction principale se fait entre modèles implémentant une variable de décision représentant le résultat net des évidences en faveur de chaque alternative, dont la règle d'arrêt est relative, et les modèles séparant ainsi l'accumulation d'évidences pour chaque alternative dans différentes unités, dont les règles d'arrêt sont absolues. Pour chaque catégorie de modèle, il existe des variantes selon que l'accumulation d'évidence soit modélisée comme un processus continu ou discret et/ou que les quantités d'évidence par unité de temps soient elle-même discrètes ou continues. **(B) Modèle de diffusion.** Le processus a deux seuils de décision, un pour chaque réponse possible (gauche ou droite). La variable de décision est initialisée en *z*. Ce point de départ n'est pas nécessairement équidistant des seuils de décision et reflète le biais *a priori* en faveur d'une des réponses. L'accumulation d'évidence se poursuit jusqu'au moment où la variable de décision croise l'un des deux seuils de décision déterminant ainsi simultanément l'option choisie et le temps de décision. Les fluctuations de la variable de décision reflètent le bruit au sein du processus d'accumulation. **(C) Modèle par compétition d'accumulateur à inhibition mutuelle (« leaky »).** Chaque unité accumule les évidences pour une des alternatives, celles-ci sont en compétition via un mécanisme d'inhibition mutuelle. Chaque unité est initialisée à 0 et possède son propre seuil de décision. La première unité atteignant le seuil de décision remportant la course, selon un mécanisme décisionnel « winner-takes-all ». Finalement, les accumulateurs présentent un mécanisme de « fuite », les évidences étant perdues en proportion de la quantité de preuve accumulée. D'après Smith et Ratcliff[14].

Processus de diffusion : Modèle de Ratcliff et modèle EZ2

Le modèle de diffusion (DDM) introduit par Ratcliff[14,16,17,19,22,38,39] en 1978 domine actuellement le domaine de la psychologie mathématique des décisions simples. Celui-ci implémente des choix binaires par accumulation d'information provenant d'un canal d'entrée bruité comme une marche aléatoire continue vers des limites absorbantes. Le processus de décision est initialisé après un temps de latence « non décisionnel » (*Ter*) rendant compte du traitement de l'information en amont du processus de décision et de l'exécution de l'action correspondante à la décision prise. Le temps de réaction est donc considéré comme la somme du temps passé à accumuler des évidences (*Td*) et du temps non décisionnel[33] (*Ter*).

$$RT = Ter + Td \qquad \text{(Eq. 4)}$$

L'évolution de la variable de décision durant la phase d'accumulation d'évidence est modélisée par l'équation différentielle stochastique décrivant la diffusion d'une particule dans un liquide (Eq. 5). La variable de décision $X(t)$ est initialisée à un niveau d'évidence *z* tel que $z \in [0,a]$ (voir Fig. 5A et 6), avant de dériver à une vitesse moyenne v vers l'un des deux seuils de décision (positionnés en 0 et en a, voir Fig. 6). La distance entre la particule et le seuil de décision $X(t)$ résulte de la somme de l'effet de sa vitesse moyenne de dérive v et d'un processus de Wiener $s * dW(t)$, bruit Gaussien de moyenne nulle et d'écart-type *s* modifiant aléatoirement la distance de la particule au seuil instant après instant. Du point de vue d'un SPRT, $X(t)$ représente donc le niveau relatif d'évidence en faveur de chaque alternative et sa valeur à l'initialisation du processus de diffusion correspond au biais *a priori* en faveur d'une des 2 réponses. L'accumulation d'évidence se poursuit jusqu'au moment où la variable de décision croise l'un des deux seuils de décision déterminant ainsi simultanément l'option choisie et le temps de décision.

$$dX(t) = v * dt + s * dW(t) \qquad \text{(Eq. 5)}$$

Dans le modèle de diffusion, les paramètres les plus importants sont donc la vitesse de dérive (*v*), qui reflète la qualité de l'information en entrée du processus de décision, la distance entre les seuils (*a*), qui reflète le conservatisme du processus, et le temps de non décision (*Ter*), qui reflète la durée des processus en amont et en aval du processus de décision (Fig. 6).

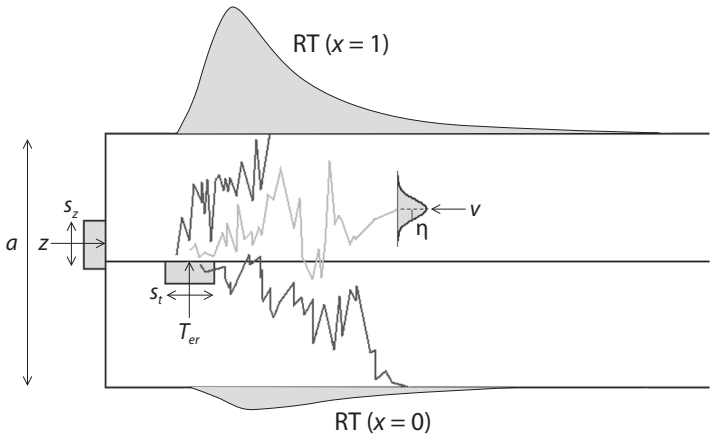

Figure 6 : Le modèle de diffusion de Ratcliff est décrit par un ensemble de 7 paramètres : **(1)** Vitesse de dérive moyenne de la variable de décision (v) **(2)** Variabilité inter-essais de la vitesse moyenne de dérive (η) **(3)** distance entre les seuils de décision (a) **(4)** Point de départ du processus (z) **(5)** Variabilité inter-essais du point de départ (sz) **(6)** Temps non-décisionnel moyen **(7)** Variabilité inter-essais du temps de non-décision (st). D'après Vandekerckhove[40].

Le modèle de diffusion inclus également des sources de variabilités supplémentaires nécessaires pour rendre compte de l'intégralité des phénomènes comportementaux observés durant les choix binaires simples[14] (Fig. 6). Tout d'abord, la vitesse de dérive moyenne varie selon une loi normale de moyenne v et d'écart-type η d'essais en essais, ce qui permet au modèle de prédire la survenue d'erreurs plus lentes que les réponses correctes. De plus, la valeur à laquelle la variable de décision est initialisée (z) varie également entre les essais : celle–ci suit une loi uniforme centrée sur z et d'amplitude cz, ce qui permet au modèle de prédire la survenue d'erreurs plus rapides que les réponses correctes. Finalement, la dernière source de variabilité inter-essais du modèle porte sur le temps de non décision. Celui-ci est distribué selon une loi uniforme de moyenne Ter et d'amplitude st, et permet au modèle de prédire correctement la pointe de la distribution des RT lié à la présence de temps de réponse contaminants.

Il est intéressant de noter, que bien que très performant pour prédire les choix binaires, le modèle de diffusion ne présente pas d'extension simple aux choix incluant plus de deux alternatives. De plus, l'estimation des 7 paramètres du modèle de diffusion repose sur l'intégralité des distributions de RT pour les décisions correctes et incorrectes. En pratique, une telle procédure nécessite donc de collecter un grand nombre d'observations, ce qui peut s'avérer impossible dans de nombreuses situations expérimentales lorsque le temps est limité et/ou les taux d'erreurs sont faibles. En effet, ajuster un tel modèle à un jeu de données de taille insuffisante conduit à une explosion de l'incertitude sur l'estimation des paramètres du modèle, et augmente leur dépendance aux valeurs d'initialisation de la procédure d'ajustement aux données.

Ce constat a motivé le développement et la validation de modèles de diffusion simplifiés[35,36,41,42], négligeant les sources de variabilité inter-essais du modèle complet afin de diminuer sa dimensionnalité. Dans cette perspective, le modèle computationnel ne vise plus à expliquer l'intégralité des phénomènes comportementaux observés, mais à fournir une estimation fiable des paramètres principaux d'un processus décisionnel par échantillonnage séquentiel, en particulier sur des jeux de données de taille plus modeste. L'argument principal des tenants de cette approche est que les effets comportementaux dépendant des sources de variabilité inter-essais, tels que la vitesse relative des erreurs et des décisions correctes, sont négligeables dans un grand nombre de paradigmes expérimentaux. Lorsqu'on utilise un tel modèle, il est donc nécessaire de mettre en balance ce risque avec la difficulté d'acquisition d'un jeu de données plus grand, les problèmes d'estimations du modèle complet, et l'importance réelle des effets comportementaux prédits par ces sources de variations inter-essais dans la situation expérimentale considérée. Le modèle de diffusion simplifié le plus récent est le modèle EZ2 de Wagenmaker *et al*[35,36,41,42]. Celui-ci utilise la variabilité intra-essai comme source unique de variabilité du processus de prise de décision (Eq. 5) et ne retient que les 4 paramètres principaux du modèle de diffusion : vitesse de dérive (v), distance entre les seuils (a), temps de non décision (Ter) et point de départ (z), estimés sur les deux premiers moments (moyenne et écart-type) des distributions de RT pour chaque type de réponse et sur la proportion d'erreur. Grace à ces hypothèses simplificatrices, il est possible d'estimer les paramètres principaux du processus de diffusion à partir d'échantillon comprenant 50 observations[36]. La limitation principale de ce modèle simplifié est sa sensibilité à la présence de temps de réaction contaminants[41,42], ce qui

nécessite de s'assurer que leur proportion soit faible (<1%) ou d'estimer une mixture de distribution uniforme et ex-Gaussienne, puis d'ajuster le modèle à partir de la moyenne et de la variance mesurée de la composante ex-Gaussienne. Ces propriétés font que le modèle EZ2 se montre plus performant que le modèle de diffusion complet pour réaliser des estimations intra-individuelles des paramètres du processus de décision[38].

Modélisation par compétition d'accumulateurs « leaky »

Le modèle de décision par compétition d'accumulateurs « leaky » (LCA), introduit par Usher et McClelland en 2001, est une évolution du modèle de diffusion inspirée par la physiologie des neurones corticaux. Celui-ci vise à proposer un modèle de décision par échantillonnage séquentiel neurobiologiquement crédible et structurellement indépendant du nombre d'options considérées[10,43]. Dans le LCA, l'information en faveur de chaque option est accumulée dans des unités indépendantes initialisées à 0 (voir Fig. 5C). Chaque unité possède une vitesse moyenne de dérive propre (*v1, v2, v3*…), ainsi qu'un seuil de décision propre (*a1, a2, a3*…). L'accumulation d'évidence dans chaque unité est décrite par un processus de diffusion auquel deux effets non-linéaires sont ajoutés : une inhibition mutuelle entre unités et une fuite d'information, modélisant la perte progressive des informations les plus anciennes. Les unités sont en compétition les unes avec les autres dans une course vers leurs seuils de décision respectifs selon une règle « winner-takes-all ». Dans le cas binaire, l'équation 5 devient donc le système d'équation 6, qui peut lui-même être facilement généralisé à *N* options (Eq. 7).

$$\begin{aligned} dX_1(t) &= (-kX_1(t) - wX_2(t) + \nu_1)dt + s_1 dW_1 \\ dX_2(t) &= (-kX_2(t) - wX_1(t) + \nu_2)dt + s_2 dW_2 \end{aligned} \qquad \text{(Eq. 6)}$$

$$dX_i(t) = (-kX(t)_i - w\sum_{\substack{j=1 \\ j\neq i}}^{N} X(t)_j + \nu_i)dt + s_i dW_i \qquad \text{(Eq. 7)}$$

Comme le modèle de diffusion, le LCA comprend plusieurs sources de variabilité inter-essais additionnelles : (1) Chaque accumulateur est initialisé à une valeur aléatoire positive suivant une loi uniforme, ce qui permet de rendre compte de la vitesse relative des erreurs et des réponse correcte lors des conditions de décision les plus faciles, (2) La

vitesse de diffusion pour un essai donné suit une loi normale ayant pour moyenne la valeur du paramètre de diffusion, (3) Enfin, le temps non décisionnel est distribué suivant une loi uniforme autour du temps non décisionnel moyen.

Une propriété intéressante du mécanisme d'inhibition mutuel entre unités est qu'il permet d'émuler le type de calcul d'évidence relative implémenté dans le DDM (Eq. 1), inscrivant ainsi le LCA dans le cadre théorique de l'inférence Bayesienne. De ce point de vue, le LCA propose donc une implémentation inspirée par la neurophysiologie d'un multiple SPRT[10], généralisation du SPRT au-delà du cas particulier des choix binaires, tout en maintenant des performances équivalentes à celles du DDM pour rendre compte du comportement observé lors de choix binaires[14,15,39].

Parmi les multiples variantes du LCA existantes, une extension particulièrement intéressante de ce modèle ajoute un signal d'urgence au processus d'accumulation de preuve sous la forme d'une amplification temporellement croissante des canaux d'entrées[44], ou d'un signal additionnel augmentant de manière hyperbolique en fonction du temps[45]. Cette étape supplémentaire permet notamment de rendre compte de notre capacité à décider même en l'absence complète d'information, quitte à répondre aléatoirement, incluant ainsi dans le modèle le coût du temps de délibération.

Modélisation par un rayon aléatoire : Modèles LATER et LBA

Une approche alternative à la modélisation du processus de décision par une marche aléatoire consiste à modéliser l'activité globale des unités accumulant des évidences par un rayon reliant l'activité basale dans l'accumulateur à son seuil de décision[29,46]. Cette hypothèse revient donc à négliger la variabilité intra-essai qu'implique le processus de diffusion au cœur des modèles précédents[29] (Eq. 5). Ces modèles de décision s'inscrivent donc dans le cadre général de la prise de décision par échantillonnage séquentiel.

Le modèle LATER (« *linear approach to threshold with ergodic rate* ») est le plus simple de cette famille[27,28,47,48]. Il vise à prédire la distribution des RT pour les choix corrects lors de décisions perceptuelles sur des stimuli aisément discriminables, mais pas les taux d'erreurs ou la distribution de RT associée. En effet, le modèle LATER a été développé pour étudier des tâches de Go/No-Go et de Stop-signals dans lesquelles les réponses inhibées ne produisent pas de quantité mesurable. Dans ce modèle (Fig. 7),

l'activité globale de la population de neurones associée à la réponse correcte est modélisée comme une droite de pente *r* reliant l'activité basale de l'accumulateur (S_0) et son seuil de décision[46] (S_T). Le modèle LATER capture la forme de la distribution des RT pour les réponses correctes en faisant l'hypothèse que la pente de la droite représentant l'activité au sein de l'accumulateur fluctue aléatoirement entre les essais selon une loi normale de moyenne *r* et d'écart type *sd*. C'est pourquoi on parle de modélisation par « rayon aléatoire ». La forme de la distribution des RT pour les réponses correctes résulte donc de la projection de la distribution Gaussienne de la pente de l'accumulateur sur le seuil de décision (Fig. 7). En formalisant la relation entre ces deux distributions, il est alors possible d'estimer les paramètres du modèle LATER à partir de la relation suivante (Eq. 8).

$$\frac{1}{RT} \rightarrow N\left(\frac{r}{s_T - s_0}, \frac{sd}{s_T - s_0}\right) \qquad \text{(Eq. 8)}$$

Finalement, le modèle LATER modélise les erreurs « rapides » (« fast guesses ») qui surviennent dans ce type de tâche par un processus accessoire distribué selon une loi normale de moyenne nulle et ayant sa propre variance[49]. La distribution des RT prédite par le modèle LATER résulte donc du mélange de ces deux processus.

Lorsque les décisions perceptuelles portent sur des stimuli aisément discriminables, le modèle LATER permet une analyse simple du comportement observé, ainsi que la représentation graphique de l'impact des manipulations expérimentales de la pente de l'accumulateur et/ou de la distance au seuil de décision sur les distributions de RT[28] (Eq. 8). Cette dernière est obtenue en représentant les percentiles de la distribution cumulée des latences en fonction de la réciproque des latences (Fig. 7, cadre inférieur gauche). Lorsque la pente de l'accumulateur varie entre deux conditions, les droites représentant les distributions de RT dans chaque condition sont parallèles l'une à l'autre (Fig. 7, cadre inférieur droit). Lorsque la distance au seuil varie, les droites représentant les distributions de RT se croisent alors à l'infini[50] (Fig. 7, cadre supérieur droit). Ce type de contrôle graphique simplifie significativement le contrôle qualitatif de l'adéquation entre le modèle et le comportement observé[51]. Finalement, des modèles associant plusieurs unités LATER en réseau ont été proposés afin de prédire les réponses

correctes et les erreurs observées lors de décisions perceptuelles de type Go-NoGo[52,53] (décision binaire dont l'une des réponse consiste à ne pas donner de réponse).

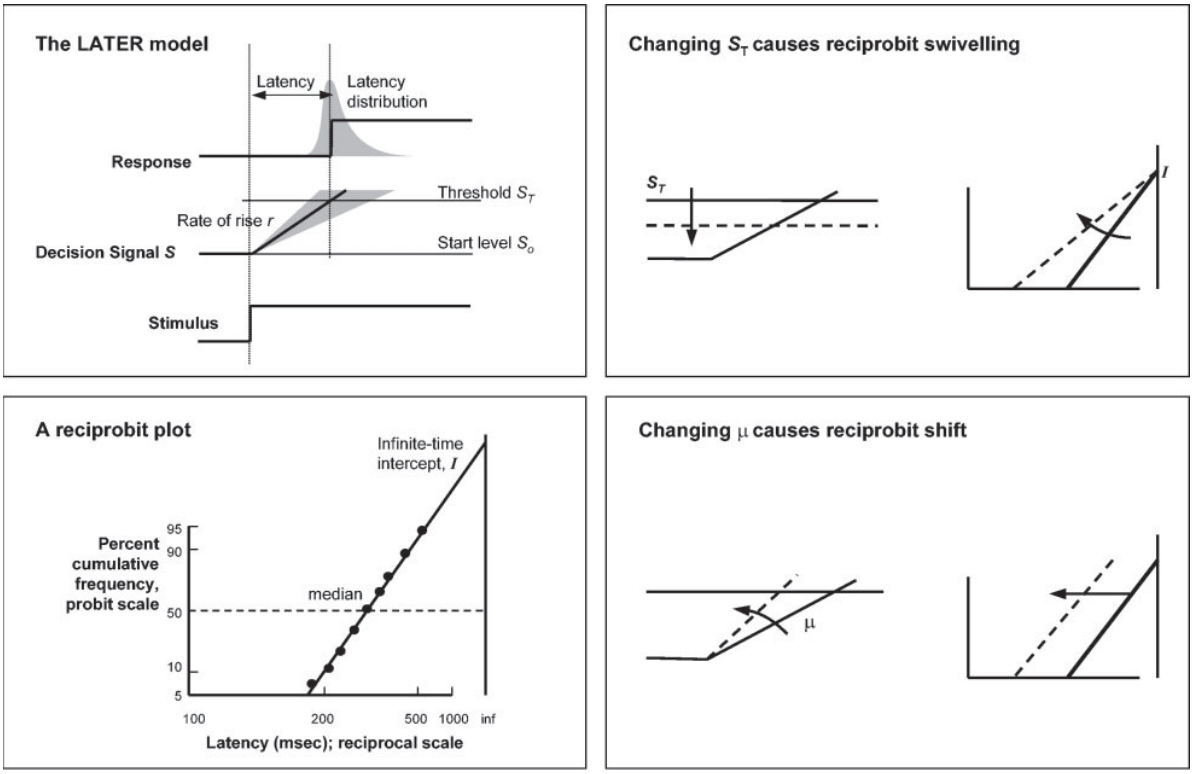

Figure 7 : Modèle LATER et graphes réciprobits. (Cadre Supérieur Gauche) Après présentation d'un stimulus, l'activité neurale augmente linéairement (r) à partir d'un niveau d'activité basale (S_0) jusqu'au seuil de décision (S_T). **(Cadre Inférieur Gauche)** Graphe Réciprobit. **(Cadre Supérieur Droit)** Représentation d'une diminution de la distance au seuil de décision sur un graphique réciprobit. **(Cadre Inférieur Droit)** Représentation d'une augmentation de la pente de l'accumulateur sur un graphique réciprobit. D'après Reddi *et al*[28].

Plus récemment, Brown et Heathcote ont proposé un modèle de décision simple basé sur une compétition entre accumulateurs linéaires indépendants : le « linear ballistic accumulator model » (LBA). En effet, le LBA est composé d'unités distinctes accumulant indépendamment les évidences en faveur de chacune des alternatives[29] (Fig. 8). Au sein de chaque unité, le processus d'accumulation est modélisé par un rayon aléatoire dont la pente fluctue d'essai en essai suivant une loi normale de moyenne spécifique à chaque unité (*d1, d2,* …) et de variance commune à l'ensemble des unités (*s*). A chaque nouvel essai, chaque unité est initialisée indépendamment suivant une loi uniforme définie sur l'intervalle [*0, A*]. Un seuil de décision est fixé chaque unité (*b1, b2,* …), représentant ainsi la quantité d'évidence devant être accumulée pour qu'une

réponse soit sélectionnée. Comme les unités accumulatrices sont engagées dans une course au seuil de décision selon une règle « winner-takes-all », l'option choisie est donc déterminée par l'unité atteignant en premier le seuil de décision. Finalement, le LBA comprend une estimation du temps non décisionnel (Eq. 4), mais pas de sa variabilité qui est considérée comme étant négligeable. A la différence du LCA, introduit dans le paragraphe précédent, l'accumulation d'évidence est donc modélisée ici comme un rayon aléatoire sans inhibition mutuelle entre unités concurrentes. De plus, les unités accumulatrices du LBA sont structurellement très proches de celles du LATER, se distinguant principalement par le fait que le LBA, contrairement au LATER, modélise la variabilité inter-essais de la valeur à laquelle l'accumulateur est initialisé[29].

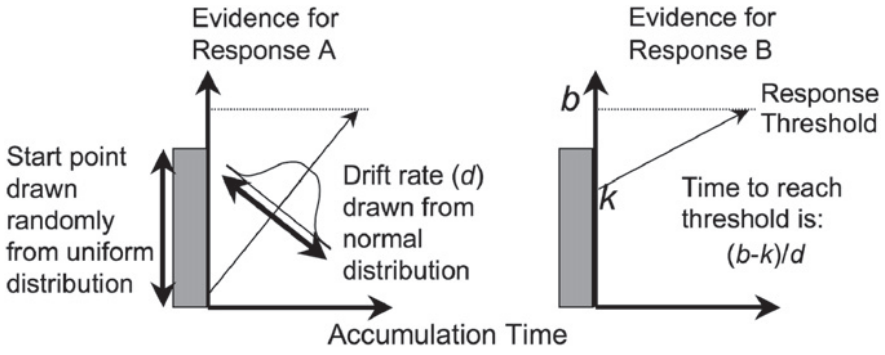

Figure 8 : Modèle LBA dans le cas d'une décision binaire. Deux unités indépendantes accumulent des évidences en faveur de chaque option. D'après Brown[29].

Le modèle LBA comprend donc 6 paramètres libres devant être ajustés aux données comportementales pour un choix binaire non biaisé. Du fait de la simplicité de son architecture, permettant d'obtenir des solutions de forme close pour les proportions de choix et les RT, cette étape est bien plus simple que pour les modèles de diffusion surtout lorsque les décisions portent sur plus de deux alternatives. En effet, l'extension du modèle LBA est mathématiquement triviale et ne complexifie pas la procédure d'ajustement du modèle[29]. Contrastant avec sa simplicité, le modèle LBA permet de prédire les phénomènes comportementaux les plus importants observés lors de décisions simples avec la même efficacité que le DDM[16,29] : Forme des distributions de RT, vitesse relative des réponses correctes et erreurs, erreurs rapides… En effet, l'ajustement du LBA et du DMM sur des données réelles produit des estimations proches

des 3 paramètres principaux des deux modèles : la valeur du seuil de décision, de la pente de l'accumulation et du temps non-décisionnel[16].

Modélisation de décision simple sans accumulation d'évidence

Opérant une rupture par rapport au cadre théorique dominant de l'inférence Bayesienne et de l'analyse par échantillonnage séquentiel, certains modèles de prise de décisions remettent en question l'hypothèse de l'accumulation progressive d'évidence durant la formation du choix. Un exemple récent de cette approche est le modèle Urgency-Gating[44,54]. Dans ce modèle, des unités indépendantes codent une variable de décision augmentant linéairement vers un seuil. Celle-ci ne représente cependant pas la sommation itérative des évidences instantanées produites par les structures cérébrales d'entrée du processus de décision, mais le produit entre (1) Un signal d'urgence – i.e. une rampe croissante indépendante du contenu informationnel de l'environnement et reflétant la pression temporelle sur la réponse -, et (2) Le niveau d'évidence instantané auquel est appliqué un filtre passe-bas. Ce type de modèle existe pour l'instant en tant que preuve de concept. En effet, il a été peu validé expérimentalement, principalement car les prédictions de ce modèle ne divergent de celles faites par les modèles par échantillonnage séquentiel que lorsque la quantité d'information sensorielle est manipulée expérimentalement durant le processus de délibération.

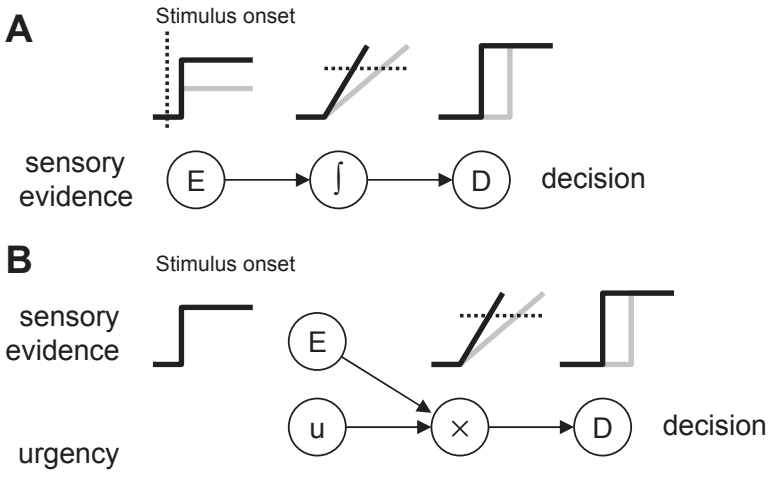

Figure 9 : (A) Modèle de décision par accumulation d'évidence. (B) Modèle « Urgency-Gating ». D'après Cisek[54]

Finalement, l'implémentation au sein d'un réseau de neurone biologique d'un filtre passe-bas et d'une opération de multiplication est plus complexe qu'une addition itérative d'évidence. De ce point de vue, les modèles urgency-gating apparaissent être moins parcimonieux que les modèles par échantillonnage séquentiel.

Analyse du comportement observé lors de décisions simples

Les modèles de décision par échantillonnage séquentiel ont été appliqués à de nombreux protocoles de décision simple, chez l'Homme et le Primate non-humain. Dans cette partie, nous illustrons la façon dont ces modèles ont permis d'étudier les mécanismes d'ajustement du processus de décision lors de nombreuses manipulations expérimentales.

- **Pression temporelle et performance**

Lorsqu'un sujet effectue une tâche de décision simple, qu'il s'agisse de rappel mnésique, de jugement lexical, de décision perceptuelle ou de choix économique, il est possible d'influencer la façon dont le sujet prend ses décisions en donnant des instructions mettant l'emphase sur la vitesse de réponse ou sur les performances.

Ce type de manipulation révèle l'existence d'un compromis entre probabilité d'erreur et temps de réponse (« speed-accuracy tradeoff ») : lorsque le sujet améliore ses performances, ses temps de réaction augmentent, et inversement[22,33]. Ce dilemme entre performances et vitesse du processus de décision, ubiquitaire dans les tâches de décision simple, est longtemps resté énigmatique. L'analyse des données comportementales issues de tâches de décisions simples montre que ce type d'instruction induit une modification de la distance au seuil de décision[22,55,56]. Ce compromis découle donc naturellement du processus d'accumulation d'évidence au cœur des modèles de décision par échantillonnage séquentiel. En effet, le seuil de décision fixe *a priori* la quantité d'évidence à accumuler pour sélectionner une option. Or, d'un point de vue Bayesien, le seuil de décision fixe également les risques de première et de deuxième espèce, c'est-à-dire le niveau de performance du processus décisionnel. Cependant, accumuler plus d'évidences prend du temps ! Le compromis entre vitesse de décision et performance reflète donc un dilemme inhérent à l'inférence Bayesienne par échantillonnage séquentiel.

Lorsque l'obtention d'une récompense est conditionnée à la réussite d'une décision perceptuelle, l'efficacité de la collecte de récompense devient une fonction du temps de décision moyen et du taux de réussite. Passer plus de temps sur chaque décision minimisera la probabilité d'erreur, maximisant ainsi la probabilité de récompense… au prix d'une diminution du nombre total de décisions prises et donc d'opportunités de gagner. Expérimentalement, on constate que des sujets engagés dans ce type de tâche ajustent leur seuil de décision afin d'adopter un compromis entre vitesse de décision et performance qui maximise la quantité de récompense récoltée et accommode le gain relatif associé à une réponse correcte[57-60].

- **Quantité d'information sensorielle**

Il est possible de manipuler la difficulté d'une tâche de décision perceptuelle en dégradant les stimuli utilisés par l'addition de quantités variables de bruit. Un exemple typique de tâche de décision perceptuelle consiste à répondre le plus rapidement possible en fonction de la direction prépondérante d'un nuage de points (**Fig. 10A**). Ce nuage est constitué d'un pourcentage fixe de points se déplaçant de manière cohérente (%coh), c'est-à-dire dans la même direction, alors que le reste des points du nuage se déplacent aléatoirement. Dans des conditions permettant un taux d'erreur faible, on observe que le temps de décision augmente à taux d'erreur constant lorsque la proportion de point se déplaçant de manière cohérente diminue (**Fig. 10B, %coh>10**). L'analyse de ce type de données par un modèle de diffusion indique que la pente de la variable de décision, qui reflète la vitesse à laquelle se fait l'accumulation d'évidence, varie en proportion inverse du niveau de dégradation du stimulus[5,22,28,61]. De ce point de vue, le temps de décision augmente car la quantité d'information sensorielle disponible par unité de temps diminue, ce qui à seuil de décision fixe, augmente le temps nécessaire pour accumuler la même quantité d'évidence. De manière intéressante, lorsque la cohérence du nuage de point augmente, le temps de réaction moyen tend vers une limite inférieure correspondant au temps non décisionnel. En revanche, lorsque le niveau de cohérence du nuage de point diminue au delà d'une certaine valeur (**Fig. 10B, %coh<10**), les sujets altèrent le compromis entre vitesse de réponse et performance de telle manière que le temps de réaction tend vers une limite supérieure idiosyncrasique, au prix d'une dégradation progressive de leurs performances. L'existence d'une telle

limite reflète le degré d'urgence associé à la décision, c'est-à-dire le temps maximum alloué par le sujet à chaque décision. Ce type de phénomène est ubiquitaire dans les tâches de décision simple[5,28,45,62], y compris les choix économiques[30,31].

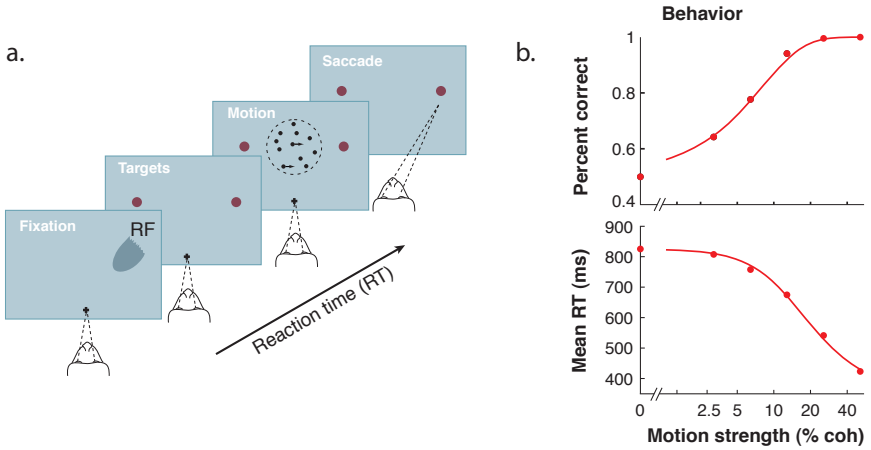

Figure 10 : Exemple de décision perceptuelle binaire. **(A)** le sujet est face à un écran, deux cibles sont affichées de part et d'autre de celui-ci. L'essai débute avec l'affichage d'un nuage de point se déplaçant aléatoirement. Une fraction des points se déplace de manière cohérente en direction d'une des cibles. Le sujet doit indiquer cette direction par une saccade oculaire vers la cible correspondante dès que possible. L'expérimentateur manipule la proportion de points se déplaçant de manière cohérente (% coh), de telle sorte que la décision est d'autant plus dure que cette proportion est faible. **(B) Panel haut :** proportion de choix en fonction du pourcentage de cohérence. **Panel bas :** temps de réaction moyen en fonction du pourcentage de cohérence. D'après Gold et Shadlen[5]

- **Arrêt du processus de décision : Réponses différées**

Dans la tâche présentée précédemment, le moment de la décision perceptuelle coïncide avec celui de la commande motrice. Il est cependant possible de dissocier ces deux phénomènes en donnant l'instruction au sujet d'attendre un signal pour indiquer son choix plutôt que de répondre dès que la décision est prise.

Si l'on continue d'afficher le stimulus et que le signal de réponse est suffisamment retardé, les SSM font alors la prédiction contre-intuitive que la probabilité d'erreur observée correspond à celle déterminée *a priori* par le seuil de décision. En d'autre terme, bien qu'il soit théoriquement possible de poursuivre l'accumulation d'évidence, le processus s'arrête au moment où la variable de décision atteint le seuil de décision indépendamment de la disponibilité d'informations supplémentaires dans

l'environnement[63]. Les taux d'erreurs observés expérimentalement confirment cette hypothèse. Ce phénomène suggère par ailleurs que la rencontre entre la variable et le seuil de décision, si elle correspond au choix d'une option, n'est cependant pas nécessairement suivie d'une action, le choix pouvant être conservé en mémoire de travail[5,64].

De plus, il est également possible de manipuler le temps d'affichage du stimulus parallèlement à la cohérence du nuage de point. Dans ce type de configuration, il est vraisemblable que la quantité totale d'information sensorielle disponible ne permette pas d'atteindre le seuil de décision pour les temps de présentation les plus courts. Globalement, le niveau de cohérence nécessaire pour obtenir un taux de 90% de réponses correctes varie comme la racine carrée de la durée d'affichage du stimulus[5,65,66]. Plusieurs hypothèses sont proposées pour expliquer ce phénomène : l'existence d'un signal d'urgence additionné aux évidences accumulées[45], ou une décroissance progressive du seuil de décision[44] qui permettrait le croisement de la variable de décision et de son seuil même en l'absence d'information ou encore un mécanisme de décision reposant sur le rapport des évidences en faveur de chaque option[22]. Bien qu'encore ouverte, cette question souligne l'existence d'une dissociation entre le processus d'accumulation d'évidence et sa règle de terminaison.

- **Quantité d'information *a priori***

Les modèles de décision par échantillonnage séquentiel réalisent une inférence Bayesienne (voir **Fig. 2**). Lorsqu'on étudie les processus de décision simple, il est donc important de distinguer les informations *a priori*, disponibles avant toute observation et basées sur les expériences passées du sujet, des informations sensorielles dont l'accumulation progressive durant la phase de délibération reflète la vraisemblance d'une alternative à un moment donné[28,50]. L'approche la plus souvent adoptée, afin d'étudier la façon dont l'information *a priori* affecte le processus de choix consiste à manipuler la fréquence relative des réponses lors de décisions perceptuelles binaires. Expérimentalement, le point de départ du processus de décision est étroitement corrélé à la fréquence relative des alternatives[22,48], biaisant ainsi le processus de décision lors de son initialisation en direction des réponses les plus probables *a priori*. Bien que le mécanisme computationnel permettant de prendre en compte cette information *a priori*

dans le processus de décision soit distinct du processus d'accumulation progressive de l'information sensorielle, on retrouve bien la règle d'additivité entre sources d'information *a priori* et sensorielle postulée dans l'équation 2, puisque la distance au seuil de décision détermine la quantité d'information nécessaire pour sélectionner une option.

c. *Neurobiologie des décisions perceptuelles*

La neurobiologie est l'étude du lien entre la structure des réseaux formés par les neurones et leur fonction. Héritiers d'Aristote, les neurobiologistes ont intensivement étudié les réseaux neuraux traitant les signaux issus des organes sensoriels et contrôlant les mouvements, la manipulation expérimentale de leurs entrées et/ou sorties s'avérant suffisamment aisée et directe pour permettre l'interprétation des activités neurales ainsi évoquées[67].

A partir des années 90 et la compréhension des règles générales d'organisation fonctionnelle des régions cérébrales sensorielles et motrices, c'est naturellement que les neurobiologistes se sont tournés vers l'étude des structures cérébrales établissant le lien entre stimulus et action, soulevant ainsi la question de la sélection de l'action sur la base des perceptions[1,3,5,68]. Bénéficiant des modèles mathématiques descriptifs développés en psychologie expérimentale, les décisions perceptuelles sont ainsi devenues un modèle privilégié pour l'étude neurobiologique des processus de décision simple.

Décision perceptuelles : Approche électrophysiologique chez le primate non-Humain

- **Organisation du système sensori-moteur**

La rétine est l'organe sensoriel assurant la transduction de la lumière en un code neural spatio-temporel. Cette information sensorielle est d'abord relayée par le noyau géniculé latéral du thalamus avant d'entrer dans le néocortex par le cortex visuel primaire (V1). V1 est située à l'extrémité occipitale du télencéphale de part et d'autre de la scissure calcarine. Ces neurones répondent préférentiellement selon l'orientation, la fréquence spatiale et temporelle des stimuli apparaissant dans leur champ récepteur, formant ainsi une carte topographique précise du champ visuel[69]. Les neurones de V1

projettent dans un système hiérarchisé d'aires visuelles secondaires puis associatives organisées en deux flux d'information suivant un axe inférieur temporal « ventral » et un axe pariétal « dorsal »[70]. Schématiquement, la voie ventrale est associée à la reconnaissance des objets (« *what* » pathway), les parties les plus caudales du cortex inférieur temporal répondant à des propriétés simples telles que la couleur des objets, les formes géométriques[71] et les parties plus rostrales à des propriétés complexes : structure d'un visage, d'un paysage… La voie dorsale assure quant à elle un traitement spatio-temporel de l'information visuelle en lien avec l'action et la perception (« *where* » pathway) via le cortex pariétal postérieur[70]. L'information visuelle en sortie de chaque flux est ensuite transmise au cortex pariétal postérieur et au cortex latéral préfrontal (Fig. 11).

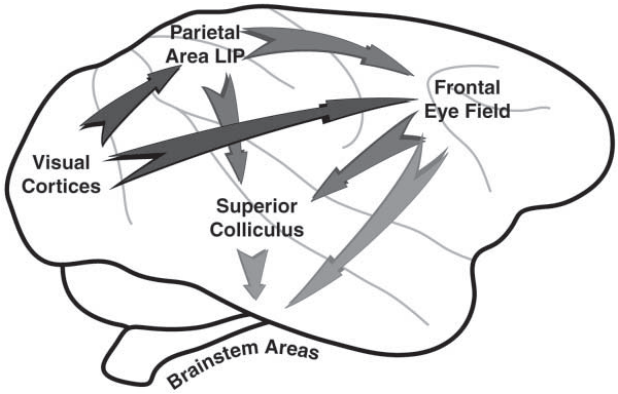

Figure 11 : Organisation sensori-motrice d'une réponse oculomotrice à un stimulus visuel. L'information sensorielle issue de la rétine entre dans le cortex par l'aire V1, à l'extrémité occipitale de l'encéphale après être passée par le noyau géniculé latéral dans le thalamus. Cette information est ensuite progressivement traitée au fur et à mesure de sa circulation au sein des aires visuelles secondaires et associatives. Cette information sensorielle influence le système oculomoteur via un réseau cortical pariéto-préfrontal comprenant la région intra-pariétale latérale (LIP) et le « frontal eye field » (FEF). Les deux régions cérébrales principales contrôlant les saccades oculaires ; le FEF et le colliculus supérieur, qui projettent à leur tour sur les noyaux pontiques contrôlant la vitesse et la position des yeux. D'après Glimcher[1].

Sur le versant moteur, le « *frontal eye field* » (FEF) est une région caudale latérale préfrontale dont la stimulation électrique déclenche des saccades oculaires[72,73]. Celle-ci est organisée topographiquement selon l'amplitude des saccades évoquées, et la direction de mouvement préférentielle des neurones y varie systématiquement de proche en proche. Le FEF est donc une région prémotrice, qui représente les commandes oculomotrices planifiées et la position des stimuli cibles. L'entrée principale

du FEF est constituée par les portions postérieures du cortex pariétal, au point de sortie du flux dorsal (LIP). Le FEF projette via les ganglions de la base sur le colliculus supérieur, qui lui-même projette sur les noyaux pontiques contrôlant la vitesse de déplacement et la position des yeux[60,74]. Le FEF est donc le point d'entrée de la voie commune finale contrôlant les saccades oculaires[75]. Par analogie avec le contrôle oculomoteur, le cortex frontal agranulaire prémoteur joue un rôle équivalent au FEF pour les mouvements corporels simples. Celui-ci projette, via les ganglions de la base, sur le cortex moteur primaire. Le cortex moteur primaire présente une organisation topographique selon les différentes parties du corps, et, de manière analogue au colliculus supérieur, les neurones y représentent la force à fournir pour un groupe de fibres musculaires donné, permettant ainsi l'exécution de mouvements simples via ses projections médullaires directes[76].

- **Prototype d'une décision perceptuelle : Saccades oculaires en direction d'un mouvement perçu**

Au sein de la voie dorsale, l'aire corticale MT (ou V5) constitue une des entrées principales du cortex pariétal postérieur[37,68]. Découverte en 1971, son étude a joué un rôle majeur dans la compréhension du cortex visuel en tant qu'ensemble hiérarchisé de modules spécialisés traitant l'information visuelle. L'activité des neurones dans MT représente la cohérence du mouvement dans une direction donnée au sein de leur champ récepteur[37,77,78]. Les neurones y sont organisés en colonnes traitant préférentiellement une direction de mouvement. Cette direction varie systématiquement selon une topographie corticale précise. Ces mêmes neurones s'avèrent également sensibles à la position relative d'un même stimulus sur les rétines, codant ainsi sa profondeur dans le champ visuel[37]. Comme le suggère la place clef de MT au sein du flux dorsal d'information visuelle, cette région est particulièrement impliquée dans la génération d'actions basées sur l'information visuelle. MT est donc un point d'entrée privilégié pour l'étude des mécanismes neurobiologiques liant information sensorielle, perception catégorielle et sélection de l'action.

Utilisant un paradigme original consistant à indiquer par une saccade oculaire le mouvement global d'un nuage de points aléatoire, Newsome *et al* ont enregistré dans MT l'activité unitaire de neurones répondant à la direction de mouvement pendant l'affichage de nuages de points dont le niveau de cohérence était systématiquement

manipulé[79]. Le protocole utilisé était similaire à celui présenté en **figure 12A**, mais avec les différences suivantes : la durée de stimulation était fixée à 2s et la réponse différée. Pour la plupart des neurones enregistrés dans cette étude, l'activité unitaire moyenne et la probabilité de catégoriser correctement le stimulus étaient significativement corrélées, suggérant que l'information sensorielle codée par ces neurones était effectivement utilisée au cours du processus de décision perceptuelle. Cette hypothèse fut confirmée par l'observation d'une relation systématique entre microstimulation dans MT et altération des performances observées : la microstimulation d'un cluster de neurones sensible à un mouvement vers la droite augmentait significativement la probabilité d'effectuer une saccade oculaire vers la droite, quelle que soit la cohérence et la direction du nuage de point présenté[80-82]. MT pouvait donc être vue comme un ensemble de détecteurs spécifiques, chacun fournissant une estimation ponctuelle de la cohérence du mouvement dans sa direction préférentielle et formant collectivement une carte corticale des mouvements dans le champ visuel. De manière similaire, la microstimulation de MT lors de jugements sur la profondeur perçue et la microstimulation de S1 lors de décisions perceptuelles vibro-tactiles ou dans le cortex inféro-temporal (sortie du flux ventral) lors de tâche de discrimination visage/maison, biaisent systématiquement la probabilité de réponse vers la valeur préférée du groupe de neurones stimulé, démontrant ainsi que les observations faites dans MT pour la direction de mouvement étaient potentiellement généralisables à l'ensemble du flux d'information sensoriel, indépendamment de la (des) dimension(s) spécifique(s) sur laquelle porte le jugement perceptuel[82,83]. La démonstration de l'existence dans MT d'une carte des mouvements dans le champ visuel servant de base à la formation des décisions perceptuelles permettait enfin d'aborder expérimentalement la question des processus convertissant l'information codée dans les cortex sensoriels en jugements catégoriels associés à la sélection d'actions.

Etudiant la prise de décision perceptuelle sur des nuages de points se déplaçant dans une direction parmi huit possibles lorsque la carte de mouvements dans MT est perturbée par microstimulation, Salzman *et al* ont démontré que la formation de décisions perceptuelles ne résultait pas d'une simple somme vectorielle pondérée des mouvements représentés dans MT mais d'un processus ségrégant l'information en faveur des différentes alternatives ouvertes au choix, suggérant ainsi une organisation du processus décisionnel perceptuel en unités décisionnelles distinctes mises en

concurrence les unes avec les autres selon une règle « winner-takes-all »[84]. Une première description formelle par Shadlen[85] du processus convertissant l'information sensorielle codée par MT en un choix catégoriel montra que, pour prédire le comportement observé dans le paradigme de Newsome[79] à partir des activités unitaires enregistrées dans MT, chaque unité décisionnelle devait faire la somme de l'information sensorielle disponible en faveur d'une des alternatives. A l'issue de la présentation du stimulus, l'unité ayant accumulé le plus d'information remporte la course pour l'accès au système moteur, déclenchant ainsi l'exécution de l'action associée à cette perception et inhibant les réponses alternatives. Expérimentalement, on constate en effet que les performances augmentent en première approximation comme la racine carrée du temps d'affichage du stimulus (Fig. 12C). Ainsi formulé, le modèle de Shadlen fait des prédictions fortes sur l'activité attendue de neurones engagés dans le processus d'accumulation d'information sensorielle : (1) leur activité doit croître progressivement lorsque l'action à venir va se faire dans leur direction préférée, (2) cette croissance se fait à une vitesse proportionnelle à la cohérence du nuage de point, et (3) lorsque la cohérence du nuage de point est nulle, l'activité unitaire de ces neurones prédit la décision à venir. Cette activité neurale mélangeant information motrice et sensorielle reflète donc bien ce qui est attendu d'un processus intermédiaire reliant système sensoriel et moteur. De plus, l'hypothèse d'une sommation de l'information sensorielle dans des unités concurrentes s'inhibant mutuellement souligne déjà la proximité entre le modèle de Shadlen, le cadre théorique de l'analyse séquentielle, et les SSM[5,11].

Afin de tester ce modèle, il était donc naturel de se tourner vers LIP et FEF, deux structures cérébrales en aval de MT, afin d'y chercher des populations de neurones susceptibles d'implémenter un processus d'accumulation de l'information sensorielle. En effet, LIP est une région pariétale postérieure dont les entrées sont principalement constituées par le cortex visuel extra-strié, en particulier MT, et qui projette sur le FEF (Fig. 11). Les neurones y sont sélectifs à la direction et à l'amplitude des saccades oculaires, et leur activité est maximale avant la production d'une saccade, partageant ainsi de nombreuses caractéristiques fonctionnelles avec le FEF. LIP possède donc les caractéristiques anatomiques et physiologiques d'une interface entre système sensoriel et moteur. Utilisant la même tâche de décision perceptuelle que Newsome[79], Shadlen *et al* ont enregistré l'activité des neurones dans le FEF et le DLPFC[86], puis dans LIP[87],

identifiant dans ces trois régions cérébrales des populations de neurones dont l'activité correspondait aux prédictions du modèle proposé par Shadlen.

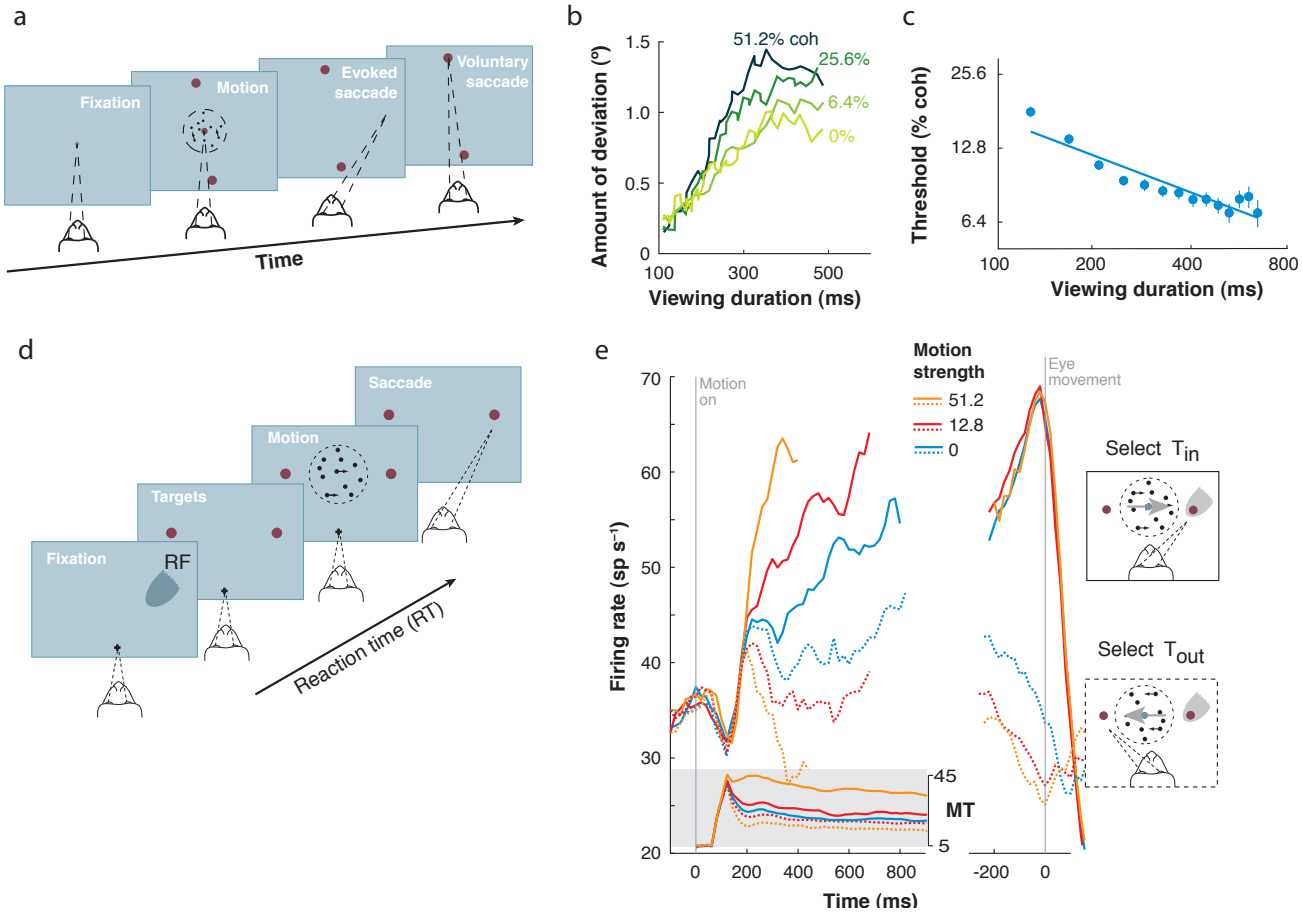

Figure 12 : (A) Le sujet est face à un écran, deux cibles sont affichées de part et d'autre de celui-ci. L'essai débute avec l'affichage d'un nuage de points se déplaçant aléatoirement. La fraction des points se déplaçant de manière cohérente est systématiquement manipulée par l'expérimentateur (% coh). Le processus de décision est interrompu par microstimulation du FEF, ce qui évoque une première saccade, suivie d'une deuxième saccade amenant le regard du singe sur une des cibles et indiquant son choix. **(B)** Déviation moyenne de la saccade évoquée en fonction de délai entre l'affichage du stimulus et la microstimulation pour les 4 niveaux de cohérences étudiés. **(C)** Cohérence évoquant 80% de réponse correcte en fonction de la durée d'affichage du stimulus. **(D)** Version « temps de réaction » du paradigme de Newsome. Le sujet doit indiquer la direction de déplacement du nuage de points par une saccade oculaire vers la cible correspondante le plus rapidement possible. L'expérimentateur manipule la proportion de points se déplaçant de manière cohérente (% coh). **(E)** Activité unitaire enregistrée dans LIP et dans MT centrée sur l'affichage du stimulus (panel gauche) et sur la réponse (panel droit). Les lignes pleines indiquent les essais aboutissant à une saccade dans le champ récepteur du neurone, alors que les lignes en pointillés indiquent les essais aboutissant à une saccade en dehors du champ récepteur. D'après Gold et Shadlen[5].

La figure 12E (panel gauche) présente l'activité unitaire enregistrée dans MT (en bas) et dans LIP (en haut). L'affichage du stimulus visuel, celui-ci évoque une activité stéréotypée qui dure approximativement 200ms. Pour les essais aboutissant à une réponse oculomotrice dans le champ récepteur du neurone, cette réponse initiale est suivie d'une activité tonique et progressivement croissante dont la pente est proportionnelle à la cohérence du nuage de points, i.e. à la quantité d'information sensorielle par unité de temps. Dans le cas contraire, son activité décline progressivement. Comme prédit par le modèle, l'activité de ces neurones est prédictive de la réponse donnée par le singe, y compris pour les essais se soldant par une réponse erronée ou ceux basés sur des stimuli non informatifs (cohérence nulle)[86,87]. Des profils de réponse identiques ont été retrouvés dans l'ensemble des régions corticales explorées (LIP, FEF, DLPFC).

La microstimulation du FEF évoque une saccade oculaire stéréotypée dont la direction et l'amplitude dépend du site de stimulation. Dans la tâche de Newsome[79], la microstimulation du FEF durant la présentation du stimulus visuel évoque également une saccade oculaire[65,66] (Fig. 12A). Cependant, le point d'arrivée observé dévie systématiquement de la position attendue en direction de la cible. Cette déviation est une fonction du délai entre l'affichage du stimulus et la microstimulation et de la cohérence du nuage de point présenté, reflétant donc la quantité d'information sensorielle accumulée par le neurones du FEF au moment de l'interruption du processus décisionnel[88] (Fig. 12B). De manière intéressante, cet effet disparaît lorsque l'action à associer à la perception n'est pas connue avant la microstimulation[66]. Ce résultat démontre la nécessité de comprendre les activités prémotrices (« *Bereitschaftspotential* »[72,89]) en terme de processus décisionnels simples dans l'espace des actions et d'accumulation d'information.

Parallèlement à ces travaux, Schall *et al* menèrent une série d'études visant à préciser les mécanismes de terminaison des processus décisionnels simples. Pour ce faire, ils proposèrent un paradigme de décision perceptuelle utilisant huit cibles arrangées radialement autour d'un point de fixation[61,62,68,90]. Le singe devait réaliser le plus rapidement possible une saccade vers la cible « *oddball* », i.e. dont la couleur différait des sept autres cibles (distracteurs). Contrairement à la tâche de Newsome, ce paradigme permet d'enregistrer l'activité neurale au moment où une action est sélectionnée de manière irrévocable suivant un hypothétique critère endogène de

terminaison du processus décisionnel. Lorsque le singe est engagé dans ce type de décision perceptuelle, l'affichage des cibles produit un pic d'activité phasique et stéréotypé des neurones du FEF[72,90].

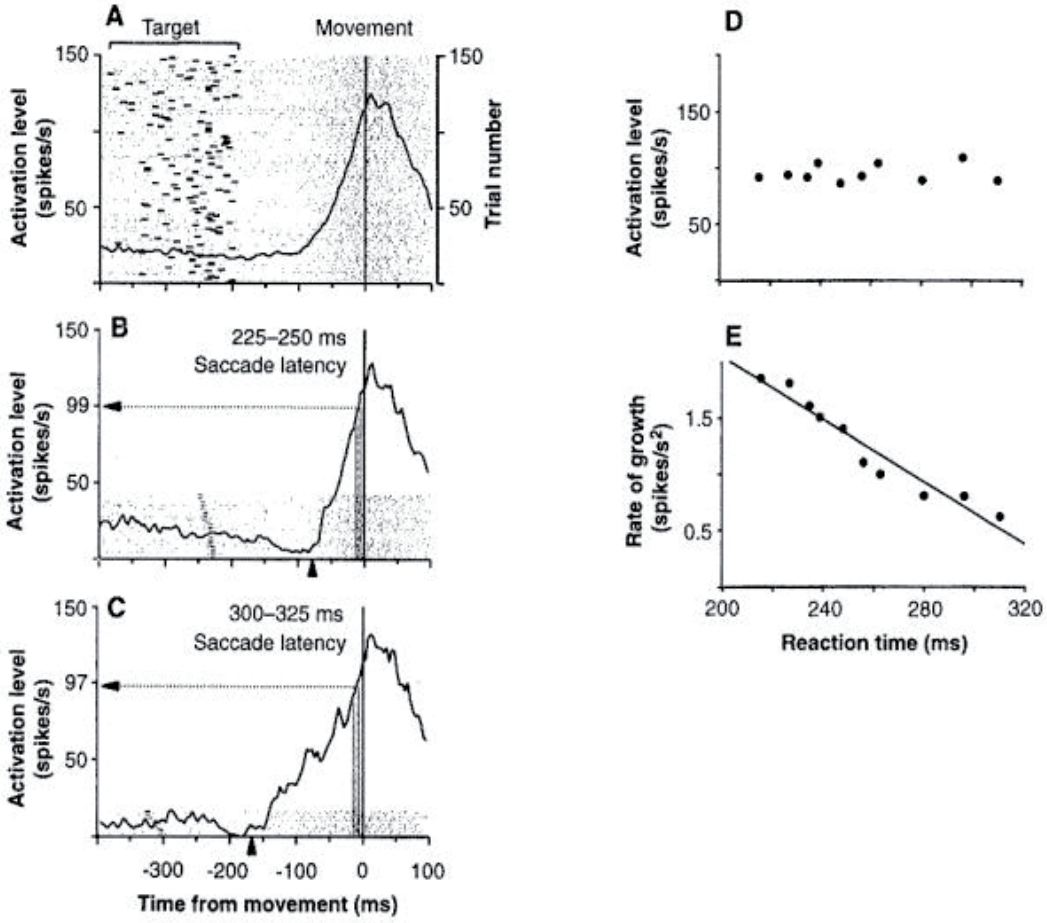

Figure 13 : Activité d'un neurone type dans le FEF durant la tâche de décision perceptuelle de Schall. (A) Activité neurale moyenne pour tous les essais aboutissant à une saccade oculaire dans le champ récepteur du neurone aligné sur la réponse. **(B)** Essais pour lesquels le RT était compris entre 225 et 250 ms. **(C)** Essais pour lesquels le RT était compris entre 300 et 325 ms. Noter la différence spontanée de pente. **(D)** Niveau d'activité moyen dans la fenêtre 10-20 ms avant la saccade oculaire en fonction du RT. **(E)** Pente de l'activité soutenue croissante pré-saccadique en fonction du RT de l'essai en cours. D'après Hanes[61].

Lorsque la cible *oddball* se trouve dans le champ récepteur du neurone, celui-ci est suivi d'une augmentation progressive du niveau d'activité culminant juste avant la production de la saccade. En revanche, lorsqu'il s'agit d'un distracteur, l'activité retourne rapidement à la ligne de base[61]. Représentant l'activité unitaire des neurones en la centrant sur les réponses survenant dans leur champ récepteur, Schall constata que la pente de l'activité tonique précédant la saccade prédisait le temps de réaction observé. De plus, l'activité neurale convergeait systématiquement vers une valeur seuil 10 et 20

ms avant la production de la saccade[61] (voir Fig. 13). Du point de vue des modèles de décision par échantillonnage séquentiel, les neurones du FEF se comportent donc comme s'ils codaient la dérive de la variable de décision pour leur alternative préférée vers un seuil de décision. Afin de tester cette hypothèse, Schall démontra qu'un modèle LATER[28,46] utilisant la pente de l'activité tonique pré-saccadique des neurones du FEF et un seuil de décision fixe prédisait correctement la distribution log-gaussienne des RT observés[61].

Suite à ces travaux, Shadlen *et al* développèrent une variante de la tâche de Newsome dans laquelle le singe indique son choix dès que possible au lieu d'attendre un signal spécifique survenant après un délai fixe, permettant ainsi la mesure de RT reflétant la durée du processus décisionnel (**Fig. 12D**). Enregistrant l'activité neurale dans LIP durant la prise de décision perceptuelle, Shadlen et ses collègues démontrèrent ainsi que la pente de l'activité soutenue pré-saccadique augmentait avec la cohérence du nuage de points et que, comme dans le FEF, l'activité des neurones du LIP convergeait vers un seuil de décision dont le croisement précédait la production d'une saccade oculaire dans le champ récepteur du neurone[91] (Fig. 12E). Comportementalement, les temps de réaction tendent vers une limite inférieure correspondant au temps non décisionnel lorsque la cohérence du nuage de point augmente (**Fig. 10B**, %coh=40). En revanche, lorsque le niveau de cohérence du nuage de points diminue, les temps de réaction augmentent progressivement, à performance constante, indiquant la nécessité de prolonger le recueil d'information pour compenser la diminution de leur qualité (**Fig. 10B,** %coh∈[20,40]). Si la baisse de la qualité des informations sensorielles se poursuit, les performances chutent progressivement au niveau du hasard, et les temps de réaction tendent vers une limite reflétant le temps maximum alloué par le sujet à chaque décision[45] (**Fig. 10B**, %coh<10). Dans cette tâche, la microstimulation de MT ou de LIP biaise la probabilité de choix et le temps de décision, ralentissant la décision lorsque la microstimulation s'oppose à la direction du stimulus et l'accélérant d'autant dans le cas inverse, confirmant le rôle de LIP comme point d'entrée de l'information sensorielle dans le processus de décision[81,92].

Ces observations comportementales et électrophysiologiques sont quantitativement prédites par un modèle neuro-computationnel du processus de décision basé sur des unités neurales biophysiques (« *spiking neurons* »). Ce modèle simule les propriétés électrophysiologiques de deux populations de neurones dans MT qui codent la

cohérence du mouvement dans des directions opposées[93]. Ces deux populations projettent sur une deuxième couche neurale qui somme itérativement l'information sensorielle en faveur de chaque réponse au sein de deux populations distinctes jusqu'à ce que l'activité de l'une des populations atteigne son seuil de décision, terminant ainsi le processus de décision. Cette deuxième couche neurale simule l'activité dans LIP sous l'hypothèse que celui-ci implémente la variable de décision d'un modèle de diffusion (Fig. 14B).

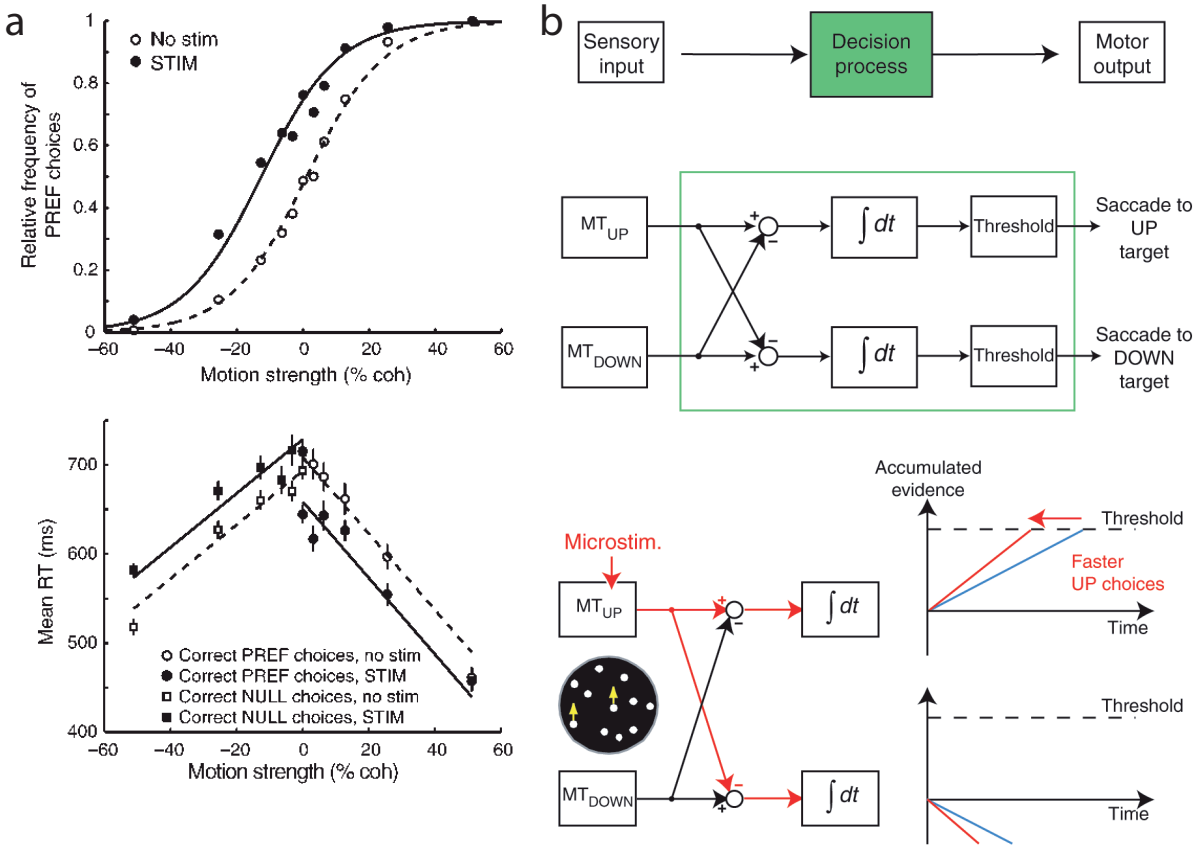

Figure 14 : (A) Panel Haut. Probabilité d'une réponse dans le champ récepteur de neurones dans LIP en fonction de la cohérence. **Panel Bas.** Temps de réaction moyen en fonction de la cohérence. Les lignes en pointillés indiquent les essais pour lesquels un cluster de neurones ayant une direction préférentielle opposée à la direction du stimulus était microstimulé dans MT. **(B) Modèle de décision proposé par Mazurek et Shadlen pour rendre compte des activités observées dans MT, LIP et du comportement décisionnel[93]. Panel Haut.** Des pools de neurones codent une estimation instantanée de la cohérence du mouvement dans une direction donnée. Celle-ci est transmise par des canaux séparés s'inhibant mutuellement à des accumulateurs distincts implémentés par une deuxième couche de neurones réalisant une intégration de l'information sensorielle sur le temps de la décision. D'après Ditterich[81]

Ce modèle démontre la capacité des modèles, neurobiologiquement plausibles, de décision par échantillonnage séquentiel à rendre compte simultanément du comportement observé et de l'activité neurale sous-jacente au processus de décision[93]. Cette référence explicite aux modèles de diffusion suggère que les neurones du LIP et du FEF implémentent une inférence Bayesienne en accumulant des évidences en faveur de chaque alternative vers un seuil de décision contrôlant le compromis entre vitesse de décision et performance[5,11] (au sens du contrôle du risque de première et de deuxième espèce).

Dans la version RT de la tâche de Newsome, l'introduction d'un pulse d'information sensorielle par l'affichage pendant un temps court d'un nuage de points de cohérence élevée par-dessus un nuage de points de « référence » permet de tester l'impact comportemental et électrophysiologique de cette perturbation de la stationnarité du transfert d'information sensorielle[94]. Cette perturbation biaise la probabilité de réponse dans la direction du pulse (préférée ou non préférée) avec une latence approximative de 250ms. De plus, le pulse d'information modifie transitoirement la pente de l'activité tonique pré-saccadique observée dans les neurones du LIP, l'augmentant lorsque le pulse d'information est congruent avec la direction de mouvement du stimulus de référence et la diminuant lorsqu'il est en sens opposé. Globalement, cette observation est cohérente avec un mécanisme d'accumulation - par addition itérative - de l'information sensorielle dans les neurones du LIP. En outre, l'existence d'un effet du pulse dans la direction non préférée sur l'activité neurale démontre la non-indépendance du processus d'accumulation d'information pour les différentes alternatives ouvertes au choix, reflétant le poids relatif des évidences en faveur de leur option préférentielle (Eq. 1). Testant explicitement l'hypothèse que l'activité soutenue des neurones dans LIP implémente la variable de décision d'un modèle de diffusion, Shadlen *et al* ont développé un paradigme dans lequel quatre formes géométriques (parmi dix) étaient présentées successivement à un singe. Celui-ci devait ensuite indiquer son choix par une saccade oculaire vers une cible rouge ou un cible verte[95]. Les formes géométriques utilisées avaient été préalablement associées au log du ratio des probabilités de récompense (évidences) pour chaque couleur via un apprentissage par renforcement préalable. Dans ce paradigme, l'activité soutenue enregistrée dans LIP corrélait à la somme des évidences fournies par chaque forme géométrique affichée entre le début de l'essai et le moment de la mesure, démontrant de manière formelle que

les neurones de LIP codent l'information sous la forme d'un poids relatif d'évidence et qu'ils réalisent la somme itérative de l'information disponible. Il existe néanmoins des mécanises additionnels participant à la formation de l'activité soutenue pré-saccadique des neurones du LIP, comme cela a été mis en évidence lors d'essais utilisant des nuages de point de cohérence nulle (non informatifs) : un signal d'urgence permet alors la croissance de l'activité neurale vers le seuil de décision en l'absence de toute information et dans l'ensemble des accumulateurs[45]. Ce mécanisme représente le coût effectif du temps de décision et permet d'implémenter une limite supérieure à la durée du processus, quitte à générer aléatoirement une réponse.

Pour conclure, le mécanisme de terminaison du processus d'accumulation par un seuil de décision fixant le niveau de conservatisme de l'inférence perceptuelle apparaît être un mécanisme élégant et parcimonieux lorsqu'une réponse doit être donnée dès que possible (notons cependant une réponse peut également être gardée en mémoire de travail avant d'être restituée dans un deuxième temps[5]). En revanche, lorsque l'information sensorielle est disponible *ad libitum*, on peut se demander si cette même stratégie est utilisée : Le sujet poursuit-il l'accumulation d'information tant que celle-ci est disponible afin de maximiser ses performances ? ou s'arrête-t-il à un seuil de décision prédéfini alors qu'il n'y a pas de pression temporelle exercée sur le processus de décision ? En enregistrant l'activité des neurones dans LIP dans une version de la tâche de Newsome où la durée de stimulation est systématiquement manipulée, on observe que lorsque l'information sensorielle n'est pas limitée, l'activité dans LIP tends vers le seuil de décision puis reste stable à cette limite jusqu'au moment de la réponse. Ce résultat démontre qu'un seuil de décision fixant *a priori* le niveau de performance existe même lorsqu'il n'y a pas de contrainte de temps ou de disponibilité de l'information et souligne la continuité fonctionnelle entre processus de décision et mémoire de travail[63].

Décisions perceptuelles : Imagerie fonctionnelle chez l'Homme

- **Identifier les réseaux impliqués dans l'accumulation d'information sensorielle**

De ces nombreux travaux de modélisation et d'électrophysiologie se dégage une description du processus de décision perceptuelle comme une accumulation d'information vers un seuil de décision permettant d'esquisser les contours d'une cartographie cérébrale des opérations élémentaires constituant les décisions simples. Tirant partie de ce corpus, établi chez le primate non-humain, Heekeren *et al* ont étudié les régions cérébrales impliquées dans le processus de décision perceptuelle chez l'Homme grâce à une tâche de classification d'images statiques bruitées de maisons et de visages administrées à un groupe de sujets sains dont l'activité hémodynamique était enregistrée dans un scanner IRM[96-98] (Fig. 15A). Après avoir visualisé le stimulus, un signal indiquait aux sujets le moment auquel ils devaient donner leur réponse, ne permettant ainsi pas l'analyse des RT. Cette réponse était donnée à l'aide d'un boitier à deux boutons placé dans leur main droite. Les performances des sujets augmentaient lorsque la proportion de bruit dans les images présentées diminuait (Fig. 15B). Plus spécifiquement, cette étude visait à identifier les régions cérébrales implémentant l'accumulation d'information sensorielle en contraignant l'analyse statistique de la réponse hémodynamique par les prédictions des modèles neuro-computationnels développés chez le singe : (1) l'activité BOLD devait varier en fonction du niveau de bruit dans l'image, puisque celle-ci conditionne la pente de la variable de décision au sein de l'accumulateur, (2) l'activité BOLD devait être corrélée à l'activité enregistrée dans les régions corticales inféro-temporales répondant préférentiellement aux images de visages et à celle répondant préférentiellement aux images de maisons, reflétant ainsi les entrées de l'accumulateur. Identifiant les voxels en région inféro-temporales répondant préférentiellement à chaque type d'image afin d'en extraire l'activité différentielle des deux populations de voxels (Fig. 15C), Heekeren *et al* démontrèrent que la partie caudale du DLPFC (MNI xyz=[-22, 24, 36]) présentait une différence d'activité significative en fonction du niveau de difficulté et que l'activité dans cette région corrélait avec la valeur absolue de l'activité différentielle enregistrée dans le cortex inférieur temporal. Ces résultats suggèrent que la partie caudale du DLPFC est impliquée dans l'accumulation d'information sensorielle lors de la prise de décision perceptuelle chez l'Homme (Fig. 15D).

Menant une expérience IRMf complémentaire dans laquelle les images bruitées étaient substituées par des nuages de points aléatoires dont le sujet indiquait la direction de mouvement par une saccade oculaire ou en appuyant sur un bouton réponse, Heekeren *et al* ont montré que la partie caudale du DLPFC fait partie d'un réseau dont l'activité BOLD varie significativement en fonction du niveau de difficulté de la décision perceptuelle, i.e. du niveau de cohérence du nuage de points, indépendamment de l'effecteur utilisé pour indiquer la réponse[97].

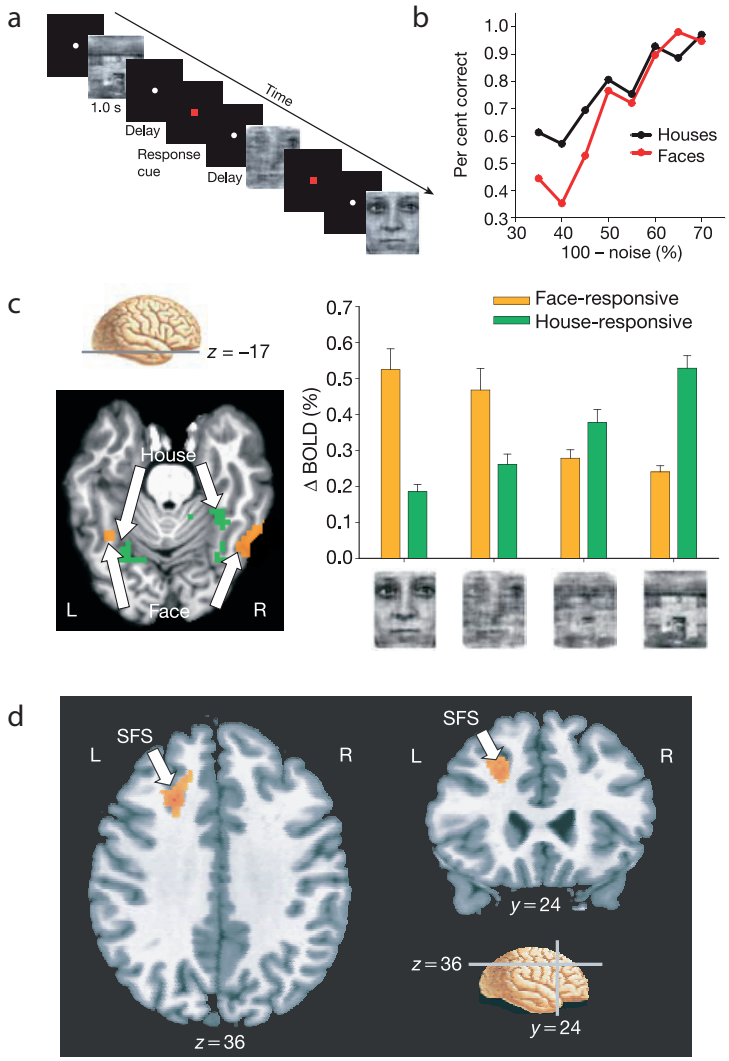

Figure 15 : (A) Tâche de catégorisation d'images bruitées de maison et de visage. (B) Performances en fonction de la proportion de niveau de bruitage de l'image présentée pour les maisons (noir) et pour les visages (rouge). (C) Voxels inféro-temporaux répondant préférentiellement aux images de maison (vert) et de visage (orange). Le graphe à droite représente l'activité BOLD évoquée en moyenne au sein des voxels répondant préférentiellement aux visages (orange) et aux maisons (vert) en fonction du stimulus présenté (visage, visage bruité, maison bruité, maison). **(D) Région dorso-latérale préfrontale caudale gauche implémentant la variable de décision d'un processus de décision par échantillonnage séquentiel.** D'après Heekeren[96].

Afin d'étudier le lien entre accumulation d'information sensorielle et sélection d'action au cours de la décision perceptuelle, Tosoni[99] *et al* ont administré une variante de la tâche de Heekeren[96,97] à des sujets sains placés dans un scanner IRM (Fig. 15A) : Une image statique de maison ou de visage, plus ou moins bruitée, était affichée pendant

un temps fixe. Après un délai, celle-ci était suivie d'un signal invitant le sujet à indiquer sa réponse par une saccade oculaire ou, selon les essais, par un mouvement de pointage. Le sujet indiquait s'il avait perçu un visage ou une maison en sélectionnant une des deux cibles affichées selon une règle d'association préétablie. Ayant préalablement identifié les régions pariétales et préfrontales dont l'activité était spécifiquement associée à chaque effecteur grâce à une tache « *localizer* », les auteurs ont examiné l'activité hémodynamique de ces régions durant la formation de la décision et la réponse. Les régions préfrontales ainsi identifiées, le FEF et le FRR (« *frontal reaching region* », région préfrontale homologue de FEF), présentaient une activité préparatoire faible ne reflétant pas le niveau de bruitage du stimulus et une réponse ample et robuste, spécifique de l'effecteur, au moment de la réponse. Par contraste, l'activité hémodynamique durant la formation de la décision dans les régions pariétales, pIPS (homologue Humain de LIP) et PRR (« *parietal reaching region* »), reflétait le niveau de bruitage du stimulus de manière spécifique à l'effecteur, indépendamment de la réponse sélectionnée. Ces régions pariétales ne répondaient pas à la visualisation passive des stimuli. Finalement, l'activité dans la partie caudale du DLPFC durant la formation de la décision perceptuelle variait significativement selon le niveau de bruitage de l'image, indépendamment du type d'image et de réponse (saccade ou pointage), reproduisant les observations de Heekeren *et al*[96,97]. Pris ensemble, ces résultats suggèrent que la partie caudale du DLPFC est impliquée dans l'accumulation d'information dont dépend l'inférence, indépendamment de la nature et du plan moteur associé à la réponse ou de son execution[98]. Par contraste, les régions pariétales impliquées dans l'accumulation d'information sensorielle sont spécifiques de l'effecteur, reflétant le plan moteur associé à la réponse et reliant ainsi choix et action.

Testant les performances de sujets sains avant et après stimulation magnétique transcrânienne à basse fréquence de la région caudale du DLPFC identifiée par Heekeren (neuroguidage, MNI xyz=[-22, 26, 36]) contre une stimulation placebo, Philiastides *et al* ont montré que la rTMS induisait transitoirement une diminution des performances associée à une augmentation des RT[100]. L'ajustement d'un modèle de diffusion à ces données révèle que ce *pattern* comportemental reflète une diminution de la vitesse d'accumulation de l'information sensorielle, ce qui traduit la dégradation du processus d'accumulation d'information par la rTMS à basse fréquence, et démontre le rôle causal de cette région cérébrale dans le processus d'accumulation d'information sous-tendant la décision perceptuelle.

- **Dynamique temporelle de la décision perceptuelle**

D'un coté, la faible résolution temporelle de l'IRMf limite l'analyse de la dynamique du processus de décision perceptuelle[101]. De l'autre, le type d'étude électrophysiologique invasive menée chez le singe est particulièrement difficile à mettre en œuvre chez l'Homme et ne peut se concevoir qu'associée à la nécessité médicale de réaliser une telle implantation, donc sur un cerveau pathologique[102]. Par contraste, l'EEG de scalp fournit une mesure directe et non-invasive de l'activité neurale avec une excellente résolution temporelle. C'est pourquoi, l'EEG reste la méthode principale d'étude de la dynamique temporelle des processus cognitifs chez l'Homme, malgré une précision spatiale et un rapport signal sur bruit médiocres.

Afin d'accommoder ces limitations, Philiastides *et al* ont développé une approche analytique originale du signal EEG reposant sur l'utilisation d'un classifieur linéaire comparant essai-par-essai l'activité de l'ensemble des électrodes aux réponses du sujet durant une tâche de classification d'images statiques dont le niveau de bruit était systématiquement manipulé[103-105] : le sujet devait identifier une image affichée pendant un temps fixe comme représentant une voiture ou un visage et indiquer sa décision à l'aide d'un boîtier réponse le plus rapidement possible (Fig. 16A). Appliquant le classifieur à des fenêtres temporelles de 60 ms couvrant de proche en proche l'ensemble du processus décisionnel, les auteurs ont identifié deux composantes EEG prédictives des performances psychophysiques des sujets : (1) La première composante, dite « précoce », corresponds à l'onde N_{170} sélective des visages classiquement observée dans ce type de paradigme et (2) la deuxième composante, dite « tardive », survenait 130 ms plus tard en moyenne et ressemble à P_{300}[106,107]. La figure 16B représente l'activité évoquée moyennée sur l'ensemble des essais (ERP) pour les électrodes FCz et PO8[104,108]. Alors que la composante précoce n'est que faiblement et inconstamment prédictive du comportement des sujets, la composante tardive permet une prédiction robuste de leur réponses[103]. La latence d'apparition de cette composante tardive reflète la difficulté de la décision, qui elle-même covarie avec RT et le niveau de bruit (Fig. 16C). Ces résultats suggèrent que la prise de décision perceptuelle chez l'homme se fait en deux temps. Il est tentant d'interpréter ces résultat à la lumière des données obtenues sur MT et LIP chez le singe : de ce point de vue, la composante précoce correspond à un niveau de traitement sensoriel et la composante tardive, prédictive du choix et dont la latence reflète la durée du processus décisionnel, représente le processus de prise de décision proprement dit[103].

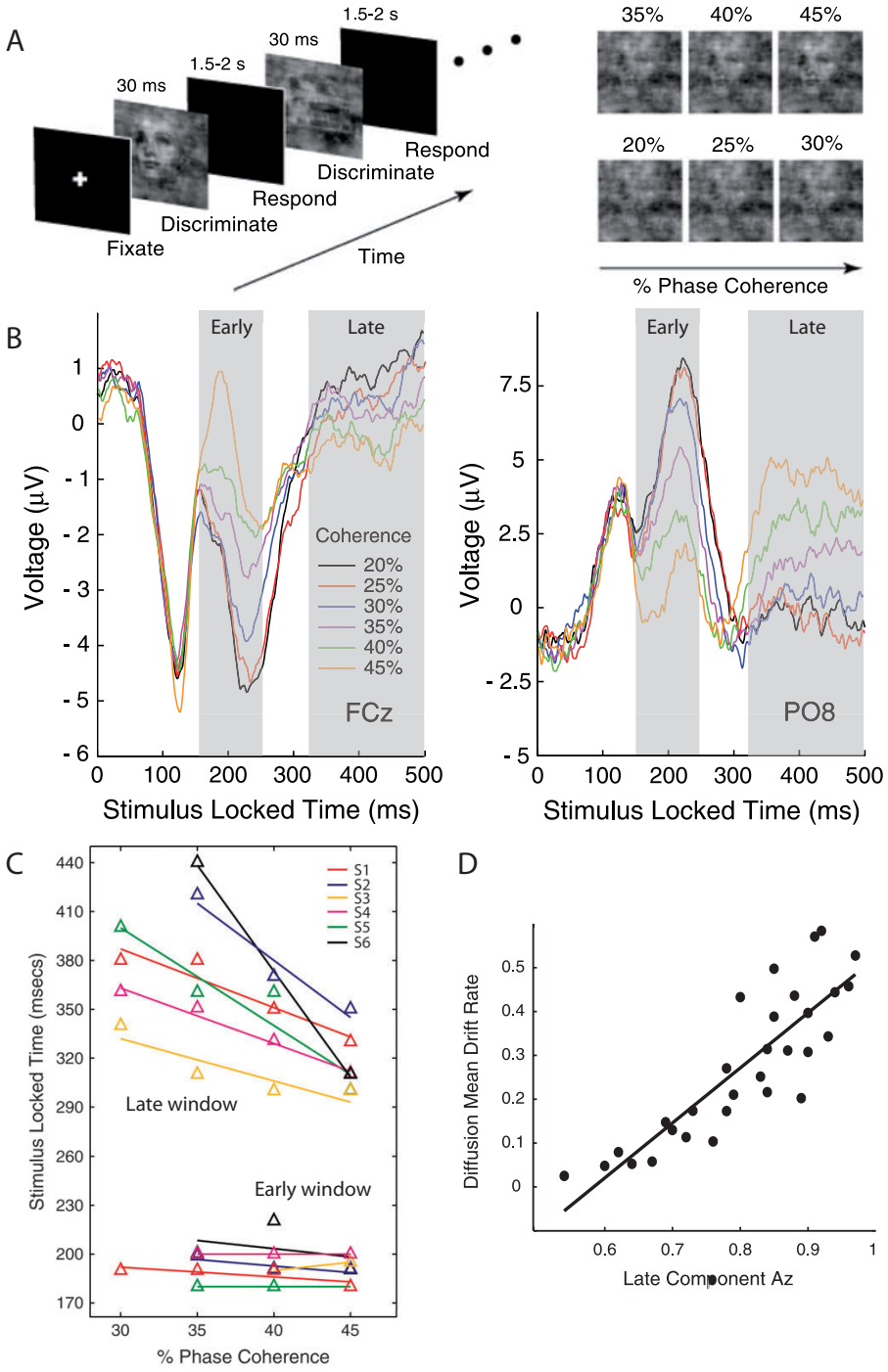

Figure 16 : (A) Paradigme de décision perceptuelle. (Panel Gauche) Une image de visage ou de voiture dont le niveau de bruit est systématiquement manipulé est présentée à un sujet. Celui-ci doit déterminer quel type d'image lui a été présenté en indiquant dès que possible sa réponse à l'aide d'un bouton réponse. **(Panel Droit)** Une image de visage à différent niveau de bruit. **(B) ERP moyen pour les électrodes FCz (Panel Gauche) et PO8 (Panel Droit) pour chaque niveau de cohérence**, indépendamment du type de stimulus ou de réponse. Les fonds grisés indiquent les composantes précoces et tardives. **(C) Latence d'apparition de la composante précoce et tardive en fonction du niveau de bruit. (D) Corrélation entre la proportion d'essais correctement prédits par le classifieur linéaire à partir de la composante tardive et vitesse de dérive du modèle de diffusion.** Chaque point correspond à un sujet et un niveau de cohérence. D'après Philiastides[103,104].

Afin de tester cette hypothèse, les auteurs ont ajusté aux données comportementales de chaque sujet un modèle de diffusion dont la vitesse de dérive, i.e. d'accumulation d'information, augmente quand la quantité de bruit présent dans l'image à classifier diminue[104] (Fig. 6). La vitesse de dérive estimée pour chaque sujet et chaque niveau de bruitage corrélait significativement avec le pourcentage de choix correctement prédit par le classifieur linéaire en se basant sur la composante tardive (Fig. 16D). De plus, lorsque des essais issus de conditions expérimentales identiques sont reclassés sur la base de l'amplitude mesurée dans la fenêtre temporelle des composantes précoces et tardives, l'ajustement d'un modèle de diffusion aux données comportementales correspondantes à ces nouvelles catégories « neurales » prédit des vitesses de dérive significativement différentes pour les essais reclassés à partir de l'amplitude de la composante EEG tardive, mais pas pour la composante précoce[105].

En conclusion, la manipulation expérimentale de la qualité de l'information induit une modification du signal EEG tardif, dont la latence est proportionnelle au niveau de difficulté de la décision et dont l'amplitude est corrélée à la vitesse d'accumulation de l'information estimée par un modèle de diffusion. De plus, la variabilité du signal EEG tardif prédit les fluctuations spontanées de qualité de l'information, démontrant ainsi que la composante EEG tardive est un marqueur électrophysiologique du processus d'accumulation sous-tendant la décision perceptuelle.

- **Neurobiologie du compromis entre vitesse de décision et performance**

La prise de décision est caractérisée par l'existence d'un dilemme entre performance et vitesse (*« speed-accuracy tradeoff »*, SAT)[22,33]. Expérimentalement, le SAT est simple à manipuler puisqu'une instruction mettant l'emphase sur la vitesse de réponse ou sur les performances suffit à induire un effet comportemental[22,55,56] (cf. p. 34). Les modèles de diffusion capturent ce phénomène par une modification de la distance au seuil de décision[55] (Fig. 5). Les paradigmes de décisions perceptuelles manipulant le SAT sont donc une voie privilégiée pour l'étude des mécanismes neurobiologiques implémentant le seuil de décision et son ajustement en réponse à une instruction.

Afin d'étudier les structures cérébrales impliquées dans la modification du SAT, Forstmann *et al* ont adapté à l'IRMf une tâche d'identification de la direction de

mouvement d'un nuage de points aléatoires dans laquelle le SAT était systématiquement manipulé grâce à une instruction affichée avant chaque décision[109]. Celle-ci indiquait au sujet s'il devait se décider rapidement (vitesse), minimiser ses erreurs (précision) ou associer les deux (intermédiaire). Comportementalement, l'instruction précédant la décision induisait une modification du SAT, puisque l'amélioration des performances se faisait au prix d'une augmentation des temps de réaction moyens. L'ajustement d'un modèle LBA à ces données montre que l'instruction « vitesse » induisait un abaissement de la distance au seuil de décision, alors que l'instruction « précision » induisait son élévation. En phase préparatoire, i.e. après avoir reçu l'instruction mais avant le début du processus de décision, l'activité BOLD dans le pré-SMA et dans le striatum antérieur était plus importante dans la condition « vitesse » que dans les conditions « intermédiaire » et « performance » (Fig. 17A). Dans ces deux régions, il y avait une corrélation interindividuelle entre la modification de la distance au seuil induite par les instructions et la différence d'activité BOLD correspondante (Fig. 17B-C), suggérant l'implication de la pré-SMA et du striatum antérieur dans la modification volontaire du SAT en réponse à une instruction. De manière intéressante, ce résultat montre également que la modification du SAT se fait avant le début de la décision elle-même[109,110].

Dans une étude complémentaire basée sur le même paradigme, les auteurs ont à nouveau quantifié l'effet comportemental d'instructions de vitesse, de précision et intermédiaire sur la distance au seuil de décision. Les sujets inclus dans cette étude bénéficiaient d'IRM structurales (3T et 7T) permettant l'analyse tractographique quantitative de la connectivité anatomique entre le STN et la pré-SMA, ainsi qu'entre la pré-SMA et le striatum antérieur (Fig. 17D). Ceux-ci ont montré une corrélation positive entre la connectivité anatomique du pré-SMA et du striatum antérieur et la modification de la distance au seuil induite par l'instruction (Fig. 17E) ; ce résultat renforce l'hypothèse que pré-SMA et striatum antérieur sont impliqués dans la modification volontaire de la distance au seuil de décision en réponse à une instruction de vitesse ou de performance[111].

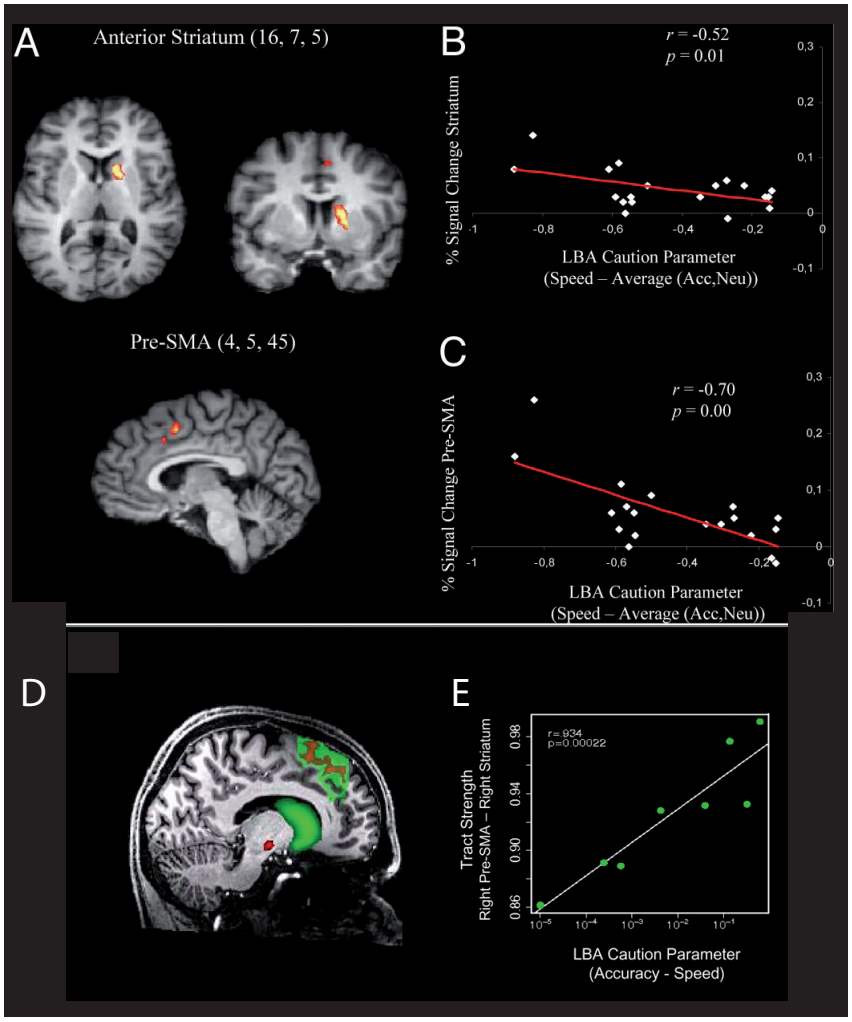

Figure 17 : (A) Activité BOLD précédant une décision perceptuelle lorsque le SAT favorise la « vitesse » comparé aux instructions « performances » et « intermédiaires ». **(B-C)** Corrélation inter-individuelle entre l'activité BOLD moyenne différentielle (Vitesse > Performance U Intermédiaire) dans le striatum antérieur **(B)** et la pré-SMA **(C)** et la variation de distance au seuil de décision induite par l'instruction. **(D)** Analyse tractographique de la connectivité anatomique entre le STN et la pré-SMA (rouge) et la pré-SMA et le striatum antérieur (vert) (E) Corrélation entre la connectivité anatomique entre la pré-SMA et le striatum antérieur et la variation de distance au seuil de décision induite par l'instruction. D'après Forstman[109,111].

Modélisation neuro-computationnelle des décisions perceptuelles

Actuellement, une nouvelle génération de modèles de décision perceptuelle émerge, ayant pour ambition de faire la synthèse des données issues de la neurobiologie et de la psychologie mathématique. Ces modèles, qu'on peut qualifier de « neuro-computationnels », ont en commun le souci du réalisme neurobiologique, leur design s'appuyant massivement sur les données électrophysiologiques et IRM disponibles pour décrire au mieux l'intégration des multiples niveaux de fonctionnement cérébraux - neurone, assemblée cellulaire et systémique - en un algorithme biologique de prise de décision[10,64]. Ces modèles proposent une compartimentation de la décision en modules spécialisés définis par les opérations élémentaires qu'ils implémentent. Certains modèles utilisent des réseaux de neurones artificiels[60,93], alors que d'autres se focalisent sur une description mathématique plus globale de l'activité dans chaque module[9,10].

Le modèle de Wang et Lo est un modèle biophysique aujourd'hui très influent décrivant un circuit cortico-sous-cortical d'opérations élémentaires qui, ensembles, forment un algorithme de décision perceptuelle. L'architecture générale de ce modèle repose sur un réseau de neurones artificiels (*« Noisy spiking leaky integrate and fire neurons »*) à quatre couches reparties en 3 modules représentant le réseau cortical pariéto-préfrontal, les ganglions de la base et le colliculus supérieur[60] (Fig. 18A). Les neurones y sont organisés en boucles cortico-sous-corticales traitant l'information en parallèle. Le premier module représente l'activité des neurones corticaux pariétaux et latéro-préfrontaux de manière indiscriminée. Des assemblées de neurones glutamatergiques y accumulent l'information issue des cortex sensoriels grâce à une boucle récurrente d'auto-excitation permettant la réverbération lente du signal neural (Fig. 18B, panel haut). Ces assemblées de neurones sont en compétition les unes avec les autres pour le seuil de décision selon une règle « *winner-takes-all* » et s'inhibent mutuellement par le truchement de neurones inhibiteurs GABAergiques, comme dans le modèle LCA de Usher et McClelland[43]. Le deuxième module représente la voie directe des ganglions de la base et comprend deux couches neurales : une couche d'entrée (le striatum) et une couche de sortie (la part réticulaire de la substance noire). Le dernier module, représentant le colliculus supérieur, comprend autant de populations de neurones phasiques que de réponses possibles et contrôle les noyaux oculomoteurs.

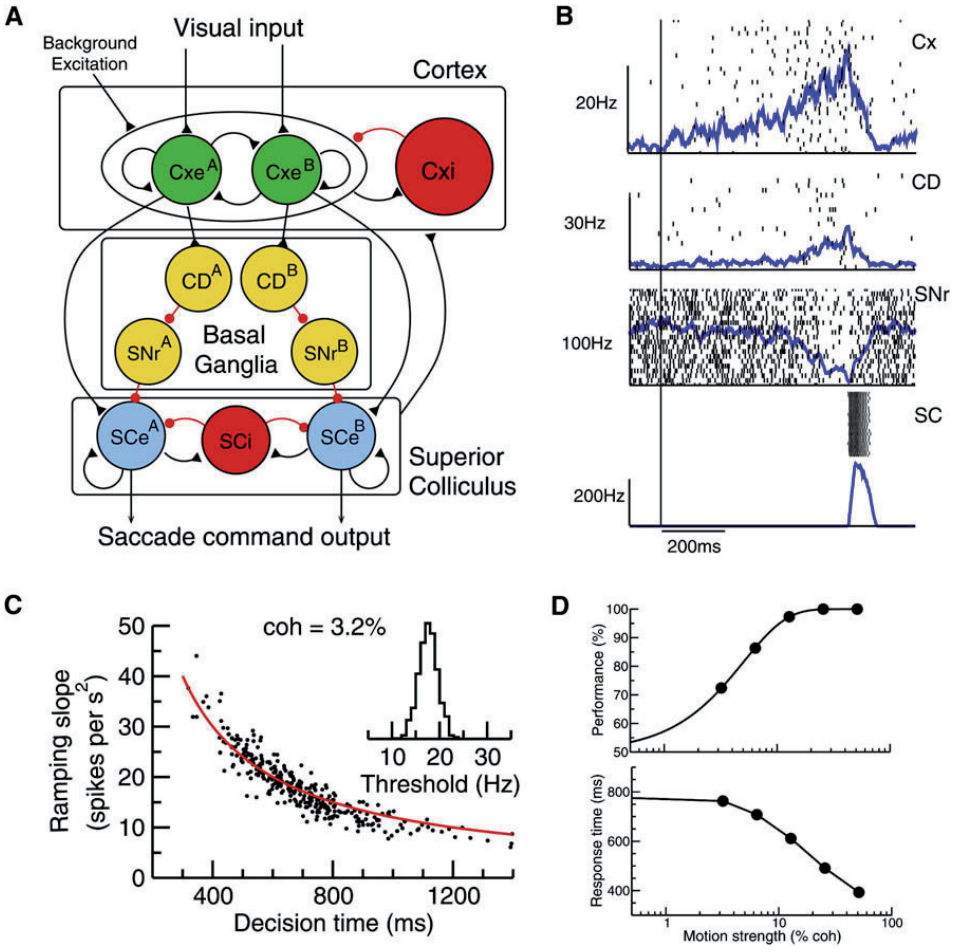

Figure 18 : (A) Représentation schématique de l'architecture du modèle de Wang et Lo. Les connections inhibitrices sont représentées en rouge et les excitatrices en noir. Chaque cercle représente une population de neurones stimulés. **(B) Simulation typique d'une décision perceptuelle par le modèle.** Activité neurale populationnelle en fonction du temps dans le cortex, le striatum, la substance noire pars reticulata et le colliculus supérieur (de haut en bas). Le fond de chaque graphique représente un « *raster plot* » de l'activité neurale, i.e. chaque ligne représente un neurone et chaque point noir représente un potentiel d'action. **(C) Pente de l'activité soutenue des neurones corticaux en fonction du temps de décision prédit par le modèle.** L'insert représente la distribution des valeurs du seuil de décision pour ces essais. **(D)** Comportement prédit par le modèle pour la tâche de Shadlen[91]. Taux de réussite (haut) et RT moyen (bas) en fonction du niveau de cohérence du nuage de points. D'après Lo[60].

En accord avec les données de la littérature[5], la pente de l'activité tonique de l'assemblée corticale augmente avec l'intensité de la stimulation correspondante (Fig. 18B, panel haut) et présente une relation exponentielle inverse au RT, conformément aux prédictions des modèles de diffusion (Fig. 18C). De plus, le modèle prédit correctement le comportement attendu lors de décisions perceptuelles sur des stimuli ayant différents niveaux de bruitage (Fig. 18D). Le module représentant les ganglions de

la base implémente quant à lui un seuil de décision en transformant le franchissement du seuil par l'activité neurale d'une assemblée corticale en une augmentation phasique de l'activité striatale, répercutée via un mécanisme de double inhibition sur le colliculus supérieur. En effet, les neurones de la SNpr exercent une inhibition tonique sur le colliculus supérieur qui est transitoirement levée par l'inhibition que le striatum exerce sur la SNpr (Fig. 18B, panels intermédiaires). Ce seuil de décision est indépendant du niveau de cohérence du stimulus (Fig. 18C, insert). Cependant, une étude de simulation évaluant la trajectoire du système dans son espace des phases indique que seule la modulation dopaminergique de l'efficacité de la synapse cortico-striatale présente des propriétés nécessaires au contrôle et à l'ajustement du seuil de décision[60]. Finalement, le colliculus supérieur exécute donc la commande oculomotrice associée à l'option sélectionnée en signalant le franchissement du seuil de décision aux noyaux oculomoteurs et réinitialise les assemblées corticales via une décharge corolaire (Fig. 18B, panel bas). Globalement, ce modèle illustre comment une décision perceptuelle peut émerger au sein d'un réseau distribué de modules spécialisés et souligne l'importance de la synapse cortico-striatale dans l'implémentation et la régulation du seuil de décision, par facilitation synaptique dopaminergique ou par des afférences corticales excitatrices accessoires.

Pour conclure, il existe actuellement 3 hypothèses principales susceptibles d'expliquer comment la distance au seuil de décision pourrait être régulée dans le cerveau humain[55] : (1) L'hypothèse *striatale*, au cœur du modèle de Lo et Wang, est celle qui celle qui rend le mieux compte des données IRMf, mais aussi des données électrophysiologiques obtenues chez le singe dans l'ensemble de ces structures[55,60,64]. (2) L'hypothèse *corticale* propose que la distance au seuil de décision soit ajustée via le niveau d'activité basale des populations de neurones corticaux accumulant les évidences. Cette hypothèse n'est pour l'instant étayée que par une seule étude IRMf portant sur le SAT[110]. (3) Une dernière hypothèse implique la voie *hyper-directe* et suggère qu'une élévation du seuil de décision peut également être obtenue par une majoration des influx excitateurs préfrontaux du STN. A l'heure actuelle, une seule étude utilisant la stimulation profonde à haute fréquence du STN (DBS-STN) chez des patients Parkinsonien implique le STN dans la régulation du seuil de décision[112]. Ces différentes hypothèses ne sont cependant pas exclusives les unes des autres et différents sources d'ajustement du seuil - SAT, information *a priori*… - pourraient reposer sur des

mécanismes neurobiologiques différents. A l'heure actuelle, la question de l'ajustement du seuil de décision reste donc ouverte.

d. Décision basée sur les valeurs : Des théories économiques du choix à la décision par échantillonnage séquentiel

Alors que les décisions perceptuelles impliquent la sélection d'une alternative sur la base des informations collectées par les organes sensoriels, les décisions basées sur les valeurs dites « économiques » impliquent quant à elles de réaliser cette sélection sur la base de la valeur subjective accordée au bien attendu en retour du choix.

Théories économiques de la décision

Depuis la célèbre correspondance de 1654 entre Pascal et Fermat jetant les bases d'une théorie des probabilités, il était admis que face à un choix dont l'issue est incertaine, un décideur « rationnel » se devait de choisir l'alternative maximisant son gain espéré, c'est-à-dire le produit de sa valeur faciale et de la probabilité de gain[113]. Comment comprendre alors que le prix d'une police d'assurance soit supérieur à la somme reversée en moyenne par l'assureur ? En conjecturant que la valeur associée à un choix n'était pas proportionnelle à la valeur faciale du bien espérée mais diminuait à la marge, Bernoulli proposa une solution simple et élégante à ces paradoxes en conceptualisant les valeurs comme des variables cachées, sous-jacentes au choix, qu'il nomme « utilités »[114]. De ce point de vue, le but de la décision économique est donc de maximiser l'utilité espérée, c'est à dire le produit de la probabilité de gain et de son utilité, cette dernière étant exprimée sur une échelle de valeur interne idiosyncrasique liée à la valeur faciale du gain par une fonction puissance[1] (Fig. 19A). L'aversion au risque, c'est à dire la dévaluation d'un bien dont l'obtention est incertaine, résulte ici de la déformation des valeurs faciales par la concavité de la fonction d'utilité (Fig. 19B). La théorie de Bernoulli, dite de « l'utilité espérée », constitue l'acte fondateur de l'économie en tant que discipline visant à formaliser une théorie normative du comportement décisionnel humain en situation de risque.

[1] Bien que d'autres paramétrisations aient été proposées, la fonction puissance reste la plus usitée.

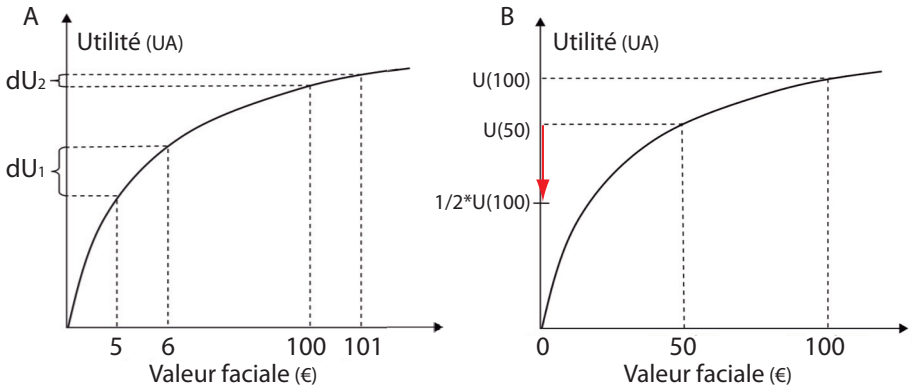

Figure 19 : Utilité en fonction de la valeur faciale du bien attendu. (A) L'utilité du gain décroit à la marge. L'utilité de 1€ est plus grande lorsqu'on a 5€ en poche (dU_1) que lorsqu'on a 100€ (dU_2). **(B) Aversion à l'incertitude.** L'utilité de 50€, U_{50}, est supérieur à l'utilité moyenne de 50% de chance d'obtenir 100€, $½*U_{100}$. En d'autre terme, l'utilité de 50€ qu'on est sûr d'obtenir est supérieure à l'utilité de 50% de chance d'obtenir 100€. Cet effet est d'autant plus prononcé que la fonction d'utilité est concave et déforme la projection des valeurs faciales dans l'espace des utilités, i.e. que son paramètre tend vers 0. D'après Glimcher[115].

Il fallut cependant attendre la première moitié du XX^{ème} siècle pour qu'une méthode de mesure des fonctions d'utilité soit proposée. La théorie de la préférence révélée de Samuelson fait l'hypothèse que, dans la mesure où les choix d'un individu se portent sur les options dont l'utilité est maximale, ceux-ci reflètent ses préférences[116,117]. L'identification de propositions équivalentes, dont les alternatives sont choisies indifféremment par le sujet, permet ainsi de mesurer la valeur relative d'offres comportant des biens de natures différentes, en quantité variable et/ou dont l'obtention est incertaine[117]. Cette approche s'enracine dans la démonstration qu'un individu ayant ordonné l'ensemble des options ouvertes au choix par utilité croissante, c'est-à-dire sur une échelle interne de valeur commune, fait des choix cohérents si ceux-ci maximisent l'utilité espérée[116]. L'articulation par Von Neumann et Morgenstern d'un ensemble d'axiomes (complétude, transitivité, continuité et indépendance des préférences révélées) à la fois nécessaire et suffisant pour que les choix d'un agent économique puissent être prédits par la maximisation de l'utilité espérée marque l'apogée de l'entreprise néoclassique dans le domaine de la théorie de la décision[118], Von Neumann et Morgenstern aboutissant à une définition formelle et normative de la rationalité intégrant les théories de l'utilité attendue et des préférences révélées.

En effet, l'identification de situations décisionnelles durant lesquelles les axiomes de Von Neumann et Morgenstern n'étaient pas respectés amena progressivement

certains économistes à se tourner vers d'autres disciplines, comme la psychologie, pour expliquer ces comportement paradoxaux[115]. Ainsi, la théorie des perspectives (« *prospect theory* ») revisite le concept d'utilité attendue de Von Neumann et Morgenstern pour mieux rendre compte de la construction et de la représentation des valeurs subjectives guidant le choix en introduisant de nombreuses modifications de sa fonction d'utilité[115,119,120] (Fig. 20) : (1) Les enjeux d'une décision risquée sont perçus en termes de gains et de pertes, définis relativement à un cadre de référence subjectif (*status quo*), (2) la fonction de liaison entre les valeurs faciales et les valeurs subjectives (concept se substituant à l'utilité) sont différentes dans le domaine des gains et des pertes. La pente à l'origine de la fonction de valeur subjective est deux fois plus importante en moyenne pour les pertes que pour les gains, induisant une asymétrie dans leurs représentations subjectives qui se traduit comportementalement par une sensibilité accrue aux pertes[119,120]. De plus, la fonction est concave dans le domaine des gains, ce qui induit une aversion au risque, alors qu'elle est convexe dans le domaine des pertes, induisant l'effet inverse, (3) finalement, les probabilités influencent la décision au travers d'une représentation subjective qui surévalue les poids des événements rares et sous-évalue les évènements fréquents.

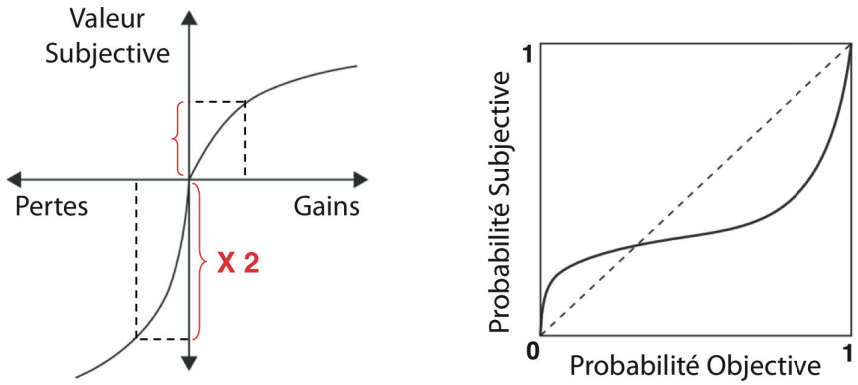

Figure 20 : Représentation des valeurs et des probabilités dans la théorie des perspectives. (Panel gauche) Valeur subjective en fonction de la valeur faciale des gains et pertes potentielles. (Panel droit) Probabilités subjectives en fonction des probabilités objectives. D'après Kahneman et Tversky[120].

La plupart des théories économiques de la décision, de la théorie de l'utilité espérée[118] à la théorie des perspectives[120], au même titre que les théories d'apprentissage par renforcement issues des travaux en intelligence artificielle[121],

partagent une même conclusion : les décideurs économiques agrègent l'ensemble des dimensions décrivant une option ouverte au choix en une mesure unique, arbitraire et subjective de sa valeur, puis choisissent l'alternative ayant la valeur subjective la plus importante. De ce point de vue, la comparaison entre alternatives de nature différente est possible du fait de l'existence de cette mesure abstraite de la valeur subjective, donnant ainsi naissance au concept de « monnaie commune ». L'hypothèse d'une monnaie commune suppose que la valeur de tout bien est convertible en une même monnaie subjective et que la comparaison de la valeur subjective entre différentes options au cœur de la décision économique se fait après conversion dans cette monnaie[3].

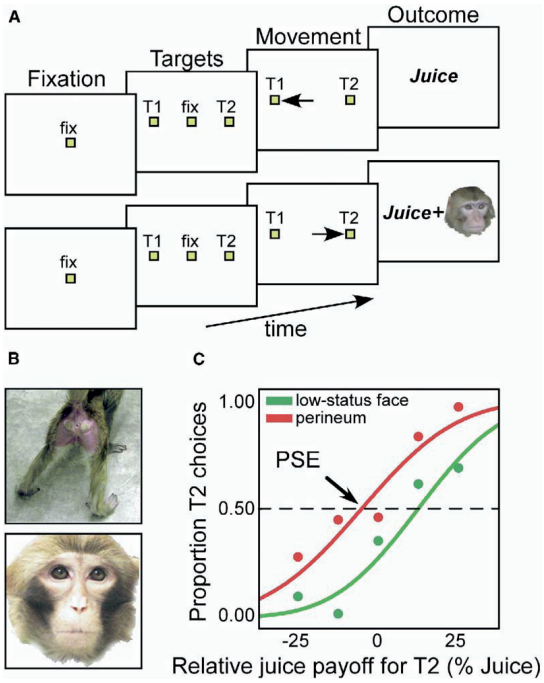

Figure 21 : (A) Paradigme de choix économiques. Des offres comprenant une option menant à une quantité fixe de jus de fruit et une option menant à une quantité variable de jus et une image sont proposées à un singe. Deux types d'images sont associées à la quantité variable de jus : de images de périnée de femelle et des images de visage de mâle dominant. Le singe connaît les enjeux lors de son choix et indique sa décision par une saccade oculaire. **(B)** Exemple d'image utilisée dans l'expérience. **(C) Courbe de réponse psychométrique.** Proportion de choix de l'option associant image et jus en fonction du bonus/malus de jus appliqué. La courbe rouge indique les essais associés à des « images de périnée » et la courbe verte les essais images de « singe dominant ». Le croisement de la courbe psychométrique avec la ligne indiquant que le singe choisit de manière équiprobable entre les deux options (en pointillé) indique le point d'équivalence subjective. D'après Deaner[122]

La figure 21 décrit une expérience comportementale menée au sein d'une colonie de singes par Deaner *et al* afin de tester l'hypothèse que la valeur de chaque option d'un choix économique est convertie en une monnaie commune préalablement à leur comparaison[122]. Des choix binaires entre une option associée à une quantité fixe de jus de fruit et une option menant à une quantité variable de jus associée à une image sont proposées à un singe. Deux types d'images sont évalués : de images de périnée de femelle et des images de visage de mâle dominant (Fig. 21B). L'intérêt de cette expérience est qu'elle permet de mesurer la valeur d'un type d'image en terme de

quantité de jus de fruit au point d'équivalence subjective, établissant ainsi une équivalence directe entre la valeur subjective de biens de nature différente (Fig. 21C). Le point d'équivalence subjective correspond à l'offre pour laquelle le singe choisit indifféremment l'une ou l'autre option, i.e. de manière équiprobable, indiquant ainsi que la valeur des deux options proposées est subjectivement identique. Dans cette expérience, les singes acceptaient de sacrifier du jus de fruit pour la possibilité de visualiser des périnées de femelle et demandaient un bonus pour être confrontés aux images de mâle dominant (Fig. 21C). Il est frappant de constater que les valeurs subjectives ainsi déterminées sont transitives : si l'option A est égale à 2 fois l'option B et que l'option B est égale à 2 fois l'option C, alors l'option A est égale à 4 fois l'option C[123,124].

Bien que le but des modèles économiques classiques soit de prédire les comportements observables d'un individu sans souci de la réalité des processus qui les sous-tendent, l'importance conceptuelle de ces résultats explique l'intérêt quasi exclusif de l'approche neuroéconomique pour la représentation dans une monnaie neurale commune des valeurs subjectives associées aux alternatives d'un choix, ou « *valuation* ». Elle explique également le peu d'intérêt accordé à l'algorithmique et à l'implémentation de la décision par les économistes, et cela malgré la démonstration précoce de la nature stochastique et dynamique du processus de choix économique[125,126].

Approche neuroéconomique des décisions basées sur les valeurs subjectives en condition d'incertitude.

- **Système dopaminergique : Apprentissage et prédiction de la valeur subjective des choix**

Dans les années 1990, une série d'études électrophysiologiques portant sur le conditionnement opérant montra que l'anticipation ou la réception de récompense était associée à une augmentation phasique de l'activité neurale dans 60 à 80% des neurones dopaminergiques[127-129]. Cette augmentation d'activité était également retrouvée au niveau de leurs cibles ; striatum, amygdale, cortex orbito-frontal et cortex cingulaire antérieur. Ensemble, ces structures constituent le « système de récompense »[127-129].

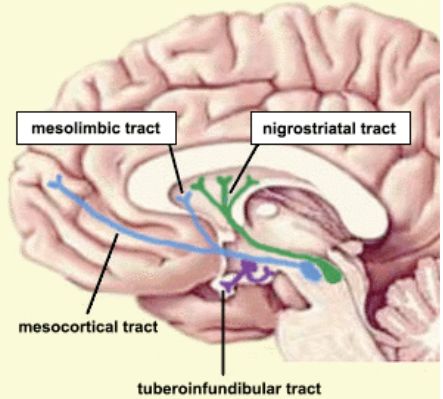

Figure 22 : Principaux faisceaux ascendants de projections des noyaux dopaminergiques mésencéphaliques. Les neurones dopaminergiques sont regroupés au sein de deux noyaux mésencéphaliques : l'aire tégmentale ventrale et la substance noire *pars compacta,* qui constituent les points de départ respectifs des voies ascendantes neuromodulatrices dites méso-cortico-limbique (bleue) et nigro-striée (vert).

Les caractéristiques électrophysiologiques des neurones dopaminergiques suggèrent cependant une fonction plus complexe que la simple détection de stimuli hédoniques. En effet, on observe une augmentation de l'activité phasique dopaminergique lors de l'obtention d'une récompense inattendue (Fig. 23A), une absence de réponse lorsqu'une récompense prédite avec certitude est reçue (Fig. 23B), et une inhibition phasique de leur activité lorsqu'une récompense prédite est omise[130,131] (Fig. 23C). Ce profil de réponse est évocateur d'un signal d'erreur de prédiction (noté δ, Fig. 24 et Eq. 9), c'est à dire d'une représentation de la différence entre ce qui était attendu (V_t) et ce qui est obtenu (Q_t).

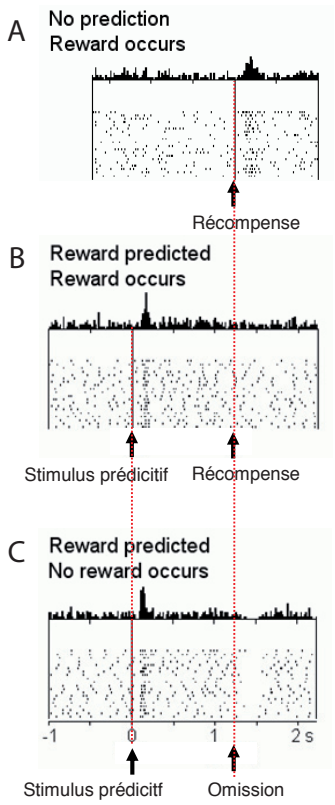

Figure 23 : Réponse phasique des neurones dopaminergiques au cours d'un paradigme de conditionnement opérant. (A) Avant apprentissage des règles de contingences, la récompense (inattendue) est associée à une augmentation phasique d'activité. **(B)** Après apprentissage des règles de contingences entre stimulus prédictif et récompense, seul le stimulus est associé à une augmentation d'activité phasique. **(C)** Si la récompense n'est pas délivrée conformément aux règles de contingence apprises, on observe une dépression phasique de l'activité des neurones dopaminergiques. D'après Schultz[131].

Les signaux d'erreur de prédiction étant au cœur des algorithmes d'apprentissage par renforcement, ces résultats furent interprétés comme impliquant les neurones dopaminergiques dans l'apprentissage des valeurs[132]. En effet, les algorithmes d'apprentissage par renforcement ont été développés dans le but de créer des intelligences artificielles capables d'apprendre par essais-erreur successifs la valeur des alternatives en situation de décision. Pour ce faire, l'algorithme calcule l'erreur de prédiction après chaque essai, puis l'utilise pour mettre à jour sa prédiction de la valeur associée à cette option avec un taux d'apprentissage α (V_{t+1} dans Eq. 9). Cet algorithme très simple, donc peu coûteux en terme de calculs, converge rapidement vers les valeurs moyennes réelles associées à chaque alternative sous réserve que celles-ci soient uniformement explorées[121]. De plus, ces modèles ne nécessitent pas d'*a priori* sur la structure de ce qui doit être appris, ce qui leur confèrent une grande versatilité pour affronter un environnement changeant et incertain.

$$V_{t+1} = V_t + \alpha * \delta_t$$
$$\delta_t = V_t - Q_t \qquad \text{(Eq. 9)}$$

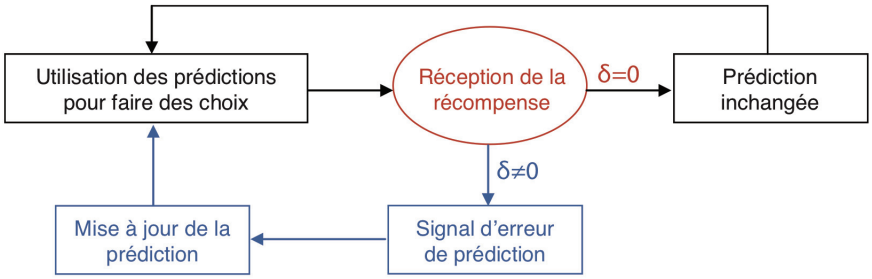

Figure 24 : Algorithme d'apprentissage par renforcement (Eq. 9).

Du point de vue de l'apprentissage par renforcement, l'activité phasique dopaminergique évoquée par l'apparition du stimulus conditionnel prédit la valeur de la récompense à venir, tandis que l'activité au moment de l'obtention de la récompense signale l'erreur de prédiction. Confirmant cette hypothèse, des études électrophysiologiques complémentaires ont montré, qu'après conditionnement, l'activité dopaminergique à l'affichage du stimulus prédictif était proportionnelle à la valeur de la récompense espérée, c'est-à-dire au produit de la quantité et de la probabilité de récompense[133,134] (Fig. 25A). De plus, l'activité phasique à la réception de la récompense est proportionnelle à la quantité de fluide obtenue comme récompense au début de l'apprentissage [134] (Fig. 25B). En revanche, après conditionnement, l'activité phasique suivant la réception d'une récompense diminue linéairement avec la probabilité de récompense reflétant ainsi la différence entre la valeur prédite et la valeur de la récompense reçue[131,133]. L'enregistrement direct de signaux d'erreur de prédiction dans la substance noire par enregistrements cérébraux profonds a récemment confirmé l'existence de ces signaux dopaminergiques d'erreur de prédiction chez l'Homme[135] (Fig. 25C et D).

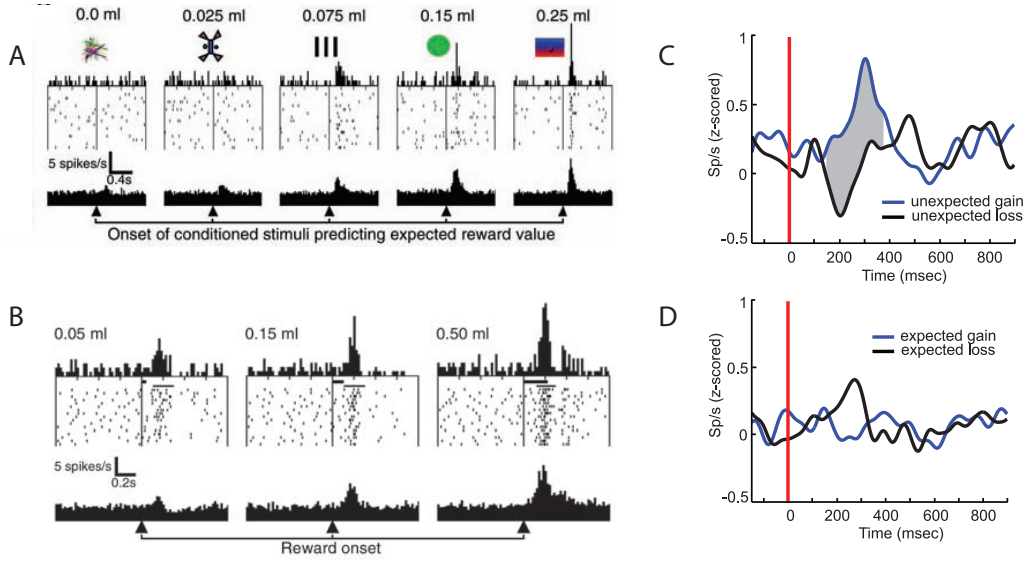

Figure 25 : (A) Activité phasique dopaminergique évoquée par la présentation de stimuli prédisant l'obtention retardée de quantité de jus en quantité croissante. **(B)** Réponse phasique évoquée par l'obtention inattendue de quantités croissantes de jus. **(C)** Activité dopaminergique évoquée par un gain monétaire (bleu) ou une perte (gris) inattendue. **(D)** Activité dopaminergique évoquée par un gain monétaire (bleu) ou une perte (gris) attendue. (A-B) sont issus d'expériences chez le singe ; (C-D) et ont été obtenues chez des patient Parkinsonien à l'occasion d'une opération neurochirurgicale fonctionnelle. D'après Tobler[134] et Zaghloul[135]

Les neurones dopaminergiques sont donc au cœur du circuit cérébral permettant l'apprentissage des valeurs par renforcement. Or, ce cadre théorique suggère que ces valeurs peuvent être utilisées pour guider nos décisions. De manière intéressante, une étude électrophysiologique récente a montré que l'activité dopaminergique phasique au moment de choix binaires corrélait à la valeur estimée de l'action qui allait être choisie, liant ainsi neurones dopaminergiques et valeurs subjectives au cours des décisions économiques[136]. Ce dernier résultat suggère l'implication des structures cérébrales cibles du système dopaminergique dans les processus de prise de décision basés sur les valeurs (Fig. 26).

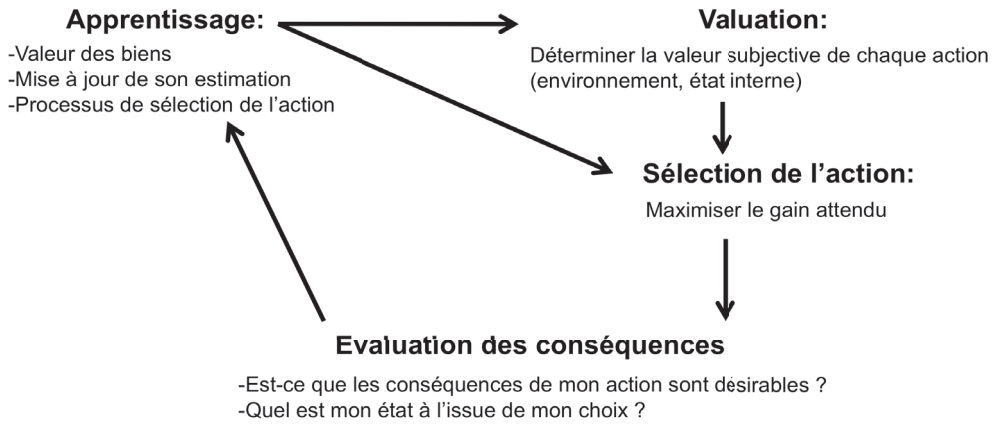

Figure 26 : Représentation schématique des étapes nécessaires à la prise de décision basée sur les valeurs subjectives lorsque les valeurs des options doivent être apprises par renforcement.

- **Le cortex orbito-frontal : Une structure tournée vers les valeurs subjectives**

Depuis le célèbre cas clinique de Phineas Gage (1823-1860), un employé des chemins de fer dont la personnalité s'était radicalement modifiée à la suite d'un accident ayant endommagé son cortex orbito-frontal (OFC), l'étude neuropsychologique de cohortes de patients lésés dans l'OFC a confirmé l'importance de cette région cérébrale dans la formation des choix basés sur les valeurs subjectives[137]. En effet, alors que l'évaluation neuropsychologique de ces patients ne révèle pas d'anomalies (QI, épreuves de Wisconsin et de la tour de Londres), ces patients se comportent de manière inadaptée et irresponsable, persévèrent dans leur échecs jusqu'à la ruine, et échouent à se conformer aux règles sociales, bien qu'ils les connaissent, jusqu'au rejet par leur entourage. Ce profil comportemental est aujourd'hui interprété comme une incapacité à prendre en compte et à réviser la valeur subjective attribuée aux alternatives d'un choix lorsque les règles d'associations entre action et conséquences ne sont pas explicites[137].

En effet, l'OFC est une région multimodale recevant des afférences de l'ensemble des cortex sensoriels[129,137,138], ainsi qu'un grand nombre de terminaisons dopaminergiques par la voie ascendante méso-cortico-limbique. Il est donc idéalement placé pour intégrer les différentes dimensions formant la valeur d'une expérience et les signaux dopaminergiques de prédiction de la valeur et d'erreur de prédiction (Fig. 27).

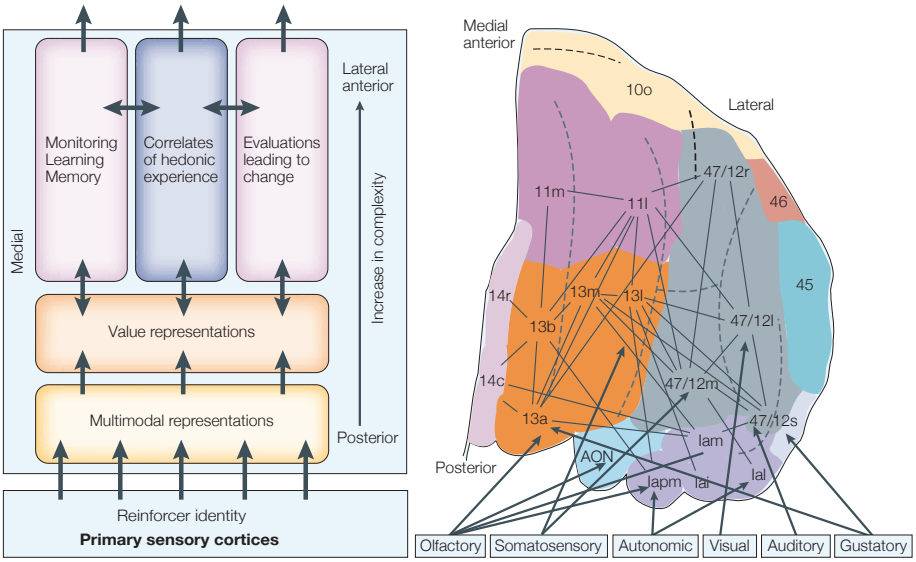

Figure 27 : (A) Modèle d'interactions entre systèmes sensoriels et système de récompense dans l'OFC. (B) Connectivité fonctionnelle au sein de l'OFC : Les informations sensorielles émanant des cortex sensoriels entrent dans l'OFC par sa part caudale. Celle-ci fait l'objet d'une intégration multimodale progressive permettant l'émergence d'une représentation centrée sur la valeur des biens et des expériences. D'après Kringelbach[139].

Chez l'Homme, de nombreuses études en IRMf suggèrent que l'OFC implémente une représentation intégrée et dynamique des valeurs subjectives[137,138]. Ainsi, l'activité cérébrale dans l'OFC corrèle avec la valeur subjective associée à une grande variété d'expériences, tel que le plaisir ressenti lors de la consommation de nourriture dont la texture, la température, l'arôme ou la marque sont manipulés[138,140] (Fig. 28B-C). Cette activité est dynamiquement ajustée : ainsi, plusieurs expériences sur la satiété montrent une extinction graduelle de l'activité cérébrale évoquée dans l'OFC par la consommation de nourriture au fur et à mesure que la faim disparaît[138]. De plus, l'OFC semble représenter sur un axe antéropostérieur les récompenses primaires, dont la valeur hédonique est immédiatement perceptible et les récompenses secondaires, dont le caractère hédonique dérive secondairement des récompenses primaires qu'il permet d'obtenir[141] (Fig. 28A). Lors de tâche de conditionnement, les neurones orbito-frontaux génèrent un signal d'anticipation de la récompense dont l'intensité reflète les préférences révélées par le singe lors de choix libres entre les différents types de récompense possible[142] (Fig. 29). L'activité de ces neurones augmente lorsque l'expérience anticipée est positive, et diminue dans le cas inverse, en fonction de l'intensité de l'expérience anticipée[143].

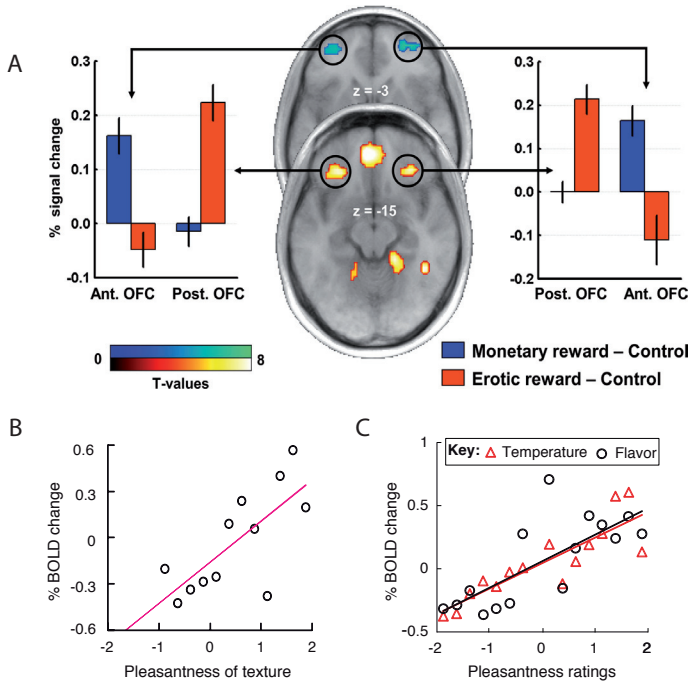

Figure 28 : Activité hémodynamique dans le cortex orbito-frontal lors de la réception de récompense. (A) Topographie de la réponse hémodynamique dans l'OFC selon la nature de la récompense : primaire (rouge) ou secondaire (bleu). **(B)** Corrélation entre l'activité hémodynamique dans l'OFC et les cotations subjectives évaluant le niveau de plaisir éprouvé durant la consommation de yaourt dont la texture est manipulée, **(C)** ainsi que la température (triangles rouges) et l'intensité de l'arôme (cercles noirs). D'après Sescousse[141] et Grabenhorst[138].

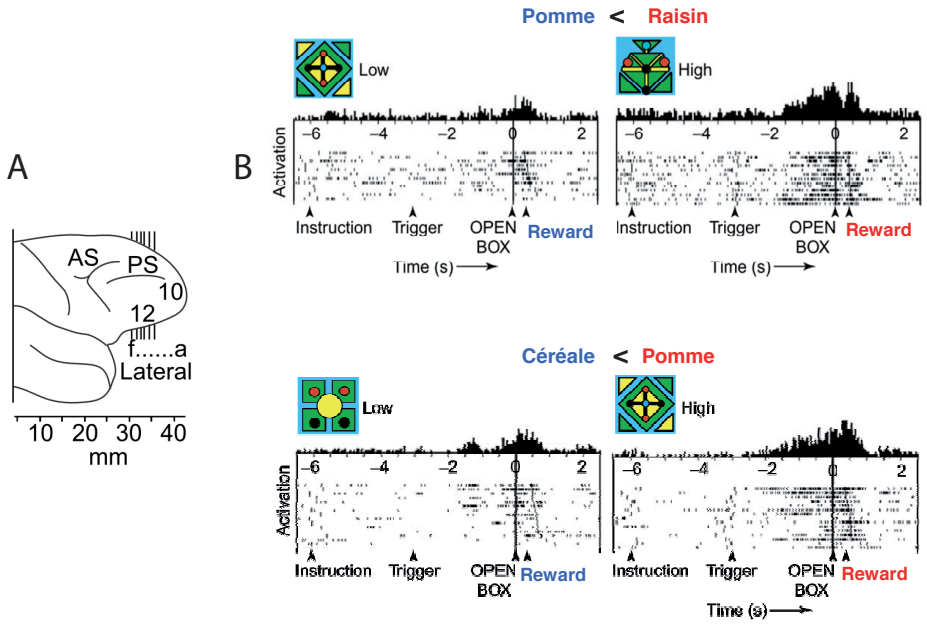

Figure 29 : Codage anticipatoire de la valeur subjective des récompenses dans le cortex orbito-frontal du singe. Les singes sont susceptibles de recevoir trois types de récompenses en quantité fixe : de la pomme, des grains de céréale ou du raisin. La récompense délivrée est annoncée en début d'essai par un symbole spécifique. Au cours d'une session, seules deux des trois récompenses sont délivrées. **(A) Plans de pénétration des électrodes. (B)** Lors des sessions où pomme et raisin sont disponibles, l'activité anticipatoire des neurones de l'OFC est plus intense pour le raisin que pour la pomme. A l'inverse, dans les sessions où pomme et céréales sont disponibles, l'activité anticipatoire des neurones de l'OFC est plus intense pour la pomme que pour le raisin. Comportementalement, les choix du singe révèlent qu'il préfère le raisin à la pomme et la pomme aux céréales. D'après Tremblay[142].

Pris ensemble, ces travaux démontrent l'implication de l'OFC dans le codage de signaux prédisant la valeur subjective des biens et expériences à venir, ainsi que de leur valeur subjective lorsqu'elles surviennent. Néanmoins, une limitation importante de ces travaux est qu'ils étudient la représentation des valeurs dans un contexte de consommation passive ou d'apprentissage par renforcement qui ne permet pas d'étudier le rôle de l'OFC dans le processus de décision économique. Une difficulté rencontrée par ces études est que le choix économique est un phénomène dynamique se divisant en plusieurs phases durant lesquelles se succèdent différents signaux de valeur. Par exemple, la « valeur décisionnelle » est définie comme étant un signal contemporain du processus de décision, sur lequel celui-ci se base pour identifier l'option maximisant la valeur subjective[144-146]. Cette notion de valeur décisionnelle doit en particulier distinguée des signaux post-décisionnels tels que la valeur subjective espérée en retour du choix ou la valeur subjective de l'expérience de consommation des biens obtenus[144-146].

Afin d'étudier le rôle de l'OFC dans la décision économique, Padoa-Schioppa *et al* ont enregistré l'activité de neurones dans cette région (Fig. 30B) pendant que des singes effectuaient des choix binaires sur la base de la quantité et du type de jus de fruit associé à chaque alternative[123,124,147,148] (Fig. 30A). Comme discuté précédemment, la plupart des théories économiques de la décision s'accordent sur le fait que les décideurs agrègent pour chaque option ouverte au choix l'ensemble de leurs caractéristiques en une mesure unique, arbitraire et subjective de leur valeur, puis choisissent l'alternative ayant la valeur subjective espérée la plus importante. Dans ce paradigme, les singes se comportent effectivement comme tel, basant leur choix sur la valeur relative qu'ils accordent à chaque type de jus - i.e. leur préférence - et sur la quantité de jus annoncée[123] (Fig. 30C-D). Les préférences ainsi révélées sont transitives au sens quantitatif, c'est-à-dire que si l'option A est égale à 1.5 fois l'option B et que l'option B est égale à 3 fois l'option C, alors l'option A est égale à 4.5 fois l'option C[123,124]. Durant la formation de la décision, suite à l'affichage de l'offre, les neurones orbito-frontaux latéraux présentent principalement deux types d'activités (Fig. 30C-D) : (1) Leur réponse est directement proportionnelle à la valeur subjective d'une des options, (2) ou à la valeur subjective de l'option qui va être choisie. L'activité des neurones codant la valeur subjective d'une des options ne dépend pas de la paire de jus proposé au choix, une propriété nécessaire pour assurer la transitivité des valeurs subjectives au travers

de l'ensemble des paires de jus de fruit utilisées dans la tâche[124]. De manière intéressante, ceux-ci s'adaptent à l'échelle des valeurs subjectives devant être représentée de telle manière que la valeur maximale sur une session expérimentale correspond au niveau d'activité maximale du neurone[134,149]. Ce mécanisme permet d'optimiser la précision de la représentation des valeurs par les neurones de l'OFC.

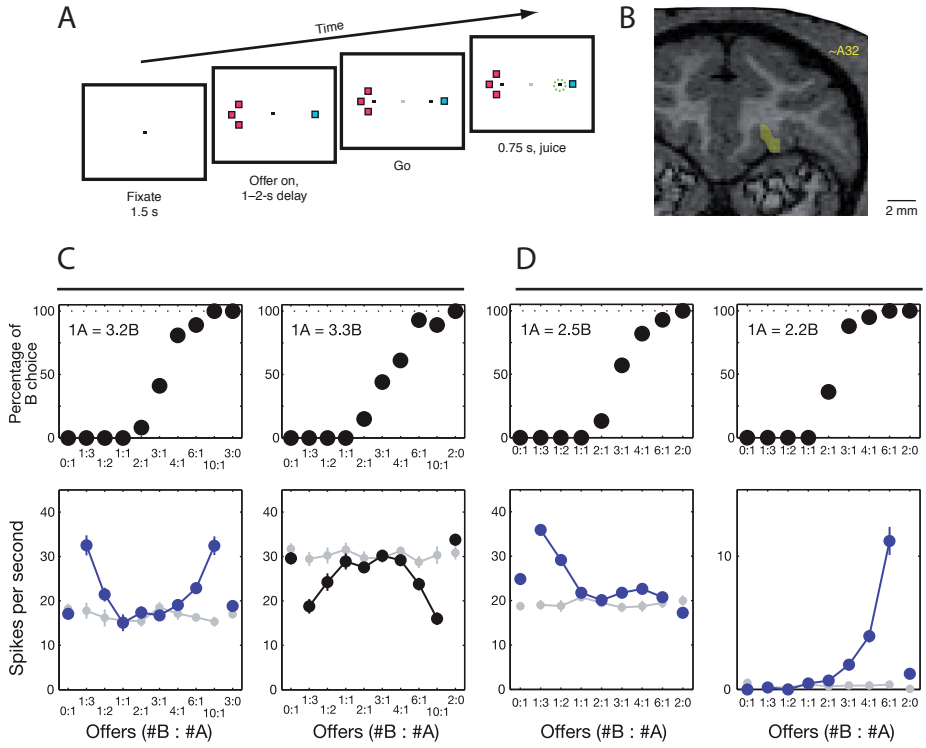

Figure 30 : Codage de la valeur subjective des options dans l'OFC latéral. (A) Paradigme de prise de décision économique. Une offre est faite au singe sous la forme de deux cibles affichées de part et d'autre de l'écran. La couleur des carrés annonce le type de jus et le nombre de carrés la quantité de jus associée à l'option. Le singe indique son choix par une saccade oculaire et obtient systématiquement la récompense annoncée. **(B)** Le cluster jaune indique la zone latérale orbito-frontale dans laquelle les neurones ont été enregistrés. **(C)** Neurones latéraux orbito-frontaux codant la valeur de l'option choisie. Les panels haut indiquent la probabilité de choisir le jus B en fonction du rapport entre la quantité de jus A et de jus B offerte. L'insert indique la valeur relative du jus 1 et du jus B. Les panels bas indiquent l'activité neurale correspondante. Celle-ci est prédictive de la valeur relative de l'option choisie en ce sens qu'elle augmente proportionnellement à la distance entre la valeur de chaque option. Une interprétation alternative est qu'ils codent la certitude du choix catégoriel. **(D)** Neurones latéraux orbito-frontaux codant la valeur d'une des options. L'activité neurale varie linéairement sélectivement avec une des deux options. D'après Padoa-Schioppa[124,147].

De plus, l'activité de ces neurones précède celle d'autres structures impliquées dans la prise de décision telle que le DLPFC, suggérant que leur activité est bien responsable de l'encodage de la valeur des options et non le reflet passif de processus d'évaluation

implémentés dans d'autres régions[150]. Finalement, les propriétés des neurones de l'OFC durant des choix basés sur les valeurs contrastent avec celle des neurones du DLPFC et du striatum, puisque contrairement à ces derniers, l'activité des neurones dans l'OFC est indépendante des caractéristiques visuo-spatiales de la tâche ainsi que de la réponse oculomotrice. Pris ensembles, ces résultats suggèrent que les neurones dans l'OFC opèrent dans l'espace abstrait et indépendant des actions représentant la valeur des options exprimée dans une monnaie neurale commune, conformément aux fonctions d'utilités des théories économiques de la décision[3,148,151,152,150].

Parallèlement à ces travaux, de nombreuses études ont été menées en IRMf afin de préciser les contours d'un « système de valuation » codant la valeur subjective espérée de chaque option dans une monnaie neurale commune pour guider le choix économique chez l'Homme. Afin d'identifier les régions cérébrales capables de représenter la valeur subjective d'un bien indépendamment de sa nature pendant la décision, Chib *et al* ont développé un paradigme de choix économiques au cours duquel des sujets installés dans un scanner IRM choisissaient entre une rémunération fixe et 80% de chance d'obtenir un bien parmi trois types[144] (argent, babioles, snacks). Avant la session IRM, la valeur subjective de chaque bien était déterminée pour chaque sujet comme sa propension à le payer (WTP, « *willingness to pay* ») lors d'une vente aux enchères de Becker–DeGroot–Marschak[153]. L'OFC médian était la seule région cérébrale dont l'activité BOLD au moment de la décision covariait avec la WTP des biens, indépendamment de leur nature (Fig. 31). Ce résultat suggère que la portion médiale de l'OFC code la valeur subjective associée aux alternatives d'une décision dans un espace monétaire commun. Au travers de la littérature, de multiples études montrent que la portion médiale du cortex orbito-frontal code au sein d'un espace monétaire commun les valeurs subjectives attribuées à chaque option ouverte au choix[145,152,154-159], qu'elles impliquent des gains et des pertes[158], qu'elles soient hédoniques ou aversives[159].

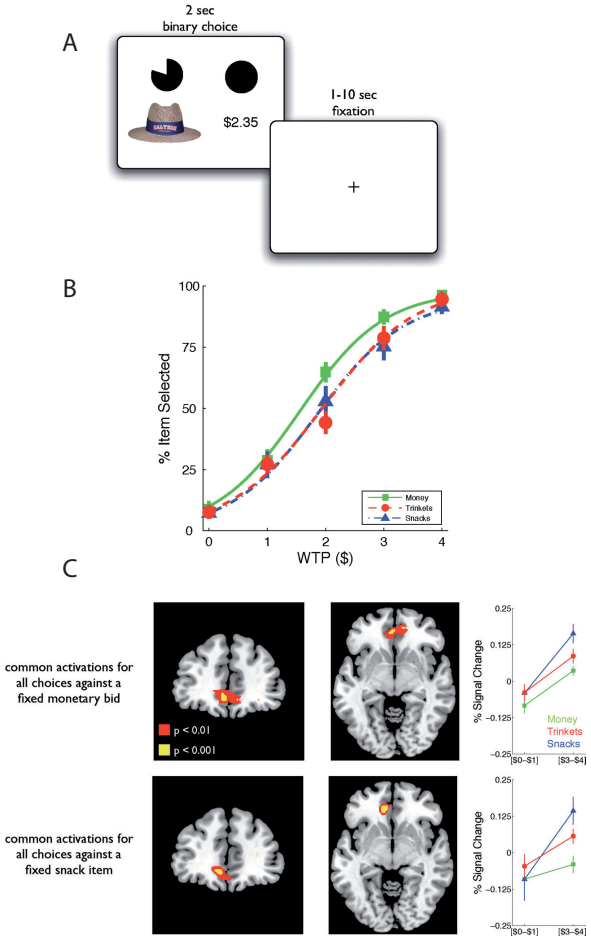

Figure 31 : (A) Décision économique binaire entre 80% de chance d'obtenir un bien et 100% de chance d'obtenir une somme fixe. (B) Probabilité de choisir l'option récompensée par un bien en fonction de sa valeur subjective (WTP). **(C)** Conjonction identifiant les régions cérébrales dont l'activité covarie avec la WTP de l'item en jeu quelque soit sa nature. D'après Chib[144].

De manière intéressante, l'activité BOLD dans la partie médiale de l'OFC corrèle aux cotations d'images, cotations qui elles-mêmes reflètent les RT mesurés lors d'une tâche de choix binaire réalisée en dehors du scanner sur des paires d'images évaluées auparavant. Cette observation suggère que l'évaluation des options d'un choix économique et la cotation d'image repose sur une même échelle de valeur subjective implémentée par l'OFC médian[160]. Pris ensemble, ces résultats démontrent la position centrale qu'occupe l'OFC médian dans la représentation des valeurs subjectives, ainsi que l'importance de cette structure pour la décision économique. En effet, l'OFC apparaît être un carrefour, permettant l'agrégation au sein des valeurs subjectives des multiples dimensions physiques et psychologiques déterminant la valeur subjective de nos buts.

Théorie des champs décisionnels : Une approche stochastique et dynamique du choix économique

Historiquement, les théories économiques de la décision se sont focalisées sur la façon dont les décideurs agrègent l'ensemble des dimensions décrivant chaque option en une mesure unique et subjective de sa valeur. La démonstration par Samuelson qu'un individu ayant ordonné l'ensemble des options ouvertes au choix par utilité croissante fait des choix cohérents tant que ceux-ci maximisent l'utilité espérée[116], ainsi que l'éviction explicite des questions portant sur l'algorithmique et l'implémentation de la décision économique par la règle du « *as if* » de Friedman[3,161], expliquent probablement le peu d'intérêt accordé par les économistes à la question de la sélection de l'option maximisant la valeur subjective espérée. Ainsi, c'est une approche déterministe et statique de la décision, faisant l'hypothèse que la sélection d'une alternative résultait d'une simple maximisation de la valeur subjective espérée, qui a longtemps prévalu (Eq. 10).

$$E\left(U_{opt}\right) = \max\left(E\left(U_1\right), E\left(U_2\right)\right) \qquad \text{(Eq. 10)}$$

Pour un choix économique binaire, ce type de fonction prédit une réponse comportementale discrète, le décideur sélectionnant systématiquement l'option 1 quand $E\left(U_1\right) > E\left(U_2\right)$ et l'option 2 quand $E\left(U_1\right) < E\left(U_2\right)$. Or, depuis les travaux menés par Mosteller dans les années 50, on sait que la sélection d'une option à l'issue d'une décision économique est un phénomène stochastique décrit par une fonction d'allure sigmoïdale associant la probabilité de choix à la différence entre les valeurs subjectives espérées associées à chaque alternative[125]. En d'autres termes, les décideurs ne prennent pas toujours la meilleure décision, des choix non-optimaux survenant de manière aléatoire. Ces résultats, maintes fois reproduits (comme témoigne les figures 21B, 30C-D et 31B), ne sont pas compatibles avec les théories déterministes de la décision économique, et ont justifié l'introduction dans les modèles économiques de fonctions « *softmax* », une famille de courbe sigmoïde dont le paramètre de température (τ) capture ce caractère stochastique du choix (Eq. 11).

$$\Pr_{option_1,\tau} = \frac{1}{1 + e^{\left(\frac{-[E(U_1)-E(U_2)]}{\tau}\right)}} \qquad \text{(Eq. 11)}$$

Ces modèles stochastiques, bien que mieux ajustés au comportement observé, ne rendent pas compte de la nature délibérative du processus de décision économique[125,126]. Ainsi, comment expliquer que le temps de décision augmente quand la différence de valeur entre options tend vers zéro[126] ou qu'une instruction mettant l'emphase sur la vitesse de décision ait un impact sur la probabilité de choix[162] ? Comme pour toute décision simple, faire un choix économique prend du temps : la durée du processus de décision économique doit donc être modélisée afin de rendre compte du comportement observé en situation de choix économique.

La théorie des champs décisionnels est une évolution récente des théories économiques classiques reposant, comme ces dernières, sur l'hypothèse d'une étape de valuation, durant laquelle une valeur subjective espérée est associée à chaque option, suivie d'une étape décisionnelle dont la nature stochastique et dynamique est capturée par un modèle de diffusion[30,31,163]. Dans le champ de la psychologie, des modèles d'architecture similaire ont été proposés, prédisant avec succès le comportement en situation de décision économique[32,163]. Par homologie avec les modèles de prise de décision perceptuelle, ces différents modèles de choix économiques considèrent tous (explicitement ou implicitement) que l'attribution d'une valeur subjective espérée à chaque option est homologue à la production d'information sensorielle par les neurones détecteurs de mouvement dans MT. La représentation interne des valeurs est donc bruitée et différents canaux fournissent l'information de valeur à des unités accumulatrices engagées dans une course pour leur seuil de décision. Comme dans les modèles de décision perceptuelle, la vitesse de dérive vers le seuil des unités accumulatrices est proportionnelle aux signaux reflétant la valeur subjective des options. La sélection de l'option maximisant la valeur subjective espérée a lieu ici aussi selon une règle winner-takes-all. De ce point de vue, l'augmentation des temps de réaction lorsque la différence de valeur subjective attendue associée à chaque option tend vers zéro traduit simplement la diminution de la vitesse d'accumulation de l'évidence en faveur d'une option[31,32,163]. De plus, l'augmentation de la proportion de choix non-optimaux (équivalent d'erreurs) lorsque l'emphase est mise sur la vitesse de décision s'explique par un ajustement du SAT via le seuil de décision comme pour les

autres types de décision simples[30,32]. Ce même type de mécanisme permet d'expliquer les renversements de préférence observés sous l'effet d'une pression temporelle[30].

L'intérêt de cette approche est double puisque l'utilisation de modèles de diffusion permet d'expliquer les interactions complexes entre temps de décision et probabilité de choix en situation de décision économique (prédiction), tout en rattachant la sélection de la meilleure option au cadre plus général de la décision par échantillonnage séquentiel (computation) et à son corpus de données neurobiologiques[3,5,31] (implémentation). Ces modèles de choix économiques, stochastiques et dynamiques, jettent donc un pont conceptuel entre théorie économique du choix et neurobiologie de la décision (Fig. 32).

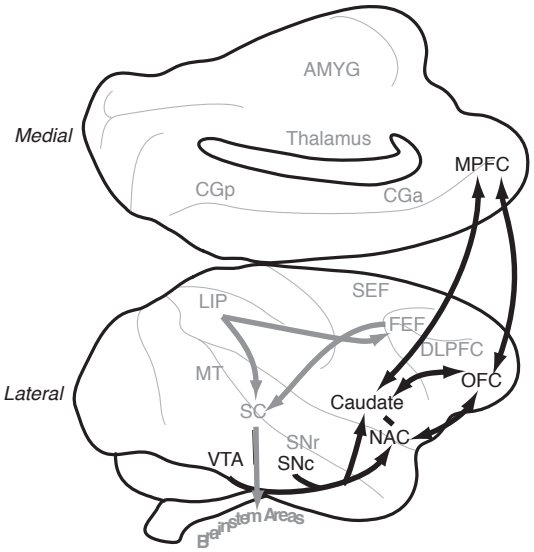

Figure 32 : Schéma mettant en rapport le réseaux pariéto-préfrontal impliqué dans la prise de décision perceptuelle et le système de valuation impliqué dans les décision économiques. D'après Glimcher[3].

3. PROBLEMATIQUE

L'étude neurobiologique des processus de décision perceptuelle, guidée par l'usage de modèles computationnels, a permis d'établir un lien clair entre l'accumulation d'information sensorielle et un réseau cortical incluant le sillon intra-pariétal et le cortex dorso-latéral préfrontal[3,5]. Afin de poursuivre cette exploration de l'architecture des réseaux biologiques impliqués dans la prise de décision, nous nous sommes d'abord intéressés aux mécanismes d'ajustement du processus de décision perceptuelle à son contexte[50]. Puis, au travers de l'étude du processus de décision économique nous soulevons la question de la capacité des mécanismes neuro-computationnels impliqués dans la décision perceptuelle à rendre compte des décisions simples dans un domaine cognitif distinct.

Question 1 : Mécanismes neuro-computationnels d'ajustement du processus de décision perceptuelle à son contexte.

Lorsque le choix de nos actions dépend de nos perceptions, l'information sensorielle est progressivement intégrée dans un réseau pariéto-préfrontal au sein duquel des assemblées neurales distinctes accumulent les preuves en faveur de chaque alternative jusqu'au franchissement d'un seuil de décision, ce qui détermine le temps de réaction et l'action exécutée[5]. Les primates ne pouvant exécuter simultanément deux décisions simples, celle-ci constitue un goulot d'étranglement cognitif[164,165]. L'optimisation de la vitesse du processus décisionnel simple est donc critique pour produire un comportement adapté à un environnement complexe, incertain et changeant. Or, ce processus de décision produit un compromis entre vitesse et performance (SAT) qui est contrôlé par la quantité d'information à accumuler pour qu'une option soit sélectionnée, i.e. la distance au seuil de décision[22,28]. L'usage de l'ensemble des sources d'information disponibles est donc critique pour minimiser la durée du processus décisionnel sans altérer ses performances.

Conformément au cadre théorique de l'inférence Bayesienne, la probabilité *a priori* de la réponse influence le processus de décision perceptuelle[48,166], celui-ci étant plus

rapide lorsque la réponse est prédictible. En effet, le logarithme de la fréquence d'une réponse influence le processus de décision perceptuel par l'ajustement de la distance au seuil de décision, suggérant que cette information *a priori* se substitue en partie à l'information sensorielle[48]. De plus, notre connaissance de la structure causale de l'environnement constitue également une source d'information *a priori* influençant la vitesse de décision[166]. Du point de vue de la théorie de l'information de Shannon, il est naturel d'exprimer cette dernière en terme d'information prédictive, c'est-à-dire du log ratio de la probabilité d'une réponse sachant le contexte et de sa probabilité marginale[8].

Afin d'étudier les mécanismes neurobiologiques et computationnels impliqués dans l'ajustement du processus de décision perceptuelle en fonction de l'information prédictive disponible, nous avons développé un paradigme original de décisions perceptuelles séquentielles formant des chaines de Markov afin de manipuler systématiquement les quantités d'information prédictive issue de l'historique des choix récents. Puis, nous avons ajusté des modèles de décision par échantillonnage séquentiel aux données comportementales recueillies et quantifié l'information prédictive disponible à chaque décision en modélisant l'apprentissage des contingences entre stimuli successifs. De plus, les modèles de décision perceptuelle étant prédictifs de l'activité des assemblées neurales accumulant l'information et régulant le seuil de décision, nous avons adopté une stratégie d'analyse des données IRMf guidée par les prédictions du modèle afin de caractériser des modules cérébraux sur la base des computations qu'ils implémentent. Nous avons ensuite réalisé des analyses de connectivité effective afin d'étudier comment l'intégration fonctionnelle de ces modules permettait l'émergence d'un algorithme de décision contextuellement optimal. Notre hypothèse de travail était que l'information *a priori* diminuerait la distance au seuil de décision, régulant ainsi dynamiquement la quantité d'information sensorielle nécessaire pour sélectionner une action et mon objectif principal était de dissocier les régions cérébrales impliquées dans la régulation du seuil de décision en fonction de l'information prédictive des régions cérébrales implémentant le processus d'accumulation d'information sensorielle.

Question 2 : Mécanismes neuro-computationnels sous-jacent au choix économique.

Il est frappant de constater à quel point les situations décisionnelles auxquelles nous sommes confrontés peuvent varier, reposant tantôt sur l'analyse perceptuelle de l'environnement, tantôt sur l'analyse économique de la valeur subjective des options considérées, ou même sur le rappel d'expériences passées.

Le champ de la psychologie mathématique a extensivement étudié ces différents types de décisions simples, démontrant la capacité des modèles de décision par échantillonnage séquentiel à rendre compte des interactions complexes entre performance et distributions de RT, indépendamment du type d'information en entrée du processus décisionnel[14,15,17,18,20,22,39,167]. Cette capacité des modèles de diffusion à rendre compte de l'ensemble des décisions simples suggère que le cerveau humain pourrait dépendre de mécanisme de diffusion pour l'ensemble des décisions simples. Cette perspective soulève la question de l'unicité des mécanismes neuro-computationnels implémentant la prise de décision au travers des différents domaines cognitifs. Or, l'intégralité des données neurobiologiques justifiant les modèles neuro-computationnel provient de paradigmes d'inférence perceptuelle.

Nous avons donc testé l'hypothèse selon laquelle les modèles neuro-computationnels décrivant les choix basés sur l'information sensorielle - i.e. les mêmes algorithmes de choix dans les mêmes régions cérébrales - puissent être pareillement impliqués dans la prise de décision basée sur les valeurs subjectives. Pour ce faire, nous avons développé et validé un modèle de diffusion simplifié, inspiré par la théorie des champs décisionnel et le modèle EZ2, pouvant être ajusté aux jeux de données de petite taille générés par les paradigmes de choix économique. Ici également, les prédictions du modèle nous ont permis de guider l'analyse des données IRMf en conjonction avec des analyses de connectivité effective.

4. RESULTATS EXPERIMENTAUX

Article 1: Decision Threshold Modulation in the Human Brain

Philippe Domenech & Jean-Claude Dreher

Publié dans The Journal of Neuroscience, October 27, 2010 • 30(43):14305–14317

Behavioral/Systems/Cognitive

Decision Threshold Modulation in the Human Brain

Philippe Domenech and Jean-Claude Dreher
Cognitive Neuroscience Center, Reward and Decision-Making Group, Centre National pour la Recherche Scientifique, Unité Mixte de Recherche 5229, 69675 Bron, France and Université Lyon 1, 69003, Lyon, France

Perceptual decisions are made when sensory evidence accumulated over time reaches a decision threshold. Because decisions are also guided by prior information, one important factor that is likely to shape how a decision is adaptively tuned to its context is the predictability of forthcoming events. However, little is known about the mechanisms underlying this contextual regulation of the perceptual decision-making process. Mathematical models of decision making predict two possible mechanisms supporting this regulation: an adjustment of the distance to the decision threshold, which leads to a change in the amount of accumulated evidence required to make a decision, or a gain control of the sensory evidence, leading to a change in the slope of the sensory evidence accumulation. Here, we show that predictability of the forthcoming event reduces the distance to the threshold of the decision. Then, combining model-driven fMRI and the framework of information theory, we show that the anterior cingulate cortex (ACC) adjusts the distance to the decision threshold in proportion to the current amount of predictive information and that the dorsolateral cortex (DLPFC) codes the accumulation of sensory evidence. Moreover, the information flow from the ACC to the DLPFC region that accumulates sensory evidence increases when optimal adjustment of the distance to the threshold requires more complex computations, reflecting the increased weight of ACC's regulation signals in the decision process. Our results characterize the respective contributions of the ACC and the DLPFC to contextually optimized decision making.

Introduction

Recent advances in neuroscience and mathematical psychology have begun to unravel the neurobiological mechanisms underlying decision making (Gold and Shadlen, 2007). Perceptual decision making, the ability to select a specific action based on our perception, proceeds from the integration of sensory evidence to a categorical choice between alternatives (Smith and Ratcliff, 2004; Lo and Wang, 2006; Bogacz, 2007a). In sequential sampling models, this gradual gathering of sensory information favoring a particular choice is defined as a drift of an abstract decision variable toward a decision threshold. A choice is made when a decision variable is equal to its decision threshold (Carpenter and Williams, 1995; Hanes and Schall, 1996; Usher and McClelland, 2001). These mathematical models of decision making received renewed interest after the demonstration by monkey electrophysiological studies that perceptual choices are made when the ramping activity of neural populations in the dorsolateral prefrontal cortex (DLPFC) and the lateral intraparietal (LIP) area reaches a given threshold (Hanes and Schall, 1996; Kim and Shadlen, 1999; Huk and Shadlen, 2005; Hanks et al., 2006). The ramping rate of this neural activity, which represents the accumulation of sensory evidence, correlates with the decision variable predicted by sequential sampling models. In humans, fMRI studies confirmed the involvement of a similar DLPFC–intraparietal network in coding the decision variable (Heekeren et al., 2004; Forstmann et al., 2008; Ivanoff et al., 2008; Tosoni et al., 2008; van Veen et al., 2008).

One important factor that is likely to shape how a decision is adaptively tuned to its context is the predictability of the forthcoming event (Luce, 1991; Dayan and Abbott, 2001; Harrison et al., 2006; Doya, 2008). However, it remains unclear how decision making is modulated by this predictive information at both the behavioral and the neural levels. Sequential sampling models predict two mechanisms that modulate the decision based on contextual information (Carpenter and Williams, 1995; Reddi et al., 2003): (1) An adjustment of the distance to the decision threshold, which leads to a change in the amount of evidence required to make a decision, but no variation in the slope of the decision variable. According to this mechanism, higher predictability of forthcoming events would reduce the distance to the decision threshold (Fig. 1*a*, top panels). (2) An adjustment of the gain of sensory evidence, leading to a change in the slope of the decision variable, but not in the distance to the threshold. According to this hypothesis, higher predictability would increase the slope of the decision variable (Fig. 1*a*, bottom panels).

Here, we manipulated the amount of contextual information available to predict which stimulus is going to appear next (Fig. 1*b*). This allowed us to distinguish between these two hypotheses by characterizing the computational mechanisms underlying the effect of predictability on decisions. Then, having found that predictability modulates the distance to the threshold of the decision and not the gain control of sensory evidence, we identified the brain regions involved in this reg-

Received May 9, 2010; revised Aug. 15, 2010; accepted Aug. 23, 2010.

This work was funded by a FP6 International reintegration grant and a Fyssen Foundation grant to J.-C.D. P.D. was supported by a French Ministry of Research scholarship and a fellowship from Le Vinatier Hospital (CSRA 05). We thank the CERMEP - Imagerie du Vivant staff for their helpful assistance and Dr. C. Summerfield and E. Koechlin for comments on an early version of the manuscript.

Correspondence should be addressed to Philippe Domenech, Cognitive Neuroscience Center, Reward and Decision-Making Group, 67 Bd Pinel, 69675 Bron, France. E-mail: pdomenech@isc.cnrs.fr.

DOI:10.1523/JNEUROSCI.2371-10.2010

 0270-6474/10/3014305-13$15.00/0

ulation, as well as those coding the decision variable. Finally, we investigated how changes in effective connectivity between these distributed brain regions lead to contextually optimized perceptual decisions.

Materials and Methods

Subjects. Fourteen healthy right-handed subjects [8 males, mean age (±SD): 25.14 ± 3.37 years, mean right-handedness score as estimated by the Edinburgh scale (±SD): 0.86 ± 0.1, mean level of higher education (±SD): 3.6 ± 2.2 years] participated in the study (Oldfield, 1971). None of the participants showed any past or current neurological or psychiatric conditions, as assessed by a medical interview and all had normal or corrected-to-normal visual acuity. None of them was on medication at the time of the study. The experiment was approved by the local ethics committee. Subjects gave their written informed consent and underwent standard medical exams before participation.

Perceptual decision-making paradigm. Participants performed a GO/NO-GO task, in which they had to press a response button for a specific target shape (presented at the beginning of each sequence) among three possible shapes (Fig. 1*b*). Each participant performed the perceptual decision task on 12 randomly ordered unique sequences. All sequences consisted of the successive presentation of blue shapes (circle, square, or triangle) displayed at the center of a screen. At the beginning of each new sequence, the participant was shown one of the three shapes on a yellow background. This shape was the target for the current sequence. After 5 s of target display, the background turned black and the perceptual decision task began. Participants were instructed to press a response button held in their right hand each time they identified the current target, as quickly and as accurately as possible. Each sequence was composed of 400 successive stimuli presented for 300 ms every 400 ms (Fig. 1*b*). A fixation cross was presented for 10 s between two successive sequences. Unbeknownst to participants, there were two types of sequences (Fig. 1*b*): in first-order sequences, the next shape was conditioned on the last shape, whereas in second-order sequences, the next shape was conditioned on the last two shapes. Figure 1*c* shows a set of transition rules for a first-order sequence. Using the framework of Shannon's information theory, we computed for each decision the surprise (Eq. 1), which measures how unlikely an event is, and the predictive information on the forthcoming stimulus (Eq. 2–3), which measures how much the knowledge of the recent history (last shape or penultimate shape) reduces this surprise. Statistical transition rules were held constant within a sequence and varied between sequences. Moreover, both first- and second-order sequences were selected to fall into three categories based on their mutual information (first-order sequences: Eq. 4; second-order sequences: Eq. 5): zero (low), one-third (medium), and two-thirds (high) of the maximum theoretical mutual information (with a tolerance margin of 5%, Eq. 6). This procedure guaranteed a broad range of predictive information values during the experiment.

To minimize potentially confounding effects classically observed during sequential choices, statistical transition rules were constrained to ensure a low repetition probability ($p_{\text{repetition}} < 0.05$) and to minimize tandem repeats in sequences (Kornblum, 1969). Moreover, the pace of perceptual decisions was chosen in accordance with the psychophysical literature, which shows that the behavioral effect of surprise on response time (RT) is minimized when repetition probability is low and the interval between two perceptual decisions is short (Kornblum, 1969) and was further adjusted to guarantee a high level of accuracy (>90%). Sequences were selected to ensure average frequencies in the 0.05–0.45 range for each stimulus, thus controlling for oddball effect (Ranganath and Rainer, 2003) by ensuring that sequences did not contain rare events. All stimuli occurred with the same probability over the whole experiment. Finally, for each sequence, we selected the most sparsely distributed shape in the range 0.25–0.4 as the target. At the end of the scanning session, participants were systematically asked about "their awareness of regularities" as in Harrison et

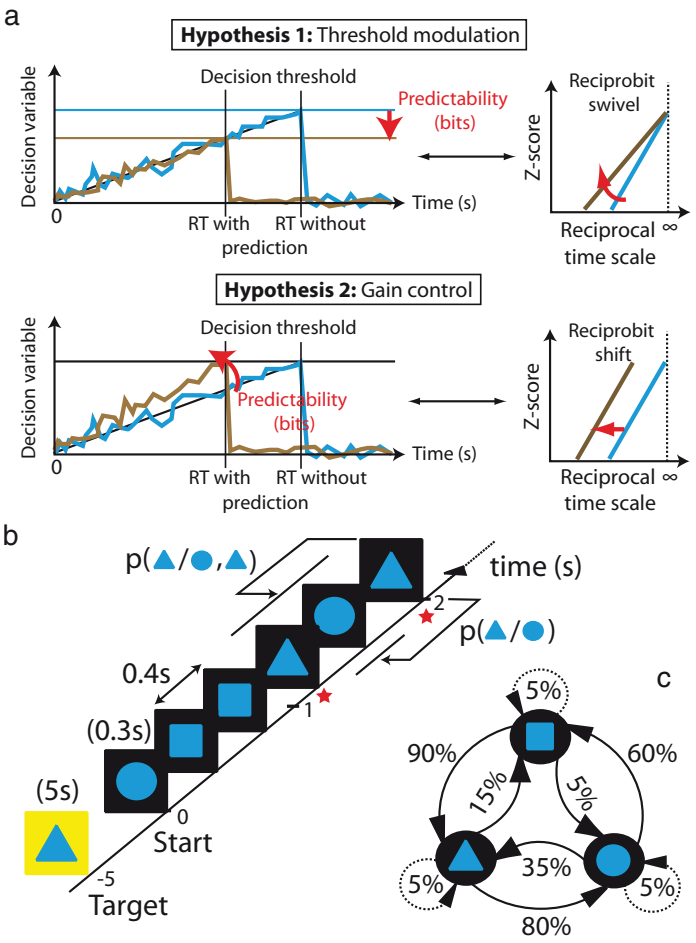

Figure 1. Hypothetical mechanisms by which predictability of forthcoming events modulates the decision-making process. ***a***, Left panels illustrate the progressive drifts of decision variables toward their respective decision threshold. They also correspond to the activity predicted by the decision model for neural populations accumulating sensory evidence. A decision is made when a decision variable equates its threshold. Right panels illustrate how the reciprobit analysis of RT distributions reveals distinct regulatory mechanisms of the decision process. Threshold modulation hypothesis: Reciprobit lines swivel toward lower RT when predictability increases (top right panel), reflecting the lowering of the decision threshold (top left panel). Gain control hypothesis: Reciprobit lines shift toward lower RT when predictability increases (bottom right panel), reflecting the faster rise of the decision variable toward the decision threshold (bottom left panel). ***b***, Task design. Participants had to identify a target shape out of three shapes by pressing a response button (red stars, ISI = 1.35 ± 0.76 s SD). Unbeknownst to the subjects, the next shape could be predicted on the basis of recent history. In first-order sequences, only the last trial had a predictive value on the next shape, whereas in second-order sequences, both the last and the penultimate trials had a predictive value on the next shape. ***c***, Example of a set of transition rules from a first-order sequence. Arrows represent transitions from one shape to the next one and transition probabilities are indicated nearby each arrow.

al. (2006). Only one subject reported he had noticed a pattern, once, during the experiment but could not give a specific example.

Working hypothesis. Bayesian formulations of perceptual decision making distinguish between the prior information (before observing the stimulus) and the accumulation of evidence in term of likelihood (during stimulus observation). In these formulations, the quantity accumulating evidence starts at different levels, according to the prior information. Evidence is then accumulated at a constant rate until the criterion is reached. In the context of our design, before the stimulus arrives, the predictive information (prior beliefs) will reset the level of activity and therefore change the distance to the decision threshold. From this perspective, the predictive information is a prior and the information conveyed by the stimulus represents the evidence entailed by its likelihood. Thus, our hypothesis was that both behavioral and fMRI data would be better explained by an adjustment of the distance to the decision threshold in proportion to the predictive information on the forthcoming stimulus than by a modulation of the slope of the decision variable.

Note that in our paradigm, we kept the level of sensory information constant (by using exactly the same three stimuli across the experiment). This does not mean that what is being integrated in the current paradigm is not sensory evidence. Indeed, perceptual decisions occur even when visual categorization may appear "unambiguous" while monkeys make saccades toward a target. For example, frontal eye field and lateral prefrontal cortex neurons exhibit a ramping activity that decrease after reaching a threshold value (Kim and Shadlen, 1999), both when manipulating the position (Hanes and Schall, 1996) or the color (Stanford et al., 2010) of unambiguous targets.

Thus, although information about local stimulus-response predictability is manipulated in the current study, it is not "integrated" over the decision process (what is being integrated is still sensory evidence). This approach mixing local stimulus-response predictability and perceptual decision making distinguishes our study from the neuroimaging literature investigating which brain regions encode measures of information theory, such as surprise and uncertainty (Huettel et al., 2005; Strange et al., 2005) or their influences on EEG components or corticospinal excitability (Bestmann et al., 2008; Mars et al., 2008).

Estimates of surprise and predictive information. In Shannon's information theory, the surprise of an event is defined by the current estimate of its marginal log-probability (abbreviated as u_t in Eq. 1). This measure has been considered as an instantaneous measure of the level of saliency (Harrison et al., 2006). For each new shape e_t, displayed at time step t, the current estimate of the surprise (u_t) is defined in the following way:

$$u_t(e_t = i) = -\log_2(\text{prob}_t(e_t = i)). \quad (1)$$

The predictive information of the upcoming event is an instantaneous measure of the loss of uncertainty about its occurrence due to the knowledge of the previous event(s) (also called "surprise reduction"). This last measure quantifies the amount of information available at a given time to predict the outcome of the ongoing perceptual decision and is poorly correlated with the surprise (a high level of predictive information does not necessarily mean that surprise is low). We computed both the predictive information conveyed by the last event (abbreviated as $p_{1,t}$ in Eq. 2) and by the last two events (abbreviated as $p_{2,t}$ in Eq. 3). For each new shape e_t, displayed at the time step t, current estimates of the predictive information ($p_{1,t}$ and $p_{2,t}$) are defined in the following way:

$$p_{1,t}(e_t = i, e_{t-1} = j) = \log_2\left(\frac{\text{prob}_t(e_t = i | e_{t-1} = j)}{\text{prob}_t(e_t = i)}\right) \quad (2)$$

$$p_{2,t}(e_t = i, e_{t-1} = j, e_{t-2} = k) = \log_2\left(\frac{\text{prob}_t(e_t = i | e_{t-1} = j, e_{t-2} = k)}{\text{prob}_t(e_t = i)}\right). \quad (3)$$

Supplemental Figure S1 (available at www.jneurosci.org as supplemental material) illustrates the trial-to-trial fluctuations of the predictive information conveyed by the last (Eq. 2) and by the last two (Eq. 3) shapes over the course of two exemplary sequences.

The average predictive information over a whole sequence of events is called the mutual information. By analogy with the predictive information, we computed the mutual information conveyed by the last event (abbreviated as $\text{Im}_{1,t}$ in Eq. 4) and by the last two events for each sequence (abbreviated as $\text{Im}_{2,t}$ in Eq. 5). Mutual information is maximum when a sequence is entirely determined (abbreviated as $\text{Im}_{\max}$ in Eq. 6). It is noteworthy that predictive information is an event-bound measure, whereas mutual information pertains to the average predictability in a sequence without relating to any specific event.

$$\text{Im}_{1,t} = \underset{t,i}{E}(p_{1,i}) \quad (4)$$

$$\text{Im}_{2,t} = \underset{t,i}{E}(p_{2,i}) \quad (5)$$

$$\text{Im}_{\max} = \log_2(k), \quad (6)$$

where k is the number of different shapes in a sequence.

Because participants learned the statistical structure of the sequence as stimuli were presented, we used a simple Bayesian learning scheme (an ideal Bayesian observer), in which all marginal and conditional probability estimates were updated after each new event. Our ideal Bayesian observer was initialized with flat prior distributions and was reset at the beginning of each new sequence to account for the lack of prior knowledge on the upcoming sequence (Harrison et al., 2006). For each new shape e_t, presented at time step t, current values of the marginal probability of the event i (Eq. 7) and of the joint probability of two successive events i and j (Eq. 8) and of three consecutive events i, j, and k (Eq. 9) are defined in the following way:

$$\text{prob}(e_t = i) = \frac{n_i^t + 1}{\sum_i n_i^t + 1} \quad (7)$$

$$\text{prob}(e_t = i, e_{t-1} = j) = \frac{n_{i,j}^t + 1}{\sum_{i,j} n_{i,j}^t + 1} \quad (8)$$

$$\text{prob}(e_t = i, e_{t-1} = j, e_{t-2} = k) = \frac{n_{i,j,k}^t + 1}{\sum_{i,j,k} n_{i,j,k}^t + 1}, \quad (9)$$

where $n_{i,j,k}^t$ is the number of triplets i, j, k at time step t; and $n_{i,j}^t$ is the number of duplets i, j at time step t.

We computed the surprise (Eq. 1) and the predictive information (Eqs. 2, 3) at each time step using the estimates provided by Equations 7–9.

Multilinear model of response times. Behavioral analyses were performed using the software packages R and Statistica (v7.1). We defined the error rate as the number of missed targets divided by the total number of targets over each sequence. Response times were calculated as the time elapsed between the onset of a target and the subject's response.

First, we searched for the best multilinear model of the observed RT using a descending strategy. The error rate, the surprise, the predictive information conveyed by the last shape and by the last two shapes (abbreviated respectively as p_1 and p_2), as well as all the first-order interactions between these explanatory variables were included in the "full" model. Akaike information criterion was minimized after the surprise and all first-order interactions were removed from the "full" model ($\beta_{\text{surprise}} = -0.015$, $p = 0.126$).

$$\text{RT} = \beta_0 + \beta_{p1} \times p1 + \beta_{p2} \times p2 + \beta_{\text{error rate}} \times (1 - \text{error rate}) + \varepsilon. \quad (10)$$

In the reduced behavioral model (Eq. 10), RTs are modeled as a weighted sum of explanatory variables in which the standardized parameter estimates of the model, such as β_{p1} and β_{p2}, are referred to as "behavioral" sensitivity because they represent the slope between response times and the amount of predictive information conveyed by the last and the penultimate shape. So, estimated βs correspond to the independent

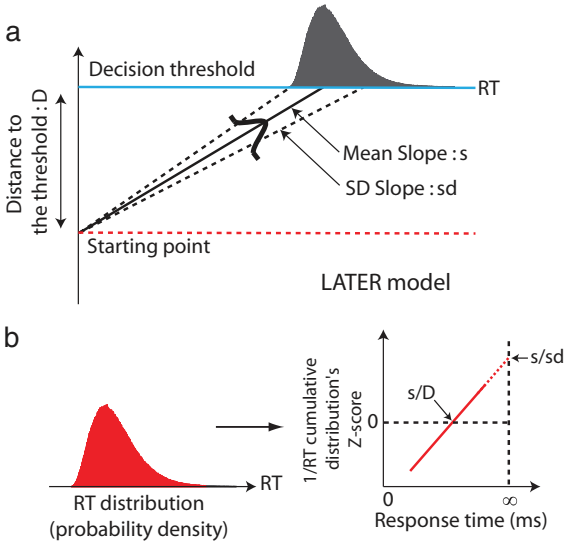

Figure 2. LATER model. ***a***, When a stimulus is presented, a decision signal rises linearly from the starting point (dashed red line) with an average slope s and a trial-to-trial standard deviation sd. When the signal reaches the decision threshold, a motor response is initiated. In the model, the amount of sensory evidence needed to reach a decision is represented by the difference between the starting point and the decision threshold, representing the distance to the threshold D (Reddi and Carpenter, 2000). ***b***, Relationship between RT distributions, reciprobit plots, and LATER model parameters. The reciprobit plot represents the cumulative 1/RT distribution, linearized by computing z-scores (probit transformation), as a function of RT. This graphical representation of RT distribution has two important features: (1) the intercept with the $x = \infty$ line solely depends on the mean slope of the decision process and is equal to s/sd; (2) the intercept with the $y = 0$ line is s/D (which depends on both the slope and the distance to the threshold).

contribution of each explanatory variable to the prediction of RT. This multilinear model is consistent with the relationship predicted by sequential sampling models of decision in which error rate and response times depend on the amount of predictive information available, while keeping the level of sensory information constant across trials. Note that, by construction of our design, there was no predictive information conveyed beyond the penultimate event available to predict the forthcoming event.

LATER model: how RT distributions are used to distinguish between the two modulation mechanisms of the decision process. In the LATER (linear approach to threshold with ergodic rate) model (Carpenter and Williams, 1995; Reddi and Carpenter, 2000; Reddi et al., 2003), the onset of a stimulus (e.g., a shape) is followed by the linear rise of a signal (decision variable) from a starting point (red dashed line) to a decision threshold D (Fig. 2*a*, blue line). A response is initiated when the decision signal reaches the threshold. On different trials, the slope of the decision signal varies randomly, but is distributed as a Gaussian probability density function with mean slope s and with standard deviation sd (Hanes and Schall, 1996). So, according to the LATER model, the distribution of RT reflects the projection of the decision variable on the decision threshold and depends on three parameters: the distance to the threshold (difference between the starting point and the decision threshold), the mean slope, and its standard deviation (as stated in Eq. 11 and Fig. 2).

Equation 11 simply expresses that, under the LATER model, the main decision process yield 1/RT following a normal distribution, with mean s/D and with standard deviation sd^2/D^2. In addition, fast guesses are modeled as an additional normal distribution, whose mean is equal to zero, and its own standard deviation.

$$1/\mathrm{RT} \rightarrow N\left(\frac{s}{D}, \frac{\mathrm{SD}^2}{D^2}\right). \quad (11)$$

Since 1/RT of the main process is normally distributed (Eq. 11), it is possible to compute z-scores that express the divergence of the observed 1/RT from the median 1/RT. Plotting z-scores of 1/RT's cumulative distribution against RT plotted on a reciprocal time axis yields a straight line, which is called a reciprobit plot (as illustrated in Fig. 2*b*). This graphical representation is useful because the resulting line intersects z-score $= 0$ at the median latency s/D, which depends on both the mean slope (s) and the distance to the threshold (D), whereas it intersects RT $= \infty$ at a point that does not vary with the distance to the decision threshold (Fig. 2*b*). Importantly, the mathematical properties of the reciprobit transformation provide us with a graphical representation that distinguishes between the two modulation mechanisms in the LATER model (see Fig. 1*a*): (1) if the modulation mechanism is an increase of the slope (sensory evidence gain control), then both intersects will vary in the same proportion and the line will shift (Fig. 1*a*, lower right panel); and (2) if the modulation mechanism is a decrease of the decision threshold, then only the z-score $= 0$ intersect will vary, which will result in a swivel of the reciprobit line around the RT $= \infty$ intersect (Fig. 1*a*, upper right panel).

To summarize, the reciprobit transformation directly allows us to derive the z-scores of 1/RTs cumulative distribution from the RT distribution. From these z-scores, it is then possible to estimate the parameters of the LATER model (distance to the decision threshold, mean slope, and sd of the slope) that best fit the data and to perform a Bayesian statistical test to identify the mechanisms of regulation that best explain the changes between conditions (decision threshold modulation or gain control of the sensory evidence).

Psychophysics: LATER model and reciprobit plots. To assess the mechanism underlying the effect of predictive information on decision, we performed a standard reciprobit analysis (Carpenter and Williams, 1995; Reddi et al., 2003).

First, we normalized each participant RT dataset to the population's average and standard deviation. Then, we pooled all the RT datasets together and collapsed the behavioral data from first- and second-order sequences using the optimal amount of predictive information. Next, we discretized each participant RT dataset into equal bins and excluded from further analysis those that did not contain enough data to allow for reliable fits of the decision model. This constraint led us to exclude the 5% lowest predictive information values from further analyses. This is because, in our experiment, the distribution of predictive information had a long tail toward low values. By the end of these preprocessing steps, we had sorted RT data into 6 bins with continuously increasing levels of predictive information ($[-0.43, -0.05, 0.25, 0.62, 1, 1.32]$ bits).

Then, we performed a reciprobit transformation on the resulting RT distributions. This transformation is based on the LATER model and makes testable predictions about how RT distributions should change according to two different modulation mechanisms: distance to the decision threshold or sensory evidence accumulation rate (Carpenter and Williams, 1995; Gold and Shadlen, 2007) (Fig. 1*a*). Plotting the reciprobit lines, which are linearized cumulative RT distributions plotted on a reciprocal time scale, highlights those changes.

In addition to this qualitative assessment of the mechanism regulating the decision process, we used a Bayesian model selection strategy to identify the regulation mechanism that most likely explained the changes observed in RT distributions across levels of predictive information. To do so, we fitted a LATER model using a standard simplex minimization routine and a likelihood-based cost function under the hypotheses that changes in RT distribution either resulted from changes in the sensory evidence accumulation rate or resulted from changes in the distance to the threshold. Model comparison was performed by fitting the LATER model for each experimental condition in such a way that either the slope or the distance to the decision threshold was fixed across condition, depending on the hypothesis tested. Finally, we computed the log likelihood ratio between the two hypotheses ($L_{\mathrm{DT}} - L_{\mathrm{Gain}}$, difference between the log likelihood of the distance to the threshold modulation, L_{DT}, and the log likelihood of the gain control mechanism, L_{Gain}) and used the cutoff value of the Bayesian factor ($L_{\mathrm{DT}} - L_{\mathrm{Gain}} \geq 2.3$) (Jeffrey, 1998) to assess the significance level of our result. For example, a log likelihood ratio equal to 4.6 indicates that a modulation of the distance to the

threshold is 100 times more likely than a gain control of the sensory evidence ($e^{4.6} = 100$).

To assess whether our finding that predictive information modulates the decision threshold depended on some specific aspect of the LATER model, we also fitted a Ratcliff's drift-diffusion model (RDM) to our data using the "D-mat" toolbox (Vandekerckhove and Tuerlinckx, 2008) (http://ppw.kuleuven.be/okp/software/dmat/). However, because the RDM has been specifically formulated for two-alternative choices, it was not possible to use its standard formulation. Because our experiment is a GO/NO-GO task, subjects only responded to one target, which implies that there were no RT distributions for false-negative trials (no response for a GO trial) and for true-negative trials (no response for a NO-GO trial). Therefore, we adapted the D-mat toolbox to fit a GO/NO-GO version of the RDM on our data: first, we modified the loss function to only fit a "hit" RT distribution (Vandekerckhove and Tuerlinckx, 2008); second, we fixed the relative position between the starting point and the boundaries, which means that the changes in the distance from the starting point to the boundary were a priori attributed to the boundary parameter. Overall, our version of the RDM ("single boundary" RDM) retained from the version implemented in the D-mat toolbox the drift-diffusion mechanism, the upper decision boundary, the explicit account of nondecision time (and of its variability), and the variability in the starting point. This version of the RDM was adequate because we only estimated parameters relating to "hit" RT distributions. Note that if we had investigated errors RT distributions and error rates, an implicit lower boundary would also have been necessary (Gomez et al., 2007; Ratcliff and McKoon, 2008).

With these modifications of the D-mat toolbox, it was possible to reliably retrieve the distance to the decision threshold and the slope parameters from synthetic RT datasets. Moreover, we assessed the ability of the "single-boundary" RDM to correctly identify the modulation mechanism underlying changes between conditions using only the hit RT distribution and a Bayesian selection strategy [Bayesian information criterion (BIC); smaller values mean a better model in terms of goodness of fit and parsimony]. In the slope condition (a synthetic RT dataset simulating a change in the slope of the accumulation of evidence), the model in which the drift rate parameter was set free between conditions had the best Bayesian information criterion (BIC drift rate = 41,162, BIC boundary = 55,167). In the threshold condition (a synthetic RT dataset simulating a change in the distance to the threshold), the model in which the boundary parameter was set free between conditions had the best Bayesian information criterion (BIC drift rate = 43,441, BIC boundary = 43,075).

Finally, we performed a Bayesian selection analysis among drift-diffusion models instantiating three alternative mechanisms (distance to the decision threshold, nondecision time, average slope of diffusion process) on our own RT dataset.

fMRI data acquisition. Subjects were scanned at the CERMEP - Imagerie du Vivant using a research dedicated 1.5 T MRI scanner (Siemens Magnetom Sonata with an eight-channel head coil). We acquired 800 echo-planar T2*-weighted functional volumes (200 volumes/run, 4 runs) per experiment. Each volume comprised 28 slices acquired continuously over 2.65 s (TE = 60 ms; interleaved acquisition; slice thickness 4 mm; 0.4 mm noncontiguous; parallel to the subject's Sylvian fissure plane; angle to AC–PC: 20–30°; in-plane resolution: 3.44×3.44 mm^2; matrix size: 64×64), allowing complete brain coverage. Additionally, T1-weighted images were acquired at the end of each experiment (MP-RAGE: TR = 1970 ms; TE = 3.93 ms; T1 = 1100 ms; resolution: $1 \times 1 \times 1$ mm^3; matrix size: 256×256). Head motions were minimized using foam padding and headphones with earplugs were used to dampen the scanner noise.

fMRI data preprocessing. Data preprocessing was performed using the Statistical Parametric Mapping software (SPM2b, Wellcome Department of Imaging Neuroscience, University College London, UK, www.fil.ion.ucl.ac.uk/spm). The first three volumes of each run were removed to allow for T1 equilibrium effects (197 volumes/run). Before statistical analysis, we applied a slice-timing correction using the time center of the volume as reference. Then, head motion correction was applied using rigid-body realignment. We used realignment parameters during the statistical analysis as covariates to model out potential nonlinear head motion artifacts. Functional and morphological images were then normalized into standard MNI space using SPM's default templates. Finally, functional volumes were resampled and smoothed with an 8 mm FWHM Gaussian kernel. A 256 s temporal "high-pass filter" regressor set was included in the design matrix to exclude low-frequency noise and artifacts.

Finally, we explored the data for potential artifacts using tsdiffana, mean and variance images (http://imaging.mrc-cbu.cam.ac.uk/imaging/DataDiagnostics). An artifact is defined as the co-occurrence of a variance spike and a mean intensity drop uncorrelated with experimental design. Only the last two volumes of one participant's session met these criteria and were modeled as confounds in the design matrix. Translational movements estimated during the realignment procedure were small as compared to the voxel size (<1 mm).

General linear model 1: main fMRI data statistical analysis. Whole-brain statistical parametric analyses were performed using a two-stage random-effect approach. We estimated independently the model parameters from each subject's dataset and then made population inferences using the parameter intersubject variance. Regressors of interest were constructed by convolving functions representing the events with the canonical hemodynamic response function. Three event-related categorical regressors ("stimulus regressor," "decision-related regressor," and "motor regressor") and three parametric regressors (surprise, predictive information conveyed by the last shape, and predictive information conveyed by the last two shapes) were used to model the events occurring during the sequences (Fig. 3).

(1) The first regressor modeled the visual stimulation as 0.3-s-long boxcar functions time locked to the onset of visual stimuli (referred to as the "stimulus regressor").

(2) The ongoing processes during perceptual decision formation (referred to as the "decision-related regressor") were modeled as boxcar functions convolved with the response time duration, time locked to each target onset. Because this condition pooled the decision-related activity regardless of the context in which it took place, it modeled the part of the decision-related activity not modulated by its context. Three parametric regressors were added to the decision-related regressor to account for the effect of surprise (Eq. 1) and predictive information (Eqs. 2, 3) on the decision process. These parametric regressors were hierarchically orthogonalized in the following order: surprise, predictive information conveyed by the last shape only, and predictive information conveyed by the last two shapes. This orthogonalization hierarchy naturally emerged from the mathematical definitions of the parameters (Büchel et al., 1998) and unambiguously separated the effect of the information conveyed by the last shape from the information conveyed by the penultimate shape into two parametric regressors. To build these regressors, we weighted each event of the decision-related regressor by the current, and continuously updated, estimates of the parameters, so that each event was characterized by its own set of parameter values.

(3) Finally, the last categorical regressor modeled the motor response associated with the button press, and was modeled as a Dirac function using the timing of the button press as onset. Thus, our model explicitly separated the motor-related activity from the decision-related activity.

Statistical inferences were performed with a threshold of $p < 0.05$ (clusterwise) familywise error (FWE) corrected across the whole brain ($p < 0.001$ voxelwise) (see supplemental Tables S1, S2, available at www.jneurosci.org as supplemental material).

Correlation between "neural" and "behavioral" sensitivity to predictive information. We reasoned that blood oxygenation level-dependent (BOLD) activity in a brain region modulating the distance to the threshold should be predictive of each participant's RT variations (Figs. 4, 5). Thus, we performed a correlation analysis between the sensitivity to predictive information estimated from brain activity and the sensitivity to predictive information estimated from response times for both the information conveyed by the last and the penultimate shape.

To measure the "behavioral" sensitivity to predictive information, we fitted the multilinear model of RT previously identified to each individual RT set, thereby estimating its βs (Eq. 10). Here, the βs are measures of the slope of the decrease in response time with increasing predictive

information conveyed by the last and the penultimate shape, regardless of the current accuracy level. This analysis yielded a behavior-based measure of the individual ability to use the predictive information conveyed by the last shape and the penultimate shape to modulate the distance to the threshold. Then, to measure the "neural" sensitivity to predictive information, we extracted for each participant, and in every brain region found to be sensitive to predictive information in the main fMRI analysis [region of interest (ROI)-based approach using MarsBaR toolbox v0.38, $p < 0.001$ voxelwise; see below, ROI analyses], the β estimates of the parametric regressors, which provided us with measures of the slopes of the decrease between event-related BOLD activity with increasing predictive information conveyed by the last shape and the penultimate shape.

Finally, we performed nonparametric correlation analyses between individual "behavioral" and "neural" sensitivity to identify the brain regions in which the slope of the relationship between predictive information and BOLD activity was predictive of the slope of the relationship between predictive information and RT (Spearman's correlation) (see supplemental Table S1, available at www.jneurosci.org as supplemental material).

General linear model 2: controlling for potential confounding effects in the anterior cingulate cortex. To assess the specificity of our fMRI findings, we performed an additional statistical parametric analysis, in which we added to the general linear model (GLM) 1 (see Figs. 3, 6) three parametric regressors to the "decision-related" regressor, orthogonalized in the following order: the first four parametric regressors controlled for the effects of error likelihood, prediction error, entropy, and surprise, whereas the following two parametric regressors modeled the modulation of BOLD signal by the predictive information conveyed by the last shape and the predictive information conveyed by the penultimate shape. This procedure ensured that any potential confounding effect from the error likelihood, prediction error, entropy, and surprise were removed from the estimation of the effects of the predictive information parametric regressors.

The error likelihood parametric regressor was computed for each sequence from participant error rates during target trials. The error prediction parametric regressor (δ_t) was computed using a standard Rescorla–Wagner algorithm (Dayan and Abbott, 2001), whose learning parameter (α) was adjusted to maximize the correlation between participants RTs and $\mathrm{Prob}_t(e_t = i|e_{t-1} = j)$, the reinforcement learning estimate of the conditional probability of a shape (e_t) at the time step t given the last shape (e_{t-1}) (Eqs. 12, 13). Finally, B_t is a binary function equal to 1 when the expected event actually occurs ($e_t = i$) and to 0 if it does not ($e_t \neq i$) (Eq. 13). The best fit of the Rescorla–Wagner algorithm was obtained for a learning rate $\alpha = 0.08$ (range explored 0.01–0.15).

$$\mathrm{Prob}_{t+1}(e_{t+1} = i|e_t = j) = \mathrm{Prob}_t(e_t = i|e_{t-1} = j) + \alpha \times \delta_t \quad (12)$$

$$\delta_t = B_t(1 - \mathrm{Prob}_t(e_t = i|e_{t-1} = j)). \quad (13)$$

Then, the entropy parametric regressor was computed for each shape from Equation 14. The entropy is classically viewed as an information-theoretic equivalent to the concept of conflict (Berlyne, 1957).

$$H_t = \underset{t,i}{E}(u_{t,i}) \quad (14)$$

General linear model 3: correlation between BOLD activity and LATER model parameters. To assess the correlation between LATER model parameters and BOLD activity, we built and estimated a second variant of GLM 1, in which we sorted the events previously included in the "decision-related" regressor (Fig. 3) into four discrete levels of predictive information ([−0.3, 0.18, 0.72, 1.22] bits), which divided the range of predictive information into bins of equal size (see above, Psychophysics: LATER model and reciprobit plots). Each bin included enough data to reliably perform individual fits of the LATER model.

Then, using these four levels of predictive information, we built four distinct categorical regressors, in which each event was modeled using a Dirac function time locked on the onset of the target. These four categorical regressors replaced the "decision-related" regressor of GLM 1 (Fig. 3). GLM 1 and GLM 3 were otherwise identical.

This procedure allowed us to perform nonparametric correlation analyses (Spearman's correlation) between BOLD activities at the time of decision averaged over the four levels of predictive information for each participant and the corresponding averaged LATER model's parameter estimates (Figs. 5*c*, 7*c*) (see below, ROI analyses).

ROI analyses. We extracted ROI average of estimated βs for the three parametric regressors included in GLM 1 and for the four categorical regressors modeling the levels of predictive information in GLM 3. To do so, ROIs were built from functional clusters from GLM 1 ($p < 0.001$, voxelwise) intersected with a 6-mm-radius sphere centered on the cluster's peak voxel using the MarsBaR toolbox (v0.38, http://marsbar.sourceforge.net).

Conjunction analysis. We performed a conjunction analysis testing the conjunction null (Nichols et al., 2005), using SPM2b to identify clusters that exhibited significant negative parametric effects for predictive information conveyed by the last and the penultimate shape at the onset of decisions. However, because conjunction tests are not as sensitive as single-contrast testing for the average effect over all contrasts and thus underestimate the underlying effect (Friston et al., 2005), and because we had a strong a priori hypothesis regarding the involvement of the DLPFC in implementing the decision variable, here inferences were performed with a level of significance of $p < 10^{-3}$ uncorrected (Fig. 7).

Structural equation modeling. First, to characterize functional subdivisions between the anterior and posterior DLPFC, we built a morphologi-

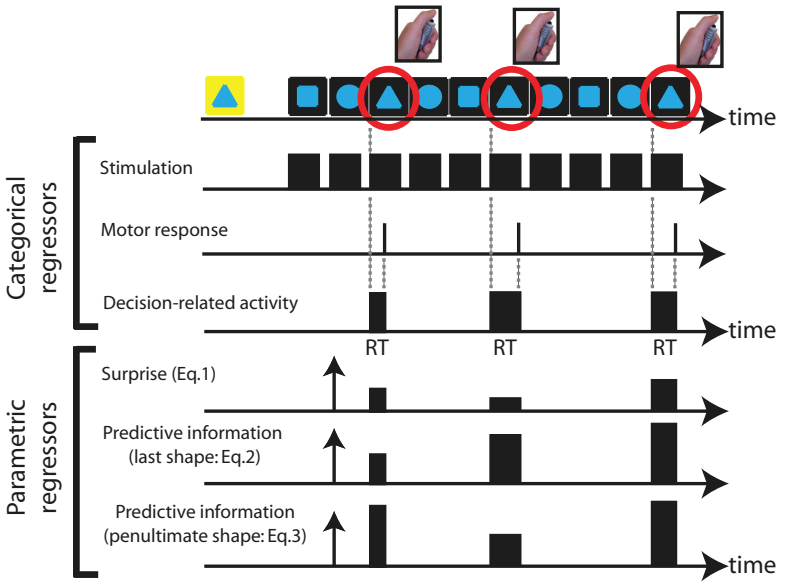

Figure 3. Regressors included in the statistical analysis of fMRI data. The main GLM included three categorical and three parametric regressors (see Materials and Methods, General linear model 1: main fMRI data statistical analysis). The three categorical regressors modeled the main steps of perceptual decision making: sensory processing, decision-related activity and motor response. Three parametric regressors were derived from the decision-related regressors and hierarchically orthogonalized. These parametric regressors modeled the modulation of BOLD activity at the time of decision by the surprise and the predictive information conveyed by the last and the penultimate shape.

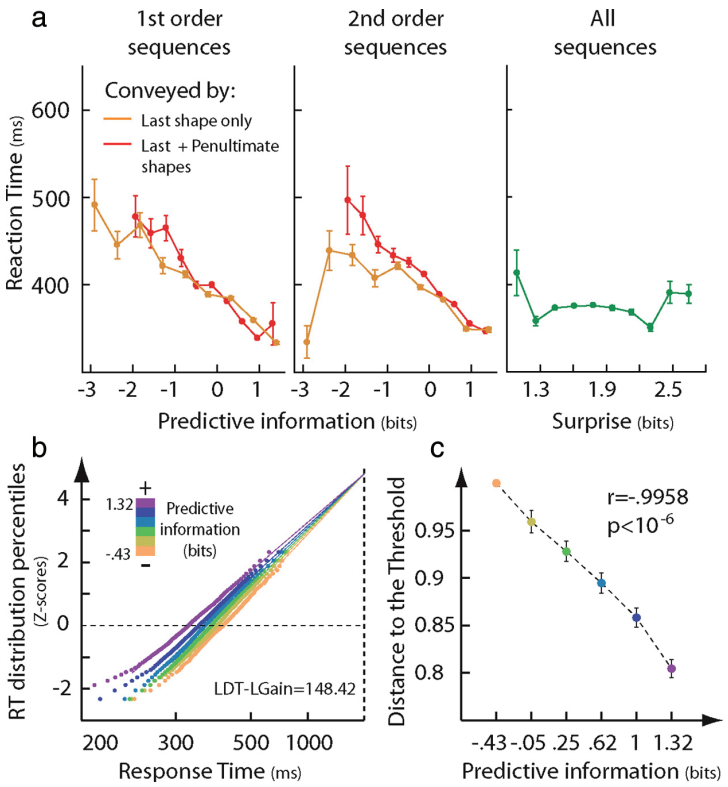

Figure 4. Higher predictive information reduces the distance to the decision threshold. ***a***, RT decreased as predictive information increased in first-order [left panel: $r_{p1} = -0.295$ (orange), $r_{p2} = -0.273$ (red), both $p < 10^{-6}$] and second-order sequences [middle panel: $r_{p1} = -0.235$ (orange), $r_{p2} = -0.292$ (red), both $p < 10^{-6}$]. During second-order sequences (middle panel), RTs were better correlated with the predictive information conveyed by the last two shapes (red) than with the predictive information conveyed by the last shape only (orange) but not during first-order sequences (left panel), indicating that all available predictive information was used in the regulation of the decision process. Finally, there was no effect of surprise (right panel, green) on RT ($r_{surprise} = -0.02$, $p = 0.126$). ***b***, Reciprobit plot based on pooled RT from all participants showing a swivel toward lower RT when predictive information increases, as hypothesized in Figure 1*a* (upper right panel). This aspect is confirmed by the log likelihood ratio ($L_{DT} - L_{Gain}$), in accordance with the hypothesis of the modulation of the distance to the threshold. ***c***, Distance to the decision threshold as a function of the level of predictive information available. Error bars represent 95% confidence intervals of the distance to the threshold. The color code represents the same levels of predictive information in both panels (from −0.43 to 1.32 bits).

cal ROI of the DLPFC (WFU PickAtlas atlas v2.4, http://fmri.wfubmc.edu, dilatation parameter = 2 voxels, bilateral mask including BA9, BA10, and BA46 from WFU PickAtlas built-in atlas, volume = 5994 voxels) and computed statistical maps of the parametric effect of the predictive information conveyed by the last shape and the penultimate shape ($p < 0.001$ voxelwise). From this analysis, we isolated four functional subregions whose activity reflected the amount of predictive information at the moment of the decision ($p < 0.05$ clusterwise, SVC): left anterior DLPFC, right anterior DLPFC, left posterior DLPFC, and right posterior DLPFC.

Then, we extracted ROI-averaged time series during first- and second-order sequences for each participant from 6-mm-radius spheres centered at the peak voxel of the four brain regions identified in the DLPFC (Fig. 8, dashed white circles) and the anterior cingulate cortex (ACC) (Fig. 8, plain white circle) ($N = 5124$ volumes for each brain region and condition, no missing values or deleted data). Structural equation modeling was performed using the Mx software package (v1.65b). Figure 8 represents the path diagram as arrows to indicate directional or symmetric connections between the functional regions included in the model. We performed a maximum-likelihood-based estimation of the model path coefficients on the correlation matrix derived from the two resulting time series and statistical inferences on path coefficient variations between the first- and second-order sequences using a nested model approach (supplemental Table S3, available at www.jneurosci.org as supplemental material) (no convergence problems or inadmissible solutions).

The overall model fit was assessed with standard goodness of fit indices, all indicated a good quality of fit (normed fit indices = 0.91, centrality index = 0.9, and relative noncentrality indices = 0.91; index values above 0.9 indicate a good quality of fit) (Mueller, 1996).

Functional connectivity analysis. To identify brain regions that were functionally coupled with the ACC, we assessed the correlation between BOLD activity in this "seed" region and BOLD activity in each voxel of the brain. To do so, we extracted the cluster-averaged time course from the functional cluster we found in the ACC (Fig. 5*a*) (ROI-based approach using MarsBaR toolbox v0.38, $p < 0.001$ voxelwise; see above, ROI analyses) and included this time course as a regressor not convolved with a hemodynamic response function in a GLM. This GLM also included a 256 s low-pass filter and head motion parameters as regressors of noninterest. We then computed group-level SPM using the standard SPM's RFX approach. Supplemental Figure S6 (available at www.jneurosci.org as supplemental material) shows the main result of this analysis with a threshold of 5% voxelwise, FWE corrected across the whole brain.

Results

Psychophysics: predictive information reduces the distance to the threshold of the decision

RT decreased linearly as predictive information increased (Fig. 4*a*, left and middle panels), showing that participants successfully used the statistical structure of sequences to predict the forthcoming shape. Moreover, participants adjusted to the actual structure of the sequences (first or second order) to exploit all the predictive information available. Indeed, RTs were better correlated with the predictive information conveyed by the last two shapes (last shape and penultimate shape, r_{p2}) (Fig. 4*a*, red line) than with the predictive information conveyed by the last shape only (r_{p1}) (Fig. 4*a*, orange line) during second-order sequences, but not during first-order sequences (Fig. 4*a*) (Hotelling's *t*, first-order sequences, $r_{p1} = r_{p2}$; $p = 0.98$; second-order sequences, $r_{p1} = r_{p2}$; $p < 10^{-6}$). We also assessed the contribution of the source (last or penultimate shape) of predictive information on decision response time by fitting a multilinear model to all participants' RTs (see Materials and Methods, Multilinear model of response times). Predictive information had the same influence on RT whether it was conveyed by the last shape ($\beta_{p1} = -0.148 \pm 10^{-2}$, $p < 10^{-5}$) or by the penultimate shape ($\beta_{p2} = -0.148 \pm 10^{-2}$, $p < 10^{-5}$; $\beta_{p1} = \beta_{p2}$, $t = -3.97 \pm 10^{-4}$, $p = 0.49$), showing that the efficiency of the modulation did not depend on the source of the information. This decrease in RT with increasing predictive information did not occur at the cost of accuracy, as shown by a factorial analysis crossing the type of sequence (first order or second order) and the predictive infor-

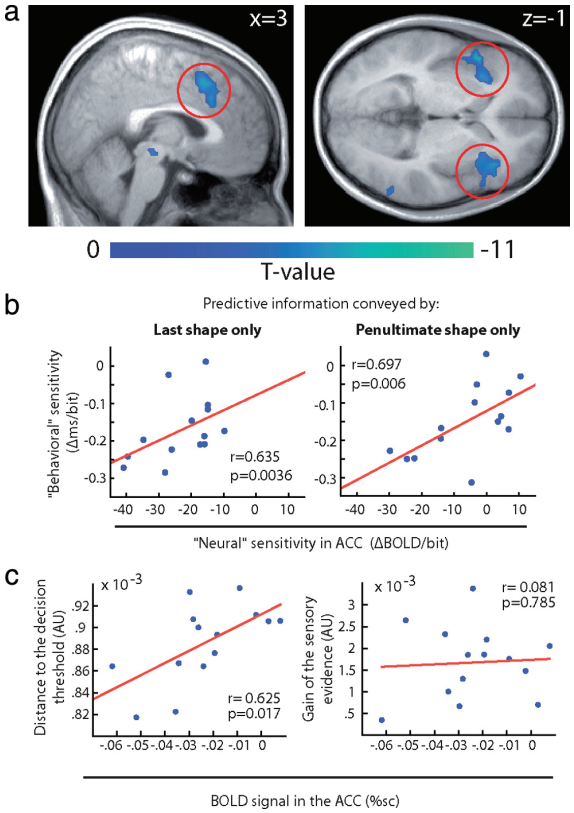

Figure 5. Event-related response in the ACC predicts individual ability to use predictive information to modulate the distance to the threshold. ***a***, Parametric response to the amount of predictive information conveyed by the last shape (rendered with a threshold of $p < 10^{-3}$ uncorrected, activations surviving a threshold of 5% clusterwise corrected across the whole brain are circled in red). The color scale represents the slope of the decrease in activity for an increasing amount of predictive information conveyed by the last shape. Note that it does not reflect deactivation. Also note that additional brain regions (not shown here) also survived the statistical threshold used and are listed in supplemental Table S1 (available at www.jneurosci.org as supplemental material). ***b***, Scatter plots of correspondence between "neural" and "behavioral" sensitivities to predictive information in the ACC ($n = 14$). For each participant, the two sensitivity measures link event-related responses in the ACC and modulation of RTs. (See Materials and Methods, Correlation between "neural" and "behavioral" sensitivity to predictive information.) Individual differences in "behavioral" sensitivity to predictive information conveyed by the last shape (left) and the penultimate shape (right) were predicted by individual differences in "neural" sensitivity in the ACC. Higher "behavioral" sensitivity to predictive information directly reflects the ability to modulate the distance to the threshold. ***c***, Scatter plots of correspondence between BOLD signal change in the ACC and the distance to the decision threshold (left panel) or the gain of the sensory evidence (right panel). Each point represents the BOLD signal change in the ACC plotted against the distance to the decision threshold estimated using the LATER model averaged over the four levels of predictive information (−0.3, 0.18, 0.72, 1.22 bits) for each subject.

mation averaged over each sequence (supplemental Fig. S2, available at www.jneurosci.org as supplemental material; Eqs. 4, 5). Finally, there was no effect of surprise on RT in our experiment, as expected from previous literature (Fig. 4*a*, right panel) (Kornblum, 1969).

Next, to identify which of the two predicted mechanisms—modulation of the distance to the threshold or gain control of the sensory evidence—mediated the effect of predictive information on decision making, we fitted a LATER model to the RT distribution of the subjects' responses and compared the likelihood of the two modulation mechanisms (Carpenter and Williams, 1995; Reddi et al., 2003). The modulation of the distance to the threshold by predictive information was significantly more likely than a gain control of the sensory evidence [log likelihood ratio, defined as the difference between the log likelihood of the distance to the threshold modulation hypothesis (L_{DT}) and the log likelihood of the gain control hypothesis (L_{Gain}), $L_{DT} - L_{Gain} = 148.42$, which is "decisive" according to Bayesian inference theory] (Jeffrey, 1998). Moreover, individual model fits showed that all the participants used predictive information to modulate their distance to the decision threshold, except for two participants for whom data did not allow to conclusively select a mechanism over the other (supplemental Fig. S3, available at www.jneurosci.org as supplemental material). Then, we performed a reciprobit analysis of the population's RT distribution (linearization of RT cumulative distribution resulting in "reciprobit lines") (see Materials and Methods, Psychophysics: LATER model and reciprobit plots, and Fig. 4*b*). This analysis provided us with a graphical representation of the mechanism modulating decision RT based on the variations of the reciprobit line for increasing amounts of predictive information: if the distance to the threshold decreases, then the line swivels around an intercept point toward lower RT (as in Fig. 1*a*, top right panel). By contrast, if the slope of the decision variable increases, then the line shifts toward lower RT (as in Fig. 1*a*, bottom right panel). The swivel of the reciprobit line with increasing levels of predictive information observed in Figure 4*b* further confirmed the reduction of the distance to the threshold by higher predictive information (supplemental Fig. S3, available at www.jneurosci.org as supplemental material). Finally, we observed a strong negative correlation between the distance to the threshold and predictive information ($r = -0.995$, $p < 10^{-6}$) (Fig. 4*c*).

These results did not depend on specific features of the LATER model since fitting a drift-diffusion model to our dataset also led to the conclusion that predictive information modulates the distance to the threshold (log likelihood ratio, $L_{DT} - L_{Gain} = 89.051$). Furthermore, there was an excellent agreement between the distance to the threshold estimated using the LATER and the drift-diffusion models for all levels of predictive information ($r = 0.99$, $p = 10^{-6}$).

Thus, our behavioral results demonstrate that the effect of predictive information on decision RT is mediated by the modulation of the distance to the decision threshold, not by gain control, and uses all the predictive information available to minimize decision RT.

Brain network responding to predictive information

In parallel with our behavioral results showing faster RTs with increasing predictive information (Fig. 4*a*), we investigated the relationship between decision-related brain activity and predictive information (see Materials and Methods, General linear model 1: main fMRI data statistical analysis; and Fig. 3). The results revealed a negative correlation between predictive information conveyed by the last shape and the BOLD activity in the ACC, the inferior frontal gyri bilaterally, the right intraparietal sulcus region (IPS), and the DLPFC bilaterally ($p < 0.05$ clusterwise corrected for multiple comparisons across the whole brain) (see Fig. 5*a* and supplemental Table S1, available at www.jneurosci.org as supplemental material).

These patterns of decision-related activity were preserved when adding prediction errors, error likelihood, entropy (which is a proxy for conflict), and surprise as potential confounds in a new analysis, supporting the specificity of the relationship between BOLD activity in all these brain regions and predictive information (supplemental Table S2, available at www.jneurosci.

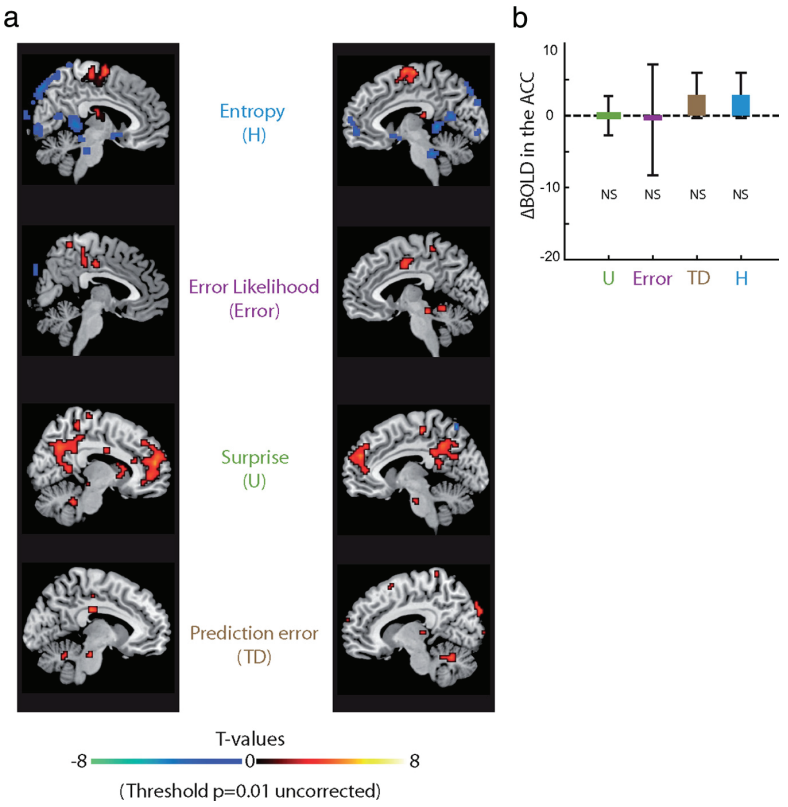

Figure 6. Whole-brain analysis of parametric responses to entropy, surprise, error likelihood and prediction error. ***a***, Statistical maps are rendered with a very lenient uncorrected threshold of $p = 0.01$ to illustrate the absence of effect of these potential confounds in the ACC. Left and right sagittal views are shown in the left and right columns. The cold color scale represents negative correlations and the hot color scale represents positive correlations. ***b***, ROI-average parametric response in the ACC to surprise (*U*), error likelihood (Error), prediction error (TD), and entropy (*H*). None of the four parametric regressors explained a significant portion of the BOLD activity in the ACC (NS, not significant).

org as supplemental material; and see Materials and Methods, General linear model 2: controlling for potential confounding effects in the anterior cingulate cortex). This additional analysis excludes alternative interpretations of the ACC's response in terms of conflict monitoring, postdecisional prediction errors, and error monitoring (Fig. 6; supplemental Fig. S4, available at www.jneurosci.org as supplemental material) (Holroyd and Coles, 2002; Botvinick et al., 2004; Brown and Braver, 2005).

The anterior cingulate cortex modulates the distance to the threshold of the decision

Within the brain regions showing a parametric response to predictive information (supplemental Table S1, available at www.jneurosci.org as supplemental material), we then assessed whether individual differences in brain activity during decision making predicted individual differences in the ability to exploit predictive information to reduce response time (see Materials and Methods, Functional connectivity analysis). From our behavioral analyses showing that the modulation of the distance to the threshold results in a linear decrease of RT with increasing predictive information (Fig. 4), we predicted that in the brain regions modulating the distance to the threshold, individual differences in "neural sensitivity," defined as the slope of the decrease in event-related activity as predictive information increased, should predict "behavioral sensitivity," i.e., the slope of the decrease in RT as predictive information increased. The ACC was the only brain region in which individual differences in event-related response ("neural" sensitivity) predicted each individual's ability to use the information available to modulate the distance to the threshold ("behavioral" sensitivity) (Fig. 5*b*). Moreover, this link between ACC's function and modulation of the distance to the decision threshold was further supported by the positive correlation between ACC's BOLD activity and distance to the decision threshold ($r = 0.625$, $p = 0.017$) (Fig. 5*c*, left panel), but not between ACC's BOLD activity and the slope of the accumulation of sensory evidence ($r = 0.081$, $p = 0.785$) (Fig. 5*c*, right panel). Together, these results demonstrate that the ACC is involved in adjusting the distance to the threshold in proportion to the current amount of predictive information.

The dorsolateral prefrontal cortex codes the decision variable

In a next step, we took advantage of basic properties of sequential sampling models to identify the brain regions computing the decision variable. First, assuming a coupling between neuronal firing rates and BOLD activity, we predicted that the BOLD response in the brain regions coding the decision variable should increase with slower decision RT and decrease when predictive information increases (i.e., when the distance to the threshold decreases). This hypothesis is based on the observation that the duration of the ramping neuronal activity coding the decision variable predicts RT and that its height correlates with the distance to the threshold (as illustrated in Fig. 1*a*, top left panel) (Hanes and Schall, 1996; Huk and Shadlen, 2005). Second, paralleling our behavioral results on RTs, the influence of predictive information on the BOLD response should not depend on the information source (last or penultimate shape) and there should be no influence of surprise on the BOLD response. Finally, BOLD response in brain regions coding the decision variable should reflect the slope of sensory evidence accumulation.

A conjunction analysis between brain regions showing decision-related activity decreasing with higher predictive information conveyed by both the last and the penultimate shapes isolated the anterior part of the right DLPFC and the right IPS ($p < 0.001$ uncorrected) (Fig. 7*a*). As expected, BOLD activity in these brain regions was identically modulated by the predictive information conveyed by the last and by the penultimate shape (Fig. 7*b*) (paired *t* test, $p_1 = p_2$, orange and red bars; right IPS: $p = 0.43$; right DLPFC: $p = 0.34$), and there was no influence of surprise on neural activity in these brain regions (Fig. 7*b*) (*t* test, $u = 0$, green bars; rIPS: $p = 0.29$; rDLPFC: $p = 0.8$).

Among these two brain regions, we assessed the correlation between BOLD response and the slope of sensory evidence accumulation (see Materials and Methods, General linear model 3: correlation between BOLD activity and LATER model parame-

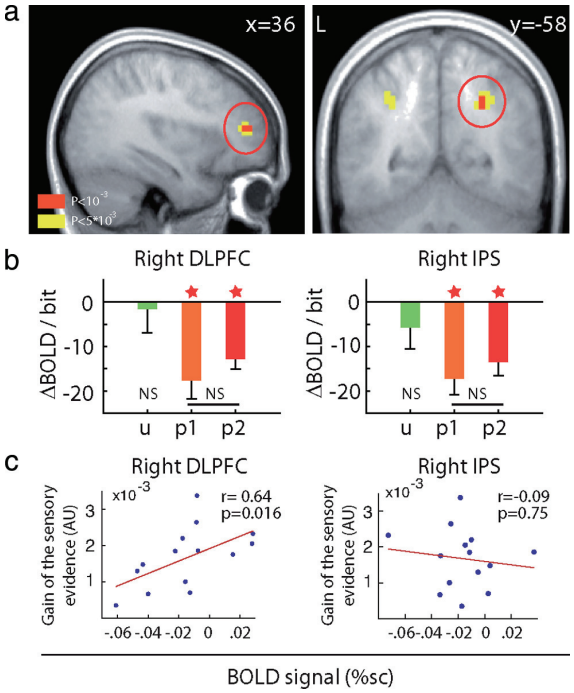

Figure 7. Brain regions coding the decision variable. ***a***, Conjunction map showing the brain regions activated during perceptual decision making in which BOLD activity is negatively modulated by the amount of predictive information conveyed by the last and the penultimate shape. We rendered our map using an uncorrected threshold of $p < 0.001$ (level of significance used for inference, red voxels) and a threshold of $p < 0.005$ to show the full extent of the activations (yellow voxels). ***b***, Average parametric response to surprise (u) and predictive information (p_1 and p_2) in these brain regions. The parametric response to the predictive information conveyed by the last shape (p_1) and the penultimate shape (p_2) was not significantly different (NS) in any of the regions identified ($p_1 = p_2$, orange and red bars; rIPS: $p = 0.43$; rDLPFC: $p = 0.34$). There was no parametric response to surprise ($u = 0$, green bars; rIPS: $p = 0.29$; rDLPFC: $p = 0.8$). ***c***, Scatter plots of correspondence between BOLD signal change in the ACC and accumulation's slope average, for each of the brain regions shown in Figure 7*a* (circled in red; see Materials and Methods, General linear model 3: correlation between BOLD activity and LATER model parameters). Each point represents the BOLD signal change in the ACC and the slope of sensory evidence accumulation estimated using the LATER model averaged over the four levels of predictive information (−0.3, 0.18, 0.72, 1.22 bits) for each subject (see supplemental Fig. S3, available at www.jneurosci.org as supplemental material).

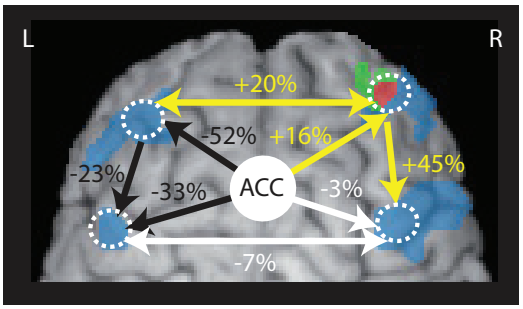

Figure 8. Diagram of effective connectivity between ACC and DLPFC. DLPFC subregions in which BOLD signal decreased as the predictive information conveyed by the last shape increased are rendered in blue, DLPFC subregions in which BOLD signal decreased as the predictive information conveyed by the penultimate shape increased are rendered in green and DLPFC subregions in which both effects were present are rendered in red ($p < 0.005$ uncorrected, for display). Red cluster corresponds to the DLPFC subregion coding the decision variable shown in Figure 7. The plain white circle represents the ACC, which is buried within the medial wall of the frontal cortex. The structural equation model included oriented path (arrows) connecting the ACC and the four functional subregions found in the DLPFC. Dashed circles white indicate the location and the extent of the spheres used for time series extraction. A yellow arrow indicates a significant increase of the path coefficient between first-order and second-order sequences, whereas a black arrow indicates a significant decrease of the path coefficient (all $p < 10^{-2}$). Finally, white arrows indicate path coefficient variations that are not significant. Variations of effective connectivity from first-order sequences to second-order sequences are indicated as relative variations next to each path (supplemental Table S3, available at www.jneurosci.org as supplemental material, indicates absolute values and statistical significance).

ters). Indeed, although the strength of sensory evidence was kept constant throughout the experiment, there were fluctuations of the slope of sensory evidence accumulation between subjects, as can be seen in supplemental Figure S3 (available at www.jneurosci.org as supplemental material). These individual fluctuations of the slope of sensory evidence accumulation correlated with BOLD activity in the right DLPFC ($r = 0.64$, $p = 0.016$), but not in the right IPS ($r = 0.09$, $p = 0.75$), thereby strongly supporting the involvement of the DLPFC in coding the decision variable (Fig. 7*c*).

Effective connectivity between the anterior cingulate cortex and the dorsolateral prefrontal cortex

Finally, having characterized the complementary computations performed in the ACC (Figs. 4, 5), which modulates the distance to the threshold, and the DLPFC region coding the decision variable (Fig. 7), we investigated whether the effective connectivity from the ACC to this DLPFC region increased when optimal regulation of the distance to the threshold required more complex computations. We formalized our hypothesis as a structural equation model (path diagram represented with arrows connecting the ACC to the DLPFC in Fig. 8), based on known anatomical pathways between the ACC and the DLPFC (Beckmann et al., 2009) and an ROI analysis of the parametric effect of predictive information in the DLPFC (Fig. 8). When comparing first-order to second-order sequences, a situation in which computation of the optimal threshold adjustment increases in complexity, the path coefficient from the ACC to the region of the DLPFC that codes the decision variable (Fig. 8, right anterior DLPFC's activation, x, y, z: 45, 45, 12) increased significantly, which was not the case for path coefficients along the other paths originating from the ACC (Fig. 8; supplemental Table S3, available at www.jneurosci.org as supplemental material). Interestingly, this effect was paralleled by an increase in the information flow from right anterior to posterior DLPFC region (right posterior DLPFC activations, x, y, z: 39, 6, 27).

Discussion

The accuracy of a perceptual decision depends on the amount of sensory evidence accumulated (Gold and Shadlen, 2007). However, gathering evidence takes time, which results in a tradeoff between a decision's speed and the accuracy achieved. Thus, optimal decision making should exploit all sources of information available, taking advantage of both the sensory evidence extracted from the environment and the knowledge of contingencies built upon past experiences (Bogacz, 2007b; Gold and Shadlen, 2007). Here, we showed that humans effectively use the predictability of forthcoming events to modulate the distance to the threshold of their decisions, substituting predictive information for sensory information in the decision process to speed up action selection without loss of accuracy (Fig. 4; supplemental Fig. S2, available at www.jneurosci.org as supplemental material). Remarkably, people both estimate and use predictive informa-

tion optimally, adjusting to environmental dynamics of varying complexity.

The key novel finding reported in this study is the coding in the ACC of a signal reflecting the adjustments of the distance to the threshold in proportion to the current amount of predictive information. This pivotal role of the ACC in the contextual guidance of the decision process is supported by two lines of evidence: (1) neural sensitivity to predictive information in the ACC accurately predicts individual fluctuations in the ability to use predictive information to modulate the distance to the threshold of the decision (Fig. 5); and (2) effective connectivity from the ACC to the DLPFC region accumulating sensory evidence increases when optimal adjustment of the distance to the threshold requires more complex computations, reflecting the increased weight of ACC's regulation signals in the decision process (Fig. 8). Overall, our results strongly support the idea that contextually optimized decisions arise from the integration of complementary computations performed in a network of specialized brain regions. In this conceptual framework, the ACC's main function is the computation of regulation signals that optimally adjust the distance to the threshold to the context.

The involvement of the DLPFC in the accumulation of sensory evidence is supported by the fact that BOLD activity observed in this brain region (1) increased with slower decision response times, (2) was negatively modulated by the amount of predictive information conveyed by the last and the penultimate shape, (3) did not depend on the source of predictive information (last or penultimate shape), and (4) is correlated with the slope of the decision variable (Fig. 7). This finding extends previous reports that the DLPFC accumulates sensory evidence related to the correct choice (Kim and Shadlen, 1999; Heekeren et al., 2004; Philiastides and Sajda, 2006; Philiastides and Heekeren, 2009). Note that we implicitly referred to sensory evidence accumulation as the computational mechanism by which a decision variable is implemented, but we acknowledge that other mechanisms have been proposed and are also possible (Ditterich, 2006; Cisek et al., 2009). Finally, the DLPFC activity we observed cannot be attributed to higher attention at the time of target appearance because this would have predicted increased BOLD response with higher predictive information (the latter being associated with faster RTs in our task). By contrast, we observed a negative correlation between predictive information and BOLD signal in this brain region (Fig. 7).

Previous fMRI studies reported a relationship between choice uncertainty and activity in the medial prefrontal cortex when subjects learn through trials and errors the probability of making a correct choice (Volz et al., 2003; Huettel et al., 2005; Volz et al., 2005; Grinband et al., 2006; Huettel, 2006; Platt and Huettel, 2008). These findings parallel studies using fMRI in humans or brain lesions in monkeys showing that one of ACC's critical functions is to build and update an extended action/reward history to guide future decisions optimally (Hampton et al., 2006; Kennerley et al., 2006; Behrens et al., 2007). Our results draw an important link between these two fields of research by showing that the ACC is involved in the regulation of the decision-making process using predictive information (a measure of the reduction of uncertainty estimated on the basis of the history of associations between successive events) and suggests that adjustment signals of the distance to the threshold in the ACC may be a general computational mechanism for the contextual guidance of decisions. Interestingly, theoretical insights into representational learning suggest that a learning signal is needed to support such a function (Williams and Goldman-Rakic, 1998; Holroyd and Coles, 2002; Friston, 2003; Dreher et al., 2006; D'Ardenne et al., 2008). The midbrain activation we observed concomitant with the ACC activation could serve such a functional role since prediction error signal has previously been found in the midbrain (although this cluster did not survive correction for multiple comparison, $p < 0.001$ uncorrected) (see Fig. 5*a*) (Dreher et al., 2006; Behrens et al., 2007; D'Ardenne et al., 2008).

Previous accounts of the ACC's function have stressed factors other than the contextual regulation of the decision-making process, such as the monitoring of errors and conflicts (Carter et al., 1998; Botvinick et al., 2004; Ridderinkhof et al., 2004), the likelihood of errors (Brown and Braver, 2005), and the role of postdecisional prediction-error signals (Holroyd and Coles, 2002). However, none of these alternative functions could account for the relationship observed here between ACC activity and predictive information. Indeed, additional fMRI analyses of our data showed that both the likelihood of error and the prediction error failed to explain our BOLD activity in the ACC at the time of decision formation (Fig. 6). Moreover, once controlled for the level of predictive information, BOLD activity in the ACC did not significantly differ between slow and fast responses, which rules out interpretations of our ACC activity in terms of conflict monitoring or spurious correlation with RT, which would have predicted that decisions with longer RTs are associated with greater levels of conflict and with higher level of ACC activity (supplemental Fig. S5, available at www.jneurosci.org as supplemental material). Moreover, in our experiment, the entropy, which has been proposed as a direct measure of conflict (Berlyne, 1957) did not account for a significant part of BOLD activity in the ACC (supplemental Table S2, available at www.jneurosci.org as supplemental material; Fig. 6).

It should be noted that ACC's regulatory function of the distance to the threshold does not necessarily imply that this brain region directly implements the threshold of the decision. In fact, a number of theoretical accounts propose that the basal ganglia implement a gating mechanism that signals, by a phasic increase of activity in the direct pathway, the moment when the activity of cortical neurons coding the decision variable crosses the decision threshold (Lo and Wang, 2006; Bogacz, 2007a, 2009; Frank et al., 2007). This phasic increase of activity would cancel the tonic inhibition exerted by the basal ganglia's output nuclei on motor command centers (Redgrave et al., 1999). Despite a current lack of direct evidence, this proposal emphasizes the potentially central role of cingulostriatal projections in conveying contextual regulation signals from the ACC to the main input structure of the basal ganglia (Kunishio and Haber, 1994; Lo and Wang, 2006). Supporting this hypothesis, we observed a strong correlation between BOLD activity in the ACC and in the striatum, showing that these two brain regions are functionally coupled when making simple decisions (supplemental Fig. S6, available at www.jneurosci.org as supplemental material; Materials and Methods, Functional connectivity analysis).

Moreover, a recent fMRI study comparing perceptual decisions with cues emphasizing speed or accuracy reported a negative correlation between individual variations of a measure for response caution (ratio between the starting point and the decision threshold) and BOLD activity at the time of the cue in both the pre-SMA and the striatum (Forstmann et al., 2008). Thus, the pre-SMA and the striatum may be involved in motor preparation of fast action when explicitly cued for speed and may implement the global slowing down observed when cueing for higher accuracy. Other recent fMRI studies also explicitly emphasized the speed of the perceptual decision at the expense of its accuracy

(Ivanoff et al., 2008; van Veen et al., 2008). By contrast, in our study, the modulation of the decision process relied upon predictive information (conveyed by recent history) on the forthcoming stimulus, a quantity that participants implicitly tracked and updated online. Our findings highlight the role of the ACC in keeping track of past events to build an inner model of contingencies and in adjusting the distance to the decision threshold and address a more general contextwise modulation of the decision process, which did not result in a simple global inhibition or facilitation of action preparation, but in a weighting of each possible outcome of the decision based on its likeliness. Consistent with our proposal, a recent fMRI study showed that individual differences in perceptual decision criterion shifts induced by expected losses correlates with BOLD activity in the ACC. Although the authors did not analyze their data within the framework of sensory evidence accumulation models, their findings indicate that asymmetric category costs may affect perceptual decision making in a similar way to changes in category expectations (Fleming et al., 2010).

In conclusion, combining psychophysics, model-driven fMRI and the framework of information theory, we characterized the influence of predictive information on two basic elements underlying the formation of human perceptual decision (distance to the threshold and decision variable). Our results reveal how these elements are coded in the human brain and shed a new light on the respective functions played by the DLPFC and the ACC in perceptual decision making. They also suggest new architectural principles governing the organization of the human frontal lobe and how the interactions between the DLPFC and the ACC are required for optimal decision making.

References

Beckmann M, Johansen-Berg H, Rushworth MF (2009) Connectivity-based parcellation of human cingulate cortex and its relation to functional specialization. J Neurosci 29:1175–1190.

Behrens TE, Woolrich MW, Walton ME, Rushworth MF (2007) Learning the value of information in an uncertain world. Nat Neurosci 10:1214–1221.

Berlyne DE (1957) Uncertainty and conflict: a point of contact between information-theory and behavior-theory concepts. Psychol Rev 64:329–339.

Bestmann S, Harrison LM, Blankenburg F, Mars RB, Haggard P, Friston KJ, Rothwell JC (2008) Influence of uncertainty and surprise on human corticospinal excitability during preparation for action. Curr Biol 18:775–780.

Bogacz R (2007a) Optimal decision network with distributed representation. Neural Netw 20:564–576.

Bogacz R (2007b) Optimal decision-making theories: linking neurobiology with behaviour. Trends Cogn Sci 11:118–125.

Bogacz R (2009) Optimal decision-making theories. In: Handbook of reward and decision making (Dreher JC, Tremblay L, eds), pp 367–389. Oxford: Academic.

Botvinick MM, Cohen JD, Carter CS (2004) Conflict monitoring and anterior cingulate cortex: an update. Trends Cogn Sci 8:539–546.

Brown JW, Braver TS (2005) Learned predictions of error likelihood in the anterior cingulate cortex. Science 307:1118–1121.

Büchel C, Holmes AP, Rees G, Friston KJ (1998) Characterizing stimulus-response functions using nonlinear regressors in parametric fMRI experiments. Neuroimage 8:140–148.

Carpenter RH, Williams ML (1995) Neural computation of log likelihood in control of saccadic eye movements. Nature 377:59–62.

Carter CS, Braver TS, Barch DM, Botvinick MM, Noll D, Cohen JD (1998) Anterior cingulate cortex, error detection, and the online monitoring of performance. Science 280:747–749.

Cisek P, Puskas GA, El-Murr S (2009) Decisions in changing conditions: the urgency-gating model. J Neurosci 29:11560–11571.

D'Ardenne K, McClure SM, Nystrom LE, Cohen JD (2008) BOLD responses reflecting dopaminergic signals in the human ventral tegmental area. Science 319:1264–1267.

Dayan P, Abbott LF (2001) Computational and mathematical modeling of neural systems, Ed 1. Cambridge, MA: MIT Press.

Ditterich J (2006) Stochastic models of decisions about motion direction: behavior and physiology. Neural Netw 19:981–1012.

Doya K (2008) Modulators of decision making. Nat Neurosci 11:410–416.

Dreher JC, Kohn P, Berman KF (2006) Neural coding of distinct statistical properties of reward information in humans. Cereb Cortex 16:561–573.

Fleming SM, Whiteley L, Hulme OJ, Sahani M, Dolan RJ (2010) Effects of category-specific costs on neural systems for perceptual decision-making. J Neurophysiol 103:3238–3247.

Forstmann BU, Dutilh G, Brown S, Neumann J, von Cramon DY, Ridderinkhof KR, Wagenmakers EJ (2008) Striatum and pre-SMA facilitate decision-making under time pressure. Proc Natl Acad Sci U S A 105:17538–17542.

Frank MJ, Samanta J, Moustafa AA, Sherman SJ (2007) Hold your horses: impulsivity, deep brain stimulation, and medication in parkinsonism. Science 318:1309–1312.

Friston K (2003) Learning and inference in the brain. Neural Netw 16: 1325–1352.

Friston KJ, Penny WD, Glaser DE (2005) Conjunction revisited. Neuroimage 25:661–667.

Gold JI, Shadlen MN (2007) The neural basis of decision making. Annu Rev Neurosci 30:535–574.

Gomez P, Ratcliff R, Perea M (2007) A model of the go/no-go task. J Exp Psychol Gen 136:389–413.

Grinband J, Hirsch J, Ferrera VP (2006) A neural representation of categorization uncertainty in the human brain. Neuron 49:757–763.

Hampton AN, Bossaerts P, O'Doherty JP (2006) The role of the ventromedial prefrontal cortex in abstract state-based inference during decision making in humans. J Neurosci 26:8360–8367.

Hanes DP, Schall JD (1996) Neural control of voluntary movement initiation. Science 274:427–430.

Hanks TD, Ditterich J, Shadlen MN (2006) Microstimulation of macaque area LIP affects decision-making in a motion discrimination task. Nat Neurosci 9:682–689.

Harrison LM, Duggins A, Friston KJ (2006) Encoding uncertainty in the hippocampus. Neural Netw 19:535–546.

Heekeren HR, Marrett S, Bandettini PA, Ungerleider LG (2004) A general mechanism for perceptual decision-making in the human brain. Nature 431:859–862.

Holroyd CB, Coles MG (2002) The neural basis of human error processing: reinforcement learning, dopamine, and the error-related negativity. Psychol Rev 109:679–709.

Huettel SA (2006) Behavioral, but not reward, risk modulates activation of prefrontal, parietal, and insular cortices. Cogn Affect Behav Neurosci 6:141–151.

Huettel SA, Song AW, McCarthy G (2005) Decisions under uncertainty: probabilistic context influences activation of prefrontal and parietal cortices. J Neurosci 25:3304–3311.

Huk AC, Shadlen MN (2005) Neural activity in macaque parietal cortex reflects temporal integration of visual motion signals during perceptual decision making. J Neurosci 25:10420–10436.

Ivanoff J, Branning P, Marois R (2008) fMRI evidence for a dual process account of the speed-accuracy tradeoff in decision-making. PLoS One 3:e2635.

Jeffrey H (1998) Theory of probability. Ed 3. Oxford: Oxford UP.

Kennerley SW, Walton ME, Behrens TE, Buckley MJ, Rushworth MF (2006) Optimal decision making and the anterior cingulate cortex. Nat Neurosci 9:940–947.

Kim JN, Shadlen MN (1999) Neural correlates of a decision in the dorsolateral prefrontal cortex of the macaque. Nat Neurosci 2:176–185.

Kornblum S (1969) Sequential determinants of information processing in serial and discrete choice reaction time. Psychol Rev 76:113–131.

Kunishio K, Haber SN (1994) Primate cingulostriatal projection: limbic striatal versus sensorimotor striatal input. J Comp Neurol 350:337–356.

Lo CC, Wang XJ (2006) Cortico-basal ganglia circuit mechanism for a decision threshold in reaction time tasks. Nat Neurosci 9:956–963.

Luce R (1991) Response times: their role in inferring elementary mental organization. Oxford: Oxford UP.

Mars RB, Debener S, Gladwin TE, Harrison LM, Haggard P, Rothwell JC, Bestmann S (2008) Trial-by-trial fluctuations in the event-related electroencephalogram reflect dynamic changes in the degree of surprise. J Neurosci 28:12539–12545.

Mueller R (1996) Basic principle of structural equation modeling. New York: Springer.
Nichols T, Brett M, Andersson J, Wager T, Poline JB (2005) Valid conjunction inference with the minimum statistic. Neuroimage 25:653–660.
Oldfield RC (1971) The assessment and analysis of handedness: the Edinburgh inventory. Neuropsychologia 9:97–113.
Philiastides MG, Heekeren HR (2009) Spatiotemporal characteristics of perceptual decision making in the human brain? In: Handbook of reward and decision making (Dreher JC, Tremblay L, eds), pp 185–212. Oxford: Academic.
Philiastides MG, Sajda P (2006) Temporal characterization of the neural correlates of perceptual decision making in the human brain. Cereb Cortex 16:509–518.
Platt ML, Huettel SA (2008) Risky business: the neuroeconomics of decision making under uncertainty. Nat Neurosci 11:398–403.
Ranganath C, Rainer G (2003) Neural mechanisms for detecting and remembering novel events. Nat Rev Neurosci 4:193–202.
Ratcliff R, McKoon G (2008) The diffusion decision model: theory and data for two-choice decision tasks. Neural Comput 20:873–922.
Reddi BA, Carpenter RH (2000) The influence of urgency on decision time. Nat Neurosci 3:827–830.
Reddi BA, Asrress KN, Carpenter RH (2003) Accuracy, information, and response time in a saccadic decision task. J Neurophysiol 90:3538–3546.
Redgrave P, Prescott TJ, Gurney K (1999) The basal ganglia: a vertebrate solution to the selection problem? Neuroscience 89:1009–1023.
Ridderinkhof KR, Ullsperger M, Crone EA, Nieuwenhuis S (2004) The role of the medial frontal cortex in cognitive control. Science 306:443–447.
Smith PL, Ratcliff R (2004) Psychology and neurobiology of simple decisions. Trends Neurosci 27:161–168.
Stanford TR, Shankar S, Massoglia DP, Costello MG, Salinas E (2010) Perceptual decision making in less than 30 milliseconds. Nat Neurosci 13:379–385.
Strange BA, Duggins A, Penny W, Dolan RJ, Friston KJ (2005) Information theory, novelty and hippocampal responses: unpredicted or unpredictable? Neural Netw 18:225–230.
Tosoni A, Galati G, Romani GL, Corbetta M (2008) Sensory-motor mechanisms in human parietal cortex underlie arbitrary visual decisions. Nat Neurosci 11:1446–1453.
Usher M, McClelland JL (2001) The time course of perceptual choice: the leaky, competing accumulator model. Psychol Rev 108:550–592.
Vandekerckhove J, Tuerlinckx F (2008) Diffusion model analysis with MATLAB: a DMAT primer. Behav Res Methods 40:61–72.
van Veen V, Krug MK, Carter CS (2008) The neural and computational basis of controlled speed-accuracy tradeoff during task performance. J Cogn Neurosci 20:1952–1965.
Volz KG, Schubotz RI, von Cramon DY (2003) Predicting events of varying probability: uncertainty investigated by fMRI. Neuroimage 19:271–280.
Volz KG, Schubotz RI, von Cramon DY (2005) Variants of uncertainty in decision-making and their neural correlates. Brain Res Bull 67:403–412.
Williams SM, Goldman-Rakic PS (1998) Widespread origin of the primate mesofrontal dopamine system. Cereb Cortex 8:321–345.

"Decision threshold modulation in the human brain":
Supplementary Figures

Philippe Domenech and Jean-Claude Dreher

Center for Cognitive Neuroscience, CNRS-Université de Lyon 1, Reward and decision making team, Lyon, France

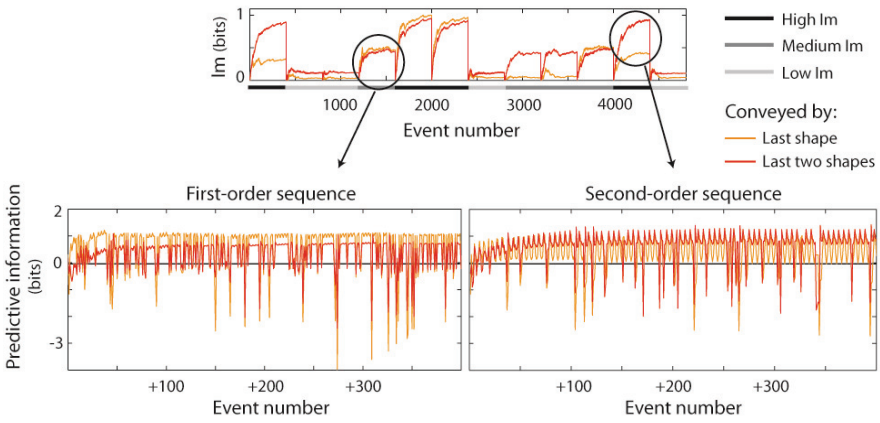

Figure S1: Illustration of the predictive information dynamic over the course of a whole experiment. The estimated mutual information was updated after each new shape and progressively rose from the beginning of each sequence to a maximum as the sequence structure was progressively disclosed (Upper panel, Eq. 4-5). Low, Medium and High level of *Im* refer to mutual information (Eq. 4-5). During second-order sequences, the mutual information of the last two shapes (red line, Eq. 3) was significantly higher than the mutual information of the last shape only (orange line, see Methods, Eq. 2) as seen in the bottom right panel. During first-order sequences, there was, on average, no extra predictive information conveyed by the penultimate shape, as reflected by the equality between mutual information (bottom left panel). Note the large trial-to-trial fluctuations of the predictive information (used as parametric regressors) during both sequence types.

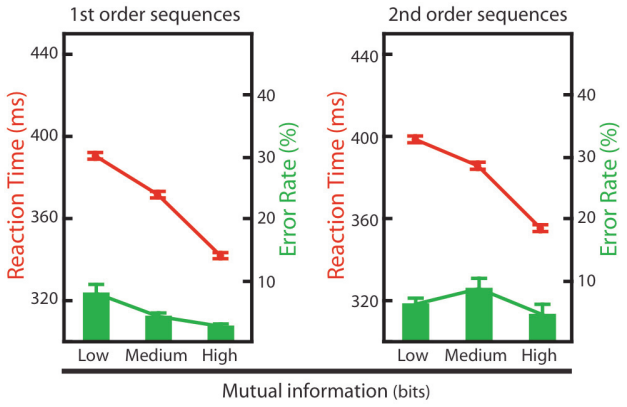

Figure S2. Relationship between increasing mutual information in first and second-order sequences and RT (red circles) and error rates (green bars). RT decreased monotonically as the mutual information of sequences increased ($F=404.1$, $p<10^{-7}$). However, this decrease in RT was not paralleled by increased error rates (Mutual information, $F=4.23$, $p=0.016$; No effect of sequence order, $F=2.79$, $p=0.096$; No interactions, $F=2.99$, $p=0.053$). RTs were on average 14.11 ms longer for second-order sequences compared to first-order sequences ($F=79$, $p<10^{-7}$, no interaction, $F=2.1$, $p=0.118$).

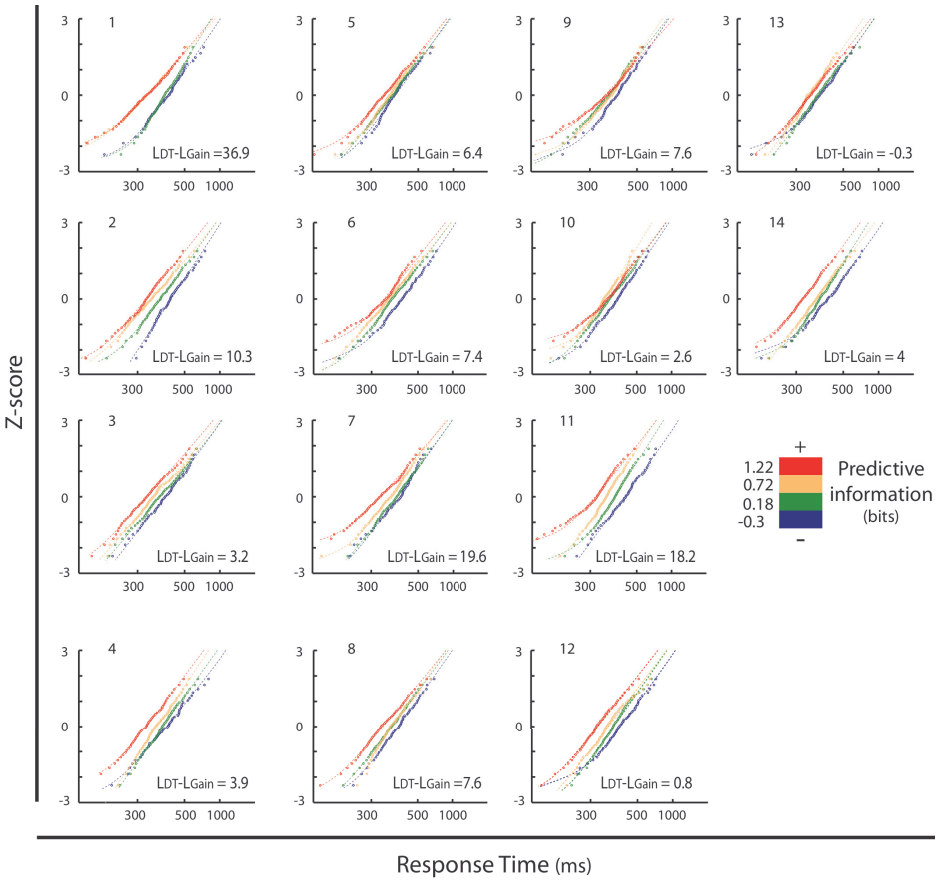

Figure S3: Reciprobit plots for each participant. Most of the individual reciprobit plots shows a clear swivel toward lower RT when predictive information increases, as hypothesized in Figure 1a (upper right panel). The values of each individual's log likelihood ratio (L_{DT}-L_{Gain}) are displayed on each reciprobit plot, favoring the distance to the threshold hypothesis in all but 2 subjects (subjects 12 and 13). For these two subjects, evidence did not allow to conclusively choose one mechanism over the other.

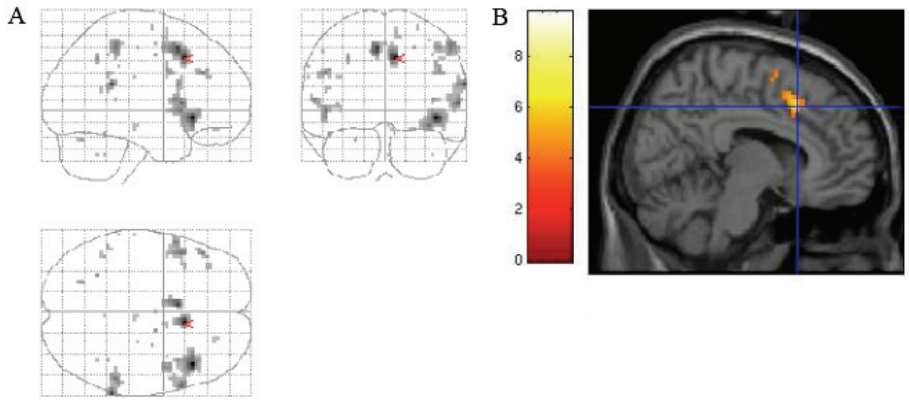

Figure S4: Whole-brain analysis of parametric responses to the amount of predictive information conveyed by the last shape when accounting for the error likelihood, the prediction error, the uncertainty and the surprise (threshold of p<0.001, see methods GLM2)**.** (A) Statistical map is rendered on a glass brain. (B) The crosshair indicates the coordinate of ACC's peak activity (x,y,z=9,18,42, Zmax=5.04).

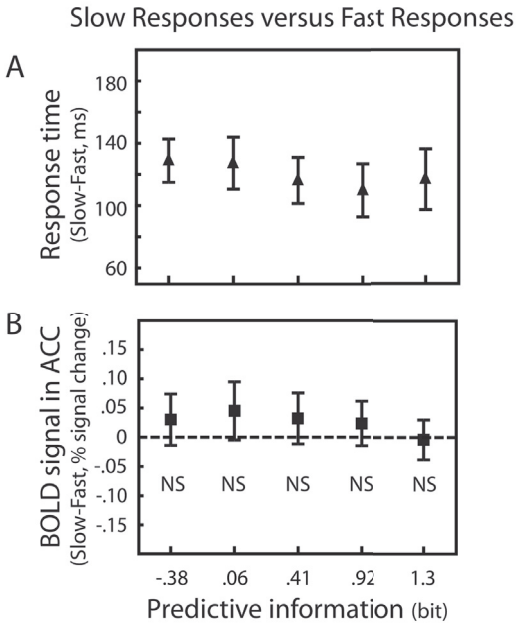

Figure S5: (A) Paired difference in RT between fast and slow responses as a function of the level of predictive information. Correct target trials were binned according to the level of predictive information ([-.43,-.05,.25,.62,1,1.32] bits) and to the response speed (fast and slow responses, according to each subject's median RT). No effect of the level of predictive information was observed on the paired difference in RT between fast and slow responses (effect of predictive information on the paired difference in RT between slow and fast responses: $F_{4,65}$=1.1242, p=0.3529). **(B) Paired difference in ACC's BOLD signal between slow and fast responses as a function of the level of predictive information.** There was no difference in ACC BOLD activity between slow and fast responses for any of the 5 levels of predictive information (T-test, -0.38 bits: p= 0.1643, .06 bits: p=0.0731, .41 bits: p=0.1353, .92 bits: p=0.2040, 1.3 bits: p=0.8053). No effect of predictive information on the paired difference in ACC BOLD activity was observed between slow and fast responses ($F_{4,65}$= 0.86, p=0.4937). Error bars in panels A and B represent 95% confidence intervals.

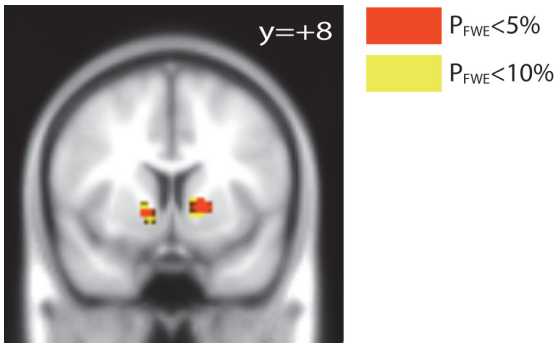

Figure S6: Group-level map of functional connectivity using the ACC as seed region. Red pixels indicate brain regions showing a significant correlation with BOLD activity in the ACC (threshold of 5% FWE whole-brain corrected).

Table S1: Whole brain analysis of parametric response to predictive information.

Location	MNI (x,y,z ;mm)	Zmax	Cluster extent (voxel)	Significance (whole-brain cluster-wise corrected)	Correlation coefficient (BOLD, sr1)	Correlation coefficient (BOLD, sr2)	Correlation coefficient (BOLD,Gain)
Predictive information conveyed by the last shape : negative parametric effect							
Anterior Cingulate Cortex	9 18 42	5.55	233	$\leq 10^{-4}$	.635-0.0036	.697-0.006	.081-NS
L IFG / Anterior Insula	-48 18 -3	5.28	184	$\leq 10^{-4}$	.393-NS	.112-NS	.103-NS
R IFG / Anterior Insula	42 24 -6	5.10	402	$\leq 10^{-4}$	.125-NS	.424-NS	.006-NS
R Intra Parietal Sulcus	36 -48 45	4.87	120	$\leq 10^{-4}$	.204-NS	.428-NS	.195-NS
R DLPFC	12 3 60	4.44	36	$\leq 10^{-4}$	.397-NS	.477-NS	.367-NS
R Superior Temporal Gyrus	63 -42 21	4.05	95	$\leq 10^{-4}$	.226-NS	.323-NS	.336-NS
L DLPFC	-42 39 33	3.67	31	0.018	.182-NS	.195-NS	-.037-NS
Predictive information conveyed by the last shape : positive parametric effect							
Posterior Cingulate Cortex	-12 -54 24	3.74	86	$\leq 10^{-4}$	N/A	N/A	N/A

Table S2: Whole brain analysis of parametric response to predictive information, including the error likelihood the prediction error and the entropy as nuisance regressors.

Location	MNI (x,y,z ;mm)	Zmax	Cluster extent (voxel)	Significance (Whole-brain cluster-wise corrected)
Predictive information conveyed by the last shape : negative parametric effect				
R Anterior Cingulate Cortex	9 18 42	5.04	50	$\leq 10^{-3}$
L Anterior Cingulate Cortex	-6 12 51	4.51	44	2.10^{-3}
L IFG / Anterior Insula	-48 15 0	4.02	50	10^{-3}
R Anterior Insula	42 24 -6	4.86	105	$\leq 10^{-4}$
R IFG	60 15 6	4.22	42	3.10^{-3}
R Intra-Parietal Sulcus	54 -39 51	3.97	40	4.10^{-3}
Predictive information conveyed by the last shape : positive parametric effect				
Posterior Cingulate Cortex	-12 -51 27	3.90	47	0.002
Middle Temporal Cortex	57 -12 -27	3.79	33	0.012

Table S3: Path coefficient variations between first and second order sequences from effective connectivity analysis. See figure 8 for the corresponding diagram of effective connectivity.

Path	Path coefficient (1^{st} order)	Path coefficient (2^{nd} order)	Significance (Chi-squared, 1 df)
ACC > Right rostral DLPFC	0.3417	0.3962	p=0.003
ACC > Right caudal DLPFC	0.2108	0.2052	p=0.779
ACC > Left rostral DLPFC	0.2819	0.134	p=0.007
ACC > Left caudal DLPFC	0.1253	0.167	p<0.001
Inter-hemispheric rostral DLPFC	0.2375	0.2867	p<0.001
Inter-hemispheric caudal DLPFC	0.07	0.0653	p=0.639
Right rostral DLPFC > Right caudal DLPFC	0.3364	0.4875	p<0.001
Left rostral DLPFC > Left caudal DLPFC	0.2618	0.2015	p<0.001

Article 2: A neuro-computational account of economic choices in the human brain

Philippe Domenech, Jerome Redouté, Rafal Bogacz and Jean-Claude Dreher

Pending Submission

A neuro-computational account of economic choices in the human brain

Philippe Domenech, Jerome Redouté, Rafal Bogacz and Jean-Claude Dreher

Reward and decision making team
Cognitive Neuroscience Center
CNRS
67 Bd Pinel, 69675 Bron, France

Text manuscript: 43

Manuscript tables: 0

Manuscript figures: 6

Supplemental material: 4 Figures, 2 Tables

Corresponding author:
Philippe Domenech
CNRS, Reward and decision-making team
Cognitive Neuroscience Center
67 Bd Pinel, 69675 Bron, France
Email: pdomenech@isc.cnrs.fr
Tel: 00 33 (0)4 37 91 12 44
Fax: 00 33 (0)4 37 91 12 10
http://www.isc.cnrs.fr/dre/

Introduction

When ordering a dessert from a set menu, choosing between the apple pie and the strawberry tart will solely depend on the subjective value attributed to each sweet: there is no correct answer, only options that are more or less desirable according to one's subjective preferences. Such decisions, made on the basis of options' subjective values, are called economic choices (Padoa-Schioppa and Assad, 2006; Padoa-Schioppa and Assad, 2008; Kable and Glimcher, 2009). Proofs in utility theory demonstrate that any value-based decision algorithm underpinned by a single common scale of options' desirability, called "common currency", yield consistent economic choices (Samuelson, 1937). So, an important assumption in economy is that value-based decision-making entails two separable stages: the aggregation of all the options' meaningful features into subjective values ordered on a common scale (valuation stage) and the selection of the option associated with the most valuable outcome (decision-making stage) (Kable and Glimcher, 2009; Rangel et al., 2008).

In the past few years, there has been a surge of interest in the brain valuation system suggested by utility theory, which yielded converging evidence linking orbito-frontal cortex (OFC) to valuation (Kable and Glimcher, 2009; Sugrue et al., 2005; Rangel and Hare, 2010). Although, early human and monkey lesion studies had already established that normal value-guided behaviors require OFC integrity (Kable and Glimcher, 2009; Wallis, 2007), recent monkeys electrophysiology recordings further demonstrated that lateral OFC (lOFC) neurons encode options' subjective values on a common scale during economic choices (Padoa-Schioppa and Assad, 2006; Freedman and Assad, 2011; Tremblay and Schultz, 1999; Deaner et al., 2005). Moreover, lOFC neurons adapt their firing rate to the range of values at stake, a mechanism that contextually optimizes the precision of value representations while preserving preference transitivity (Padoa-Schioppa and Assad, 2008; Padoa-Schioppa, 2009; Tobler et

al., 2005). By contrast with striatal and dorso-lateral prefrontal (DLPFC) neurons, lOFC neurons value-related activity is independent of sensory-motor contingencies, suggesting that these neurons represent subjective values within an action-independent option-based common space, as hypothesized by utility theory (Kable and Glimcher, 2009; Freedman and Assad, 2011; Padoa-Schioppa, 2010; Wunderlich et al., 2010; Wallis and Miller, 2003). On the other hand, human fMRI studies have emphasized the role of the ventro-medial prefrontal cortex (vmPFC), the medial portion of the OFC, in coding decision value signals during economic choices (Kable and Glimcher, 2009; Rangel and Hare, 2010). Decision value signals putatively arise at the onset of economic choices to be fed into a decision-making mechanism (Chib et al., 2009; Peters and Büchel, 2010; Hare et al., 2008). Hence, decision values must be distinguished from post-decisional values such as the expected value associated with a choice (chosen option value) or the subjective value experienced during goods consumption (Chib et al., 2009; Peters and Büchel, 2010; Hare et al., 2008) (outcome value). Decision value signals may be computed in the vmPFC as a difference between the expected values assigned to each option (Philiastides et al., 2010; Basten et al., 2010). Moreover, the vmPFC commonly encodes the subjective values of different types of goods (Chib et al., 2009), appetitive and aversive (Plassmann et al., 2010), as well as prospects of monetary gains and losses (Tom et al., 2007), within an action-independent option-based value space (Wunderlich et al., 2010; Hare et al., 2008; Plassmann et al., 2007; Kahnt et al., 2010b; Wunderlich et al., 2009; Philiastides et al., 2010).

Despite many apparent similarities, lOFC and vmPFC have very different anatomical connectivity (Price, 2007), suggesting distinct functions for these two portions of the OFC. However, lOFC and vmPFC unique contributions to economic choices remain unclear. In a recent study that examined monkeys performing value-based decisions before and after selective lOFC or vmPFC lesions, lOFC-lesioned monkeys behaved as if they had become

unable to correctly learn option values, whereas vmPFC-lesioned monkeys became less efficient decision-makers, making sub-optimal choices more frequently (Noonan et al., 2010). Baring this one exception, previous studies on economic choices have focused on characterizing the brain valuation system. As a consequence, very little is known on how the distinct functional networks within the OFC interact with the brain decision-making systems to transform decision value signals into economic choices.

To address this question, central to our understanding of Human's everyday behavior, we designed an economic choice paradigm in which male heterosexual participants chose freely between two options, one of which was probabilistically rewarded by an erotic picture (erotic picture option) and the other one by a small amount of fruit juice (0.75 mL, drink option). When confronted with such an offer, participants compared each option's expected subjective value to select the most valuable option of the pair and indicated their choices with a two-responses button box (**Fig. 1A**). Such economic choices bear many similarities with binary perceptual decisions. Indeed, perceptual decision-making paradigms typically involve forming categorical judgments upon noisy sensory information to select the correct option. To do so, participants compare the sensory evidence supporting each alternative, mirroring the situation faced during economic choices in the domain of perception. Sequential sampling models of decision-making, such as the drift diffusion models, accurately describe the relationship between choice probability and decision time in perceptual decisions under many experimental conditions (Gold and Shadlen, 2007). In drift-diffusion models, the difference in sensory evidence supporting each option drives an abstract decision variable from an intermediate starting point toward one of two boundaries. Each boundary represents the decision threshold for one alternative: a choice is made when the decision variable reaches one of the boundaries. When the difference in sensory evidence increases, the slope of the decision variable gets steeper, which results in lower decision times mean and variance.

During perceptual decision-making, neural populations in monkey lateral intra-parietal and dorso-lateral prefrontal cortices exhibit a ramping activity that breaks down after reaching a decision threshold. At the single neuron level, the ramping rate of this neural activity, which represents the accumulation of sensory evidence, correlates with the decision variable predicted by drift-diffusion models (Gold and Shadlen, 2007). At the population level, because distinct cell assemblies accumulate the difference in evidence supporting concurrent options toward a decision threshold, the resulting activity correlates with the absolute value of the decision variable predicted by the drift-diffusion model (Wang, 2008). Multiple fMRI studies confirmed that a homologous parieto-prefrontal network accumulates sensory evidence to form perceptual decisions in the human brain (Gold and Shadlen, 2007; Heekeren et al., 2008). The ability of sequential sampling models to provide a unified account of perceptual decisions, from neural activity to choice behavior, recently started a debate about whether the sequential sampling decision process implemented in the human parieto-prefrontal cortical network may be a general decision-making mechanism, whose function extends across cognitive domains (Kable and Glimcher, 2009; Rangel and Hare, 2010; Freedman and Assad, 2011; Gold and Shadlen, 2007). This view has found some support from decision field theory, a recent development of utility theory describing value-based decisions as a drift-diffusion decision process driven by the difference between option values that accounts for the relationship between choice probability and decision time during economic choices, as well as preference reversals between choice probability and selling price (Busemeyer et al., 2006; Milica Milosavljevic et al., 2010).

Here, we tested the hypothesis that the vmPFC is a pre-decisional hub coding a decision value signal based on the difference between option's expected subjective values and that the lOFC, by contrast, is primarily involved in tracking decisional subjective values across the course of each trial. We further hypothesized that economic choices are

implemented in the human brain as a two-stage process in which the vmPFC decision value signal drives a sequential sampling decision process implemented in the parieto-prefrontal cortical network.

Behavioral results

In our experiment, participants chose between two options that probabilistically yielded different goods: an erotic picture or a drop of juice (**Fig. 1**). We observed that their choices depended on the probability of being rewarded associated with each option and on the relative value between erotic pictures and fruit juice, reflecting participant's subjective preferences (**Fig. 2A**).

To explore how participants made their choices, we first assessed their preference for juice over erotic pictures by performing a logistic regression analysis on each participant choice pattern (**Methods, Eq. 1**). Our logistic model expressed the probability of choosing the juice option as a function of the probability of reward for the juice option, for the picture option and the trial number, which accounted for a possible drift of the preference over the experiment. We computed the preference as the ratio between the model's betas for the probabilities of reward associated with the juice and the erotic picture options (Padoa-Schioppa and Assad, 2006). Hence, we measured preference as the relative value of a drop of juice (0.75 mL) against an erotic picture and reported preferences as equivalent offers expressing "how many" drops of juices were subjectively equivalent to an erotic picture (**Fig. 2A and S1)**: 6 participants out of 14 had a preference greater than 1, revealing their preference for erotic pictures (mean preference: 0.95+/-0.3 SD). Furthermore, an AIC-based selection of individual logistic models ruled out a drift of preference across the experiment in 11 participants out of 14. For the three remaining participants, this drift was an order of magnitude below the effect of reward probabilities (% reward probability effect: 6.8%,

23.1%, 11.8%) and thus could be neglected. Preference's stability over the experiment was further supported by the lack of difference between pre and post-experiment desirability ratings for fruit juice (paired T test, p=0.208).

Then, for each participant, we computed a decision value per offer by subtracting the expected subjective value of the juice option to the expected subjective value of the picture option (**Eq. 3**). This procedure allowed us to place each offer on a common "currency" scale. **Figure 2A** shows three individuals choice patterns illustrating the range of sigmoid relationships observed between decision value and choice probability in our sample. Indeed, some subjects were poor decision-makers as they frequently chose the option with the lower expected subjective value even when decision value grew larger (**Fig. 2A, left panel**), whereas others almost always picked up the option with the highest expected subjective value (**Fig. 2A, right panel**). By homology with perceptual decision-making (Grinband et al., 2006; Freedman and Assad, 2011), we quantified participants' value-based decision-making efficiency as the full width at middle height of the choice uncertainty curve (Bell shaped green curve, **Fig. 2A**, **Eq. 6**). Consistent with previous reports (Grinband et al., 2006; Busemeyer and Townsend, 1993), RTs linearly increased with choice uncertainty (**Fig. 2B**), indicating that participants slowed down when decision value tended toward subjective equivalence. Overall, our behavioral results emphasize the complex relationship between decision value, choice probability and RT. These interdependencies are likely to reflect the elementary computations underpinning economic choices.

Thus, to investigate the computational mechanisms underlying economic choices, we fitted mEZ2 drift-diffusion models to each participant behavioral data set (**see Methods**). Indeed, drift-diffusion models have successfully provided a neurobiologically plausible account of the tradeoff between response probability and decision duration in many decision-making settings (Gold and Shadlen, 2007; Ratcliff and McKoon, 2008). By homology, we

hypothesized that value-based decision-making could be described as a two-steps process: A decision value is computed by comparing each option's expected subjective values (valuation stage), which drives, in turn, a drift-diffusion decision process implementing the probabilistic selection of one of the options (Freedman and Assad, 2011; Busemeyer and Townsend, 1993; Kable and Glimcher, 2009; Heekeren et al., 2008; Rangel and Hare, 2010; Milica Milosavljevic et al., 2010) (decision-making stage). **Figure 3A** illustrates the drift-diffusion model that best fit our participants' behavior: a decision variable is initialized half-ways between an upper and a lower boundary, corresponding respectively to the decision threshold for choosing the fruit juice and the erotic picture option. After a pre-decisional processing latency (Non-decision time, noted "Tnd" in **Fig. 3A**), the decision value neural signal progressively drives the decision variable toward one of the boundaries. The subject commits to a choice once the decision variable crosses one of the decision thresholds. Finally, a gain parameter amplifying the influence of the decision value on the drift-diffusion process accounted for individual variations in the decisional weight conveyed by each value unit (**Fig. 3A**).

As can be seen from **figure 3 (panels E-G)**, the mEZ2 drift-diffusion model provided excellent fits for choice probability (r=0.926) and mean RTs (r=0.883) and despite small numbers of observations per condition, it accounted for RT standard deviation with good accuracy (r=0.562). Moreover, there was a good agreement between preferences estimated using the logistic regression approach and the mEZ2 drift-diffusion model (r=0.9326) (**Fig. 3B**). More complex models including additional modulation mechanisms, such as adjusting the distance between boundaries or the non-decisional time for choice uncertainty, or initializing the decision variable with an offset proportional to decision value, did not outperform the simpler model ($\Delta AIC_{DT\text{-}simple}$=2.1431, $\Delta AIC_{Tnd\text{-}simple}$=1.9751, $\Delta AIC_{SP\text{-}simple}$ =1.9263). Overall, our results support the idea that the brain implements value-based

decision-making as a drift-diffusion process driven by the offer's decision value and show how the decision process' slowing down nearby the subjective equivalence point results from the decision variable's projection onto the accumulator boundaries (**Fig. 2B and 3A**).

Economic decision efficiency in the mEZ2 model depends on both the drift-diffusion process's gain and the decision threshold, which posits an exponential relationship between decision efficiency and these two parameters (Wagenmakers et al., 2007, 2008). Here, we show that inter-individual variations in decision efficiency were almost entirely explained by our model's gain parameter, which captures individual decisional weights per value unit ($r_{log\text{-}Gain,Efficiency}$=-0.9773, $p<10^{-6}$, Fig. **3**C), not by the distance to the decision threshold ($r_{log\ DT,Efficiency}$=0.429, p=0.125). So, our result provides, for the first time, a computationally tractable explanation to decision-making efficiency in value-based decisions.

fMRI results

Having found behavioral evidence supporting our hypothesis that value-based decision-making is a two-steps process in which the current offer's decision value is fed into a drift diffusion process, we then investigated how the human brain may implement each of these steps (valuation and decision) and whether they involved common or distinct brain networks (Freedman and Assad, 2011; Kable and Glimcher, 2009; Heekeren et al., 2008; Rangel and Hare, 2010).

We first focused on the brain regions coding subjective values. Indeed, despite the wealth of experimental data linking OFC to valuation and dopaminergic reinforcement learning, the respective contribution of the lOFC and the vmPFC, two anatomically distinct parts of the OFC (Price, 2007), to valuation and value-based decision-making remains unclear (Grabenhorst and Rolls, 2011; Wallis, 2007; Murray et al., 2007; Kringelbach, 2005). To account for our *a priori* that the OFC was involved in representing subjective values, we

performed the following analysis within a morphological ROI of the OFC (**see Methods**). First, we found that BOLD activity at decision onset correlated significantly with decision value in two OFC regions: the lOFC and the vmPFC (5% FWE corrected clusterwise, F**ig 4A**). Then, we performed post-hoc analyses estimating separately the effects of the drink and picture option's expected values and showed that, in these two OFC regions, BOLD activity at decision onset increased when the probability of being rewarded associated with the erotic picture option increased and decreased when the probability of being rewarded associated with the drink option increased (yellow bar graphs**, Fig 4B)**. However, only the lOFC encoded the value of the chosen option when committing to choice, as there was a positive correlation between BOLD activity in the lOFC, but not in the vmPFC (**Fig. 4B**, red bar graphs in **Fig. 4B**). These findings extend to human cognition previous observations that monkey lOFC neurons code the subjective values of options on a common currency scale during economic choices (Padoa-Schioppa and Assad, 2006; Padoa-Schioppa and Assad, 2008; Tremblay and Schultz, 1999).

To further characterize the respective contributions of lOFC and vmPFC to value-based decision-making, we investigated the relationship between regional BOLD activity at decision onset and mEZ2 drift-diffusion model parameters. On one hand, we found a positive correlation between BOLD activity and the gain of the decision variable in the vmPFC (F**ig. 4C,** r=0.666, p=0.009), but not in the lOFC (F**ig. 4C,** r=0.031, p=0.914). Because the gain parameter captures the decisional weight per value unit, it is a crucial feature of the decision value signal that is integrated over time in the drift-diffusion process (**Fig. 3A**). As a consequence, our results demonstrate that the vmPFC codes a difference-based decision value signal scaled to drive a drift-diffusion decision process and generalize to economic decision-making previous observations that the vmPFC computes the difference in probabilistic evidence supporting each option during binary value-based decisions (Kahnt et al., 2010b;

Philiastides et al., 2010). On the other hand, there was a significant correlation between the decision value's parametric effect and the value range in the lOFC (F**ig. 4D,** r=0.722, p=0.003), but not in the vmPFC (F**ig. 4D,** r=0.094, p=0.749), such that the slope of the regression line between BOLD activity in the lOFC and decision value tended to be steeper when value range tended to be narrower. This result is consistent with previous observations of neural activity adaptation to value range in monkeys lOFC, an important property of brain regions involved in representing values that maintains computational efficiency over widely varying value ranges (Tremblay and Schultz, 1999; Wallis and Kennerley, 2010; Padoa-Schioppa, 2009). Taken together, our results support the idea that lateral and medial parts of the OFC have distinct functions, which reflect their distinct cortico-cortical connection patterns (Price, 2007). Putting our results in the light of recent literature (Chib et al., 2009; Rangel and Hare, 2010; Hare et al., 2010; Kang et al., 2011; Wunderlich et al., 2010; Plassmann et al., 2007, 2010), we propose that the vmPFC may function as a pre-decisional hub that aggregates and scales subjective values into a neural decision value signal fit to drive a drift-diffusion decision process. By contrast, the lOFC appears to be primarily involved in coding and tracking subjective values. Our proposal shed a new light on a recent monkey lesion studies showing that selective lesions in the lOFC disrupted option value learning, whereas selective lesions in the vmPFC disrupted value-based decision-making: the vmPFC-lesioned monkeys made sub-optimal choices more frequently, the hallmark of less efficient decision-making (Noonan et al., 2010).

Alternatively, our results may be interpreted as supporting the implementation of a drift-diffusion process by the vmPFC as opposed to our hypothesis of a two-steps process in which distinct brain regions implement the valuation and the drift-diffusion decision-making process (Padoa-Schioppa, 2010; Noonan et al., 2010; Grabenhorst and Rolls, 2011). Despite an abundant literature on perceptual decision-making linking action selection based on a drift-

diffusion process with the parietal and the dorso-lateral prefrontal cortices (Heekeren et al., 2008; Heekeren et al., 2004, 2006; Domenech and Dreher, 2010), it is possible that different brain regions implement decision-making in different cognitive domains. However, reviewing this literature indicates that a critical feature of the brain regions implementing sequential sampling decision-making process is that their BOLD activity correlates positively with RTs and negatively with the absolute drift-diffusion process decision variable's slope (Gold and Shadlen, 2007; Hanes and Schall, 1996) (**Figure 5B). Figure 4B** (blue bar graph) shows that there was no correlation between BOLD activity and RTs in the vmPFC or the lOFC, thereby excluding a direct implementation of a drift diffusion decision process in these brain regions. This result further supports our proposal that the vmPFC stands upstream of the actual decision-making stage (Kable and Glimcher, 2009; Rangel and Hare, 2010; Philiastides et al., 2010).

To further explore the functional dissociation between lOFC and vmPFC, we reasoned that if one of these two OFC regions, presumably the vmPFC, drove a drift-diffusion decision-making process, then the brain regions implementing it would be revealed by the increased information flow coming from the OFC during decision formation. To test this hypothesis, we performed a PPI analysis to assess changes in both OFC regions effective connectivity when participants engaged in economic decision formation (**see Methods**). We found that effective connectivity increased during decision formation between the vmPFC and a right lateralized network including the inferior parietal lobule, the dorso-lateral prefrontal cortex (rDLPFC), two brain regions whose involvement in the implementation of a drift-diffusion processes during perceptual decisions has received strong experimental supports (Heekeren et al., 2008; Heekeren et al., 2004, 2006; Domenech and Dreher, 2010), and the anterior insula (5% FWE corrected clusterwise, **Fig. 5A, Table S1**). Moreover, effective connectivity decreased during decision formation between the vmPFC and a set of brain

regions including the right inferior temporal gyrus and the resting-state network, defined as the posterior cingulate gyri, the anterior medial frontal cortex (BA10) and the angular gyri. The resting state network has been involved in top-down biases on sensory processing, filtering irrelevant stimuli, reorienting attention and broadcasting predictive codes toward sensory cortices in conjunction with perceptual decision-making (Corbetta et al., 2008; Summerfield and Egner, 2009) (5% FWE corrected clusterwise, **Fig. 5A, Table S1**). It is noteworthy that the parieto-dorsolateral prefrontal cortex and the rest-state network are known to be spontaneously anti-correlated, a feature thought to be functionally important (Corbetta et al., 2008). Here, we report an increased level of anti-correlation between the vmPFC and the rest-state brain network during economic decision formation. By contrast, there was no increase in the effective connectivity with lOFC during decision formation, which suggests either that it does not participate directly to value-based decision–making or that its role is mediated by the vmPFC (**Fig. S4, Table S1**).

Having characterized a network of brain regions whose effective connectivity with the vmPFC increases during economic decision formation, we then assessed whether BOLD activity within this network may contain the neural signature of a drift-diffusion process integrating vmPFC's decision value signal. Assuming a coupling between neuronal firing rates and hemodynamic response, BOLD activity in the brain regions coding the decision variable should decrease when the modulus of the decision value increases because, unlike drift-diffusion models formulation (**Fig. 3A)**, competing cortical assemblies implement the integration of the net evidence supporting each option, which results in a positive ramping activity at the population level (Gold and Shadlen, 2007; Lo and Wang, 2006; Churchland et al., 2008) (**Fig. 5B)**. Moreover, residual BOLD activity in the brain regions coding the decision variable should also correlate positively with decision time. **Figure 5B** illustrates how steeper accumulation slopes, yielding shorter RTs on average, result in lower BOLD

activity at decision onset after convolution with the canonical hemodynamic response function. We found that BOLD activity in the right DLPFC correlated negatively with the modulus of the decision value (p=0.03 FWE SVC clusterwise, Fig. 5**C)**. Moreover, post-hoc analyses indicated that residual BOLD activity in the right DLPFC was positively correlated with RTs (T-test, p= 0.02, **Fig.** 5**D)**. Taken together, these results support our view that economic decisions are implemented in the human brain as a two steps process in which the vmPFC builds a decision value signal by computing the difference between options' expected subjective values and drives a drift diffusion process, implemented in the right DLPFC, that integrates this difference signal over time to select the option with the higher subjective value. These results shed a new light on how applying rTMS to the right DLPFC alters human economic choices by tempering with sequential sampling decision-making process it implements, thus paralleling in the economic domain manipulations of perceptual choices by microstimulation of monkey parietal cortex (Hanks et al., 2006; Camus et al., 2009).

Finally, having demonstrated that the vmPFC acts as a pre-decisional hub driving the sequential sampling decision-making process, we investigated the neurobiological correlates of optimal economic choices. Building upon our findings that mEZ2's gain parameter accurately predicted participant's economic efficiency as decision-makers (**Fig. 3C**) and that average BOLD activity at decision onset in the vmPFC correlated with mEZ2's gain parameter (**Fig. 4C**), we searched the brain for regions in which effective connectivity with the vmPFC during decision formation depended on whether the forthcoming choice was optimal. We reasoned that the emergence of optimal choices may depend on the decision-making process' drive by the vmPFC and/or on the contribution of vmPFC's inputs to decision value computation. Whereas effective connectivity between the vmPFC and the right DLPFC accounts for the first, effective connectivity between the vmPFC and its input brain regions should accounts for the latter. Contrasting optimal and suboptimal choices, we found

that the effective connectivity with the vmPFC increased in the right internal globus pallidus, an output structure of the basal ganglia system, and in a large associative visual cortical network that included the fusiform gyri, the inferior occipital and temporal cortices and the parahippocampus, when choices were optimal (**Fig. 6**). We did not find any connectivity changes with the vmPFC in the OFC, the amygdala or the DLPFC even at a very liberal threshold of 0.01. There was no brain region associated with a decrease in effective connectivity with the vmPFC. These results rule out the hypothesis that optimal choices are associated with an increased connectivity between the vmPFC and the right DLPFC and emphasize the contribution of vmPFC inputs to the computation of a decision value signal that accurately describes the proposed offer. Because of previous experimental evidence showing that visual associative cortices code for option reward likelihoods during value-based decisions, a source of probabilistic evidence used by the vmPFC to compute a difference-based decision value signal (Philiastides et al., 2010), we interpreted these results as supporting our hypothesis that optimal choices were associated with a higher contribution of external vmPFC inputs in the computation of the decision value signal. Interestingly, the parahippocampal gyri and the vmPFC are anatomically closely interconnected, suggesting that it may serve as a relay for economic decision-related information between associative visual cortices and the vmPFC (Price, 2007). Finally, our results provide further evidence excluding the hypothesis that the lOFC may directly contribute to value-based decision-making, even through the vmPFC. As a control, we tested for changes in effective connectivity during choices formation between the lOFC and the rest of the brain when comparing optimal and suboptimal choices and found no significant changes. Overall, our results support the view that the lOFC tracks values at the different steps of economic decision, without directly contributing to value-based decision-making.

Discussion

Our findings demonstrate that economic choices are implemented in the human brain as a two-step process, spatially dissociating the computation of a difference based decision value signal (valuation stage) and the probabilistic selection of one of the options by a sequential sampling decision process (decision-making stage). This neuro-computational approach to economic choices allowed us to characterize a new medio-lateral functional dissociation within the human OFC. More specifically, we showed that during economic choices, the medial portion of the OFC (vmPFC) operates as a pre-decisional hub in which external probabilistic evidence and inner subjective preferences are aggregated into a common decision value signal (**Fig. 4 and 6**). Crucially, this signal correlates with the difference between option's expected subjective values and is scaled to the decisional weight per unit of subjective value (**Eq. 3 and Fig. 4)**, which are the two key features of the drift-diffusion decision process' input, as illustrated in **figure 3A**. Moreover, this decision value signal coded in the vmPFC drives a sequential sampling decision process implemented in the DLPFC, as demonstrated by the increase in effective connectivity during economic choices between the vmPFC and the right DLPFC, and the correlation between trial-by-trial BOLD activity in the right DLPFC and the slope of the sequential sampling model (**Fig.** 5). Taken together, our results demonstrate the pivotal role of the vmPFC in computing the input to the sequential sampling decision-making process during economic choice formation.

This new insight into vmPFC's function unifies previously scattered observations of ventro-medial prefrontal activations during decision-making paradigms within a general neuro-computational framework. For example, the human vmPFC is the only brain region in which multivariate pattern analysis of BOLD activity predicts the value associated with complex sensory cues on which perceptual decisions probabilistically yielding reward feedbacks are performed (Kahnt et al., 2010a). Moreover, the vmPFC uses the probabilistic

evidence of reward coded in visual associative cortices to compute a difference-based signal that may guide the decision, which echoes with our own finding that effective connectivity between associative visual cortices and vmPFC increases when choices are optimal (**Fig. 6**) (Philiastides et al., 2010). Finally, a recent fMRI study examining cost-benefit-based decisions, based on the premises that the amygdala should be the decision input for costs and the striatum the input for gains, found that the effective connectivity between the difference in BOLD activity of the two brain region and the vmPFC correlated with the average slope of a power diffusion model suggesting again that the vmPFC may compute a difference-based signal (Basten et al., 2010). Consistent with our model, in all these paradigms the vmPFC computed a difference-based signal reflecting the values on which the ongoing decision was based.

By contrast, we found no evidence involving the lateral portion of the OFC in economic decision-making (**Fig. 4 and S4)**. Although BOLD activity in the lOFC correlated with decision value, its activity did not reflect the decisional weight of subjective values, demonstrating that lOFC activity was not suited to drive the decision process. Moreover, whole brain lOFC's effective connectivity did not increase during decision formation nor varied between optimal and suboptimal choices, which further supported our conclusion that participants did not rely on lOFC's value-related activity to make their choices. Instead, lOFC functional features suggested a role in tracking the subjective values at stakes before and after decisions (**Fig. 4**). Indeed, parametric response to decision value in the lOFC adapted to the range of values at stake, a slow adaptation mechanism that optimizes the precision of value coding, and the lOFC coded for the value of the chosen option, a post-decisional value signal arising when participants committed to a choice. Interestingly, selective lesions of the lOFC have been shown to impair the learning of option values when choices are based on values. Indeed, choice behavior of lOFC lesioned monkeys suggested that they were unable to

correctly pair up option values estimates with the outcome of choices, leading to erroneous updates and cancelling Thorndike's "law of effect" (Noonan et al., 2010). In our task, as well as in previous studies on economic choices (Padoa-Schioppa and Assad, 2006; Padoa-Schioppa and Assad, 2008), participants did not have to learn by trial and errors the contingencies between options and outcomes because visual cues explicitly provided all the information relevant to the choice. However, option values had to be updated after each choice to account for the repeated consumption of goods, which was susceptible to progressively shift preferences, as illustrated by the minor drifts observed in three of our participants. Thus, we propose that the lOFC tracks the subjective values at stake during the successive phases of an economic choice to appropriately update the value of the chosen option.

The ability of sequential sampling models to provide a unified account of perceptual decisions, which is supported by many studies linking a parieto-prefrontal network with the accumulation of sensory evidence toward a decision threshold to form perceptual decisions (Gold and Shadlen, 2007; Heekeren et al., 2008), have recently fueled a theoretical debate about whether sequential sampling decision process may be a general decision-making mechanism in the human brain, whose function extends across cognitive domains (Kable and Glimcher, 2009; Rangel and Hare, 2010; Freedman and Assad, 2011; Gold and Shadlen, 2007). Our results strongly support this view, as we demonstrate here that the role of the DLPFC in implementing sequential sampling decision process extends to the domain economic choices. Moreover, sequential sampling models accurately account for behavior during memory retrieval tasks, suggesting that the DLPFC might be similarly engaged in decision-making based on memories (Ratcliff and McKoon, 2008; Gold and Shadlen, 2007). Thus, we propose that the DLPFC implements sequential sampling process as a general mechanism for making decisions, whether based on sensory evidence or subjective values.

When performing perceptual decisions on random motion dot clouds, specialized neural populations in associative visual cortices encode moment-to-moment level of sensory evidence for each direction of motion and directly project to the LIP/DLPFC network where sensory evidence are progressively accumulated until it reaches a decision threshold (Gold and Shadlen, 2007). In contrast with perceptual decisions, economic choices involve an additional brain region between before the DLPFC's sequential sampling decision process. The vmPFC aggregates all relevant sources of information into a unique difference-based value signal, which in turn drives a sequential sampling decision-making process during economic choice formation. This difference of functional architectures raises the question of why the vmPFC has evolved into a pre-decisional hub computing subjective values whereas it has no equivalent for perceptual decision-making? To compute the subjective value attributed to a fruit, one has to combine many sources of information such as fruit size, color, texture, fragrance, but also past experiences, memories, hunger, emotions and cognitions (Hare et al., 2009; Coricelli et al., 2005; Philiastides et al., 2010). Clearly, a crucial difference between perceptual decisions and economic choices pertains to the complexity of the information on which decisions are made. Thus, a first hypothesis is that a pre-decisional hub dedicated to the computation of subjective values is needed because of the complexity of the computations needed to aggregate all these sources of information into a single neural common currency measuring the worth of prospects. Another interesting feature of the vmPFC is that it is involved in coding subjective values even in the absence of actual decisions, during imaginary economic choices or subjective ratings of pictures (Lebreton et al., 2009; Kang et al., 2011). In this later example, vmPFC BOLD activity during subjective ratings correlated with subject's revealed preferences estimated using a binary choice task performed outside the scanner, supporting the hypothesis that the vmPFC performs the same computations in both tasks (Lebreton et al., 2009). Furthermore, combined expected values during multi-attribute

subjective ratings are predicted by multivariate pattern of BOLD activity in the vmPFC, thus confirming the ability of the vmPFC to aggregate very different kind of information into a value based signal even outside the context of value-based decision (Kahnt et al., 2010a). Interestingly, this ability to perform the same function inside and outside the context of decision-making seems to generalize to the lOFC since neurons in monkey lOFC code the subjective values associated with visual cues during simple conditioning tasks, in the absence of any decision (Tremblay and Schultz, 1999) and contrasting BOLD activity at feedback for rewarded and unrewarded choices (**Fig. S4**) revealed the very same pattern than our previous studies on prediction error signals in operant conditioning tasks using the same erotic pictures and fruit juice delivery device (Sescousse et al., 2010) **(ELISE)**, suggesting that similar process are engaged whether a feedback results from a choice or not.

Conclusion

Our findings bridge economics and neuro-computational views on value-based decision-making within a unified theoretical framework characterizing the computations preformed in keys prefrontal brain regions. Here, in accordance with economic view on value-based choices, in particular decision field theory, we show that decision are implemented as a two-steps process in which the DLPFC implements the selection of the appropriate option using a sequential sampling decision process and the vmPFC the computation of a decision value signal that drive the DLPFC. Our results highlight the need to further fractionate the concept of "valuation" into its core cognitive components by further exploring electrophysiological activity in the vmPFC and the lOFC during economic choices, in order to further validate our model and demonstrate the power of model-driven fMRI in challenging complex cognitive questions.

Materials and Methods

Participants

Eighteen right-handed healthy volunteers (mean age: 21.5+/-3 years SD, mean handedness score: 0.812+/-0.2 SD) with no history of neurological or psychiatric conditions were screened for inclusion through a medical interview and standardized questionnaires assessing major depressive disorder (Beck Depression Inventory 21, mean score: 2.9+/-3.58 SD), erotic picture induced arousal (Sexual Assessment Inventory, global score: 93.3+/-13.2 SD, subtotal on erotic picture related items [3,14,20,23]: 11.56+/-2.67 SD on 20), as well as the absence of sexual dysfunctions and heterosexual orientation (Brief Sexual Function Questionnaire, 79.33+/-21.87 SD). All subjects gave written informed consent to be part of the experiment, which was approved by the local ethics committee (CPP, Centre Léon Berard).

Out of the initial pool of 18 subjects, we excluded one subject who scored above BDI criterion for a major depressive episode and another one who had a previously undiagnosed cerebral anatomical abnormality. We further excluded two subjects from subsequent analyses: One subject always chose the option rewarded by erotic pictures preventing the estimation of his preference and the other one exhibited an inconsistent choice pattern that included transitivity violations, casting doubts on this subject's comprehension of experimental instructions.

Value-based decision-making paradigm

Participants were asked to choose between two options (offer), one of which was probabilistically rewarded by an erotic picture (erotic picture option) and the other one by a small amount of fruit juice (0.75 ml, drink option). At the beginning of each new choice trial

(decision onset), two cues were displayed around a central fixation cross (**Fig. 1A**). Each cue indicated the probability of obtaining the reward as a pie chart and its type as a pictogram. Erotic picture and drink options were randomly displayed on the left or right side of the fixation cross. 31 different offers were built by systematically varying the reward probabilities (p=[0.25, 0.5, 0.75, 1]) associated with the two options. Each offer was repeated 16 times during the course of the experiment. Moreover, 8 additional offers consisting of one option never rewarded against another one probabilistically rewarded (p=[0.5, 1]) were also built, but repeated only 8 times (**Fig. 1B**). Following the decision onset, the participants were given 3 seconds to indicate their choice (left or right option) using a two-responses button box (commitment to decision). Immediately after the subject's choice, the chosen option was highlighted (350 ms) and a small arrow circling around the chosen cue symbolized a real-time drawing from the reward distribution indicated by the cue (jittered 3530-4830 ms). Then, upon "picture" choices, a picture of a slightly dressed or nude woman (rewarded trial) or a neutral scrambled image (unrewarded trial) was displayed on the screen for 2.5 seconds. Upon "drink" choices, a picture showing a glass filled with juice was displayed on the screen for 2.5 seconds while 0.75 mL of fruit juice was simultaneously delivered to the subject's mouth through a polythene tube mounted on an automated syringe pump (rewarded trials) or a neutral scrambled image (and no fruit juice) was displayed without any fluid delivery (unrewarded trials). To promote a high level of motivation throughout the experimental session, participants were asked to avoid sexual intercourses for 24h and drinking for 12h prior to the scanning session. Moreover, they were told that drinking would not be allowed for a few hours after the scanning session.

The experiment was split into 4 runs of 70 choice trials. On average, each choice trial lasted 14 s and was followed by a 4-6 s inter-trial interval (**Fig. 1A**). Conditions order was randomized and counterbalanced across sessions and sessions order was counterbalanced

across subjects. Immediately before and after the fMRI session, participants were presented with motivational questionnaires to quote, using rating scales numbered from 1 to 5, their desire for various drinks (including the apple juice used in our experiment). Theses questionnaires allowed us to assess their motivation for drink and its stability over the experimental session.

Stimuli

Three kinds of stimuli were used in our experiment (**Fig. 1A**): (1) "Erotic pictures" showed slightly dressed or nude women and were selected to induce moderate to high sexual arousal but no negative emotion such as disgust (Redouté et al., 2000). Each picture was presented only once during the experimental session to preclude habituation effects. (2) The "fruit juice" reward consisted of 0.75 mL of apple juice directly delivered to the participant mouth. The amount of fruit juice delivered for each rewarded trial was experimentally set during pretests to minimize satiety effects potentially arising from repeated deliveries of the reward. (3) Neutral pictures were scrambled versions of the erotic pictures used in the experiment. This procedure allowed us to remove all spatial information while preserving the original chromaticity and luminance.

Measuring preferences

In our experiment, participants chose between two options that probabilistically yielded different goods. Behaviorally, their choices depended on the probability of being rewarded, as well as on the relative value between goods. To measure preferences for fruit juice over erotic pictures ($\mathbf{R_{drink/picture}}$), we fitted to each participant's choice pattern a logistic model that predicted the probability of choosing the "drink" option as a function of the probabilities of being rewarded and of a time variable (trial number) (**Eq. 1)**. This time

variable accounted for potential drifts in participants' preferences that may arise from repeated deliveries of goods, thereby modeling out this potential confound from the estimation of the subjective values. Because our method measures subjective values on a common value scale, which is defined up to a scaling factor, we computed the preference as the ratio of the estimated subjective value for fruit juice and erotic pictures (**Betas in Eq. 2**). Then, using this measure of preference ($\mathbf{R_{drink/picture}}$), we also computed the decision value for each offer, defined as the difference between the expected subjective values associated with each option (Chib et al., 2009) (**Eq. 3**). The expected value associated with each option was computed as the product between the subjective value of the prospect (1 for erotic pictures, R for juice) and the probability of being rewarded. We computed the value range as the difference between the maximum and the minimum subjective values available during the course of the experiment **(Eq. 4**).

When presented with an offer whose decision value was null, participants were equally likely to choose both options because they were perceived as being subjectively equivalent. For clarity, we report preferences as "equivalent offers" matching the number of 0.75 mL juice drops to the subjective value of an erotic picture (1 picture = $\mathbf{R_{drink/picture}}$ juice drop, **Fig. 2A**).

$$Logit\big(P(Choice = Drink)\big) = \beta_{cst} + \beta_{time} * trial\ number + \beta_{fruit\ juice} * P_{drink\,option} + \beta_{erotic\,picture} * P_{picture\,option} + \varepsilon \quad \textbf{(Eq.} 1)$$

$$R_{drink/picture} = \left| \frac{\beta_{fruit\ juice}}{\beta_{erotic\ picture}} \right| \quad \textbf{(Eq.} 2)$$

$$DV = R_{drink/picture} * P_{drink\,option} - P_{picture\,option} \quad \textbf{(Eq.} 3)$$

$$Value\,Range = R_{drink/picture} + 1 \quad \textbf{(}\text{Eq. } 4)$$

Our method to measure preference was highly consistent (R^2=0.98) with alternative approaches such as plotting choice probabilities against objective quantities and identifying the offer to which each participant was indifferent (Padoa-Schioppa and Assad, 2006; Padoa-Schioppa and Assad, 2008).

To illustrate each participant's choice pattern, we plotted the probability of choosing the "drink" option against the decision value for each offer and fitted a three parameters Weibull function weighted to equal 0.5 when decision value is null (subjective equivalence point) (**Eq. 5**). We then computed the choice uncertainty associated with each offer as proposed by Grinband *et al.*(Grinband et al., 2006) (**Eq. 6**), which reflects the uncertainty on choice outcome when the expected subjective value is known for each option *a priori*. Finally, we measured the efficiency of each participant as a decision-maker by computing the choice uncertainty function's full width at half maximum (FWHM). This measure decreases as the ability of an agent to choose optimally – that is, to always pick the option with the highest expected subjective value – increases (**Fig. 2A, right panel**).

$$P_{Choice=Drink}(DV;\alpha,\beta,\gamma) = 1 - \exp\left(-\left(\frac{DV+\gamma}{\alpha}\right)^{\beta}\right) \qquad \text{with: } \gamma \geq -\min(DV),\ P_{Choice=Drink}(0;\alpha,\beta,\gamma) = 0.5 \quad \textbf{(Eq. 5)}$$

$$CU(DV;\alpha,\beta,\gamma) = \frac{\left|\left|0.5 - P_{Choice=Drink}(DV;\alpha,\beta,\gamma)\right| - 0.5\right|}{0.5} \quad \textbf{(Eq. 6)}$$

EZ2 Drift diffusion model: Adaptations to value-based decisions

We used modified EZ2 drift diffusion models (mEZ2) to fit the mean RTs, RT variances and choice probabilities for each participant and investigate the computational mechanisms underlying value-based decision-making. EZ2 drift diffusion models are well suited to small data sets as they predicts the first two moments of each choice's RT distribution and choice probability rather than full RT distributions (Wagenmakers et al.,

2007, 2008; Wagenmakers and Brown, 2007; van Ravenzwaaij and Oberauer, 2009; Grasman et al., 2009; Ratcliff and Tuerlinckx, 2002; Ratcliff, 2008). Nevertheless, EZ2 models retain most features of the Ratcliff's drift diffusion model, as they are a simplified variant in which inter-trial parameters variability (slope, non-decision time and starting point) is neglected (Wagenmakers et al., 2007, 2008). By contrast, more simplistic fitting procedures such as power rate "diffusion models" are unable to account for RT variances, do not allow for mechanistic hypothesis testing, as only the slope of the accumulation can vary and as bias and performance estimates are, to the best of our knowledge, currently unavailable (Padoa-Schioppa and Assad, 2006; Palmer et al., 2005). Hence, building upon a robust EZ2 drift diffusion model (Wagenmakers et al., 2007, 2008), we developed and validated a variant able to account for value-based decision-making from data sets small enough to be recorded during a typical fMRI session.

To do so, we reparametrized an EZ2 model according to several mechanistic hypotheses on the relationship between slope, decision threshold, non-decision time, starting point and decision value. **Figure 3A** illustrates our main model, in which the slope is equal to the decision value weighted by a "gain" parameter and the starting point is set at mid distance from the accumulator boundaries. The decision threshold and the non-decision time are unchanged compared to the original formulation of the model. Hence, our main model has four parameters: preference, gain, decision threshold and non-decision time. We set the accumulator internal noise (scale parameter) to 1 for all participants, as determined by an exploratory analysis of the parameter space. Moreover, we built three additional models on top of our main model to investigate whether complementary mechanisms may participate to the decision-making process: (1) the decision value biases the starting point, (2) the absolute value of the decision value modulates the decision threshold, (3) the decision value modulates non-decision time.

EZ models have been shown to be sensitive to contaminant RTs (Ratcliff, 2008) and filtering strategies assuming RT distribution mixtures have been proposed as a remedy (Wagenmakers et al., 2008). However, this approach is not suited to the size of our data sets because contaminant proportion estimates are biased when sample size is less than 50. We addressed this issue by fitting our mEZ2 model on logRT distributions and by filtering contaminant RTs (highpass: 300 ms, low-pass: +4 DS). We fitted our mEZ2 model to mean RTs, RT variances and choice probabilities with a bounded NM simplex algorithm optimizing the sum across offers of the squared differences weighted by standard deviations. To obtain a worst case estimate of the proportion of contaminant in our data set, we modeled pooled Z-scored RTs for all offers and participants as a mixture of Ex-Gaussian and uniform distributions using previously validated methodology (Wagenmakers et al., 2008) (Proportion of contaminant RT=0.72%, n=3901). **Figure S2** provides the results of parameter retrieval Monte Carlo validation studies (n=2000 synthetic experiments) estimating error bias and 95% confidence interval for each parameter under different levels of contaminant RTs (Wagenmakers et al., 2007, 2008) and shows that our mEZ2 model provide unbiased and precise parameter estimates when synthetic data sets mimicking our experiment are provided as input.

MRI Data Acquisition

Participants were scanned at the CERMEP - imagerie du vivant using a research dedicated 1.5T MRI scanner (Siemens Magnetom Sonata with an eight-channel head coil). We acquired 1016 echo-planar T2*-weighted functional volumes over 4 runs, each run lasting about 15 minutes (404 volumes/run). Each volume comprised 26 axial slices acquired continuously over 2.5 s (TE=60 ms; ascending interleaved acquisition; slice thickness 4 mm; 0.4 mm noncontiguous; axial AC–PC; in-plane resolution: 3.44*3.44 mm2; matrix size:

64*64 in a 220x220 mm field of view), allowing complete brain coverage. Additionally, T1-weighted anatomical images were acquired at the end of each experimental session (MP-RAGE: TR=1970ms; TE=3.93ms; T1=1100ms; resolution: 1*1*1 mm3; matrix size: 256*256). Head motions were minimized using foam padding and headphones with earplugs were used to dampen the scanner noise. The participants were instructed to keep the fruit juice in their mouth as long as the associated picture showing a fruit juice glass was displayed and to wait for the inter-trial interval to swallow in order to reduce movement artifacts.

fMRI Data analysis

Preprocessing. Data were processed and analyzed using SPM5 software (Wellcome Department Of Imaging Neuroscience, University College London, UK, www. fil.ion.ucl.ac.uk/spm). The first eight volumes of each run were removed to allow for T1 equilibrium effects (400 volumes/run). Image preprocessing consisted of slice timing interpolation, motion correction (six-parameters, rigid body transformation). We used realignment parameters during the statistical analysis as covariates to model out potential nonlinear head motion artifacts. Functional and morphological images were then normalized into standard MNI space using EPI Montreal Neurological Institute template. Then, functional volumes were resampled and spatially smoothed with an isotropic 8 mm FWHM Gaussian kernel. A 128 s temporal "high-pass filter" regressor set was included in the design matrix to exclude low-frequency noise and artifacts.

Finally, we explored the data for potential artifacts using tsdiffana, mean and variance images (http://imaging.mrc-cbu.cam.ac.uk/imaging/DataDiagnostics). An artifact is defined as the co-occurrence of a variance spike and a mean intensity drop uncorrelated with experimental design. We did not exclude any volume using these criteria. Translational

movements estimated during the realignment procedure were small as compared to voxel size (>1 mm).

Main General Linear Model. Whole-brain statistical parametric analyses were performed using a two-stage random-effect approach. We estimated independently the model parameters from each subject's dataset and then made population inferences using the parameter inter-subject variance. Regressors were constructed by convolving functions representing the events with the canonical hemodynamic response function. Five event-related categorical regressors were used to model choice trials ("Decision onset", "Commitment to choice", "Wait", "Picture reward" and "Drink reward", **Fig. 1C**). In accordance with drift diffusion model account of decision-making, ongoing processes during value-based decision formation were modeled as Dirac functions time locked to each decision onset (Decision onset) to which we added two parametric regressors: response time and decision value (**Eq. 3**). On the other hand, processes associated with decision threshold crossing or motor responses were modeled as a Dirac function time locked to the response button press (Commitment to choice) to which we added two parametric regressors: a "left-right" regressor that was equal to 1 when the option selected was displayed on right of the fixation cross and to 0 otherwise and a "chosen value" regressor, equal to the expected subjective value of the chosen option. Feedbacks on choices were included in the model as two categorical regressors (Drink feedback and Picture feedback) modeled as 2.5s long boxcar functions time locket on the onset of feedbacks. Rewarded and Unrewarded trials were modeled as a parametric regressor equal to 0 when a scrambled picture was delivered and to 1 otherwise. Finally, processes unrelated to decision were modeled as boxcars time locked on the decision onset whose duration equal the time between the decision onset and the feedback onset (Wait). While designing our model, we controlled for multi-colinearity by computing the variance

inflation factor for each parametric regressor within each categorical regressor and by rejecting combinations of parametric regressors that yielded a VIF superior to 4 for at least one of the regressor(O'brien, 2007). Parametric regressors were then estimated on the basis of the variance they uniquely explained. Statistical inferences were performed with a threshold of 5% FWE corrected cluterwise using WFU pick-atlas built-in morphological of the OFC and small volume correction (voxelwise threshold: 10^{-3} uncorrected).

Psycho-physiological interaction analysis. To identify brain regions whose effective connectivity with lOFC and vmPFC changed significantly during decision formation, we performed a psycho-physiological interaction analysis. First, we extracted individual ROI-averaged BOLD activity time series from vmPFC and lOFC functional regions using Marsbar toolbox (v0.42, threshold $p<10^{-3}$ voxelwise, **Fig. 4A**). Then, we estimated a PPI-GLM including five regressors: (1) a psychological regressor, modeling decision formation as RT-long boxcars time-locked with decision onsets and convolved with the canonical HRF. (2-3) BOLD activity time-courses in the two seed regions and (4-5) interactions between time-courses from each seed region and the psychological regressor. Finally, the PPI-GLM also included realignment parameters as non-interest covariates to model out potential nonlinear head motion artifacts. Statistical inferences were performed with a threshold of 5% (cluterwise) FWE corrected across the whole brain (voxelwise threshold: 10^{-3} uncorrected).

We ran two variants of this model that contrasted optimal and non-optimal choices and included only one seed region per analysis. Optimal choices were defined as choices in which the subjective value of the chosen option was greater than the value of the unchosen option (**Fig. 6**).

Region-of-interest analyses. To further characterize the role of the brain regions, we identified in the OFC and the DLPFC (**Fig. 4A** and 5**A**), we extracted ROI-averaged regression line slope estimates (parametric regressors) or ROI-averaged percent signal

changes (categorical regressors) using a leave-one-out cross-validation approach, that prevented circularity biases in the post-hoc ROI-based inferences we performed (Kriegeskorte et al., 2009, 2010). To do so, we built individual ROIs by computing a statistical map for each participant and for each contrast from the whole subject group minus the participant him/herself (threshold $p<10^{-3}$ voxelwise), hence explicitly splitting the subject's ROI-averaged parameter estimate from the data used for voxels selection.

ROI analyses were performed on three alternative versions of the main GLM (**see Main General Linear Model**). In a first variant of the main GLM (GLM1), we aimed to estimate average BOLD response amplitude during the decision-making process to assess its relationship to mEZ2 parameter estimates. To do so, we built and estimated a new GLM that retained the categorical regressors for decision onset, wait, picture and drink feedback, from the main GLM without parametric regressors. In a second variant (GLM2), we aimed to assess separately the relationship between BOLD activity and the expected value associated with the drink option, on one hand, and BOLD activity and the expected value associated with the picture option, on the other hand. So, we built and estimated a second model based on the main GLM, in which we substituted the expected value associated with the drink and with the picture options to the decision variable parametric regressor. GLM2 was otherwise identical to the main GLM. In a third variant (GML3), we aimed to identify candidate brain regions implementing our decision model's decision variable. Based on previous electrophysiological literature (Gold and Shadlen, 2007; Kim and Shadlen, 1999; Hanes and Schall, 1996), we hypothesized that event-related BOLD activity in such brain region would negatively correlate with the absolute value of the decision value as illustrated in **figure** 5**B**. Thus, we built and estimated a third variant of the main GLM, in which we substituted the absolute value of the decision value multiplied by each individual's gain parameter estimate to the

decision value parametric regressor in the main GLM. GLM3 was otherwise identical to the main GLM.

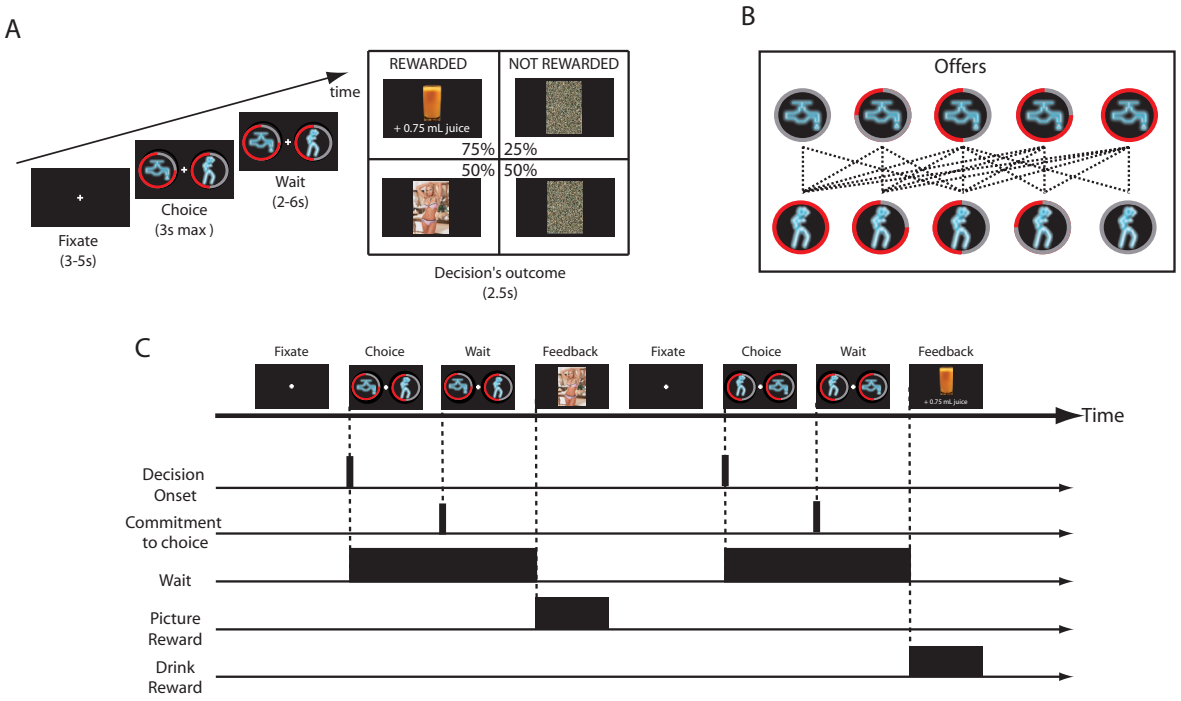

Figure 1: Experimental paradigm. (A) Participants were asked to choose between two options, one of which was probabilistically rewarded by an erotic picture and the other one by a fixed amount of fruit juice delivered to the subject mouth by a computer-driven pump. Here, the participant could choose between 75% chances of drinking 0.75 mL juice or 50% chances of viewing an erotic picture by pressing one of two responses button according to the position of the chosen option relative to the central fixation cross. After a random delay, the participant received the chosen goods according to his choice and the probability of reward associated ("rewarded" choice trials). A scrambled picture was displayed when the choice did not yield the expected good ("not rewarded" choice trials). **(B)** Thirty-nine different offers were built by systematically varying the reward probabilities (p=[0.25, 0.5, 0.75, 1]) associated with the drink and the picture options. **(C)** The main GLM included five event-related categorical regressors to model choice trials: Decision onset, Commitment to choice, Wait, Picture reward and Drink reward. In accordance with drift diffusion model accounts of decision-making, ongoing processes during value-based decision formation were modeled as Dirac functions time locked to each decision onset (Decision onset) and the processes associated with decision threshold crossing or motor responses were modeled as a Dirac function time locked to the response button press. Parametric regressors associated with each categorical regressor modeled events all the variables events and quantities relating to the decision process.

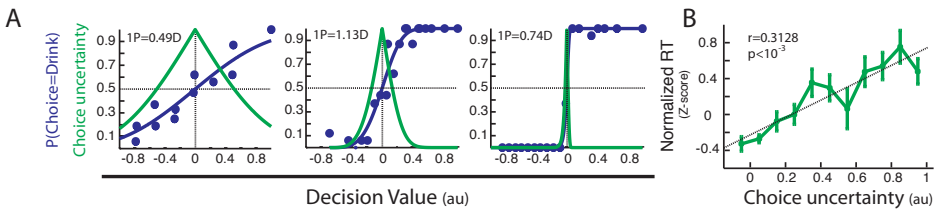

Figure 2: Behavioral results. (A) Probability of choosing the drink option (Blue sigmoid curve) and choice uncertainty (Bell shaped green curve) as a function of the decision value. Here, we show choice data from three participants. Plain blue circles represent measured probabilities of choosing the drink option given the decision value of the offer. **Figure S1** provides choice patterns for all the participants in our experiment. Dashed lines intersect at the point of subjective equivalence where decision value is null, choice probability at chance level and choice uncertainty is maximal. Preferences are reported (Insert: 1P=x*D) as equivalent offers expressing "how much" drops of juices (x*D) were subjectively equivalent to one erotic picture (1P). **(B)** Normalized response times as a function of choice uncertainty. Error bars represent standard errors.

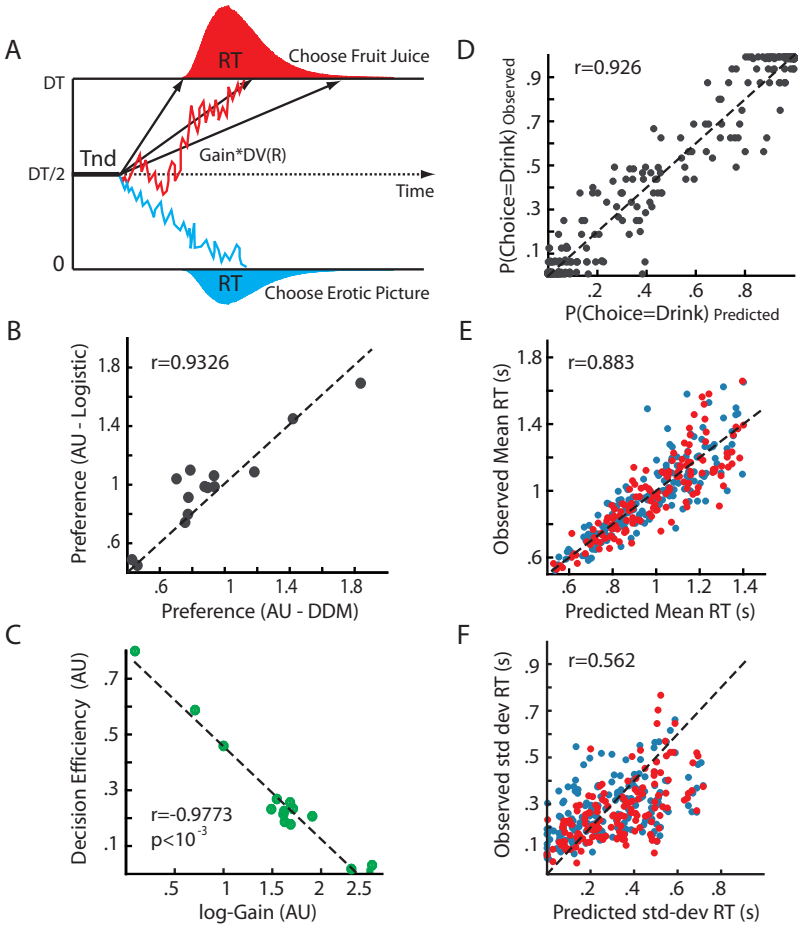

Figure 3: mEZ2 drift-diffusion model and behavioral fits. (A) The decision variable is initialized half-ways between an upper (DT) and a lower boundary (0), corresponding respectively to the decision threshold for choosing the fruit juice (red) and the erotic picture option (blue). After a fixed pre-decisional processing latency (Non-decision time, Tnd), the decision value neural signal progressively drives the decision variable, which represents the accumulation of the decision value weighted by a gain parameter, toward one of the boundaries. The decision value is the difference between the expected subjective value of the drink and the picture option, the decision value (noted DV(R), as it is a function of the preference, R). The gain parameter models the decisional weight conveyed by each value unit on each participant behavioral choices. A choice is made when the decision variable crosses one of the boundaries. (B) Revealed preference estimated using logistic regressions plotted against the preference estimated using the mEZ2 model. Each data point represents a participant. (C) Economic decision efficiency as a function of the logarithm of the gain parameter. Here, the decision efficiency is defined as the FWHM of the choice uncertainty curve for each participant because the wider the curve peak, the less optimal the choices are made by the participant (green bell shaped curve in **Fig. 2A**). Each data point represents a participant. (D-F**)** Probability of choosing the drink option (D), the mean RT (E) and the standard deviation of the RT (F) measured plotted against the mEZ2 model predictions. Each participant data set was fit separately, however we pooled here the data from all the participants for display. Thus, each plain black circle in panel D represents the probability of choosing the drink option for one of the thirty-nine offers made to one participant. In panel E-F, plain red circles represent the offers followed by a drink choice, whereas plain blue circles represent the offers followed by a picture choice. Data points tend to be aligned on the identity lines (dashed lines in panel D-F), as the model predictions are more accurate.

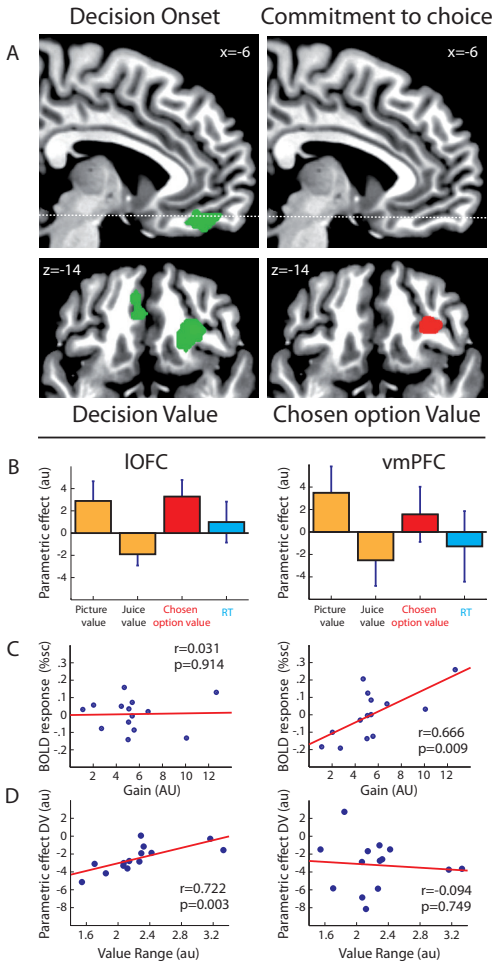

Figure 4: Mediolateral functional specialization in the OFC. (A) Parametric response to subjective values in the OFC (threshold of $p<10^{-3}$ voxelwise for display). OFC clusters showing a significant parametric response to the offer's decision value at decision onset are rendered in green (left column) and those showing a parametric response to the expected value of the chosen option at the time of commitment to choice are rendered in red (right column). (B) Bar graphs reporting the slope of the regression line between BOLD activity and the picture and juice expected value (yellow bars), the expected value of the chosen option (red bars) and response time (blue bars), in the lOFC (left graph) and the vmPFC (right graph). Error bars indicate 95% confidence intervals. In the lOFC, there was a significant parametric effect of the picture (T-test, p=0.0043), of the drink (T-test, p=0.0014) and of the chosen option (T-test, p=0.0013) expected values. In the vmPFC, there was a significant parametric effect of the picture (T-test, p=0.0124), of the drink (T-test, p=0.0384) and of the chosen option (T-test, p=0.252) expected values. By contrast, there was no parametric effect of RTs in both the vmPFC (T-test, p=0.5043) and the lOFC (T-test, p=0.3835). (C) Scatterplots of correspondence between mean BOLD activity at decision onset and the gain parameter estimated using the mEZ2 drift-diffusion model in the lOFC (left graph) and the vmPFC (right graph). (D) Scatterplots of correspondence between the slope of the regression line between BOLD activity at decision onset and the decision value (parametric effect of DV) and the value range (the difference between the maximal and the minimal subjective value in the experiment) in the lOFC (left graph) and the vmPFC (right graph). Please note that the significances of the linear relationship between parametric effect of decision value and value range observed were only marginally affected when removing the two most extremes subjects (value range > 2.5).

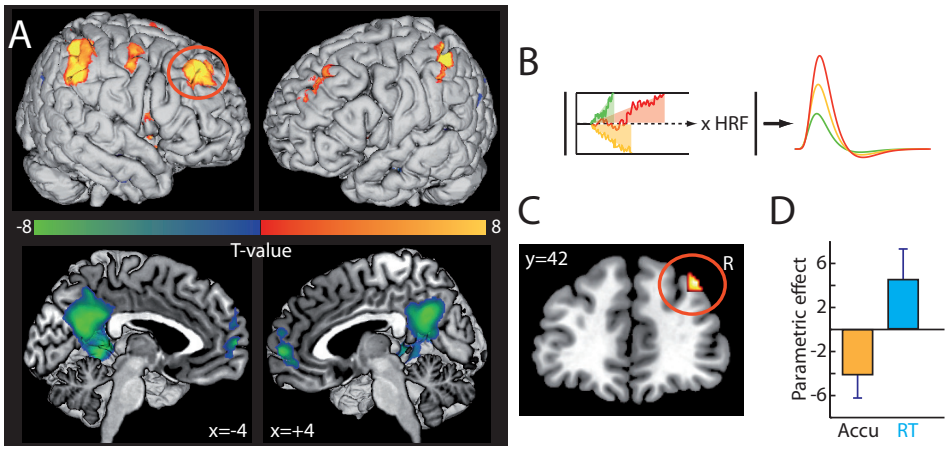

Figure 5: Brain region implementing a drift-diffusion decision process. (A) Psycho-physiological interaction whole-brain analysis between vmPFC and other brain areas during economic choices formation (PPI). Positive PPIs are rendered using a hot scale and negative PPIs are rendered using a cold scale (threshold for display, $p<10^{-3}$ voxelwise). (B) mEZ2 drift-diffusion model predictions on BOLD activity of brain region implementing this process: convolving predicted neural activity with the hemodynamic response function predicted lower BOLD activity for steeper accumulations of the decision value (green) and higher BOLD activity for longer RT (red). (C) Brain regions whose BOLD activity correlates negatively with the absolute value of the drift-diffusion process accumulation slope (MNI, xyz: 38, 42,42, 10^{-3} voxelwise, p=0.03 FWE cluster corrected) among the brain regions exhibiting a positive PPI with the vmPFC during decision formation. (D) Bar graphs reporting the slope of the regression line between BOLD activity and the absolute value of the drift-diffusion process accumulation slope (yellow bars, T-test, p=0.0029) and response times (blue bars, T-test, p= 0.02). Error bars represent 95% confidence intervals.

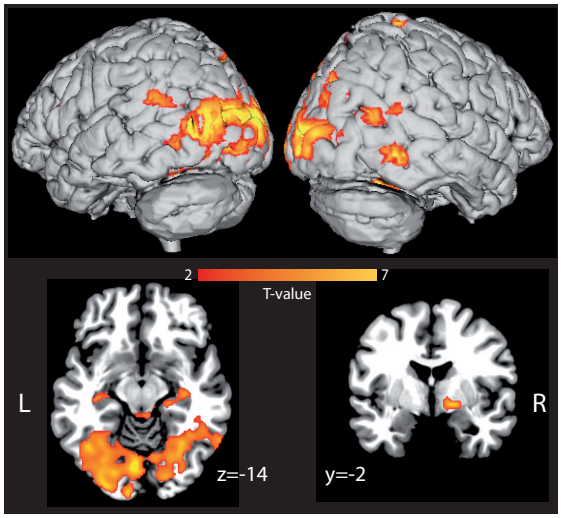

Figure 6: vmPFC input brain regions associated with optimal economic choices. We performed a psycho-physiological whole-brain analysis of vmPFC effective connectivity during economic choice formation by contrasting optimal and suboptimal choices. Positive PPIs are rendered using a hot scale and negative PPIs are rendered using a cold scale (threshold for display, $p<10^{-3}$ voxelwise).

Bibliography

Basten, U., Biele, G., Heekeren, H. R., and Fiebach, C. J. (2010). How the brain integrates costs and benefits during decision making. Proc. Natl. Acad. Sci. U.S.A *107*, 21767-21772.

Bogacz, R. (2007). Optimal decision-making theories: linking neurobiology with behaviour. Trends Cogn. Sci. (Regul. Ed.) *11*, 118-125.

Busemeyer, J. R., and Townsend, J. T. (1993). Decision field theory: a dynamic-cognitive approach to decision making in an uncertain environment. Psychol Rev *100*, 432-459.

Busemeyer, J. R., Jessup, R. K., Johnson, J. G., and Townsend, J. T. (2006). Building bridges between neural models and complex decision making behaviour. Neural Netw *19*, 1047-1058.

Camus, M., Halelamien, N., Plassmann, H., Shimojo, S., O'Doherty, J., Camerer, C., and Rangel, A. (2009). Repetitive transcranial magnetic stimulation over the right dorsolateral prefrontal cortex decreases valuations during food choices. Eur. J. Neurosci *30*, 1980-1988.

Chib, V. S., Rangel, A., Shimojo, S., and O'Doherty, J. P. (2009). Evidence for a common representation of decision values for dissimilar goods in human ventromedial prefrontal cortex. J. Neurosci *29*, 12315-12320.

Churchland, A. K., Kiani, R., and Shadlen, M. N. (2008). Decision-making with multiple alternatives. Nat. Neurosci *11*, 693-702.

Corbetta, M., Patel, G., and Shulman, G. L. (2008). The reorienting system of the human brain: from environment to theory of mind. Neuron *58*, 306-324.

Coricelli, G., Critchley, H. D., Joffily, M., O'Doherty, J. P., Sirigu, A., and Dolan, R. J. (2005). Regret and its avoidance: a neuroimaging study of choice behavior. Nat. Neurosci *8*, 1255-1262.

Deaner, R. O., Khera, A. V., and Platt, M. L. (2005). Monkeys pay per view: adaptive valuation of social images by rhesus macaques. Curr. Biol *15*, 543-548.

Domenech, P., and Dreher, J.-C. (2010). Decision threshold modulation in the human brain. J. Neurosci *30*, 14305-14317.

Frank, M. J., Samanta, J., Moustafa, A. A., and Sherman, S. J. (2007). Hold your horses: impulsivity, deep brain stimulation, and medication in parkinsonism. Science *318*, 1309-1312.

Freedman, D. J., and Assad, J. A. (2011). A proposed common neural mechanism for categorization and perceptual decisions. Nat Neurosci *14*, 143-146.

Gold, J. I., and Shadlen, M. N. (2007). The neural basis of decision making. Annu. Rev. Neurosci *30*, 535-574.

Grabenhorst, F., and Rolls, E. T. (2011). Value, pleasure and choice in the ventral prefrontal cortex. Trends Cogn. Sci. (Regul. Ed.) *15*, 56-67.

Grasman, R. P. P. P., Wagenmakers, E.-J., and van der Maas, H. L. J. (2009). On the mean and variance of response times under the diffusion model with an application to parameter estimation. Journal of Mathematical Psychology *53*, 55-68.

Grinband, J., Hirsch, J., and Ferrera, V. P. (2006). A neural representation of categorization uncertainty in the human brain. Neuron *49*, 757-763.

Hanes, D. P., and Schall, J. D. (1996). Neural control of voluntary movement initiation. Science *274*, 427-430.

Hanks, T. D., Ditterich, J., and Shadlen, M. N. (2006). Microstimulation of macaque area LIP affects decision-making in a motion discrimination task. Nat. Neurosci *9*, 682-689.

Hare, T. A., Camerer, C. F., Knoepfle, D. T., and Rangel, A. (2010). Value computations in ventral medial prefrontal cortex during charitable decision making incorporate input from regions involved in social cognition. J. Neurosci *30*, 583-590.

Hare, T. A., Camerer, C. F., and Rangel, A. (2009). Self-control in decision-making involves modulation of the vmPFC valuation system. Science *324*, 646-648.

Hare, T. A., O'Doherty, J., Camerer, C. F., Schultz, W., and Rangel, A. (2008). Dissociating the Role of the Orbitofrontal Cortex and the Striatum in the Computation of Goal Values and Prediction Errors. J. Neurosci. *28*, 5623-5630.

Heekeren, H. R., Marrett, S., Bandettini, P. A., and Ungerleider, L. G. (2004). A general mechanism for perceptual decision-making in the human brain. Nature *431*, 859-862.
Heekeren, H. R., Marrett, S., Ruff, D. A., Bandettini, P. A., and Ungerleider, L. G. (2006). Involvement of human left dorsolateral prefrontal cortex in perceptual decision making is independent of response modality. Proc. Natl. Acad. Sci. U.S.A *103*, 10023-10028.
Heekeren, H. R., Marrett, S., and Ungerleider, L. G. (2008). The neural systems that mediate human perceptual decision making. Nat. Rev. Neurosci *9*, 467-479.
Kable, J. W., and Glimcher, P. W. (2009). The neurobiology of decision: consensus and controversy. Neuron *63*, 733-745.
Kahnt, T., Heinzle, J., Park, S. Q., and Haynes, J.-D. (2010a). Decoding different roles for vmPFC and dlPFC in multi-attribute decision making. Neuroimage.
Kahnt, T., Heinzle, J., Park, S. Q., and Haynes, J.-D. (2010b). The neural code of reward anticipation in human orbitofrontal cortex. Proc. Natl. Acad. Sci. U.S.A *107*, 6010-6015.
Kang, M. J., Rangel, A., Camus, M., and Camerer, C. F. (2011). Hypothetical and real choice differentially activate common valuation areas. J. Neurosci *31*, 461-468.
Kim, J. N., and Shadlen, M. N. (1999). Neural correlates of a decision in the dorsolateral prefrontal cortex of the macaque. Nat. Neurosci *2*, 176-185.
Kriegeskorte, N., Lindquist, M. A., Nichols, T. E., Poldrack, R. A., and Vul, E. (2010). Everything you never wanted to know about circular analysis, but were afraid to ask. J. Cereb. Blood Flow Metab *30*, 1551-1557.
Kriegeskorte, N., Simmons, W. K., Bellgowan, P. S. F., and Baker, C. I. (2009). Circular analysis in systems neuroscience: the dangers of double dipping. Nat. Neurosci *12*, 535-540.
Kringelbach, M. L. (2005). The human orbitofrontal cortex: linking reward to hedonic experience. Nat. Rev. Neurosci *6*, 691-702.
Lebreton, M., Jorge, S., Michel, V., Thirion, B., and Pessiglione, M. (2009). An automatic valuation system in the human brain: evidence from functional neuroimaging. Neuron *64*, 431-439.
Lo, C.-C., and Wang, X.-J. (2006). Cortico-basal ganglia circuit mechanism for a decision threshold in reaction time tasks. Nat. Neurosci *9*, 956-963.
Milica Milosavljevic, Jonathan Malmaud, Alexander Huth, Christof Koch, and Antonio Rangel (2010). The Drift Diffusion Model can account for the accuracy and reaction time of value-based choices under high and low time pressure. Judgment and Decision Making *5*, 437-449.
Murray, E. A., O'Doherty, J. P., and Schoenbaum, G. (2007). What we know and do not know about the functions of the orbitofrontal cortex after 20 years of cross-species studies. J. Neurosci *27*, 8166-8169.
Noonan, M. P., Walton, M. E., Behrens, T. E. J., Sallet, J., Buckley, M. J., and Rushworth, M. F. S. (2010). Separate value comparison and learning mechanisms in macaque medial and lateral orbitofrontal cortex. Proceedings of the National Academy of Sciences *107*, 20547 -20552.
O'brien, R. M. (2007). A Caution Regarding Rules of Thumb for Variance Inflation Factors. Qual Quant *41*, 673-690.
Padoa-Schioppa, C. (2010). Neurobiology of Economic Choice: A Good-Based Model. Annu Rev Neurosci.
Padoa-Schioppa, C. (2009). Range-adapting representation of economic value in the orbitofrontal cortex. J. Neurosci *29*, 14004-14014.
Padoa-Schioppa, C., and Assad, J. A. (2008). The representation of economic value in the orbitofrontal cortex is invariant for changes of menu. Nat. Neurosci *11*, 95-102.
Padoa-Schioppa, C., and Assad, J. A. (2006). Neurons in the orbitofrontal cortex encode economic value. Nature *441*, 223-226.
Palmer, J., Huk, A. C., and Shadlen, M. N. (2005). The effect of stimulus strength on the speed and accuracy of a perceptual decision. J Vis *5*, 376-404.
Peters, J., and Büchel, C. (2010). Neural representations of subjective reward value. Behav. Brain Res *213*, 135-141.
Philiastides, M. G., Biele, G., and Heekeren, H. R. (2010). A mechanistic account of value computation in the human brain. Proc. Natl. Acad. Sci. U.S.A *107*, 9430-9435.

Plassmann, H., O'Doherty, J. P., and Rangel, A. (2010). Appetitive and aversive goal values are encoded in the medial orbitofrontal cortex at the time of decision making. J. Neurosci *30*, 10799-10808.
Plassmann, H., O'Doherty, J., and Rangel, A. (2007). Orbitofrontal cortex encodes willingness to pay in everyday economic transactions. J. Neurosci *27*, 9984-9988.
Price, J. L. (2007). Definition of the orbital cortex in relation to specific connections with limbic and visceral structures and other cortical regions. Ann. N. Y. Acad. Sci *1121*, 54-71.
Rangel, A., Camerer, C., and Montague, P. R. (2008). A framework for studying the neurobiology of value-based decision making. Nat. Rev. Neurosci *9*, 545-556.
Rangel, A., and Hare, T. (2010). Neural computations associated with goal-directed choice. Curr. Opin. Neurobiol *20*, 262-270.
Ratcliff, R. (2008). The EZ diffusion method: too EZ? Psychon Bull Rev *15*, 1218-1228.
Ratcliff, R., and McKoon, G. (2008). The diffusion decision model: theory and data for two-choice decision tasks. Neural Comput *20*, 873-922.
Ratcliff, R., and Tuerlinckx, F. (2002). Estimating parameters of the diffusion model: approaches to dealing with contaminant reaction times and parameter variability. Psychon Bull Rev *9*, 438-481.
van Ravenzwaaij, D., and Oberauer, K. (2009). How to use the diffusion model: Parameter recovery of three methods: EZ, fast-dm, and DMAT. Journal of Mathematical Psychology *53*, 463-473.
Redouté, J., Stoléru, S., Grégoire, M. C., Costes, N., Cinotti, L., Lavenne, F., Le Bars, D., Forest, M. G., and Pujol, J. F. (2000). Brain processing of visual sexual stimuli in human males. Hum Brain Mapp *11*, 162-177.
Samuelson, P. A. (1937). A Note on Measurement of Utility. The Review of Economic Studies *4*, 155-161.
Sescousse, G., Redouté, J., and Dreher, J.-C. (2010). The architecture of reward value coding in the human orbitofrontal cortex. J. Neurosci *30*, 13095-13104.
Simen, P., Contreras, D., Buck, C., Hu, P., Holmes, P., and Cohen, J. D. (2009). Reward rate optimization in two-alternative decision making: empirical tests of theoretical predictions. J Exp Psychol Hum Percept Perform *35*, 1865-1897.
Sugrue, L. P., Corrado, G. S., and Newsome, W. T. (2005). Choosing the greater of two goods: neural currencies for valuation and decision making. Nat. Rev. Neurosci *6*, 363-375.
Summerfield, C., and Egner, T. (2009). Expectation (and attention) in visual cognition. Trends in Cognitive Sciences *13*, 403-409.
Summerfield, C., and Koechlin, E. (2010). Economic value biases uncertain perceptual choices in the parietal and prefrontal cortices. Front Hum Neurosci *4*, 208.
Teichert, T., and Ferrera, V. P. Suboptimal Integration of Reward Magnitude and Prior Reward Likelihood in Categorical Decisions by Monkeys. Front Neurosci *4*.
Tobler, P. N., Fiorillo, C. D., and Schultz, W. (2005). Adaptive coding of reward value by dopamine neurons. Science *307*, 1642-1645.
Tom, S. M., Fox, C. R., Trepel, C., and Poldrack, R. A. (2007). The neural basis of loss aversion in decision-making under risk. Science *315*, 515-518.
Tremblay, L., and Schultz, W. (1999). Relative reward preference in primate orbitofrontal cortex. Nature *398*, 704-708.
Wagenmakers, E.-J., and Brown, S. (2007). On the linear relation between the mean and the standard deviation of a response time distribution. Psychol Rev *114*, 830-841.
Wagenmakers, E.-J., van der Maas, H. L. J., Dolan, C. V., and Grasman, R. P. P. P. (2008). EZ does it! Extensions of the EZ-diffusion model. Psychon Bull Rev *15*, 1229-1235.
Wagenmakers, E.-J., van der Maas, H. L. J., and Grasman, R. P. P. P. (2007). An EZ-diffusion model for response time and accuracy. Psychon Bull Rev *14*, 3-22.
Wallis, J. D. (2007). Orbitofrontal cortex and its contribution to decision-making. Annu. Rev. Neurosci *30*, 31-56.
Wallis, J. D., and Kennerley, S. W. (2010). Heterogeneous reward signals in prefrontal cortex. Curr. Opin. Neurobiol *20*, 191-198.
Wallis, J. D., and Miller, E. K. (2003). Neuronal activity in primate dorsolateral and orbital prefrontal cortex during performance of a reward preference task. Eur. J. Neurosci *18*, 2069-2081.
Wang, X.-J. (2008). Decision making in recurrent neuronal circuits. Neuron *60*, 215-234.

Wunderlich, K., Rangel, A., and O'Doherty, J. P. (2010). Economic choices can be made using only stimulus values. Proc. Natl. Acad. Sci. U.S.A *107*, 15005-15010.
Wunderlich, K., Rangel, A., and O'Doherty, J. P. (2009). Neural computations underlying action-based decision making in the human brain. Proc. Natl. Acad. Sci. U.S.A *106*, 17199-17204.

Supplementary legends

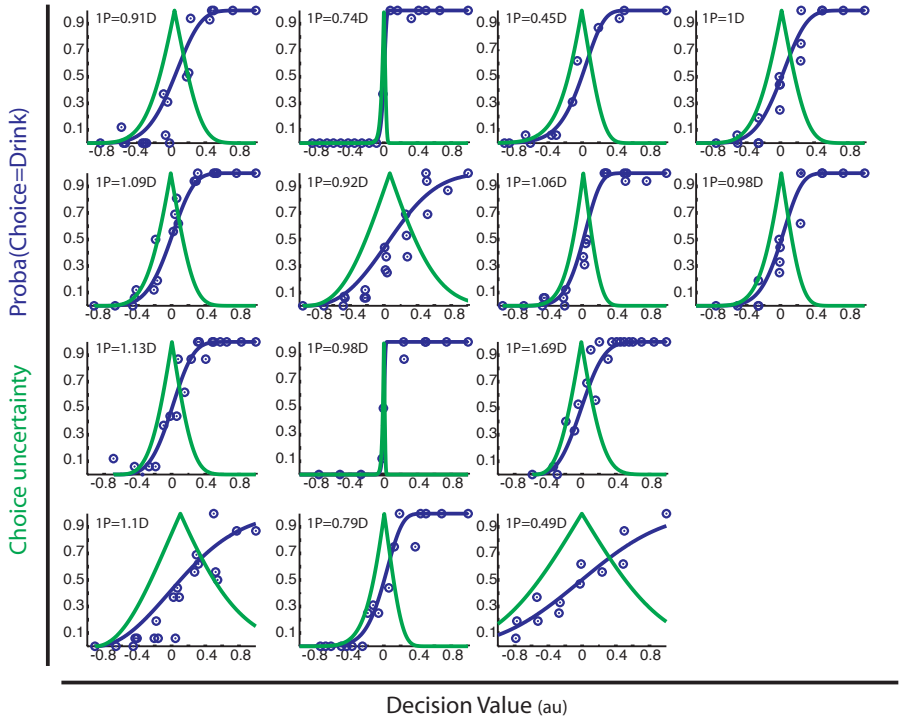

Figure S1: Behavioral results: choice patterns and RT. Probability of choosing the drink option (Blue sigmoid curve) and choice uncertainty (Bell shaped green curve) as a function of the decision value. Plain blue circles represent measured probabilities of choosing the drink option given the decision value of the offer. Dashed lines intersect at the point of subjective equivalence where decision value is null, choice probability at chance level and choice uncertainty is maximal. Preferences are reported (Insert: 1P=x*D) as equivalent offers expressing "how much" drops of juices (x*D) were subjectively equivalent to one erotic picture (1P).

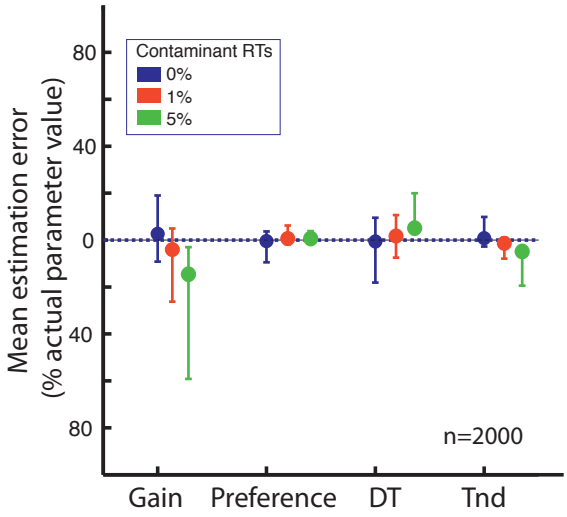

Figure S2: Parameter retrieval Monte Carlo validation study of the mEZ2 drift-diffusion model. We simulated 2000 experiments and fitted mEZ2 models to each synthetic data set. Here, we report estimations of the mean error on each parameter of the mEZ2 model (plain colored circles, % of the actual parameter value) and 95% confidence intervals (error bars) under three level of uniformly distributed contaminant RTs (see Methods). Level of contaminant RTs in our experiment was below 1%, thus mEZ2 model provided unbiased and accurate estimations of all the parameters.

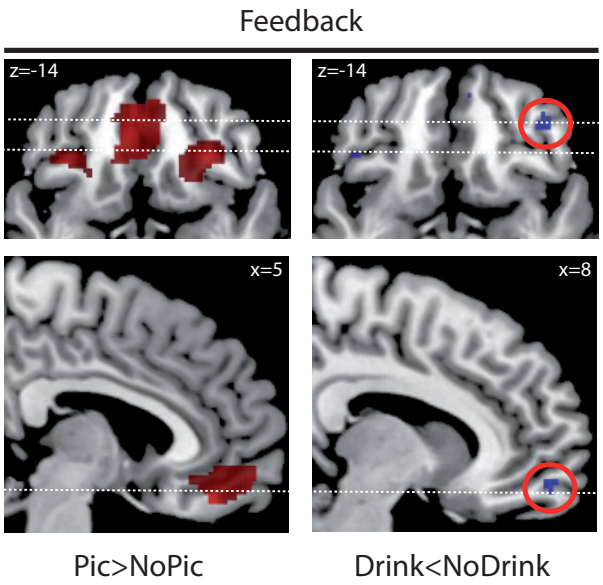

Figure S3: OFC regions responding to picture and juice decision outcomes (threshold of $p<10^{-3}$ voxelwise for display). Left column, OFC clusters significantly responding at the time of picture reward are rendered in red (Rewarded > Not rewarded). Right column, OFC clusters significantly responding at the time of drink reward are rendered in blue (Not rewarded > rewarded). Interestingly, signed OFC BOLD responses at the outcome were consistent with the coding of the decision variable in the OFC during economic decisions. OFC foci at the outcome correspond to meta-analytic coordinates for visual and drink reward consumption.

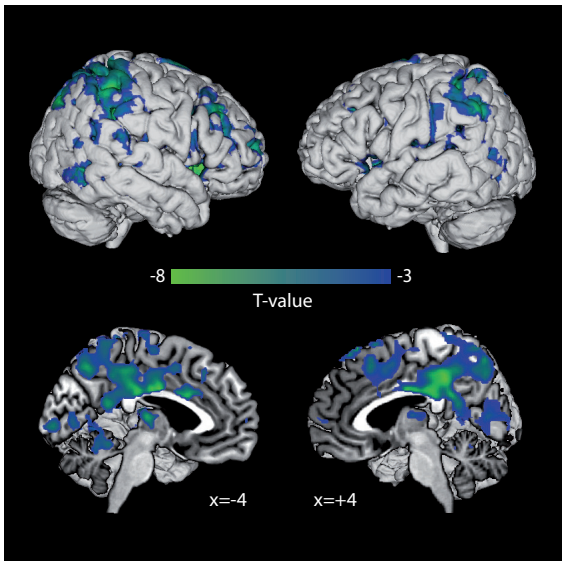

Figure S4: Psycho-physiological interaction whole-brain analysis between lOFC and other brain areas during economic choices formation (PPI). Negative PPIs are rendered using a cold scale (threshold for display, $p<10^{-3}$ voxelwise). There was no brain regions showed positive PPI with lOFC during decision formation.

5. DISCUSSION GENERALE

a. Activités neurales soutenues : Intégration et maintenance de l'information dans le cortex latéral préfrontal

Le cortex préfrontal latéral est caractérisé par sa capacité à maintenir une activité neurale entre une stimulation brève et la production d'une réponse comportementale adaptée[168]. Historiquement, cette activité neurale persistante, protégée des interférences externe et reflétant le maintien d'informations pertinentes pour la tâche en cours, a été associée au concept psychologique de mémoire de travail[169]. En effet, le lien entre LPFC et mémoire de travail s'appuie sur un ensemble de résultats convergeant et robustes[169] : (1) Les activité soutenues sont présentes dans le LPFC lorsqu'une information pertinente doit être conservée pour guider, après un délai, la sélection d'une action ; (2) cette activité soutenue disparaît lorsque ces informations ne sont plus pertinentes pour la tâche en cours d'exécution ; (3) Si l'activité ne persiste pas jusqu'au moment de produire la réponse, alors les performances s'effondrent, indiquant que l'information nécessaire pour guider la sélection de l'action n'est plus disponible, (4) l'intensité de l'activité soutenue reflète la quantité d'information à maintenir en mémoire ; (5) Finalement, l'information représentée, tel que la direction d'une saccade oculaire, peut être décodée du pattern d'activité des neurones. Bien que les mécanismes biologiques permettant à l'activité neurale de se maintenir dans ces neurones ne soit pas élucidée, l'hypothèse actuellement prévalente propose que les activités persistantes résultent de la réverbération de l'information au sein de réseaux de neurones récurrents, c'est-à-dire comportant des boucles directes de rétroaction positives[60,64]. Alternativement, d'autres auteurs ont proposé que ces activités soutenues puissent également dépendre de changement rapide d'efficacité synaptique[170]. Ces deux hypothèses ne s'excluent d'ailleurs pas mutuellement[169].

D'un autre coté, les travaux sur la décision perceptuelle ont fourni un ensemble de résultats tout aussi robustes associant le LPFC à la sélection de l'action sur la base d'information sensorielle (voir p.38). De plus, les résultats expérimentaux rapportés dans cette thèse démontrent l'implication du DLPFC dans le processus d'accumulation d'information sensorielle durant la décision perceptuelle et d'information sur les valeurs

subjectives espérée durant la décision économique. Ces deux types de décisions simples reposent sur un mécanisme d'intégration progressive de l'information en faveur de chaque option qui dépend directement de la capacité du DLPFC à maintenir l'information sensorielle déjà accumulée pour additionner itérativement les nouveaux éléments d'information au fur et à mesure de leur observation[60,64].

Mémoire de travail et processus de décision constituent donc les deux faces d'un même phénomène neurobiologique : l'existence d'activités soutenues dans le LPFC[168]. Ainsi, lors d'une tâche de mémoire de travail « spatiale » dans laquelle un premier stimulus informe le sujet de la réponse qui doit être produite à l'affichage d'un second stimulus, l'activité dans le DLPFC témoigne du maintien de l'activité évoquée par l'instruction jusqu'à la réponse du sujet. L'affichage des cibles (deuxième stimulus indiquant qu'une réponse oculomotrice doit être donnée) évoque dans le DLPFC une activité BOLD croissant linéairement jusqu'à une valeur seuil (Fig. 33A). De ce point de vue, l'activité soutenue précédant la réponse peut également être interprétée comme le maintien de l'information en faveur d'une des réponses transmise par le premier stimulus et le pic d'activité au moment de l'affichage du deuxième stimulus, comme l'accumulation d'information sensorielle supplémentaire nécessaire à la sélection finale de l'action adéquate. De plus, lorsque des formes géométriques simples sont associées à un choix binaire de manière à prédire partiellement la réponse correcte, l'intensité de l'activité soutenue dans LIP corrèle directement à la quantité d'évidence cumulée en faveur de leur option préférée au fur et à mesure que de nouvelles formes géométrique sont affichées, démontrant ainsi que l'intensité de l'activité neurale codant la variable de décision représente le log ratio de la vraisemblance de l'alternative préférée[95]. L'activité des neurone implémentant la variable de décision du processus de diffusion est donc simultanément, et de manière indissociable, capable de stocker et d'intégrer l'information (Fig. 33B). Finalement, la démonstration que lorsque l'information sensorielle est illimitée, l'accumulation d'information tends vers le seuil de décision défini *a priori,* qui une fois atteint représente l'option sélectionnée (assemblée neurale ayant gagnée la course au seuil) ainsi que le niveau de confiance associé à la décision (l'intensité de l'activité soutenue est égale au seuil de décision, c'est à dire au log ratio des probabilités *a posteriori*) illustre bien cette continuité fonctionnelle entre processus d'accumulation d'information et mémoire de travail[63].

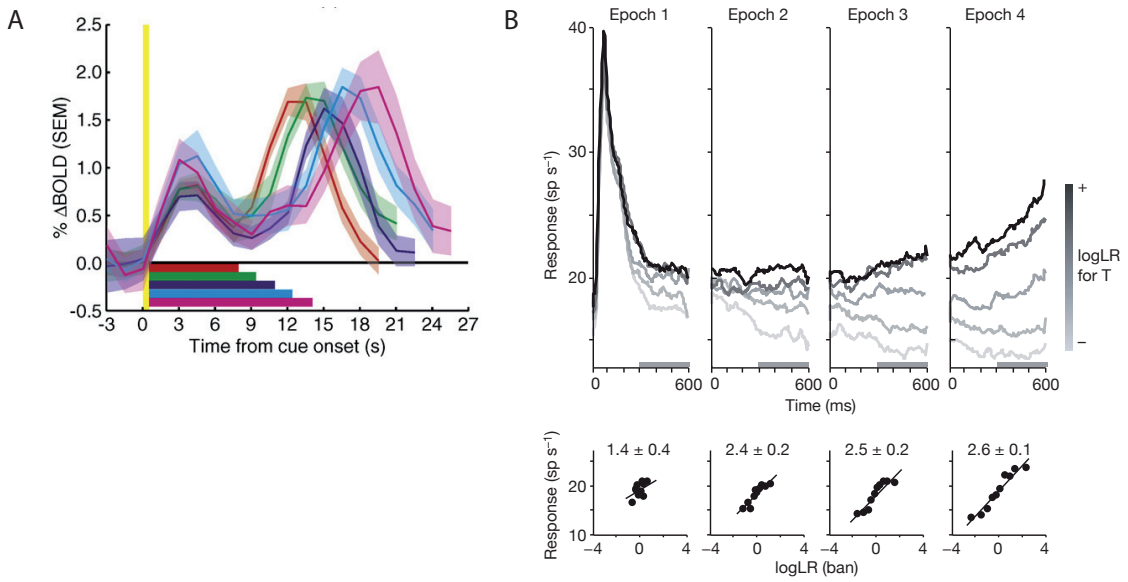

Figure 33 : (A) PSTH de l'activité BOLD évoquée dans le DLPFC lors d'un paradigme de mémoire de travail spatiale. Les barres colorées indiquent la durée d'intervalle de rétention pour le PSTH correspondant. **(B) Activité de neurones dans LIP lors d'une décision binaire basée sur la quantité d'évidence transmise par quatre figures géométriques présentées successivement. Panel Haut** : Activité populationnelle à l'affichage de chaque stimulus en fonction de la quantité d'évidence cumulée depuis le début de l'essai. **Panel Bas : L**es graphes rapportent l'activité moyenne en fonction de la quantité d'évidence cumulée après l'affichage de chaque nouveau stimulus. D'après Curtis, Romo et Yang[5,95,169].

Cette continuité fonctionnelle n'est pas intuitive du point de vue des modèles de diffusion. En effet, ces modèles ont été développés pour rendre compte du comportement observé au cours de décisions simples et, bien qu'ils fournissent une bonne approximation de l'activité du réseau pariéto-préfrontal dans certaines situations expérimentales, ceux-ci ne peuvent pas rendre compte intégralement de la dynamique non-linéaire des réseaux neuraux biologiques. Les modèles neuro-computationnels actuels de décisions simples sont construits autour de l'hypothèse que les activités neurales soutenues observées dans le réseau cortical pariéto-préfrontal sont au cœur du processus décisionnel (voir p.58 et les Fig. 18 et 34). L'architecture des réseaux de neurones biophysiques simulant ces régions corticales comprend donc des boucles récurrentes excitatrices qui modélisent l'effet synaptique du glutamate sur le récepteur NMDA et permettent la réverbération lente d'information dans le réseau. Cette architecture, initialement développée pour modéliser la rétention d'information en mémoire de travail dans le réseau pariéto-préfrontal, permet également de réaliser l'intégration des entrées sensorielles dans les assemblées neurales[64,171].

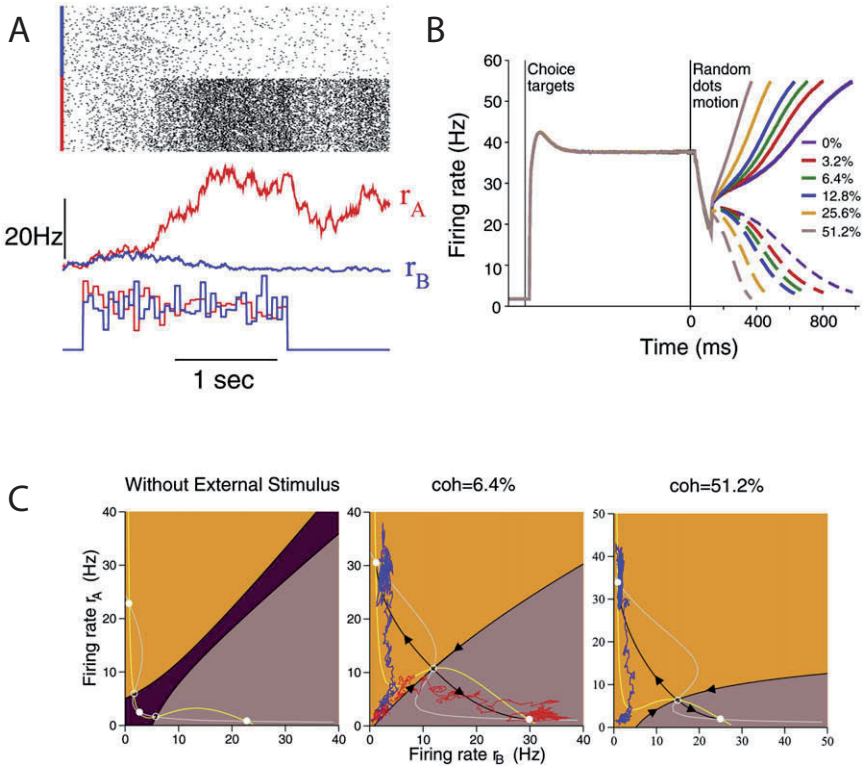

Figure 34 : Modèle de décision perceptuelle de Wang et Lo. (A) Activité des deux populations de neurones corticales lors d'une décision binaire sur la direction de mouvement d'un nuage de points aléatoire. Les couleurs en ordonnée indique l'assemblée neural à laquelle appartient le neurone (rouge : préfère la direction de mouvement du stimulus, bleu : préfère la direction opposée). Chaque point indique un potentiel d'action. Les potentiels d'actions sont représentés en fonction du temps. **(B) Activité moyennée des assemblées de neurones accumulant l'information** dans la direction de stimulation (lignes pleines) ou opposée (lignes pointillées) pour différents niveaux de cohérence de mouvement. **(C) Plan de phase pour les deux populations de neurones.** Le graphe rapporte l'activité de l'assemblée de neurone bleue en fonction de l'activité de l'assemblée de neurone rouge pour trois niveau de cohérence (0%, 6.4% et 51%). Les couleurs de fond indiquent les bassins attracteurs du système : dominance de la population bleue, dominance de la population rouge, ex-æquo. Les points jaunes indiquent la position des attracteurs et les lignes jaunes indiquent les trajectoires du système dans le plan de phase. **Panel gauche**, en l'absence de stimulation, trois attracteurs ponctuels co-existent, le système tendant à se maintenir dans un état ex-aequo à basse activité neurale, ou basculer vers la dominance d'une des assemblées de façon équiprobable. **Panel milieu et droite**, en présence d'information sensorielle les transitions de phases sont modifiées de façon à élargir d'autant le bassin attracteur correspondant au choix correct. L'attracteur « ex-aequo » disparaît, le système étant forcé d'évoluer vers un des deux attracteurs qui représente la croisée du seuil de décision. D'après Wang[64].

Il devient ainsi possible de rendre compte du processus de décision simple et du maintien en mémoire de travail du choix effectué comme un phénomène unique (Fig. 34C). Lors d'une décision perceptuelle, le système se dirige progressivement vers un des attracteurs, ce qui correspond à l'augmentation progressive de l'activité de l'assemblée de neurones menant la course (Fig. 34A-B). Lorsque le seuil de décision est atteint et que le système se stabilise sur un des attracteurs, le maintien du choix en mémoire de travail et sa protection des perturbations extérieures résulte naturellement de la diminution rapide de l'influence de nouvelles informations sur la position du système à proximité de l'attracteur. Cette protection n'est d'ailleurs pas absolue puisqu'un renversement des entrées sensorielles peut malgré tout éloigner le système de l'attracteur. De plus, contrairement aux premiers modèles neuro-computationnels qui reproduisaient *ad integrum* le mécanisme de diffusion dans leur réseau, ce modèle prédit correctement les RT pour les erreurs, principalement à cause du ralentissement qu'implique le passage d'un bassin attracteur à l'autre[91,93].

Malgré leurs limitations, les modèles de diffusion conservent cependant un intérêt important pour les sciences expérimentales car leur relative simplicité permet capturer le processus de décision grâce à un ensemble de paramètres réduit, susceptible d'être estimés sur des jeux de données réels. Cette capacité à rendre compte des processus décisionnels souligne l'importance du mécanisme d'accumulation d'information vers un seuil qui est au cœur de l'implémentation biologique du choix.

b. Régulation contextuelle du processus de décision ou détection du conflit : quel rôle pour le cortex cingulaire antérieur ?

La « théorie du conflit » fait l'hypothèse que la fonction principale de l'ACC est de détecter la survenue de conflit entre options comportementales afin d'ajuster le niveau de contrôle cognitif[172,173]. Il y a conflit lorsqu'un effort mental supplémentaire est nécessaire pour effectuer une tâche[172] : Lire le nom d'une couleur écrite avec des caractères d'une couleur différente, ne pas appuyer sur un bouton lorsqu'un stimulus rare survient, indiquer la direction d'une flèche encadrée de flèches parasites pointant la direction opposée, augmenter le nombre d'alternatives ouvertes au choix… Comportementalement, le conflit se traduit par une augmentation des RT[172], éventuellement associée à une diminution des performances s'atténuant lorsque des

essais difficiles sont répétés[173]. Cette théorie a été fortement popularisée par les multiples études IRMf démontrant une augmentation de l'activité BOLD en situation de conflit dans l'ACC (et/ou la pré-SMA), le DLPFC et le cortex pariétal postérieur[173-175], et une corrélation entre l'activité BOLD dans l'ACC et l'activité BOLD dans le DLPFC à l'essai suivant[176]. Ensemble, ces résultat furent interprétés comme validant un modèle dans lequel l'ACC signale la présence de conflit au DLPFC, qui à son tour augmente le contrôle cognitif afin d'ajuster la quantité de « ressources attentionnelles » à la difficulté de la tâche[172,173,176]. Malgré sa séduisante simplicité un certain nombre de résultats expérimentaux remettent en question cette théorie[173,177,175,178] : (1) Chez le primate, les lésions de l'ACC n'ont pas d'impact sur les performances et les RT observés en situation de conflit[179-182], (2) Les enregistrement électrophysiologiques chez le singe ne retrouvent pas de neurones codant le conflit dans l'ACC[183,184], (3) En début de tâche, la présence de conflit à l'essai précédent est associée à une activité basale soutenue plus élevée dans les neurones du DLPFC, mais pas dans l'ACC, et seule la lésion spécifique du DLPFC, pas de l'ACC, modifie les performances[173,179], (4) L'ACC est constamment retrouvé dans les tâches IRMf de prise de décision, y compris lorsqu'elles n'impliquent pas de situation de conflit[185], (5) L'augmentation de l'activité BOLD dans l'ACC est mieux expliquée par les RT que par le niveau de conflit[177], (6) Finalement, la théorie du conflit ne rend pas compte de manière satisfaisante des nombreux résultats impliquant l'ACC dans le monitoring des erreurs.

En effet, l'activité BOLD augmente dans l'ACC en cas d'erreur dans l'exécution d'une tâche[175,186,186,187]. De plus, l'ACC est le générateur de l'ERN (« *early related negativity* »), une onde EEG évoquée par les feedback négatifs sur l'issue des décisions, comme le démontre la corrélation essai par essai entre le signal BOLD dans l'ACC et amplitude de l'ERN[188]. Ce signal d'erreur est associé à un ajustement comportemental comme le montre la corrélation entre l'amplitude de l'ERN et le RT à l'essai suivant[188]. Contrairement à ce qui est observé pour le conflit, les données électrophysiologiques obtenues chez le singe confirment que les neurones dans l'ACC signalent la survenue d'erreur. Ces signaux d'erreur semblent d'ailleurs guider comportementalement la prise de décision en fournissant un feedback sur leurs conséquences[183,189,190]. De plus, le fait que les neurones dans l'ACC répondent au renforcement positif des actions[191,192] et à l'omission d'un renforçateur positif attendu[189] suggère que le codage des conséquences des actions dans l'ACC n'est pas restreint à la survenue d'erreur, mais constitue plutôt

un signal reflétant la déviation entre les conséquences attendues et effectives d'une action[193]. Chez l'homme, un faisceau convergeant de résultats suggère que l'ERN reflète l'arrivée et l'intégration des signaux d'erreur de prédiction dopaminergique dans l'ACC[194]. Pris ensemble ces résultats impliquent l'ACC dans l'évaluation des conséquences de nos choix et suggèrent qu'il pourrait avoir une fonction « régulatrice » du processus de décision en guidant la sélection de l'action sur la base des conséquences des actions passée[195]. En accord avec cette hypothèse, la lésion sélective de l'ACC rend les singes incapables d'apprendre les relations de contingence entre les options et leurs valeurs afin de guider leur processus de décision[196]. De plus, l'étude en IRMf, chez l'Homme, de décisions basées sur les valeurs montre que l'activité BOLD dans l'ACC au moment de l'évaluation des conséquences du choix prédit l'ajustement du taux d'apprentissage à la volatilité de la valeur des options, lorsque celles-ci doivent être apprises par essais-erreurs[197]. Pris ensemble, ces résultats démontrent comment l'apprentissage des contingences entre options et valeurs à partir des conséquences de nos choix permet de guider nos décisions futures.

Nos travaux démontrent le rôle de l'ACC dans l'ajustement de la distance au seuil de décision en fonction de l'information prédictive, établissant ainsi un lien entre l'apprentissage des contingences dans l'environnement, la prédiction de l'issue de la décision et un mécanisme computationnel permettant de guider le processus décisionnel : la modulation de la distance au seuil de décision[50]. L'implication de la pré-SMA et de ses projections striatales dans la modification de la distance au seuil de décision lors d'instructions modifiant le SAT suggère que l'ajustement de la distance au seuil de décision via ses projections striatales pourrait être une fonction générale de la portion dorsale du MPFC[109,111]. De plus, l'étude neuropsychologique de patients lésés au niveau de l'ACC (mais dont la pré-SMA est préservée) montre que les capacités d'ajustement du SAT n'est pas altérée chez ces patient[198], indiquant une dissociation entre l'ACC et la pré-SMA dans le type de régulation du processus de décision implémenté[199].

c. Cortex orbito-frontal : un carrefour entre valeurs subjectives et décision ?

En accord avec l'importante littérature neuroéconomique existante (p. 66), nos travaux impliquent l'OFC dans le phénomène de valuation, c'est-à-dire dans la représentation des valeurs subjectives espérées des options. Dans la plupart des théories économiques du choix, cette étape de valuation est un préalable nécessaire à la sélection de l'option maximisant la valeur subjective espérée.

Par ailleurs, nos résultats démontrent que l'OFC n'est pas une structure fonctionnellement homogène. En effet, bien que la valeur subjective des options soit représentée dans l'OFC médial et latéral durant la formation du choix, nos résultats montrent que seule la portion médiale de l'OFC participe au processus de décision économique. Cette spécialisation fonctionnelle reflète probablement les importantes différences de connectivité anatomique de ces deux portions de l'OFC[200]. Le codage de la valeur subjective des options dans la portion latérale de l'OFC avait déjà été observé lors d'enregistrements électrophysiologiques chez le singe[124,147]. Cette activité neurale avait été interprétée comme étant liée au processus de décision économique car elle survenait durant la formation du choix et qu'elle corrélait à la valeur subjective des options. Confirmant nos conclusions, une étude de lésion sélective, menée récemment sur des singes engagés dans un paradigme de décision basé sur les valeurs, a montré que la lésion sélective de l'OFC latéral perturbait l'apprentissage de la valeur des options à partir des conséquences des choix. En revanche, la lésion de la partie médiale de l'OFC résultait en une augmentation de la proportion de choix sub-optimaux, c'est-à-dire ne maximisant pas la valeur subjective du choix, sans altération de ses capacités d'apprentissage[201]. Pris ensemble, ces résultats confirment le rôle central de l'OFC dans la représentation des valeurs subjective et souligne la dissociation fonctionnelle entre sa portion latérale qui semble être impliquée dans l'apprentissage des valeurs et sa partie médiale qui est impliquée dans la représentation des valeurs subjectives sous-tendant la décision économique.

6. PERSPECTIVES

L'architecture des réseaux biologiques impliqués dans la prise de décision, la nature des algorithmes qu'ils implémentent et surtout, l'étude des relations entre structure biologique et computation est au cœur constitue le fil conducteur de cette thèse. Pris ensemble, les travaux rassemblés ici participent à l'établissement d'une cartographie des modules computationnels du cortex préfrontal humain et de leur intégration fonctionnelle au cours des décisions simples.

La neurobiologie, lorsqu'elle est guidée par l'usage de modèles computationnels, permet de décrire le cerveau humain comme un ordinateur biologique implémentant des algorithmes sophistiqués pour percevoir le monde, prendre des décisions et les transformer en actions. Pour le psychiatre, la compréhension de l'organisation neuro-computationnelle du cerveau humain est indissociablement liée à l'étude expérimentale et théorique des conditions neurobiologiques aboutissant aux dysfonctions de ces algorithmes. Clairement, la relecture de la physiopathologie des maladies mentales du point de vue des neurosciences computationnelles est porteuse d'espoir pour l'identification de nouvelles cibles et le développement de nouvelles méthodes diagnostiques et thérapeutiques.

7. REFERENCES

1. Glimcher, P. Decisions, decisions, decisions: choosing a biological science of choice. *Neuron* **36**, 323-332 (2002).
2. Cohen, J.D. & Blum, K.I. Reward and decision. *Neuron* **36**, 193-198 (2002).
3. Kable, J.W. & Glimcher, P.W. The neurobiology of decision: consensus and controversy. *Neuron* **63**, 733-745 (2009).
4. Pascal, B. *Pensées*. (1824).
5. Gold, J.I. & Shadlen, M.N. The neural basis of decision making. *Annu. Rev. Neurosci* **30**, 535-574 (2007).
6. Corrado, G. & Doya, K. Understanding neural coding through the model-based analysis of decision making. *J. Neurosci* **27**, 8178-8180 (2007).
7. Dehaene, S., Kerszberg, M. & Changeux, J.P. A neuronal model of a global workspace in effortful cognitive tasks. *Proc. Natl. Acad. Sci. U.S.A* **95**, 14529-14534 (1998).
8. Shannon, C.E. A Mathematical Theory of Communication. *Bell System Technical Journal* 379 (1948).
9. Bogacz, R. Optimal decision network with distributed representation. *Neural Netw* **20**, 564-576 (2007).
10. Bogacz, R. & Gurney, K. The basal ganglia and cortex implement optimal decision making between alternative actions. *Neural Comput* **19**, 442-477 (2007).
11. Gold, J.I. & Shadlen, M.N. Banburismus and the brain: decoding the relationship between sensory stimuli, decisions, and reward. *Neuron* **36**, 299-308 (2002).
12. Wald, A. *Sequential Analysis*. (Courier Dover Publications: 2004).
13. Bogacz, R. Optimal decision-making theories: linking neurobiology with behaviour. *Trends Cogn. Sci. (Regul. Ed.)* **11**, 118-125 (2007).
14. Smith, P.L. & Ratcliff, R. Psychology and neurobiology of simple decisions. *Trends Neurosci* **27**, 161-168 (2004).
15. Ratcliff, R. & Smith, P.L. A comparison of sequential sampling models for two-choice reaction time. *Psychol Rev* **111**, 333-367 (2004).
16. Donkin, C., Brown, S., Heathcote, A. & Wagenmakers, E.-J. Diffusion versus linear ballistic accumulation: different models but the same conclusions about psychological processes? *Psychon Bull Rev* **18**, 61-69 (2011).
17. Ratcliff, R. A theory of memory retrieval. *Psychological Review* **85**, 59-108 (1978).
18. Ratcliff, R. A theory of order relations in perceptual matching. *Psychological Review* **88**, 552-572 (1981).
19. Ratcliff, R. & Tuerlinckx, F. Estimating parameters of the diffusion model: approaches to dealing with contaminant reaction times and parameter variability. *Psychon Bull Rev* **9**, 438-481 (2002).
20. Ratcliff, R. & Rouder, J.N. Modeling Response Times for Two-Choice Decisions. *Psychological Science* **9**, 347 -356 (1998).
21. Ratcliff, R. & Rouder, J.N. A diffusion model account of masking in two-choice letter identification. *J Exp Psychol Hum Percept Perform* **26**, 127-140 (2000).
22. Ratcliff, R. & McKoon, G. The diffusion decision model: theory and data for two-choice decision tasks. *Neural Comput* **20**, 873-922 (2008).
23. Ratcliff, R., Van Zandt, T. & McKoon, G. Connectionist and diffusion models of reaction time. *Psychol Rev* **106**, 261-300 (1999).
24. Ratcliff, R., Gomez, P. & McKoon, G. A diffusion model account of the lexical

decision task. *Psychol Rev* **111**, 159-182 (2004).
25. Voss, A., Rothermund, K. & Voss, J. Interpreting the parameters of the diffusion model: an empirical validation. *Mem Cognit* **32**, 1206-1220 (2004).
26. Smith, P.L. Psychophysically Principled Models of Visual Simple Reaction Time,. *Psychological Review* **102**, 567-593 (1995).
27. Reddi, B.A. & Carpenter, R.H. The influence of urgency on decision time. *Nat. Neurosci* **3**, 827-830 (2000).
28. Reddi, B.A.J., Asrress, K.N. & Carpenter, R.H.S. Accuracy, information, and response time in a saccadic decision task. *J. Neurophysiol* **90**, 3538-3546 (2003).
29. Brown, S.D. & Heathcote, A. The simplest complete model of choice response time: linear ballistic accumulation. *Cogn Psychol* **57**, 153-178 (2008).
30. Busemeyer, J.R. & Townsend, J.T. Decision field theory: a dynamic-cognitive approach to decision making in an uncertain environment. *Psychol Rev* **100**, 432-459 (1993).
31. Busemeyer, J.R., Jessup, R.K., Johnson, J.G. & Townsend, J.T. Building bridges between neural models and complex decision making behaviour. *Neural Netw* **19**, 1047-1058 (2006).
32. Milica Milosavljevic, Jonathan Malmaud, Alexander Huth, Christof Koch & Antonio Rangel The Drift Diffusion Model can account for the accuracy and reaction time of value-based choices under high and low time pressure. *Judgment and Decision Making* **5**, 437-449 (2010).
33. Luce, R.D. *Response Times: Their Role in Inferring Elementary Mental Organization*. (Oxford University Press: 1991).
34. Grasman, R.P.P.P., Wagenmakers, E.-J. & van der Maas, H.L.J. On the mean and variance of response times under the diffusion model with an application to parameter estimation. *Journal of Mathematical Psychology* **53**, 55-68 (2009).
35. Wagenmakers, E.-J. & Brown, S. On the linear relation between the mean and the standard deviation of a response time distribution. *Psychol Rev* **114**, 830-841 (2007).
36. Wagenmakers, E.-J., van der Maas, H.L.J. & Grasman, R.P.P.P. An EZ-diffusion model for response time and accuracy. *Psychon Bull Rev* **14**, 3-22 (2007).
37. Born, R.T. & Bradley, D.C. Structure and function of visual area MT. *Annu. Rev. Neurosci* **28**, 157-189 (2005).
38. van Ravenzwaaij, D. & Oberauer, K. How to use the diffusion model: Parameter recovery of three methods: EZ, fast-dm, and DMAT. *Journal of Mathematical Psychology* **53**, 463-473 (2009).
39. Leite, F.P. & Ratcliff, R. Modeling reaction time and accuracy of multiple-alternative decisions. *Atten Percept Psychophys* **72**, 246-273 (2010).
40. Vandekerckhove, J. & Tuerlinckx, F. Fitting the Ratcliff diffusion model to experimental data. *Psychon Bull Rev* **14**, 1011-1026 (2007).
41. Wagenmakers, E.-J., van der Maas, H.L.J., Dolan, C.V. & Grasman, R.P.P.P. EZ does it! Extensions of the EZ-diffusion model. *Psychon Bull Rev* **15**, 1229-1235 (2008).
42. Ratcliff, R. The EZ diffusion method: too EZ? *Psychon Bull Rev* **15**, 1218-1228 (2008).
43. Usher, M. & McClelland, J.L. The time course of perceptual choice: the leaky, competing accumulator model. *Psychol Rev* **108**, 550-592 (2001).
44. Ditterich, J. Stochastic models of decisions about motion direction: behavior and physiology. *Neural Netw* **19**, 981-1012 (2006).
45. Churchland, A.K., Kiani, R. & Shadlen, M.N. Decision-making with multiple alternatives. *Nat. Neurosci* **11**, 693-702 (2008).
46. Carpenter, R.H.S. oculomotor procrastination. *Eye Movements: Cognition and Visual Perception* 237–246 (1981).

47. Carpenter, R.H.S. Contrast, probability, and saccadic latency; evidence for independence of detection and decision. *Curr. Biol* **14**, 1576-1580 (2004).
48. Carpenter, R.H. & Williams, M.L. Neural computation of log likelihood in control of saccadic eye movements. *Nature* **377**, 59-62 (1995).
49. Fuchs, A.F. *Contemporary ocular motor and vestibular research: a tribute to David A. Robinson : international meeting Eibsee, 1993*. (G. Thieme Verlag: 1994).
50. Domenech, P. & Dreher, J.-C. Decision threshold modulation in the human brain. *J. Neurosci* **30**, 14305-14317 (2010).
51. Noorani, I. & Carpenter, R.H.S. Full reaction time distributions reveal the complexity of neural decision-making. *Eur. J. Neurosci* **33**, 1948-1951 (2011).
52. Carpenter, R.H.S., Reddi, B.A.J. & Anderson, A.J. A simple two-stage model predicts response time distributions. *J. Physiol. (Lond.)* **587**, 4051-4062 (2009).
53. Noorani, I., Gao, M.J., Pearson, B.C. & Carpenter, R.H.S. Predicting the timing of wrong decisions with LATER. *Exp Brain Res* **209**, 587-598 (2011).
54. Cisek, P., Puskas, G.A. & El-Murr, S. Decisions in changing conditions: the urgency-gating model. *J. Neurosci* **29**, 11560-11571 (2009).
55. Bogacz, R., Wagenmakers, E.-J., Forstmann, B.U. & Nieuwenhuis, S. The neural basis of the speed-accuracy tradeoff. *Trends Neurosci* **33**, 10-16 (2010).
56. Dreher, J.-C. & Tremblay, L. *Handbook of Reward and Decision Making*. (Academic Press Inc: 2009).
57. Simen, P. et al. Reward rate optimization in two-alternative decision making: empirical tests of theoretical predictions. *J Exp Psychol Hum Percept Perform* **35**, 1865-1897 (2009).
58. Simen, P., Cohen, J.D. & Holmes, P. Rapid decision threshold modulation by reward rate in a neural network. *Neural Netw* **19**, 1013-1026 (2006).
59. Summerfield, C. & Koechlin, E. Economic value biases uncertain perceptual choices in the parietal and prefrontal cortices. *Front Hum Neurosci* **4**, 208 (2010).
60. Lo, C.-C. & Wang, X.-J. Cortico-basal ganglia circuit mechanism for a decision threshold in reaction time tasks. *Nat. Neurosci* **9**, 956-963 (2006).
61. Hanes, D.P. & Schall, J.D. Neural control of voluntary movement initiation. *Science* **274**, 427-430 (1996).
62. Schall, J.D., Purcell, B.A., Heitz, R.P., Logan, G.D. & Palmeri, T.J. Neural mechanisms of saccade target selection: gated accumulator model of the visual-motor cascade. *Eur. J. Neurosci* **33**, 1991-2002 (2011).
63. Kiani, R., Hanks, T.D. & Shadlen, M.N. Bounded integration in parietal cortex underlies decisions even when viewing duration is dictated by the environment. *J. Neurosci* **28**, 3017-3029 (2008).
64. Wang, X.-J. Decision making in recurrent neuronal circuits. *Neuron* **60**, 215-234 (2008).
65. Gold, J.I. & Shadlen, M.N. Representation of a perceptual decision in developing oculomotor commands. *Nature* **404**, 390-394 (2000).
66. Gold, J.I. & Shadlen, M.N. The influence of behavioral context on the representation of a perceptual decision in developing oculomotor commands. *J. Neurosci* **23**, 632-651 (2003).
67. Glimcher, P.W. The neurobiology of visual-saccadic decision making. *Annu. Rev. Neurosci* **26**, 133-179 (2003).
68. Schall, J.D. Neural basis of deciding, choosing and acting. *Nat. Rev. Neurosci* **2**, 33-42 (2001).
69. Van Essen, D.C., Anderson, C.H. & Felleman, D.J. Information processing in the primate visual system: an integrated systems perspective. *Science* **255**, 419-423 (1992).

70. Ungerleider, L.G. & Haxby, J.V. « What » and « where » in the human brain. *Curr. Opin. Neurobiol* **4**, 157-165 (1994).
71. Grill-Spector, K., Kourtzi, Z. & Kanwisher, N. The lateral occipital complex and its role in object recognition. *Vision Res* **41**, 1409-1422 (2001).
72. Bruce, C.J. & Goldberg, M.E. Primate frontal eye fields. I. Single neurons discharging before saccades. *J. Neurophysiol* **53**, 603-635 (1985).
73. Bruce, C.J., Goldberg, M.E., Bushnell, M.C. & Stanton, G.B. Primate frontal eye fields. II. Physiological and anatomical correlates of electrically evoked eye movements. *J. Neurophysiol* **54**, 714-734 (1985).
74. Alexander, G.E., DeLong, M.R. & Strick, P.L. Parallel organization of functionally segregated circuits linking basal ganglia and cortex. *Annu. Rev. Neurosci* **9**, 357-381 (1986).
75. Glimcher, P.W. Making choices: the neurophysiology of visual-saccadic decision making. *Trends Neurosci* **24**, 654-659 (2001).
76. Kandel, E.R., Schwartz, J.H. & Jessell, T.M. *Principles of neural science*. (McGraw-Hill, Health Professions Division: 2000).
77. Dubner, R. & Zeki, S.M. Response properties and receptive fields of cells in an anatomically defined region of the superior temporal sulcus in the monkey. *Brain Res* **35**, 528-532 (1971).
78. Van Essen, D.C., Maunsell, J.H. & Bixby, J.L. The middle temporal visual area in the macaque: myeloarchitecture, connections, functional properties and topographic organization. *J. Comp. Neurol* **199**, 293-326 (1981).
79. Newsome, W.T., Britten, K.H. & Movshon, J.A. Neuronal correlates of a perceptual decision. *Nature* **341**, 52-54 (1989).
80. Salzman, C.D., Britten, K.H. & Newsome, W.T. Cortical microstimulation influences perceptual judgements of motion direction. *Nature* **346**, 174-177 (1990).
81. Ditterich, J., Mazurek, M.E. & Shadlen, M.N. Microstimulation of visual cortex affects the speed of perceptual decisions. *Nat. Neurosci* **6**, 891-898 (2003).
82. Cohen, M.R. & Newsome, W.T. What electrical microstimulation has revealed about the neural basis of cognition. *Curr. Opin. Neurobiol* **14**, 169-177 (2004).
83. Afraz, S.-R., Kiani, R. & Esteky, H. Microstimulation of inferotemporal cortex influences face categorization. *Nature* **442**, 692-695 (2006).
84. Salzman, C.D. & Newsome, W.T. Neural mechanisms for forming a perceptual decision. *Science* **264**, 231-237 (1994).
85. Shadlen, M.N., Britten, K.H., Newsome, W.T. & Movshon, J.A. A computational analysis of the relationship between neuronal and behavioral responses to visual motion. *J. Neurosci* **16**, 1486-1510 (1996).
86. Kim, J.N. & Shadlen, M.N. Neural correlates of a decision in the dorsolateral prefrontal cortex of the macaque. *Nat. Neurosci* **2**, 176-185 (1999).
87. Shadlen, M.N. & Newsome, W.T. Neural basis of a perceptual decision in the parietal cortex (area LIP) of the rhesus monkey. *J. Neurophysiol* **86**, 1916-1936 (2001).
88. Schiller, P.H. & Sandell, J.H. Interactions between visually and electrically elicited saccades before and after superior colliculus and frontal eye field ablations in the rhesus monkey. *Exp Brain Res* **49**, 381-392 (1983).
89. Kornhuber, H.H. & Deecke, L. [Changes in the brain potential in voluntary movements in man: Readiness potential and reafferent potentials]. *Pflugers Arch Gesamte Physiol Menschen Tiere* **284**, 1-17 (1965).
90. Schall, J.D., Hanes, D.P., Thompson, K.G. & King, D.J. Saccade target selection in frontal eye field of macaque. I. Visual and premovement activation. *J. Neurosci* **15**, 6905-6918 (1995).
91. Roitman, J.D. & Shadlen, M.N. Response of neurons in the lateral intraparietal area

during a combined visual discrimination reaction time task. *J. Neurosci* **22**, 9475-9489 (2002).
92. Hanks, T.D., Ditterich, J. & Shadlen, M.N. Microstimulation of macaque area LIP affects decision-making in a motion discrimination task. *Nat. Neurosci* **9**, 682-689 (2006).
93. Mazurek, M.E., Roitman, J.D., Ditterich, J. & Shadlen, M.N. A role for neural integrators in perceptual decision making. *Cereb. Cortex* **13**, 1257-1269 (2003).
94. Huk, A.C. & Shadlen, M.N. Neural activity in macaque parietal cortex reflects temporal integration of visual motion signals during perceptual decision making. *J. Neurosci* **25**, 10420-10436 (2005).
95. Yang, T. & Shadlen, M.N. Probabilistic reasoning by neurons. *Nature* **447**, 1075-1080 (2007).
96. Heekeren, H.R., Marrett, S., Bandettini, P.A. & Ungerleider, L.G. A general mechanism for perceptual decision-making in the human brain. *Nature* **431**, 859-862 (2004).
97. Heekeren, H.R., Marrett, S., Ruff, D.A., Bandettini, P.A. & Ungerleider, L.G. Involvement of human left dorsolateral prefrontal cortex in perceptual decision making is independent of response modality. *Proc. Natl. Acad. Sci. U.S.A* **103**, 10023-10028 (2006).
98. Heekeren, H.R., Marrett, S. & Ungerleider, L.G. The neural systems that mediate human perceptual decision making. *Nat. Rev. Neurosci* **9**, 467-479 (2008).
99. Tosoni, A., Galati, G., Romani, G.L. & Corbetta, M. Sensory-motor mechanisms in human parietal cortex underlie arbitrary visual decisions. *Nat. Neurosci* **11**, 1446-1453 (2008).
100. Philiastides, M.G., Auksztulewicz, R., Heekeren, H.R. & Blankenburg, F. Causal Role of Dorsolateral Prefrontal Cortex in Human Perceptual Decision Making. *Curr Biol* (2011).doi:10.1016/j.cub.2011.04.034
101. Logothetis, N.K. What we can do and what we cannot do with fMRI. *Nature* **453**, 869-878 (2008).
102. Lachaux, J.P., Rudrauf, D. & Kahane, P. Intracranial EEG and human brain mapping. *J. Physiol. Paris* **97**, 613-628 (2003).
103. Philiastides, M.G. & Sajda, P. Temporal characterization of the neural correlates of perceptual decision making in the human brain. *Cereb. Cortex* **16**, 509-518 (2006).
104. Philiastides, M.G., Ratcliff, R. & Sajda, P. Neural representation of task difficulty and decision making during perceptual categorization: a timing diagram. *J. Neurosci* **26**, 8965-8975 (2006).
105. Ratcliff, R., Philiastides, M.G. & Sajda, P. Quality of evidence for perceptual decision making is indexed by trial-to-trial variability of the EEG. *Proc. Natl. Acad. Sci. U.S.A* **106**, 6539-6544 (2009).
106. Linden, D.E.J. The p300: where in the brain is it produced and what does it tell us? *Neuroscientist* **11**, 563-576 (2005).
107. Johnson, J.S. & Olshausen, B.A. Timecourse of neural signatures of object recognition. *J Vis* **3**, 499-512 (2003).
108. Niedermeyer, E. & Silva, F.H.L. da *Electroencephalography: basic principles, clinical applications, and related fields*. (Lippincott Williams & Wilkins: 2005).
109. Forstmann, B.U. et al. Striatum and pre-SMA facilitate decision-making under time pressure. *Proc. Natl. Acad. Sci. U.S.A* **105**, 17538-17542 (2008).
110. Ivanoff, J., Branning, P. & Marois, R. fMRI evidence for a dual process account of the speed-accuracy tradeoff in decision-making. *PLoS ONE* **3**, e2635 (2008).
111. Forstmann, B.U. et al. Cortico-striatal connections predict control over speed and accuracy in perceptual decision making. *Proc. Natl. Acad. Sci. U.S.A* **107**, 15916-15920 (2010).
112. Frank, M.J., Samanta, J., Moustafa, A.A. & Sherman, S.J. Hold your horses:

impulsivity, deep brain stimulation, and medication in parkinsonism. *Science* **318**, 1309-1312 (2007).
113. Pascal, B. *Pensées*. (L. de Bure: 1823).
114. Bernoulli, D. Exposition of a New Theory on the Measurement of Risk. *Econometrica* **22**, 23-36 (1954).
115. Glimcher, P.W., Camerer, C., Poldrack, R.A. & Fehr, E. *Neuroeconomics: Decision Making and the Brain*. (Academic Press: 2008).
116. Samuelson, P.A. A Note on Measurement of Utility. *The Review of Economic Studies* **4**, 155-161 (1937).
117. Samuelson, P. A Note on the Pure Theory of Consumer's Behavior. *economica* **5**, 61-71 (1938).
118. Neumann, J.V., Morgenstern, O., Rubinstein, A. & Kuhn, H.W. *Theory of games and economic behavior*. (Greenwood Publishing Group: 2007).
119. Trepel, C., Fox, C.R. & Poldrack, R.A. Prospect theory on the brain? Toward a cognitive neuroscience of decision under risk. *Brain Res Cogn Brain Res* **23**, 34-50 (2005).
120. Kahneman, D. & Tversky, A. Prospect Theory: An Analysis of Decision under Risk. *Econometrica* **47**, 263-291 (1979).
121. Sutton, R.S. & Barto, A.G. *Reinforcement learning: an introduction*. (MIT Press: 1998).
122. Deaner, R.O., Khera, A.V. & Platt, M.L. Monkeys pay per view: adaptive valuation of social images by rhesus macaques. *Curr. Biol* **15**, 543-548 (2005).
123. Padoa-Schioppa, C., Jandolo, L. & Visalberghi, E. Multi-stage mental process for economic choice in capuchins. *Cognition* **99**, B1-B13 (2006).
124. Padoa-Schioppa, C. & Assad, J.A. The representation of economic value in the orbitofrontal cortex is invariant for changes of menu. *Nat. Neurosci* **11**, 95-102 (2008).
125. Mosteller, F. & Nogee, P. An Experimental Measurement of Utility. *Journal of Political Economy* **59**, 371-404 (1951).
126. Dashiell, J.F. Affective Value-Distances as a Determinant of Esthetic Judgment-Times. *The American Journal of Psychology* **50**, 57-67 (1937).
127. Schultz, W. Neural coding of basic reward terms of animal learning theory, game theory, microeconomics and behavioural ecology. *Curr. Opin. Neurobiol* **14**, 139-147 (2004).
128. Schultz, W. Behavioral dopamine signals. *Trends Neurosci* **30**, 203-210 (2007).
129. Wallis, J.D. Orbitofrontal cortex and its contribution to decision-making. *Annu. Rev. Neurosci* **30**, 31-56 (2007).
130. Schultz, W. Dopamine neurons and their role in reward mechanisms. *Curr. Opin. Neurobiol* **7**, 191-197 (1997).
131. Bayer, H.M. & Glimcher, P.W. Midbrain dopamine neurons encode a quantitative reward prediction error signal. *Neuron* **47**, 129-141 (2005).
132. Schultz, W., Dayan, P. & Montague, P.R. A neural substrate of prediction and reward. *Science* **275**, 1593-1599 (1997).
133. Fiorillo, C.D., Tobler, P.N. & Schultz, W. Discrete coding of reward probability and uncertainty by dopamine neurons. *Science* **299**, 1898-1902 (2003).
134. Tobler, P.N., Fiorillo, C.D. & Schultz, W. Adaptive coding of reward value by dopamine neurons. *Science* **307**, 1642-1645 (2005).
135. Zaghloul, K.A. et al. Human substantia nigra neurons encode unexpected financial rewards. *Science* **323**, 1496-1499 (2009).
136. Morris, G., Nevet, A., Arkadir, D., Vaadia, E. & Bergman, H. Midbrain dopamine neurons encode decisions for future action. *Nat. Neurosci* **9**, 1057-1063 (2006).
137. Kringelbach, M.L. & Rolls, E.T. The functional neuroanatomy of the human orbitofrontal cortex: evidence from neuroimaging and neuropsychology. *Prog. Neurobiol* **72**,

341-372 (2004).
138. Grabenhorst, F. & Rolls, E.T. Value, pleasure and choice in the ventral prefrontal cortex. *Trends Cogn. Sci. (Regul. Ed.)* **15**, 56-67 (2011).
139. Kringelbach, M.L. The human orbitofrontal cortex: linking reward to hedonic experience. *Nat. Rev. Neurosci* **6**, 691-702 (2005).
140. McClure, S.M. et al. Neural correlates of behavioral preference for culturally familiar drinks. *Neuron* **44**, 379-387 (2004).
141. Sescousse, G., Redouté, J. & Dreher, J.-C. The architecture of reward value coding in the human orbitofrontal cortex. *J. Neurosci* **30**, 13095-13104 (2010).
142. Tremblay, L. & Schultz, W. Relative reward preference in primate orbitofrontal cortex. *Nature* **398**, 704-708 (1999).
143. Roesch, M.R. & Olson, C.R. Neuronal activity related to reward value and motivation in primate frontal cortex. *Science* **304**, 307-310 (2004).
144. Chib, V.S., Rangel, A., Shimojo, S. & O'Doherty, J.P. Evidence for a common representation of decision values for dissimilar goods in human ventromedial prefrontal cortex. *J. Neurosci* **29**, 12315-12320 (2009).
145. Hare, T.A., O'Doherty, J., Camerer, C.F., Schultz, W. & Rangel, A. Dissociating the Role of the Orbitofrontal Cortex and the Striatum in the Computation of Goal Values and Prediction Errors. *J. Neurosci.* **28**, 5623-5630 (2008).
146. Peters, J. & Büchel, C. Neural representations of subjective reward value. *Behav. Brain Res* **213**, 135-141 (2010).
147. Padoa-Schioppa, C. & Assad, J.A. Neurons in the orbitofrontal cortex encode economic value. *Nature* **441**, 223-226 (2006).
148. Padoa-Schioppa, C. Neurobiology of Economic Choice: A Good-Based Model. *Annu Rev Neurosci* (2010).doi:10.1146/annurev-neuro-061010-113648
149. Padoa-Schioppa, C. Range-adapting representation of economic value in the orbitofrontal cortex. *J. Neurosci* **29**, 14004-14014 (2009).
150. Wallis, J.D. & Miller, E.K. Neuronal activity in primate dorsolateral and orbital prefrontal cortex during performance of a reward preference task. *Eur. J. Neurosci* **18**, 2069-2081 (2003).
151. Freedman, D.J. & Assad, J.A. A proposed common neural mechanism for categorization and perceptual decisions. *Nat Neurosci* **14**, 143-146 (2011).
152. Wunderlich, K., Rangel, A. & O'Doherty, J.P. Economic choices can be made using only stimulus values. *Proc. Natl. Acad. Sci. U.S.A* **107**, 15005-15010 (2010).
153. Becker, G.M., DeGroot, M.H. & Marschak, J. Measuring utility by a single-response sequential method. *Behav Sci* **9**, 226-232 (1964).
154. Plassmann, H., O'Doherty, J. & Rangel, A. Orbitofrontal cortex encodes willingness to pay in everyday economic transactions. *J. Neurosci* **27**, 9984-9988 (2007).
155. Kahnt, T., Heinzle, J., Park, S.Q. & Haynes, J.-D. The neural code of reward anticipation in human orbitofrontal cortex. *Proc. Natl. Acad. Sci. U.S.A* **107**, 6010-6015 (2010).
156. Wunderlich, K., Rangel, A. & O'Doherty, J.P. Neural computations underlying action-based decision making in the human brain. *Proc. Natl. Acad. Sci. U.S.A* **106**, 17199-17204 (2009).
157. Philiastides, M.G., Biele, G. & Heekeren, H.R. A mechanistic account of value computation in the human brain. *Proc. Natl. Acad. Sci. U.S.A* **107**, 9430-9435 (2010).
158. Tom, S.M., Fox, C.R., Trepel, C. & Poldrack, R.A. The neural basis of loss aversion in decision-making under risk. *Science* **315**, 515-518 (2007).
159. Plassmann, H., O'Doherty, J.P. & Rangel, A. Appetitive and aversive goal values are encoded in the medial orbitofrontal cortex at the time of decision making. *J. Neurosci* **30**,

10799-10808 (2010).
160. Lebreton, M., Jorge, S., Michel, V., Thirion, B. & Pessiglione, M. An automatic valuation system in the human brain: evidence from functional neuroimaging. *Neuron* **64**, 431-439 (2009).
161. Hausman, D.M. *The Philosophy of economics: an anthology*. (Cambridge University Press: 1994).
162. Ben Zur, H. & Breznitz, S.J. The effect of time pressure on risky choice behavior. *Acta Psychologica* **47**, 89-104 (1981).
163. Usher, M. & McClelland, J.L. Loss aversion and inhibition in dynamical models of multialternative choice. *Psychol Rev* **111**, 757-769 (2004).
164. Sigman, M. & Dehaene, S. Parsing a cognitive task: a characterization of the mind's bottleneck. *PLoS Biol* **3**, e37 (2005).
165. Sigman, M. & Dehaene, S. Dynamics of the central bottleneck: dual-task and task uncertainty. *PLoS Biol* **4**, e220 (2006).
166. Kornblum, S. Sequential determinants of information processing in serial and discrete choice reaction time. *Psychological Review* **76**, 113-131 (1969).
167. Gomez, P., Ratcliff, R. & Perea, M. A model of the go/no-go task. *J Exp Psychol Gen* **136**, 389-413 (2007).
168. Lee, D., Rushworth, M.F.S., Walton, M.E., Watanabe, M. & Sakagami, M. Functional specialization of the primate frontal cortex during decision making. *J. Neurosci* **27**, 8170-8173 (2007).
169. Curtis, C.E. & Lee, D. Beyond working memory: the role of persistent activity in decision making. *Trends Cogn. Sci. (Regul. Ed.)* **14**, 216-222 (2010).
170. Mongillo, G., Barak, O. & Tsodyks, M. Synaptic theory of working memory. *Science* **319**, 1543-1546 (2008).
171. Wang, X.J. Synaptic reverberation underlying mnemonic persistent activity. *Trends Neurosci* **24**, 455-463 (2001).
172. Botvinick, M.M., Cohen, J.D. & Carter, C.S. Conflict monitoring and anterior cingulate cortex: an update. *Trends Cogn. Sci. (Regul. Ed.)* **8**, 539-546 (2004).
173. Mansouri, F.A., Tanaka, K. & Buckley, M.J. Conflict-induced behavioural adjustment: a clue to the executive functions of the prefrontal cortex. *Nat. Rev. Neurosci* **10**, 141-152 (2009).
174. Nachev, P., Kennard, C. & Husain, M. Functional role of the supplementary and pre-supplementary motor areas. *Nat. Rev. Neurosci* **9**, 856-869 (2008).
175. Ridderinkhof, K.R., Ullsperger, M., Crone, E.A. & Nieuwenhuis, S. The role of the medial frontal cortex in cognitive control. *Science* **306**, 443-447 (2004).
176. Kerns, J.G. et al. Anterior cingulate conflict monitoring and adjustments in control. *Science* **303**, 1023-1026 (2004).
177. Grinband, J. et al. The dorsal medial frontal cortex is sensitive to time on task, not response conflict or error likelihood. *Neuroimage* **57**, 303-311 (2011).
178. Rushworth, M.F.S., Buckley, M.J., Behrens, T.E.J., Walton, M.E. & Bannerman, D.M. Functional organization of the medial frontal cortex. *Curr. Opin. Neurobiol* **17**, 220-227 (2007).
179. Mansouri, F.A., Buckley, M.J. & Tanaka, K. Mnemonic function of the dorsolateral prefrontal cortex in conflict-induced behavioral adjustment. *Science* **318**, 987-990 (2007).
180. Turken, A.U. & Swick, D. Response selection in the human anterior cingulate cortex. *Nat. Neurosci* **2**, 920-924 (1999).
181. Swick, D. & Turken, A.U. Dissociation between conflict detection and error monitoring in the human anterior cingulate cortex. *Proc. Natl. Acad. Sci. U.S.A* **99**, 16354-16359 (2002).

182. Hayward, G., Goodwin, G.M. & Harmer, C.J. The role of the anterior cingulate cortex in the counting Stroop task. *Exp Brain Res* **154**, 355-358 (2004).
183. Ito, S., Stuphorn, V., Brown, J.W. & Schall, J.D. Performance monitoring by the anterior cingulate cortex during saccade countermanding. *Science* **302**, 120-122 (2003).
184. Nakamura, K., Roesch, M.R. & Olson, C.R. Neuronal activity in macaque SEF and ACC during performance of tasks involving conflict. *J. Neurophysiol* **93**, 884-908 (2005).
185. Roelofs, A., van Turennout, M. & Coles, M.G.H. Anterior cingulate cortex activity can be independent of response conflict in Stroop-like tasks. *Proc. Natl. Acad. Sci. U.S.A* **103**, 13884-13889 (2006).
186. Holroyd, C.B. et al. Dorsal anterior cingulate cortex shows fMRI response to internal and external error signals. *Nat Neurosci* **7**, 497-498 (2004).
187. Carter, C.S. et al. Anterior cingulate cortex, error detection, and the online monitoring of performance. *Science* **280**, 747-749 (1998).
188. Debener, S. et al. Trial-by-trial coupling of concurrent electroencephalogram and functional magnetic resonance imaging identifies the dynamics of performance monitoring. *J. Neurosci* **25**, 11730-11737 (2005).
189. Shima, K. & Tanji, J. Role for cingulate motor area cells in voluntary movement selection based on reward. *Science* **282**, 1335-1338 (1998).
190. Procyk, E., Tanaka, Y.L. & Joseph, J.P. Anterior cingulate activity during routine and non-routine sequential behaviors in macaques. *Nat. Neurosci* **3**, 502-508 (2000).
191. Shidara, M. & Richmond, B.J. Anterior cingulate: single neuronal signals related to degree of reward expectancy. *Science* **296**, 1709-1711 (2002).
192. Matsumoto, K., Suzuki, W. & Tanaka, K. Neuronal correlates of goal-based motor selection in the prefrontal cortex. *Science* **301**, 229-232 (2003).
193. Amiez, C., Joseph, J.-P. & Procyk, E. Anterior cingulate error-related activity is modulated by predicted reward. *Eur. J. Neurosci* **21**, 3447-3452 (2005).
194. Nieuwenhuis, S., Holroyd, C.B., Mol, N. & Coles, M.G.H. Reinforcement-related brain potentials from medial frontal cortex: origins and functional significance. *Neurosci Biobehav Rev* **28**, 441-448 (2004).
195. Rushworth, M.F.S. & Behrens, T.E.J. Choice, uncertainty and value in prefrontal and cingulate cortex. *Nat. Neurosci* **11**, 389-397 (2008).
196. Kennerley, S.W., Walton, M.E., Behrens, T.E.J., Buckley, M.J. & Rushworth, M.F.S. Optimal decision making and the anterior cingulate cortex. *Nat. Neurosci* **9**, 940-947 (2006).
197. Behrens, T.E.J., Woolrich, M.W., Walton, M.E. & Rushworth, M.F.S. Learning the value of information in an uncertain world. *Nat. Neurosci* **10**, 1214-1221 (2007).
198. Fellows, L.K. & Farah, M.J. Is anterior cingulate cortex necessary for cognitive control? *Brain* **128**, 788-796 (2005).
199. Kouneiher, F., Charron, S. & Koechlin, E. Motivation and cognitive control in the human prefrontal cortex. *Nat. Neurosci* **12**, 939-945 (2009).
200. Price, J.L. Definition of the orbital cortex in relation to specific connections with limbic and visceral structures and other cortical regions. *Ann. N. Y. Acad. Sci* **1121**, 54-71 (2007).
201. Noonan, M.P. et al. Separate value comparison and learning mechanisms in macaque medial and lateral orbitofrontal cortex. *Proceedings of the National Academy of Sciences* **107**, 20547 -20552 (2010).
202. Friston, K. The free-energy principle: a unified brain theory? *Nat. Rev. Neurosci* **11**, 127-138 (2010).
203. Friston, K. The free-energy principle: a rough guide to the brain? *Trends Cogn. Sci. (Regul. Ed.)* **13**, 293-301 (2009).
204. Gold, J.I. & Shadlen, M.N. Neural computations that underlie decisions about sensory

stimuli. *Trends Cogn. Sci. (Regul. Ed.)* **5**, 10-16 (2001).
205. Rangel, A. & Hare, T. Neural computations associated with goal-directed choice. *Curr. Opin. Neurobiol* **20**, 262-270 (2010).

8. PUBLICATIONS ET COMMUNICATIONS

a. Articles scientifiques :

Publié en 2011 :

- V. Chambon, **P. Domenech**, E. Pacherie, E. Koechlin, P. Baraduc, C. Farrer, « What are they up to? The role of sensory evidence and prior knowledge in action understanding », **PLoS ONE**, 2011.
- T. Fassier, N. Guffon, T. D'Amato, D. Vital-Durand, **P. Domenech**, « Misdiagnosed postpartum psychosis revealing a late-onset urea cycle disorder: a clinical case conference », **American Journal of Psychiatry**, 2011.
- G. Barbalat, V. Chambon*, **P. Domenech***, C. Ody, E. Koechlin, C. Farrer, « Impaired hierarchical control within the lateral prefrontal cortex in schizophrenia » (*Equally contributing), **Biological Psychiatry**, 2011.

Publié en 2010 :

- **P. Domenech,** JC. Dreher, « Decision threshold modulation in the human brain », **Journal of Neuroscience**, 2010. Comment by N. Myers and V. Wyart in Frontiers in human neuroscience, 2011.

En préparation :

- G. Sescousse, G. Barbalat*, **P. Domenech***, JC. Dreher, « Exacerbated responses specific to monetary rewards in pathological gamblers », **pending submission**.
- **P. Domenech**, J. Redouté, R. Bogacz, JC Dreher, «A mechanistic account of efficient economic decision-making », **pending submission**.
- G. Barbalat, P. Fourneret, F. Ramus, **P. Domenech «** Impaired perceptual decision-making in dyslexia », **pending submission**.
- G. Barbalat, P. Fourneret, **P. Domenech «** Perceptual decision-making in dyslexia, an fMRI study ».
- **P. Domenech**, M. Ulla, JC. Dreher, F. Duriff, « STN-DBS, but not DOPAtherapy, restores the ability to contextually adjusts decision-making in parkinsonian patients ».
- G. Sescousse, **P. Domenech***, G. Barbalat*, JC. Dreher, « A neurobiological approach to the Gambler's Fallacy ».
- G. Sescousse, **P. Domenech***, G. Barbalat*, JC. Dreher, « Gambler's Fallacy and pathological gambling : an fMRI study ».
- V. Chambon, **P. Domenech**, E. Pacherie, E. Koechlin, P. Baraduc, C. Farrer, « Sensory evidence and prior knowledge in action understanding : an fMRI study ».

b. Communications internationales et prix :

2010 :

- **Society for Neuroscience (**SFN) : « Exacerbated responses specific to monetary rewards in pathological gamblers », poster, communication orale (collaboration avec G. Sescousse).

2008 :

- **Society for Neuroscience (**SFN) : «Distinguishing two brain systems involved in choosing between different types of rewards », communication orale.
- **Exciting Biologies: Biology of Cognition** (Cell press-NEURON) : "Choosing between two types of rewards reveals a new functional antero-posterior organization in the medial wall of the frontal cortex", poster.

2007 :

- **Human Brain Mapping** (HBM) : « Uncertainty and predictability during rapid perceptual decision making », communication orale, poster et « travel award ».
- **Computational Cognitive Neuroscience** (SFN-CCN) : « Predictability, surprise and perceptual decision making », communication orale, poster, « travel award ».
- **Society for Neuroscience (**SFN) : « Common reward currency allowing choice between rewards of different nature », poster.

c. Publications pédagogiques :

Publié en 2010 : G. Barbalat, **P. Domenech**, M. Vernet, P. Fourneret, « Approche neuro-économique de la prise risque à l'adolescence », **Encéphale**.
Publié en 2008 : F. Guenole, **P. Domenech**, L. Garma, A. Nicolas, « Sommeil et schizophrénie : une revue des données expérimentales », **Médecine du sommeil**.
Publié en 2007 : C. Danion, **P. Domenech**, C. Demily, N. Franck, « Symptômes psychotiques dans les affections médicales générales de l'adulte », **EMC**.

d. Communications en Français :

2010 : T. Fassier, P. Domenech, N. Guffon, D. Vital-Durand, « Miraculous treatment of late-onset urea cycle disorder (UCD), initially misdiagnosed as post- partum psychosis: a case report and review of the pathophysiology-oriented management », **Congrès de physiologie, de pharmacologie et de thérapeutique**.
2008: G. Barbalat, P. Domenech, M. Vernet, P. Fourneret, « Approche neuro-économique de la prise risque à l'adolescence », **Congrès de l'Encéphale**.
2007 : L. Jasse, A. Prouteau, G. Bailly, P. Domenech, N. Franck, « Remédiation cognitive par utilisation du jeu d'échecs dans la schizophrénie », **Congrès de l'Encéphale**.

9. ANNEXES : AUTRES PUBLICATIONS

Article 3 : What are they up to ? The role of sensory evidence and prior knowledge in action understanding

Valérian Chambon, Philippe Domenech, Elisabeth Pacherie, Etienne Koechlin, Pierre Baraduc and Chlöé Farrer

Publié dans PLoS ONE (2011) vol. 6 (2) pp. e17133

OPEN ACCESS Freely available online

PLoS one

What Are They Up To? The Role of Sensory Evidence and Prior Knowledge in Action Understanding

Valerian Chambon[1]*, Philippe Domenech[1], Elisabeth Pacherie[2], Etienne Koechlin[3], Pierre Baraduc[1], Chlöé Farrer[4,5]

1 Centre de Neuroscience Cognitive, Université de Lyon, CNRS, Bron, France, **2** Institut Jean Nicod, EHESS, DEC-ENS, CNRS, Paris, France, **3** INSERM, Ecole Normale Supérieure, Université Pierre et Marie Curie, Paris, France, **4** Centre de Recherche Cerveau et Cognition, Université de Toulouse, UPS-CNRS, Toulouse, France, **5** Faculté de Médecine de Rangueil, Toulouse, France

Abstract

Explaining or predicting the behaviour of our conspecifics requires the ability to infer the intentions that motivate it. Such inferences are assumed to rely on two types of information: (1) the sensory information conveyed by movement kinematics and (2) the observer's prior expectations – acquired from past experience or derived from prior knowledge. However, the respective contribution of these two sources of information is still controversial. This controversy stems in part from the fact that "intention" is an umbrella term that may embrace various sub-types each being assigned different scopes and targets. We hypothesized that variations in the scope and target of intentions may account for variations in the contribution of visual kinematics and prior knowledge to the intention inference process. To test this hypothesis, we conducted four behavioural experiments in which participants were instructed to identify different types of intention: basic intentions (i.e. simple goal of a motor act), superordinate intentions (i.e. general goal of a sequence of motor acts), or social intentions (i.e. intentions accomplished in a context of reciprocal interaction). For each of the above-mentioned intentions, we varied (1) the amount of visual information available from the action scene and (2) participant's prior expectations concerning the intention that was more likely to be accomplished. First, we showed that intentional judgments depend on a consistent interaction between visual information and participant's prior expectations. Moreover, we demonstrated that this interaction varied according to the type of intention to be inferred, with participant's priors rather than perceptual evidence exerting a greater effect on the inference of social and superordinate intentions. The results are discussed by appealing to the specific properties of each type of intention considered and further interpreted in the light of a hierarchical model of action representation.

Citation: Chambon V, Domenech P, Pacherie E, Koechlin E, Baraduc P, et al. (2011) What Are They Up To? The Role of Sensory Evidence and Prior Knowledge in Action Understanding. PLoS ONE 6(2): e17133. doi:10.1371/journal.pone.0017133

Editor: Angela Sirigu, French National Centre for Scientific Research, France

Received November 11, 2010; **Accepted** January 20, 2011; **Published** February 18, 2011

Funding: This research was supported by a grant of the Agence Nationale de la Recherche obtained by C.F. (ANR-ZR81). V.C. and P.D. were supported by scholarships from the French Ministry of Research. The funders had no role in study design, data collection and analysis, decision to publish, or preparation of the manuscript.

Competing Interests: The authors have declared that no competing interests exist.

* E-mail: valerian.chambon@isc.cnrs.fr

Introduction

Intentional inference: perceptual information and top-down prior knowledge

Explaining or predicting the behaviour of our conspecifics requires the ability to properly appreciate the causes that motivate it. As these causes are hidden – intentions, like beliefs or desires, are unobservable states –, it has long been a matter of speculation how one may infer them from patterns of visible behaviour alone. Indeed, visual information conveyed by the movement kinematics is often noisy, ambiguous or incomplete. As a result, visual information generally under-constraints the space of candidate causes (i.e. the many competing intentions) that are logically consistent with what is observed [1–3]. One way to solve this problem is to assume that this space of possible intentions is further constrained by the observer's prior expectations. These expectations are derived from prior knowledge that may originate from the past experience of the viewer (through expertise: [4,5]; or learning of statistical regularities: [6]), from her intuitive theories [7,8], or reputational knowledge [9,10], as well as from contextual information surrounding the action scene [5,11]. This prior knowledge has been demonstrated to be crucial to account for the robustness of our everyday inferences [12]. Indeed, it makes possible inductive inference about the agent's intentions, even in cases of noisy signals or incomplete data [13–15].

However, although most authors agree that prior knowledge and perceptual information both contribute to the process of inferring intentions, the precise contribution of each type of information remains controversial [16–23]. The controversy stems in part from the fact that "intention" is an umbrella term used in the empirical and philosophical literature to refer to representations of actions that can differ in both their content and format, as well as in their temporal properties and in the role they play in the guidance of actions [24–29]. Intentions can therefore be distinguished into several sub-types according to one or several of these factors. In the present study, we propose a typology of intentions and hypothesize that this typology might be a key element in understanding how perceptual information and prior knowledge contribute to the process by which intentions are inferred.

Varieties of intentions

The intentional typology we present below is primarily motivated by the necessity to take into account two dimensions of variation in the content of intentions that may make an important difference to the processes involved in their inference. The first dimension of variation concerns the scope of the intention; i.e., the more-or-less complex nature of its goal. Here we can draw a distinction between *basic intentions* and *superordinate intentions*. *Basic intentions* are directed at simple motor goals (i.e. goals that can be realized by basic actions such as lifting an arm, pressing a button, or reaching for an object). These intentions are sensorimotor representations where the goal is represented directly in terms of the motor commands needed to achieve it. The relation between basic intention and motor act is thus one-to-one when that act is successfully completed [17]. In contrast, s*uperordinate intentions* are intentions directed at somewhat more complex or general goals, the achievement of which typically involves the completion of a number of subgoals or substeps. Depending on the complexity of the general goal, these subgoals may themselves be decomposed into further subgoals, ultimately reaching the level of basic actions. The achievement of a superordinate intention will thus require the execution of a combination of basic actions each guided by a corresponding basic intention. Different combinations of motor acts can be used to accomplish the same general goal and, conversely, a same motor act (or even series of motor acts) can be part of combinations aimed at different general goals.

The second dimension of variation we were interested in concerns the target of the intentions. Neither basic nor superordinate intentions are necessarily directed at inanimate objects. They may also target a third party or be achieved in a context of social interaction [11,30–33]. The content of intentions is thus also modulated by the relational structure in which an action takes place. We call intentions directed at an object, *non-social* intentions, and intentions directed at a third party, *social* intentions.

By combining these two dimensions, we obtain the following typology: i) *non-social* basic intention, ii) *non-social* superordinate intention, iii) *social* basic intention, and iv) *social* superordinate intention. Owing to their different scopes and targets, basic and superordinate, social and non-social, intentions are naturally assigned different functional roles, different types of content and different temporal scales. The present study aims at investigating whether these functional differences are reflected in the respective contribution of perceptual information and prior expectations to intentional judgments.

Overview of the present study

We conducted four experiments in which participants were requested to identify one intention underlying an action scene. Each experiment involved one type of intention with a specific scope (basic *vs.* superordinate) and a specific target (social *vs.* non-social). Interactions between prior expectations and visual information were examined within a Bayesian probabilistic framework. This conceptual framework is particularly well-suited to account for how accurate predictions on hidden world states are made in situations where available sensory information does not sufficiently constrain the number of potential solutions [13,15,34]. Before the onset of an action sequence, each of the agent's possible intentions was first assigned a certain 'level of belief', termed *a priori probability* (the probability that intention X is the real cause of the observed behaviour estimated from past experiences). Then the observer progressively gathers sensory information (visual input) as the action sequence is disclosed and both sources of information (sensory and *a priori*) are combined and used to infer the intention underlying the observed behaviour. Thus, the process by which intentions are inferred is considered as reflecting a trade-off between the sensory information and the prior probability of each candidate intention [14]. Finally, the chosen intention is that which maximizes the *posterior probability* value, *i.e.* the probability that intention X is true *given* what is observed.

In the present study, these two terms – *a priori* probability and sensory information – were manipulated using a two-step procedure. Prior expectations the participants had about the agent's possible intentions were manipulated by increasing the *a priori* probability that one intention (termed *likely intention*) was achieved, to the detriment of other intentions (*unlikely intentions*) with the same scope and target. Sensory information available from an action scene was then manipulated in a second step by modulating the degree of completeness (i.e. the duration) of the action sequences, resulting in actions scenes with varying amounts of visual information.

We first predicted that judgements about intentions would follow the general principles of Bayesian inference. Specifically, we expected that the amount of visual information would interact with participants' prior expectations such that the lower the reliability of the external visual input, the more participants' responses would depend upon their own internal expectations. That is, they should respond more frequently in the direction of the *likely* intention. And vice versa, the higher the amount of visual information, the less the participants should rely on their prior expectations.

Second, we predicted that the shape of the interaction between these two sources of information would be a function of the *type* of intention, depending on both its scope and target. Along the dimension of the scope, we hypothesised that participants' judgement about basic intentions should primarily rely on sensory information available from the action scene. This prediction is motivated by the pragmatic content of the basic intention: "grasping a glass of water" directly denotes the corresponding intention of "grasping that glass". In this case, perceiving the action itself – i.e. processing the associated visual kinematics – is enough to successfully determine the nature of the underlying intention [35]. On the other hand, we expected performance in judging superordinate intentions to be significantly influenced by participants' prior expectations. As already mentioned, the same sequence of motor acts can be part of combinations aimed at different general goals or superordinate intentions. In this specific case, sensory information carried by movement kinematics is not sufficient to infer the corresponding intention, as it under-constraints the set of candidate intentions congruent with this movement [1,2,17,36]. We consequently predicted that this perceptual uncertainty should encourage participants to 'mistrust' what they observe and, hence, to rely more on their prior expectations.

Along the dimension of target, finally, we expected participants' reliance on their prior expectations to increase when basic and superordinate intentions are directed at another agent. The structure of social interaction meets indeed particular, often irrepressible, expectations, such as those provided by reputational knowledge [9,10,37]. Indeed, knowledge about individual's reputation has been robustly demonstrated to have a strong impact on predicting how the observed agent will behave [12]. In line with other recent suggestions, we thus hypothesised that the weight of these *a priori* expectations would increase when the observed action fits into a context of social interaction.

Materials and Methods

Non-social experiments

In the first experiment, participants were instructed to infer the *basic intention* (to lift, to rotate, or to transport) of an actor manipulating meaningless objects (fig. 1, **A**). In the second

experiment, participants were instructed to infer the *superordinate intention* (i.e. the general goal) underlying a sequence of motor acts (fig. 1, **B**).

Social experiments

The third (fig. 1, **C**) and fourth experiments (fig. 1, **D**) presented two actors engaged in a social game in which they could either cooperate or defect by coordinating their action (joint-action condition) or by refusing to join their action to the achievement of a shared goal (defective condition). Participants were instructed to infer the nature of the second player's social intention (i.e. cooperative or defective intention). In both these experiments, the bias was assigned according to the way the second player responded to the strategy adopted by the opponent in the previous round. Participants were therefore biased towards the reputation of the second player rather than towards one particular type of social intention. Finally, as in the two previous non-social experiments, both *basic intentions* (single motor acts) and *superordinate intentions* (sequences of motor acts leading to the construction of a shape) were considered in the last two experiments.

Ethics Statement

All participants gave written informed consent for the study which was approved by the local Ethical Committee (Comité de Protection des Personnes SUD-EST IV, no. B80631-60).

Experiment 1: non-social basic intention

Participants. 30 healthy subjects (15 males, 15 females, mean age = 35.13, S.D. = 9.33 and laterality score mean = 0.88, S.D. = 0.31; [38]) participated in this experiment. They all reported normal or corrected-to-normal visual acuity. Participants received 10 euros for taking part in the study.

Stimuli. Visual stimuli were incomplete movies representing an actor's hand performing a simple manipulation of a meaningless object. The duration of the video sequences was varied on 4 distinct levels, ranging from 1480 ms to 1880 ms after movement onset. Each movie was characterized by one basic intention (to transport, to rotate, or to lift an object) and participants were instructed to infer the basic intention in each video. There were three white rectangular objects of similar size (3 cm×6 cm) and orientation, positioned at equal distance (16.8 cm) from the starting position of the actor's hand (figure 1, A). All the movies were performed by a single actor and only featured her naked arm. Each action was performed as often with one object as with the others.

Movies were equalized for temporal homogeneity (see **Supporting Text S1, part 1,** and **Figure S1**). Furthermore, all the movies were unique, i.e., they were presented only once to prevent any influence of memorized kinematic parameters on participants' performance in the experiment.

Procedure. Participants were comfortably sat at a distance of 60 cm from a 19″ computer monitor. Each trial started with the observation of an incomplete movie, and then a response screen appeared for 2500 ms representing the first letter of each possible intention (T for 'transport', L for 'lift', or R for 'rotate'). Participants were requested to respond by pressing, as quickly and accurately as possible, one of the three keyboard presses corresponding to the three possible intentions. Once a response was given, the next trial started.

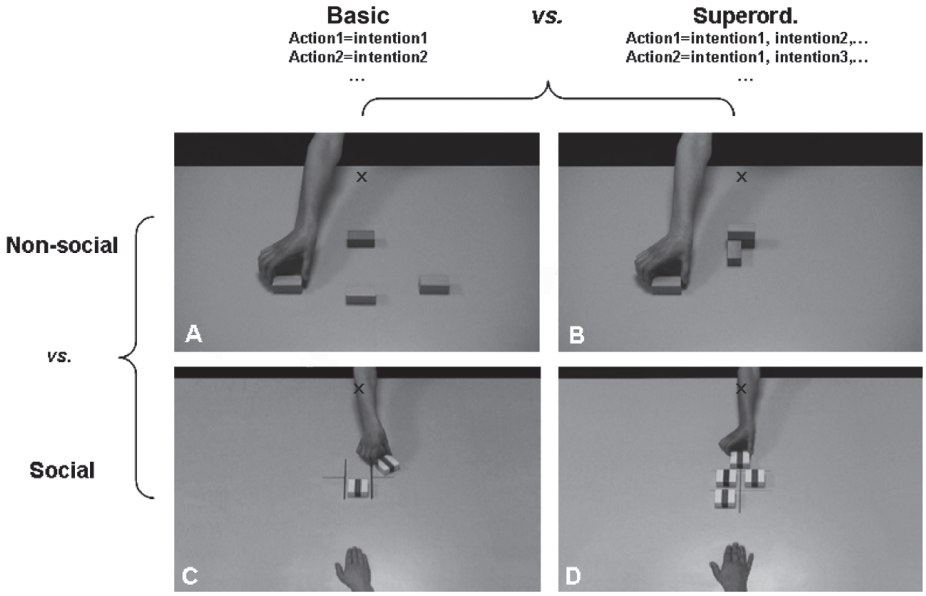

Figure 1. Examples of stimuli for each of the four experiments. BASIC NON-SOCIAL intention experiment (**A**); SUPERORDINATE NON-SOCIAL intention experiment (**B**); BASIC SOCIAL intention experiment (**C**); SUPERORDINATE SOCIAL intention experiment (**D**). The black cross indicates the starting position of the hand.
doi:10.1371/journal.pone.0017133.g001

The design was composed of two experimental sessions. A first baseline session was characterized by a flat (unbiased) prior probability distribution with all basic intentions having the same probability. In a second bias session, participants were biased towards one intention (likely intention, 55%) to the detriment of the others (unlikely intentions, 22% each). The bias was randomly assigned so that each basic intention was equally biased across participants.

In both sessions, trials were organized into OVERT blocks in which movies consisted of a constant and very high amount of visual information (1880 ms), alternating with COVERT blocks in which movies consisted of varying and lower amounts of visual information presented in a random order (LOW = 1480 ms, MODERATE = 1560 ms, and HIGH = 1640) (see **Supporting Text S1, part 2**, for the selection of these amounts of visual information[58,59]; **Figure S2**). Each experimental sequence (one overt block followed by one covert block) was repeated 9 times over each session (see figure 2, A) and each participant performed the trials in a different random order.

The reason for block interleaving was that it enabled us to maintain the bias constant across the bias session. Indeed, by regularly inserting overt blocks of movies with different probabilities, we ensured that participants were continuously biased towards one intention over the whole session. Furthermore, even though the baseline session did not include any bias assignment, and therefore was not concerned with bias maintenance, it contained the same trial organization (block interleaving) to allow a direct comparison of the performance between the two sessions.

Prior to running the experiment, participants undertook a training session to get familiar with the task. The training consisted of 3 baseline experimental sequences (non-biased probability distribution) with interleaved blocks. The 72 movies (3×24) presented during the training session were distinct from those used in the experiment.

Design and statistical analyses. One group of statistical analyses was performed for each session independently (baseline and bias sessions), on the two dependant variables (participants' hits and reaction times for correct responses). In the overt blocks of the baseline session, one two-tailed t-test was conducted on participants' reaction times (RTs) between the future 'likely' intention (the one towards which participants were subsequently biased in the bias session) and the future 'unlikely' intentions. The same test was conducted in the bias session between likely and unlikely intentions. In the covert blocks, a 2×3 repeated-measures ANOVA was performed for each session on both RTs and hits. The first two-level factor was the bias (future 'likely' vs. future 'unlikely' intentions OR likely vs. unlikely intention) and the second three-level factor was the amount of visual information (LOW, MODERATE and HIGH). Post-hoc Fisher tests were then performed to identify differences between conditions.

Another group of analyses was conducted in order to assess the magnitude of the bias effect on participants' performance. To do so, we looked at whether increasing the probability of one intention concomitantly affected the selection of intentions with lower probability. Two-tailed t-tests on RTs and hits for unlikely intentions were thus performed between the baseline and the bias sessions. We predicted that selecting an unlikely intention should be more demanding in the bias session – as it concomitantly requires inhibiting a competing biased intention – than in the baseline session, where all intentions had the same probability of occurring. In the following, the resulting "cost" (i.e. increased RTs and decreased hits for unlikely intentions) was considered as an indirect measure of the bias effect.

For all analyses, a $p<.05$ was taken as the criterion for significance and an eta squared ($\hat{\eta}$) was used as a measure of effect size. These analyses were performed using the statistical software *Statistica 7* (www.statsoft.com).

Experiment 2: non-social superordinate intention

Participants. 30 new participants (15 males, 15 females, mean age = 36.59, S.D. = 8.12 and laterality score mean = 0.79, S.D. = 0.19) took part in this experiment. They all reported normal or corrected-to-normal visual acuity and received 10 euros for taking part in the study.

Stimuli. As with the non-social basic experiment, test material consisted of incomplete movie clips showing an actor's hand manipulating meaningless objects. However, contrary to experiment 1, movies in the superordinate experiment represented a sequence of *three* successive manipulations (to transport, rotate, or lift the object) leading to the construction of a meaningless shape. Each sequence was therefore characterized by an underlying superordinate intention, represented by one final shape (s1, s2 or s3). The objects used in the first experiment were also used in this second experiment (figure 1, B). The first action was performed on one of the three objects, the second action on one of the two objects left, and the third action on the remaining object. After each action, the hand came back to the starting position. The incompleteness of the video sequences was controlled so that the duration of the last action was varied on 3 distinct levels (1480 ms, 1560 ms or 1640 ms after this action starts). All the movies were made with the same actor as in experiment 1. Finally, temporal homogeneity of the movies was controlled and each trial was unique.

Procedure. The organization of the trials was the same as in the non-social basic experiment (see figure 2, B, 'Superordinate exp.'). However, the task was further constrained. First, to ensure that participants paid attention to the overall sequence of actions, they were asked to identify what the last (not-yet completed) action of this sequence was, by pressing as quickly and accurately as possible, one of the three corresponding keyboard presses (T, L, or R). This response depended upon having inferred the superordinate intention of this sequence (i.e. the final shape being achieved by a set of three successive actions). Second, to ensure that participants were biased towards the superordinate intention itself and not towards the last final action only, commutative sequences were used so that each shape could be constructed from distinct sequences of actions sets. Sequences shown in the covert blocks were thus distinct from those used in the overt blocks (e.g. the shape s1 could be obtained from the sequence 'lift-lift-rotate' in an overt block, but from the sequence 'lift-rotate-lift' in a covert block). Finally, the intention could not be inferred solely from the motor acts composing the sequence. Indeed, although the probability of each shape being constructed was manipulated in the bias session (i.e. one particular shape had a higher probability), the probabilities of the individual actions (lift, rotate, or transport) were held equal at each step of that sequence. Finally a training session was conducted with movies distinct from those used in the experimental sessions.

Experiment 3: social basic intention

Participants. 30 novel subjects (15 males, 15 females, mean age = 32.9, S.D. = 10, and laterality score mean = 0.80, S.D. = 0.11) participated in this experiment. They all reported normal or corrected-to-normal visual acuity and received 10 euros for taking part in the study.

Stimuli. Visual stimuli consisted of incomplete movies showing two players' hands (opposite each other) manipulating

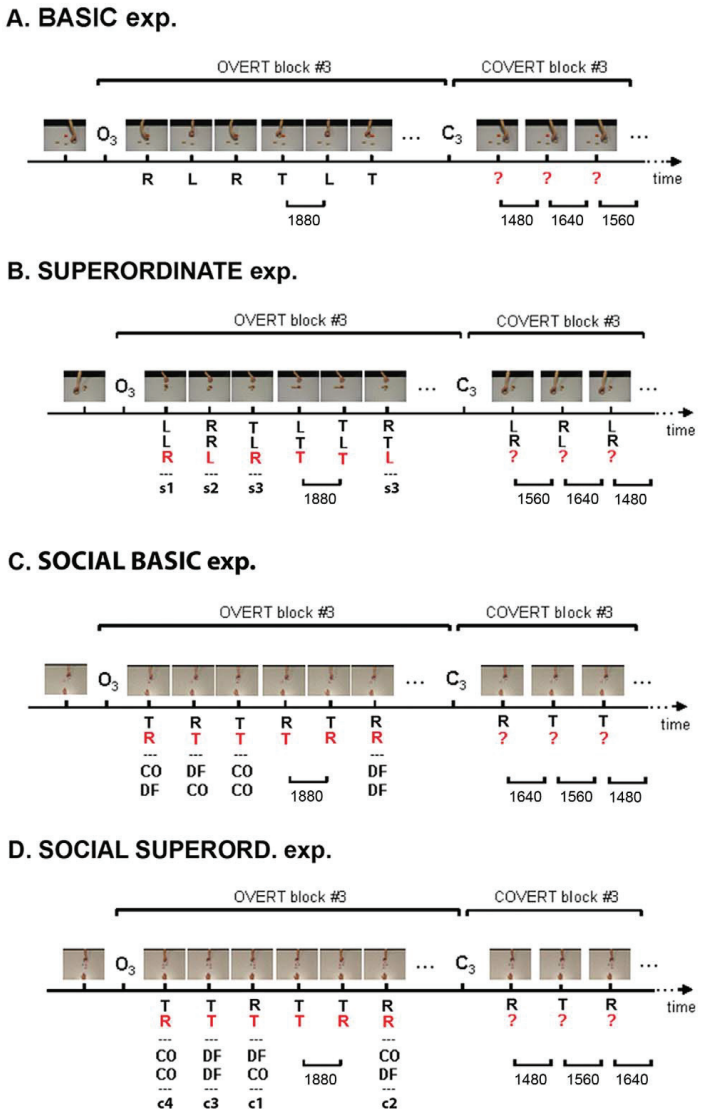

Figure 2. Experimental designs. Examples of a typical experimental sequence (one OVERT block followed by one COVERT block) used in both the baseline and the bias sessions. *OVERT blocks (O)*: 18 movies with a very high and constant amount of visual information (1880 ms). *COVERT blocks (C)*: 9 movies with three amounts of visual information (1480, 1560, and 1640 ms). In the 4 experiments, the probability of all intentions was held equal across the block, except in OVERT blocks of the bias session, where one particular intention had a greater probability to be accomplished than the other ones. **In the BASIC exp.**, subjects had to identify a single action (*labels*: **L**: "lift" action; **R**: "rotate" action; **T**: "transport" action). **In the SUPERORDINATE exp.**, subjects had to identify the final action (red letter) of a sequence leading to *shape 1*, *2*, or *3* (**s1**: shape 1). **In the SUPERORD. SOCIAL exp.**, subjects had to identify the action of the second player (red letter) leading to *configuration 1*, *2*, *3*, or *4* (**c1**: configuration 1). In both **BASIC and SUPERORD. SOCIAL exp.**, the action or the configuration achieved by each player indicated either a cooperative or a defective strategy (**CO**: cooperate; **DF**: defect). In each experiment, a probabilistic bias was assigned to one particular action (basic), shape (superordinate) or strategy (social). The red interrogation mark indicates the action (basic: single action; superordinate: last action of the sequence) for which the amount of visual information varied.

doi:10.1371/journal.pone.0017133.g002

meaningless objects. Two objects (printed with a blue or a red line) were placed on the sides of a grid that was situated in the centre of the scene (figure 1, C). The objects were of similar size (5.8 cm×5.8 cm) and located at equal distance from the starting position of each player's hand (figure 1, C). The two actors played one after the other by moving the object towards the middle of the grid (termed 'bank') or by rotating it so that it remained at its own place. Movies were partitioned so that the last action (i.e. the action performed by the second player) was incomplete (1480 ms, 1560 ms, or 1640 ms after the last action starts).Here, each motor act directly denoted the social intention of the player: each player could either cooperate with the other one, by moving the object towards the central bank (transport), or defect, by leaving the object at its own place (rotate). Consequently, there were four possible combinations of intentions, or strategies: either both players cooperated (transport/transport) or defected (rotate/rotate), or the first player defected and the second cooperated (rotate/transport), or the first player cooperated and the second defected (transport/rotate). Finally, temporal homogeneity of the movies was controlled and each trial was unique.

Procedure. For each trial, participants were instructed to observe the incomplete movie and infer what the last action (i.e. the one performed by the second player) was. This response required the participant to have inferred the second player's intention (to defect or to cooperate) which itself depended upon the first player's strategy. Participants were asked to give their answer by pressing, as quickly and accurately as possible, one of the two keyboard keys corresponding to the two possible last actions (T for 'transport', or R for 'rotate') susceptible to achieve the second player's intention. Once a response was given, the next trial started.

In the baseline session, all combinations of strategies were counterbalanced over the blocks (i.e. whatever the first player did the second player was just as likely to defect or to cooperate). In the bias session, on the other hand, the probability that the second player did whatever the opponent did in the previous round was increased, thus biasing participants to perceive the second actor as a "tit-for-tat" player (i.e. as being more inclined to cooperate if the first player had previously cooperated, and to defect if the first player had previously defected). The rationale for biasing the second player's reputation in such a way was twofold. First, tit-for-tat (TFT) reputation implies that individuals respond to their opponent's actions in a mirrored (i.e. correlated) fashion. Therefore, successfully predicting intentions of a TFT-like player necessarily involves taking into account what the first player has done, and by consequence, ensured that participants paid attention to the whole sequence of actions (both actor 1′s play and actor 2′s play). Second, contrary to other common types of reputation such as "always defect", or "always cooperate", TFT may equally imply cooperative as well as defective strategies. The probability that the second actor behaves as a tit-for-tat player could thus be increased without otherwise increasing the probability of one intention (e.g. cooperate) to the detriment of the other one (e.g. defect). Holding equal the probability of both these strategies was here crucial to nullify their potential kinematic differences on participants' performance (see [39]) and also to avoid stereotyped responses (e.g. always responding 'cooperate' or 'defect'). Finally, a tit-for-tat strategy is known to be a more intuitive and successful strategy than alternative ones, such as "always cooperating", "always defecting" or "acting randomly" [40–42]. We thus chose to experimentally strengthen this already existing *a priori* bias by increasing the probability that the second player's action mirrors her opponent's one while holding equal both the probability of each single act (to rotate or to transport) and the overall probability of each intention (to defect or to cooperate) (figure 2, C, 'Social Basic exp.'). Thus, in the baseline session, the second player was as likely to play tit-for-tat as she was to play the other types of strategy. In the bias session, however, the probability that the second actor played tit-for-tat was increased so that she was more likely to cooperate (rather than defect) if the first player had previously cooperated, and to defect (rather than cooperate) if the first player had previously cooperated. Finally a training session was conducted with movies distinct from those used in the experimental sessions.

Experiment 4: social superordinate intention

Participants. 30 novel participants (15 males, 15 females, mean age = 34.27, S.D. = 9.42, and laterality score mean = 0.83, S.D. = 0.26) participated in this last experiment. They all reported normal or corrected-to-normal visual acuity and received 10 euros for taking part in the study.

Stimuli. As in the social basic experiment, the stimuli of this last experiment represented two players' hands manipulating objects. However, in the present experiment, the actors played in turn with the goal of vertically aligning three objects (see figure 1, D). The goal of the first player was to align the objects according to the color (red), irrespective of the orientation, while the goal of the second player was to align the objects according to the orientation, irrespective of the color. A third configuration could be obtained by the alignment of the objects according to both the orientation and the color. As in the social basic experiment, the two social intentions were of a defective or a cooperative nature. However, in the present experiment, the social intention was denoted by the sequence of the players' motor acts (i.e. the final configuration), rather than by the single action performed by each player. Indeed, a defective or a cooperative strategy could be equally achieved by rotating or transporting the object. Each player could adopt a defective strategy by manipulating the object in such a way that it prevented the creation of one configuration, or adopt a cooperative strategy in order to achieve another configuration. The four possible final configurations were therefore: either both players defected (configuration 3) or cooperated (configuration 4), or the first player defected and the second cooperated (configuration 1), or the first player cooperated and the second defected (configuration 2). As for previous experiments, only the last action (i.e. the action performed by the second player) was made incomplete (1480 ms, 1560 ms or 1640 ms). Finally, temporal homogeneity of the movies was controlled and each trial was unique.

Procedure. Participants were instructed to infer the social superordinate intention of the second player by indicating which action allowed the accomplishment of that intention. A correct response therefore required having correctly inferred the second player's intention (to defect or to cooperate) which itself depended upon the first player's strategy. Participants were asked to give their answer by pressing, as quickly and accurately as possible, one of the two keyboard keys corresponding to the two possible actions (T for 'transport' or R for 'rotate') congruent with the second player's social intention. The organization of trials in the social superordinate experiment was the same as for the social basic experiment (see figure 2, D). Tit-for-tat reputation (i.e. the second player did whatever the opponent did in the previous round) was chosen to be biased across participants. Likewise, commutative sequences were also used so that each pattern could be obtained from distinct sequences of actions ensuring that the different strategies could not be predicted from motor acts solely. Furthermore, both the overall probability of each strategy (cooperative or defective) and each action (to rotate or to

transport) were held equal across the blocks. Finally a training session was conducted with movies distinct from those used in the experimental sessions.

'Bias effect': between-experiment comparisons

Finally, some analyses were conducted to directly assess whether the contribution of prior knowledge to the inference of an intention depended upon the target (basic vs. superordinate) and the scope (non-social vs. social) of the intention. Student tests were first conducted on the overall performance in the bias session between the basic experiments and the superordinate ones, and between the non-social experiments and the social ones. Second, the bias effects for each dimension (scope and target) were compared with each other. A score reflecting the effect of each type of intention (basic, superordinate, social, non-social intention) was calculated by subtracting, in each experiment, participants' hit rate for the likely intention from the hit rate for the unlikely intentions. The resulting scores were then entered in a 2 (basic vs. superordinate) ×2 (social vs. non-social) ×3 (amounts of information) factorial ANOVA.

Results

Experiment 1: non-social basic intention

For each session, two-tailed t-tests were performed between the two unlikely intentions on both RTs and hits. As no significant differences appeared (all $p>.05$), performances for these two unlikely intentions were pooled for subsequent analyses.

Overt blocks. As expected, participants performed the task well when the amount of visual information was very high (percentage of mean correct responses = 98%, S.D. = 2.4, and 96.8%, S.D. = 3.4 in the baseline and the bias sessions, respectively). Furthermore, in the baseline session, there were no significant differences among hits and RTs between the (future) 'likely intention' (i.e. the one towards which participants will be biased in the subsequent bias session) and the 'unlikely intention', indicating that prior to biasing participants, there was no *a priori* bias towards one intention rather than another (two-tailed *t*-tests, all $p>0.2$, see figure 3, 'Basic exp.', baseline session).

The only significant difference was found in the bias session, with faster RTs for the likely intention vs. unlikely intentions (two-tailed *t*-tests, all $p<.001$). Subsequent analyses of RTs across time were carried out by independently comparing RTs for likely basic intention and RTs for unlikely basic intentions across the different blocks. The bias was found to have a cumulative effect over time, with RTs for the likely intention progressively decreasing up to block 8 (minimal RT = 337 ms) and then remaining constant until the end of the session (blocks 1–3 *vs.* blocks 4–6: $t = 3.09$, $p<.005$; blocks 4–6 *vs.* blocks 7–9: $t = 2.08$, $p<.05$) (see figure 3, 'Basic exp.').

Covert Blocks. The 3 (amounts of information) ×2 (likely vs. unlikely intentions) repeated-measures ANOVA revealed significant effects on both participants' RTs and hits. In the baseline session, a significant effect of the amount of visual information was obtained (RTs: $F(2,116) = 167.13$, $p<.001$, $\acute{\eta} = 0.74$, and hits: $F(2,116) = 277.44$, $p<.001$, $\acute{\eta} = 0.82$). As expected, RTs were found to decrease and hits to improve as the amount of visual information increased. There were, however, no significant effects of the intention presented (future 'likely' or future 'unlikely' intention) nor of the interaction between the intention and the amount of visual information (both $p>0.05$), showing that improved performance for higher amounts of information was independent of the presented intention (Im1, Im2, or Im3) (see table 1 and figure 4, 'Baseline session').

In the bias session, in addition to the effect of amount of visual information (RTs: $F(2,116) = 98.8$, $p<.001$, $\acute{\eta} = 0.62$; hits: ($F(2,116) = 190.92$, $p<.001$, $\acute{\eta} = 0.76$), an effect of the bias (RTs: $F(1,58) = 18.51$, $p<.001$, $\acute{\eta} = 0.24$; hits: ($F(1,58) = 19.81$, $p<.001$, $\acute{\eta} = 0.25$) as well as of the interaction (RTs: $F(2,116) = 13.98$, $p<.001$, $\acute{\eta} = 0.19$; hits: $F(2,116) = 5.44$, $p = .005$, $\acute{\eta} = 0.08$) were also observed. Post-hoc tests indicated that participants were more accurate and faster in recognizing the likely intention in low information condition only (LSD Fisher tests, RTs: LOW = $p<.001$; MODERATE = $p<.005$ and HIGH = *ns*; Hits: LOW = $p<.001$; MODERATE = *ns*. and HIGH = *ns*.) (see table 1 and figure 4, 'Bias session').

Effect of the bias on the unlikely intention. We were also interested in evaluating the influence of the bias on the selection of the unlikely intentions. Comparing the performance for the unlikely intention between the two sessions revealed no significant differences for any amount of visual information (two-tailed t-tests, RTs and hits: all $p>0.05$). This result indicates that switching from the baseline to the bias session (i.e. increasing the probability of one intention to the detriment of others) did not significantly affect the inference of basic intentions with lower probabilities.

Preliminary discussion. As expected, basic intentions were better inferred as the actions were presented with a high amount of visual information. Performances were also influenced by the probability distribution of the intentions, with a significant increase in participants' hits and decrease in RTs for the likely (i.e. biased) intention. Finally, the bias significantly interacted with the amount of visual information: participants responded more often towards the likely intention when action scenes were presented with a low amount of visual information. When the amount of visual information was sufficient, prior expectations then exerted less influence on intention inference.

Experiment 2: non-social superordinate intention

Statistical analyses were similar to those conducted in the first experiment. Responses for the two unlikely superordinate intentions were pooled for subsequent analyses as there were no significant differences among both hits and RTs between these responses (for each session, two-tailed *t*-tests, $p>0.15$).

Overt blocks. As for experiment 1, participants performed the task well when the amount of visual information was very high (1880 ms), in both the baseline (mean correct responses percentage: 98.6%, S.D. = 2.3) and the bias sessions (percentage of mean correct responses: 98.1%, S.D. = 3.1). Furthermore, in the baseline session participants were equally rapid at inferring the last action of the sequence, whatever the superordinate intention being accomplished (two-tailed *t*-tests, all $p>.35$).

In the bias session, however, although there were no significant differences among hits between likely and unlikely intentions, RTs for the likely intention were found to significantly decrease (two-tailed t-tests, likely *vs.* unlikely intentions, all $p<.001$). This decrease increased over time as revealed by a cumulative effect of the bias across blocks. Indeed, RTs decreased up to block 7 (minimal RT = 424 ms) and then remained constant until the end of the session (blocks 1–3 *vs.* blocks 4–6: $t = 4.04$, $p<.001$; blocks 4–6 *vs.* blocks 7–9: $t = 0.83$, $p>.05$) (see figure 3, 'Superordinate exp.').

Covert blocks. In both the baseline and the bias sessions, the amount of visual information significantly affected participants' hits and latencies with decreased RTs (baseline: $F(2,116) = 423,68$, $p<.001$, $\acute{\eta} = 0.87$; bias session: ($F(2,116) = 523.9$, $p<.001$; $\acute{\eta} = 0.9$) and a greater number of hits as the amount of visual information increased (baseline: $F(2,116) = 249.18$, $p<.001$, $\acute{\eta} = 0.81$; bias

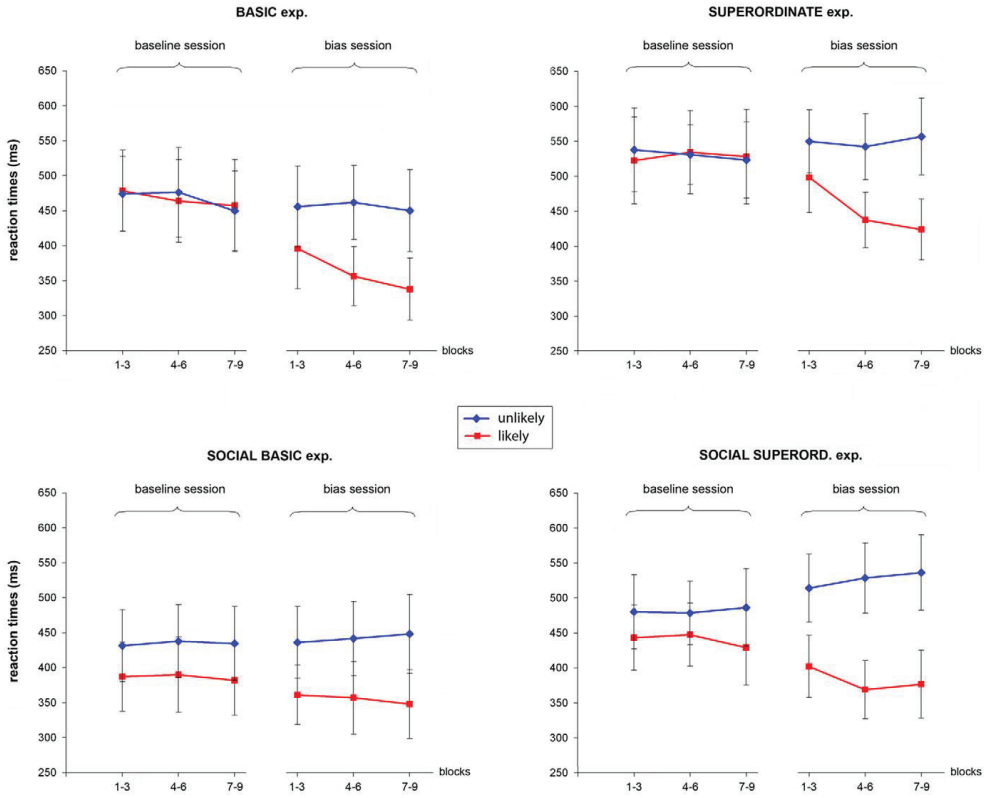

Figure 3. OVERT blocks: mean reaction times of the likely and the unlikely intentions across time. Baseline and bias sessions: (1-3): the first three overt blocks of the session; (4-6) the intermediate three blocks; and (7-9) the three last blocks of the session.
doi:10.1371/journal.pone.0017133.g003

session: ($F(2,116) = 199.03$, $p<.001$; $\acute{\eta} = 0.77$) (see table 2 and figure 5).

In the bias session, a significant effect of the bias was also observed with faster RTs and increased hits for actions congruent with the likely superordinate intention (RTs: $F(1,58) = 47.04$, $p<.001$, $\acute{\eta} = 0.44$; and hits: $F(1,58) = 62.09$, $p<.001$, $\acute{\eta} = 0.51$). Finally, the bias was found to significantly interact with the amount of visual information in such a way that the number of hits was significantly higher and RTs faster for the likely intention as the amount of visual information decreased (RTs: $F(2,116) = 15.3$,

Table 1. NON-SOCIAL BASIC intention experiment (COVERT blocks).

Experiment		Hits (%)			RTs (ms)		
Session	**Intention**	**LOW**	**MODERATE**	**HIGH**	**LOW**	**MODERATE**	**HIGH**
BASIC							
Baseline	Unlikely	42.5±11.6	63.3±14.7	94.7±7	1153±303	894±205	579±193
	Likely	44.4±20.6	66±11.9	93.8±10.2	1092±288	866±247	601±143
Bias	Unlikely	38.3±14.7	62.2±15.4	91.3±8	1190±380	975±294	628±206
	Likely	57.2±17.3	69.4±15.8	95.5±7.4	817±270	659±223	552±159

Mean reaction times (± SD) for likely and unlikely intentions for each amount of visual information (LOW, MODERATE, HIGH).
doi:10.1371/journal.pone.0017133.t001

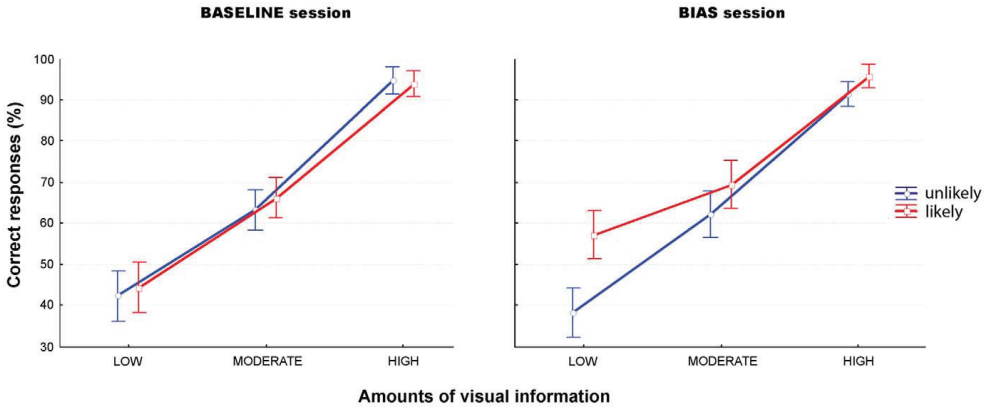

Figure 4. Non-social basic intention experiment (COVERT blocks). Mean percentage of correct responses (± SD) for likely (red) and unlikely (blue) intentions for each amount of visual information (low, moderate, high).
doi:10.1371/journal.pone.0017133.g004

$p<.001$, $\acute{\eta}=0.2$; and hits: $F(2,116)=9.28$, $p<.001$; $\acute{\eta}=0.13$). Post-hoc tests further indicated that participants were more accurate and faster in recognizing the likely intention in both low and moderate amount of visual information conditions (LSD Fisher: low, $p<.001$; moderate, $p=.005$, high, $p<.05$ for RTs; and low, $p<.001$; moderate, $p<.001$; high = *ns.* for hits) (see table 2 and figure 5, 'Bias session').

Effect of the bias on the unlikely intention. The number of correct responses for unlikely intentions significantly decreased in the bias session, compared to the baseline session, for both low and moderate amounts of visual information (two-tailed t-tests: all $t(30)>2.33$, all $p<0.02$). Likewise, RTs significantly decreased in the moderate amount of visual information condition (two-tailed t-tests: $t(30)=-2.09$, $p=0.04$).

Preliminary discussion. Two results make the present experiment diverge from the previous one. First, the bias effect was greater in the second experiment, as it was observed in condition of low amount of visual information as well as in condition of moderate amount of information. Second, a 'switch effect' was also observed in both these conditions, with an increasing number of correct responses and decreasing latencies for the likely intention, accompanied by decreased hits and increased RTs for the unlikely intentions. This effect reflects the cost associated with the selection of an unlikely superordinate intention. Indeed, the increasing difficulty in disengaging from prior expectations to select a less privileged representation (i.e. unlikely intentions) reveals the greater extent to which participants rely on the bias for making their response.

Experiment 3: social basic intention

Statistical analyses were similar to those conducted in the previous experiments. Two-tailed t-tests revealed no significant differences among both participants' RTs and hits between the TFT intentions (coop/coop *vs.* def/def: two-tailed *t*-tests, all $p>.2$) and between the alternative ones (coop/def *vs.* def/coop, two-tailed *t*-tests, all $p>.15$). Performances for def/def were therefore pooled with those of coop/coop (i.e. TFT or likely intentions) and performances for def/coop were pooled with those of coop/def (i.e. alternative or unlikely intentions) for the subsequent analyses.

Overt blocks. Participants performed the task well in both the baseline and the bias sessions (percentage mean correct responses: 98%, and S.D. = 2.5 and S.D. = 2.8). In the baseline session, RT analyses revealed a significant effect of the type of reputation, with participants being faster at inferring an action that was embedded within a tit-for-tat strategy than within an

Table 2. Non-social superordinate intention experiment (COVERT blocks).

Experiment		Hits (%)			RTs (ms)		
Session	**Intention**	**LOW**	**MODERATE**	**HIGH**	**LOW**	**MODERATE**	**HIGH**
SUPERORDINATE							
Baseline	Unlikely	50±15	68.7±12.1	97±6.3	1605±314	1241±218	745±153
	Likely	48.3±15.9	70±15.2	96.6±8.6	1676±304	1211±244	783±128
Bias	Unlikely	40.8±15.7	61.6±12.2	93.3±11.7	1689±307	1357±262	809±161
	Likely	65±14	77.5±12	98.7±5	1221±209	1014±183	600±138

Mean reaction times (± SD) for likely and unlikely intentions for each amount of visual information (low, moderate, high).
doi:10.1371/journal.pone.0017133.t002

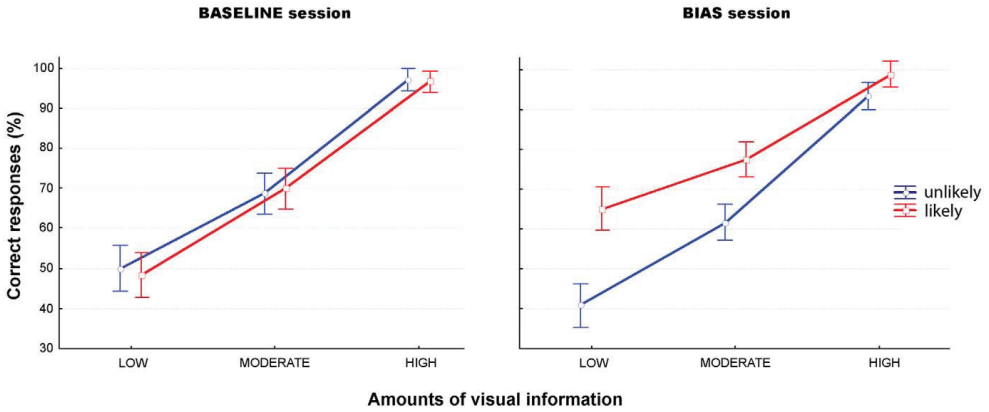

Figure 5. Non-social superordinate intention experiment (COVERT blocks). Mean percentage of correct responses (± SD) for likely (red) and unlikely (blue) intentions for each amount of visual information (low, moderate, high).
doi:10.1371/journal.pone.0017133.g005

alternative strategy (e.g. always defect or always cooperate) (two-tailed *t*-tests, all $p<.05$). Crucially, this result confirmed the existence of an inherent preference towards TFT reputation. This effect was maintained after the bias assignment as revealed by faster RTs for the likely intention (i.e. the TFT intention) in the bias session (two-tailed t-tests, likely *vs.* unlikely intentions, all $p<.001$). However, RTs for likely intentions did not significantly decrease with time (blocks 1–3 *vs.* blocks 4–6: $t=0.35$, $p>.05$; blocks 4–6 *vs.* blocks 7–9: $t=-0.68$, $p>.05$) (see figure 3, 'Social Basic exp.').

Covert blocks. *Baseline session.* ANOVAs performed on both hits and RTs showed a significant main effect of the amount of visual information with decreased RTs ($F(2,116)=80.44$, $p<.001$; $\acute{\eta}=.58$) and a greater number of hits ($F(2,116)=209.02$, $p<.001$, $\acute{\eta}=.78$) as the amount of visual information increased. In addition, the main effect of the type of reputation – previously observed in the overt blocks – was also significant in the covert blocks among RTs only ($F(1, 58)=4.7$, $p<.05$, $\acute{\eta}=.07$). The second player's action was more rapidly inferred when it was embedded within a TFT intention than within an "always defecting" or an "always cooperating" intention. The type of reputation did not, however, interact with the amount of visual information (see table 3 and figure 6, 'Baseline session").

Bias session. There were significant main effects of the amount of visual information and of the bias on both the RTs (main effect of amount of visual information: $F(2,116)=114.49$, $p<.001$, $\acute{\eta}=.66$; main effect of the bias, $F(1,58)=25.29$, $p<.001$, $\acute{\eta}=.3$) and the hits (main effect of amount of visual information: $F(2,116)=170.34$, $p<.001$, $\acute{\eta}=.74$; main effect of the bias, $F(1,58)=34.75$, $p<.001$, $\acute{\eta}=.37$), as well as a significant effect of the interaction between these two factors (RTs: $F(2,116)=9.23$, $p<.001$, $\acute{\eta}=.13$; hits: $F(2,116)=8.28$, $p<.001$, $\acute{\eta}=.12$). Participants' performance (slower RTs and higher hits) for actions congruent with a biased (i.e. likely) social intention improved as the amount of visual information decreased. Furthermore, the bias significantly affected participants' hits for all amounts of information (LSD Fisher: low, $p<.001$; moderate, $p=.005$; high, $p=$ *ns* for RTs; low, $p<.001$; moderate, $p=.05$; high, $p=.05$ for hits) (see table 3 and figure 6, 'Bias session').

Effect of the bias on the unlikely intention. When comparing performance for unlikely intentions between the baseline and the bias sessions, we found significant differences between these sessions for a high amount of visual information only, with participants' RTs for unlikely intentions significantly decreasing in this condition (two-tailed t-tests: $t(30)=2.26$, $p=0.03$).

Table 3. Social basic intention experiment (COVERT blocks).

Experiment		Hits (%)			RTs (ms)		
Session	**Intention**	**LOW**	**MODERATE**	**HIGH**	**LOW**	**MODERATE**	**HIGH**
SOCIAL BASIC							
Baseline	Unlikely	45.8±13.4	66.6±11.7	90.8±9.3	1159±263	990±220	888±210
	Likely	52.2±12.5	68±12.3	92.2±7.5	1053±232	899±213	750±169
Bias	Unlikely	41.6±17.3	66.3±14.4	86.6±11.6	1217±297	1041±282	788±229
	Likely	64.9±13.7	75.2±10.6	95.5±6.4	846±220	748±216	607±158

Mean reaction times (± SD) for likely and unlikely intentions for each amount of visual information (low, moderate, high).
doi:10.1371/journal.pone.0017133.t003

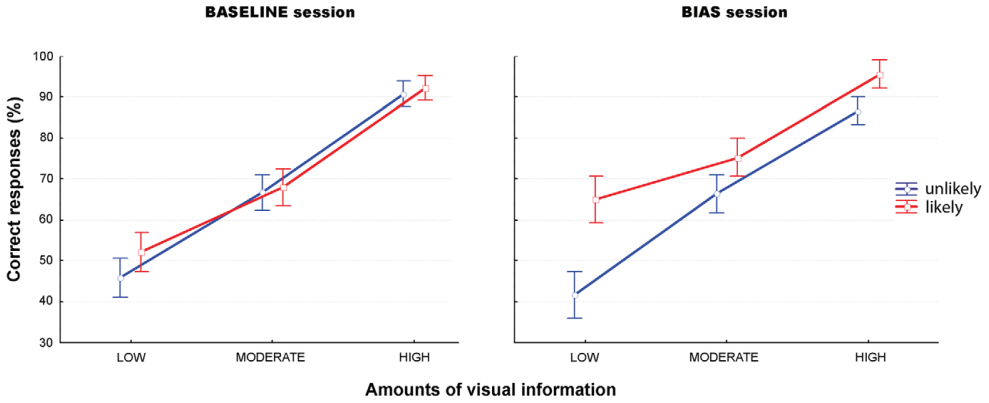

Figure 6. Social basic intention experiment (COVERT blocks). Mean percentage of correct responses (± SD) for likely (red) and unlikely (blue) intentions for each amount of visual information (low, moderate, high).
doi:10.1371/journal.pone.0017133.g006

Preliminary discussion. Two results make the present experiment diverge from the two previous ones. First, in the baseline session, where no bias was assigned, participants were faster at predicting an action associated with a tit-for-tat (TFT) intention. Interestingly, this early preference for TFT strategies differed from several aspects of the probabilistic bias that was imposed on participants in the second session. Not only did this preference not interact with the amount of visual information but its effect on performance remained constant over time. Second, the effect of the probabilistic bias was significant for any amount of visual information showing that prior expectations contributed to the inference even in conditions in which the visual information was highly reliable. By increasing the probability that the second player does whatever the opponent did in the previous round, we forced participants to perceive the second player as a 'tit-for-tat' player, rather than an altruist (always cooperate), an egoistic (always defect), or a 'random' player, hence generating progressively reinforced expectations that might prevail on relevant perceptual cues – as it is the case in conditions of high amount of visual information.

Experiment 4: social superordinate intention

Statistical analyses were similar to those conducted in the first three experiments. Two-tailed t-tests revealed no significant differences among both participants' RTs and hits between the two likely combinations (coop/coop *vs.* def/def: two-tailed *t*-tests, all $p>.2$) and between the two unlikely combinations (coop/def *vs.* def/coop, two-tailed *t*-tests, all $p>.15$). Performances for def/def were therefore pooled with those of coop/coop (TFT or likely intentions) and performances for def/coop were pooled with those of coop/def (unlikely intentions).

Overt blocks. Participants performed the task well in both the baseline (percentage mean correct responses: 97.5%, S.D. = 2.8) and the bias sessions (percentage mean correct responses: 98.4%, S.D. = 2.6). In the baseline session, RT analyses revealed a significant effect of the type of reputation (two-tailed *t*-tests, all $p<.05$), with participants being faster at inferring an action that was embedded within a tit-for-tat strategy than within an alternative strategy (i.e. always defect or always coop). RTs for the likely intention also significantly decreased in the bias session (two-tailed t-tests, likely *vs.* unlikely intentions, all $p<.001$) and this decrease was found to increase over time up to block 6 (minimal RT = 369 ms), (blocks 1–3 *vs.* blocks 4–6: $t=-2.11$, $p<.05$; blocks 4–6 *vs.* blocks 7–9: $t=-0.44$, $p>.05$) (see figure 3, 'Social superord. exp.").

Covert blocks. *Baseline session.* As the amount of visual information increased, decreased RTs ($F(2,116)=93.23$, $p<.001$, $\acute{\eta}=.61$) and increased hits ($F(2,116)=281.6$, $p<.001$, $\acute{\eta}=.82$) were observed for actions accomplishing the likely social intention. In addition, as in the overt blocks, actions were better and more rapidly inferred when they were embedded within a tit-for-tat strategy than within an alternative strategy (RTs: $F(1,58,)=4.16$, $p<.05$, $\acute{\eta}=.06$, and hits: $F(1,58)=7.96$, $p<.01$, $\acute{\eta}=.12$). The effect of reputation did not, however, interact with the amount of visual information showing that the type of strategy affected participants' performance independently of the amount of visual information (see table 4 and figure 7, 'Baseline session').

Bias session. There were significant main effects of the amount of visual information and of the bias on both the RTs (main effect of amount of visual information: $F(2,116)=163.11$, $p<.001$, $\acute{\eta}=.73$; main effect of the bias $F(1,58)=52.03$, $p<.001$, $\acute{\eta}=.47$) and the hits (main effect of amount of visual information: $F(2,116)=198.77$, $p<.001$, $\acute{\eta}=.77$; main effect of the bias $F(1,58)=92.16$, $p<.001$, $\acute{\eta}=.61$), as well as a significant effect of the interaction between these two factors (RTs: $F(2,116)=27.74$, $p<.001$, $\acute{\eta}=.32$, and hits: $F(2,116)=4.41$, $p=.01$, $\acute{\eta}=.07$). Participants' performance (slower RTs and higher percentage of hits) for likely social intentions improved to a large extent as the amount of visual information decreased, although the bias effect was observed for all amounts of visual information as revealed by the Post-hoc (LSD Fisher: low, $p<.001$; moderate, $p<.001$; high, $p=.01$ for RTs and low, $p<.001$; moderate, $p<.001$; high, $p<.001$ for hits) (see table 4 and figure 7, 'Bias session').

Effect of the bias on the unlikely intention. We found that reaction times for unlikely intentions significantly increased in the bias session, compared to the baseline session, for all amounts of visual information (two-tailed t-tests: all $t(30)<-2.07$, all $p<0.05$). The number of correct responses for unlikely intentions also significantly decreased in the bias session, for both low and high amounts of visual information (two-tailed t-tests: all $t(30)>2.33$, all

Table 4. SOCIAL SUPERORDINATE intention experiment (COVERT blocks).

Experiment		Hits (%)			RTs (ms)		
Session	**Intention**	**LOW**	**MODERATE**	**HIGH**	**LOW**	**MODERATE**	**HIGH**
SOCIAL SUPERORD.							
Baseline	Unlikely	44.1±14.5	62.4±11.5	86.1±9.1	1282±288	1049±237	877±198
	Likely	53±12.7	68.3±12.2	90.5±7.8	1102±277	957±217	816±175
Bias	Unlikely	36.1±15.2	56.3±14.6	80.2±11.8	1488±328	1197±271	961±230
	Likely	64.1±12.2	76.1±11.7	97.2±5.9	923±219	785±192	704±151

Mean reaction times (± SD) for likely and unlikely intentions for each amount of visual information (LOW, MODERATE, HIGH).
doi:10.1371/journal.pone.0017133.t004

$p<0.02$). This effect did not reach significance in the moderate amount of visual information condition (two-tailed t-test: $t(30) = 1.8$, $p = 0.07$).

Preliminary discussion. As for the social basic experiment, the bias effect was of major importance. First, in the baseline session, analyses of latencies and accuracy data revealed that, prior to the bias assignment, participants exhibited an early preference for social intentions congruent with a tit-for-tat reputation. Second, in the bias session, the bias significantly impacted on performances for all amounts of visual information revealing an increase in the difficulty with which the observer could disengage from his prior expectations, even in the case where these expectations interfered with the visual cues (e.g. in condition of high amount of visual information). Consistent with this interpretation is the observation that participants' hits for the unlikely intentions were found to significantly decrease in the bias session – as the selection of these unlikely intentions required inhibiting the activation of the likely intention representation.

'Bias effect': between-experiment comparisons

Contrasting the overall performance between experiments revealed no significant differences, showing that overall participants performed at comparable levels across the four experiments. Comparing the bias effect between experiments revealed significant effects of both the scope and the target of the intention. The bias effect was indeed significantly increased for the superordinate intention compared with the basic intention ($F(1,116) = 8.36$, $p<.005$, $\acute{\eta} = .81$) and for the social intention compared with the non-social intention ($F(1,116) = 5.06$, $p = .02$, $\acute{\eta} = .61$). Furthermore, these differences were observed for different amounts of information according to the dimension itself. Indeed, along the scope dimension, the bias had a significantly greater effect when inferring a superordinate intention than a basic one in the conditions with a moderate amount of visual information (post-hoc Fisher test, $p = .014$). Along the target dimension, on the other hand, the only significant difference was observed for a high amount of visual information with a greater bias effect for inferring social intentions than non-social ones (post-hoc Fisher test, $p = .0035$) (see figure 8).

Preliminary discussion. Comparing the bias effect across the four experiments, two main results emerged. First, consistent with the previous results, we found that the bias differentially affected performance according to the scope and the target of the intention. The bias effect was indeed significantly more important in superordinate conditions than in basic ones and in social conditions than in non-social ones. Second, this effect varied according to the amount of visual information available to the participants. It was significantly

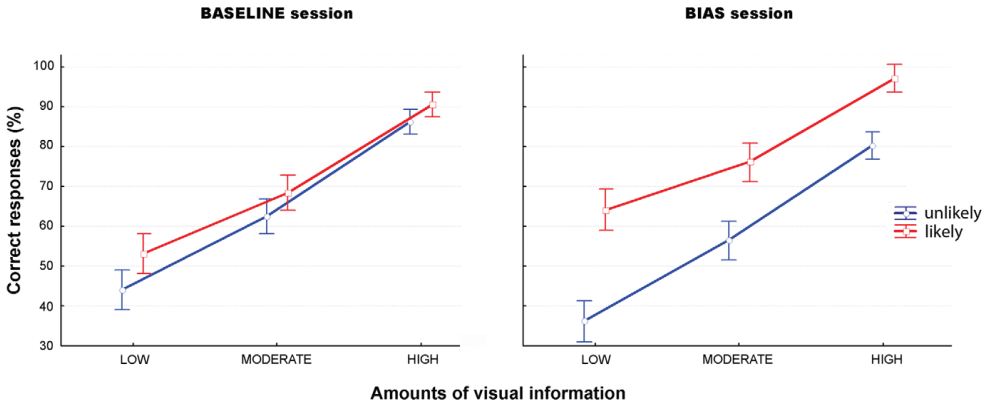

Figure 7. SOCIAL SUPERORDINATE intention experiment (COVERT blocks). Mean percentage of correct responses (± SD) for likely (red) and unlikely (blue) intentions for each amount of visual information (LOW, MODERATE, HIGH).
doi:10.1371/journal.pone.0017133.g007

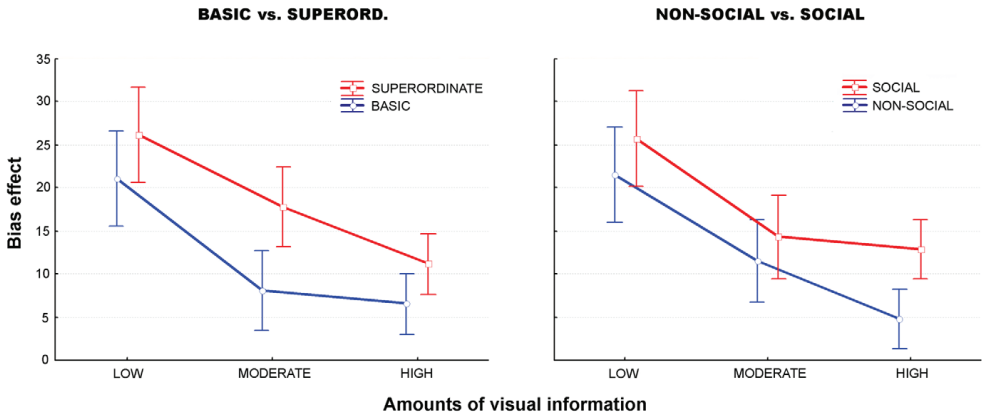

Figure 8. Mean score (± SD) of the bias effect expressed as a percentage of correct responses. Left panel: comparison between intentions with same target but different scopes (BASIC vs. SUPERORD.). **Right panel**: comparison between intentions with same scope but different targets (SOCIAL vs. NON-SOCIAL).
doi:10.1371/journal.pone.0017133.g008

more important for superordinate intentions than for basic intentions in condition of moderate amount of visual information and greater for social intentions compared to non-social intentions in condition of high amount of visual information.

Discussion

The present study aimed at investigating how two distinct sources of information – perceptual (bottom-up) evidence and *prior* (top-down) expectations – interact to enable one to make an intentional inference. To do so, we manipulated the participants' prior expectations about the probability of the underlying intention while varying the amount of visual information in the action scene. Our second purpose was to determine whether the contribution of these two sources of information would vary depending on the scope (basic vs. superordinate intention) and the target of the intention (social vs. non-social intention) that had to be inferred. To test this second hypothesis, we therefore manipulated the type of intention underlying the observed action using four distinct tasks (basic non-social, superordinate non-social, basic social, and superordinate social tasks).

Two main results emerged. First, we observed that the intentional judgment indeed rests on an interplay between the participants' prior expectations (their probability of being true varied across the blocks) and the reliability of the sensory information available from the action scene. When this reliability decreased, the bias effect (i.e. the contribution of prior expectations) on performance increased, with participants responding more towards intentions they estimated as being the most likely cause of the observed behaviour. Second, this interaction was found to vary according to the *type* of intention, defined here by its scope (basic vs. superordinate) or its target (social vs. non-social). Indeed, directly comparing performance between intentions of different scopes but identical targets, and between intentions with the same scope but distinct targets, revealed an increase in the bias effect for both superordinate and social intentions. While this effect was only observed when the amount of visual information was low in the basic task, it was found to be significant for both low and moderate amounts of information in the superordinate task, and for any amount of visual information in the social conditions.

Taken together, these results indicate that the degree to which the participants' prior knowledge contributes is sensitive to the type of intention that is focused on. As the intention being considered becomes more abstract (from basic to superordinate, and from non-social to social intentions), the inference problem becomes less constrained (i.e. the number of intentions congruent with visuomotor inputs increases): in this condition, participants' prior expectations exerted an increasing influence on their responses, to the detriment of the sensory information available from the action scene.

Interaction between perceptual and prior information

In the 4 experiments in the present study, the degree to which prior expectations contributed strongly depended on the reliability of the visual information conveyed by the video scenes. In low amount of visual information conditions, whatever the type of intention, participants tended to give priority to likely intentions at the expense of unlikely intentions; that is, they relied mostly on the intention they estimated to be the most likely cause of what was observed. This tendency towards favouring prior knowledge over perceptual information may further be accounted for by considering intentional inference as an *inverse problem* [1–3,14]. Inverse problems characterise situations in which the same sensory input can have different causes. This type of problem is commonly encountered in ambiguous perceptual tasks – such as those using bi-stable or degraded stimuli – the resolution of which requires appealing to prior knowledge or making further assumptions about the nature of the observed phenomenon [43]. The significant contribution of prior expectations in conditions of high visual ambiguity precisely suggests that when sensory information was not sufficient to unambiguously infer one intention, participants compensated by massively appealing to their prior knowledge (i.e. about the space of the agent's possible intentions). This strategy resulted in preferentially selecting actions achieving the intention with the highest probability to occur.

Overall, this result reinforces the idea that in situations of sparse or incomplete data a successful inference depends on an adaptive integration between bottom-up information (from the observation of behaviour) and top-down prior knowledge about goals or intentions [13]. This integration is consistent with a mechanism complementing the available perceptual information when it does not sufficiently constrain the number of potential solutions, namely, the many competing intentions congruent with what is observed. In line with this assumption, some authors have suggested that inferring another person's intention necessarily requires sensorimotor information to be complemented with information about mental states and attitudes [23]. It has been demonstrated that prior expectations are already used frequently by children, even at a very early age. This tendency combines with a tendency to interpret actions as being directed towards a goal ('teleological obsession', [3]). When the visual information is not sufficient for interpreting the action as a goal directed one [44], or when the action is incomplete [45], children posit states of the world occasionally counterfactual to the perceptual evidence (such as the presence of occluded physical objects). The results of the present study are consistent with the existence of such a mechanism of data completion/correction operating through the default use of prior expectations. Crucially, however, we further show that reliance on this mechanism also depends on the type of the intention to be inferred, according to its scope (basic vs. superordinate) or its target (non-social vs. social).

Basic vs. superordinate intentions

Both non-social basic and superordinate experiments required recognising one motor act, with the superordinate condition also requiring the final goal of the sequence (i.e. the shape being constructed) to be taken into account. Yet, across both experiments, prior expectations were found to differentially contribute to the participants' responses. In the basic non-social experiment, a bias response towards the likely intention was only observed in the condition where the amount of visual information was low. When participants were exposed to a moderate amount of visual information, these expectations no longer exerted an influence on performance, which then substantially depended upon the processing of the visual information alone. On the other hand, a heightened contribution of these expectations is observed in the superordinate experiments since they significantly influenced participants' performance in conditions of both low and moderate amounts of visual information.

The increase in response bias in the superordinate experiment cannot be explained by differences in complexity between both tasks since participants performed at comparable levels across basic and superordinate experiments showing that the differences between both experiments in terms of contribution of prior information are accounted for by the type of intention being considered. This result may be explained by differences in the relationship between these two types of intentions and action. While basic intention stands to action in a one-to-one relation (basic intentions like 'transport', 'rotate', or 'lift' an object are indeed directly accessible to the viewer from mere observation of the motor acts), superordinate intention stands to action in a many-to-one relation since the very same intention can be achieved by several distinct (commutative) sequences of actions. In the present study, this commutative property resulted in an ability of participants to infer the underlying intention solely on the basis of visual information arising from the first two actions. However, the present results also suggest that, despite the unpredictability of the sequence, participants still initiated a response, before observing the last action, by appealing massively to their prior expectations. Participants' dependence on priors in this condition could precisely account for the fact that *simulating* the motor acts composing the sequence (through motor mirroring, [46–47]) was of little help to infer the final superordinate intention. Those motor acts were indeed interchangeable within the sequence itself, and, as a consequence, they did predict neither the subsequent action nor the intention eventually achieved.

This early use of prior expectations might be accounted for by the existence of a system that pre-processes the current action chain depending on the sequences previously encountered. Observing the beginning of an action, or a sequence of actions, would automatically activate a representation of the likely intention that would be progressively suppressed or reinforced as the amount of visual information increases. Such a pre-processing would be particularly salient in superordinate conditions, where the beginning of the act chain proved to be of little importance for inferring the final intention it achieved. As such, it would explain why selecting an unlikely intention in bias sessions induced a significant cost on participants' performance. In these sessions, selecting an unlikely intention would indeed imply disengaging from the early activation of a likely intention. Finally, such pre-processing may account for why prior expectations are favoured over visual information in conditions of moderate perceptual uncertainty, as it would account for the role that priors continue to play when the amount of perceptual information increases. In superordinate conditions, the current sequence of actions would pre-activate the representation of the likely intention (i.e. the intention with the highest probability) to such an extent that a greater amount of visual information would be required to counteract it.

Non-social vs. social intentions

Social experiments were characterized by participants' responses over-relying on prior expectations as revealed by responses massively shifting towards likely intentions (i.e. 'tit-for-tat" intention: cooperation if previous cooperation, defection if previous defection) whatever the amount of visual information available from the action scene. This increased reliance on prior knowledge cannot be accounted for by differences in terms of complexity between non-social and social experiments, namely a greater memory load due to the requirement of tracking two successive intentions – the first and the second player's ones. Indeed, participants performed equally well, in terms of correct responses and reaction times, in both the social and non-social experiments. Additionally, the effect of facilitation associated with TFT strategy in the basic social experiment cannot be explained by a visual priming effect of the first player's action on the second player's one, which could have occurred when the latter performed the same action as the former. Indeed, TFT strategy was also found to be favoured in the superordinate social experiment; yet in this study TFT strategy did not necessarily imply that the action of the first player should be reproduced by the second player.

The dependence of the participants on their prior knowledge appears to reflect some expectations driven by the social context of the task. It is well-known that even basic movements, like the relative movements of geometrical figures, automatically induce participants to perceive the figures as socially interacting [48–50], and elicit strong expectations about the intentional causes of their movements (e.g. striking, kissing, etc.). Situations identified as involving social interactions are generally prone to trigger specific expectations concerning the way agents are likely to behave in such situations [12]. These expectations may be derived from perceiving the other as an interaction partner rather than a

competitor in a joint-action task [51], and from knowledge of diverse origins, such as that provided by group stereotypes [52], social-specific naive theories [53], or an individual's reputation acquired from experience of reciprocal social interactions [10]. In the present experiment, increased dependence on prior knowledge for inferring social intentions, regardless of their scope, seems precisely to fall within this type of expectation. Indeed, during the whole task, increasing the frequency of the second player adopting a TFT strategy amounted to progressively assigning a specific reputation to that player. A bias in the response towards a "tit-for-tat" mode of reciprocation reveals that participants did integrate this reputational knowledge and made their response accordingly.

The pervasive effect of these specific expectations is also well illustrated in the baseline condition by the early preference of participants for the TFT reciprocation. Even before being biased in this direction, participants tended to infer more rapidly that the second player was more inclined to mirror the first player's strategy. This early preference was probabilistically reinforced in the bias session and, as a consequence, exerted a greater influence on the participants' performance since it persisted even when the reliability of the visual information was high. Indeed, while in the basic non-social experiment the very same motor act presented alone was inferred from a much lower amount of visual information, in the social experiment a bias response towards the likely social intention was still observed for a higher amount of visual information. This shows that the influence of these expectations in the bias session was such that the participants had difficulty disengaging from their *a priori* expectations, resulting in predicting a play congruent with prior expectations but counterfactual to perceptual evidence. Similarly, these difficulties could account for the cost in performance associated with the selection of intentions that did not meet these expectations. In the bias session, participants were indeed significantly less accurate and were slower to select an unlikely intention (i.e. always defect, always cooperate) when this selection required concomitantly inhibiting the competing tit-for-tat intention.

Simulation vs. reasoning accounts of action understanding

The two main results of the present study (interaction between prior expectations and perceptual information and the modulation of this interaction as a function of the type of intention) may help reconcile the two major accounts of action understanding developed over the last decade. On the simulation account, we understand our conspecifics' intention by literally simulating their action via the activation of our own motor planning system. The result of this process of internal replication is the selection, in the observer's own repertoire, of the intention that would have caused the very same action. This type of explanation stresses the role of sensory information, derived from the kinematics of the movement, in action understanding [35]– irrespective of whether the action is complete (the goal achieved is fully visible) or only partially performed (the goal is hidden but can be predicted from the unfolding action) [see 46]. In contrast, the "theory theory" account postulates that action understanding is based on specialized inferential processes and mostly emphasizes the contribution of the context-related prior knowledge. This knowledge can either be derived from our intuitive theories of human behaviour, or from the subject's past experiences and rules she has drawn from them [8,54,55].

A wealth of empirical data and theoretical works nowadays converges on the idea that these two major classes of mechanisms play a complementary role in intention inference [10,22,23,56]. The results of the present study comfort these observations. By suggesting that intentional judgment relies on a relative balance of bottom-up sensory and top-down prior information, they plead in favour of a *hybrid* model of action understanding. In such a model, the observer would mobilize either low-level simulation or high-order inferential mechanisms depending on whether the current sensory evidence is, or is not, reliable enough to elicit simulation from observation.

Recently, Kilner and colleagues proposed a theoretical framework that attempts to further account for how these two classes of mechanisms may interact to enable one's understanding of other people's intentions [1]. This framework relies on the hierarchical architecture of action representations ranging from the intention level to the kinematics level (see also [57]). In this architecture, the selection of one type of action representation would result from the resolution of the inverse problem at each level of the hierarchy. Basically, each level uses a model to generate a prediction of the representations in the level below. This prediction is then compared with the representation at the subordinate level and prediction errors arising from that comparison are returned to the higher level to adjust its representation. This adjustment is generalised to the different levels of the hierarchy (intention, motor command and kinematics). The most likely cause of the observed action is then inferred by minimising the prediction error at all the levels of this hierarchy [1,2]. Given visual kinematics, goal expectations are first generated, from these goal representations motor commands are then predicted and given these motor commands, kinematics are in turn predicted. In this framework, top-down influences are therefore dynamically generated since the estimates produced at the higher levels become prior expectations for the lower levels.

Our results can be consistently interpreted in the light of the Kilner's hierarchical model. A basic intention can be directly predicted from the observation of the current motor act, provided the related visual information is sufficient to enable comparison with expected kinematics at higher levels. In this case, participants' performance is strongly dependent on minimising the prediction error that arises from this comparison. However, this comparison also closely depends on the reliability of the current movement kinematics; when the amount of visual information is too low, this comparison cannot be made, and, as a result, subordinate levels cannot adjust their representation to higher estimates of the hierarchy. We observed that, when this comparison could not be carried out, participants consistently appealed to their prior knowledge. In a hierarchical model of action representations, such an over-reliance on priors could be made possible by the existence of a short circuitry of recursive loops between subordinate and higher levels of the cortical hierarchy. These recursive loops would be mobilized when data is sparse to shortcut the automatic comparison process between observed and expected kinematics movement. Importantly, the engagement of this mechanism proved to be dependent on the amount of visual information available from the action scene, but independent from the scope and target of the intention, since it was observed to operate at the lowest levels of visual information in each of the four experimental conditions.

Noteworthily, the engagement of these recursive loops is also sensitive to variations in the relationship between the observed action and its goal. Superordinate conditions indeed involved a greater recourse to participants' prior expectations even when the visual information significantly increased to a moderate (non-social) or even a high level (social). This greater dependence on prior expectations can be explained by the fact that, in superordinate conditions, many competing intentions are congruent with the visual information conveyed by the current motor act.

Thus, whereas minimising the prediction error between expected and current kinematics may be sufficient to predict the agent's single act (e.g. to rotate), it may not be to infer unambiguously which of the multiple superordinate intentions (e.g. final shapes) it contributes to accomplish. As a consequence, we found the weight of the decision to be mostly carried by participants' prior expectations, suggesting, in this situation of accrued perceptual uncertainty, an early shortcut of the comparison process between levels of the action representation hierarchy. Crucially, this shortcut was independent of the amount of information, since it occurred even when the visual information was high enough for the participant to be normally confident about what she is seeing. This observation suggests that recursive loops of this kind could be mostly recruited in contexts where relying on one's prior expectations is a better guarantee for accurate inference, even if such expectations can occasionally go against perceptual evidence.

Conclusion

Our results shed light on how sensory information, derived from the kinematics of the observed action, interacts with prior expectations to enable one's understanding of other people's intentions. We first showed that the contribution of participants' prior knowledge was sensitive to the availability of the sensory information from the action scene. A greater contribution of this knowledge was observed in conditions of sparse visual information, suggesting the engagement of a mechanism of data completion operating through the default use of prior expectations.

Second, we found that the priors' contribution also depended on the type of intention that was inferred. An increased reliance on priors was indeed observed in conditions where the agent's intention could not be predicted by the sole visible, current motor act, but further required estimating the superordinate goal this act contributed to achieve. In this case, participants' expectations – being progressively acquired from observation – were found to most frequently supersede the visual information conveyed by the current motor kinematics. Thus, the more participants responded towards the biased (e.g. expected) intentions, the more the visual information tended to play a confirmatory, rather than a predictive role. Such a shift in the contribution of visual evidence is likely to account for why participants, in this condition, mostly over-relied on their priors to make their decision, even though it ran counter to the perceptual evidence.

Crucially, an over-reliance on priors was also massively observed in social conditions. We suggested that the early influence of social-specific expectations (e.g. expectations on how agents are the most likely to behave in a context of reciprocal interaction) may account for this important shift in the response toward participants' priors. Contexts of social interaction are indeed prone to elicit modular, high-level expectations, which may contribute to giving priority to some intentional causes (e.g. cooperation if previous cooperation, defection if previous defection) at the expense of other competing causes. These *a priori* expectations, being acquired from experience (probabilistic bias) or derived from domain-specific knowledge (TFT reciprocation), were found to favour some action representations so that less sensory evidence was needed for the participants to be confident about their decision, *i.e.* about which kind of intention was most likely the cause of the observed action.

Supporting Information

Text S1 Pre-tests: intra- and inter-sequence comparisons; selection of LOW, MODERATE and HIGH amounts of information.
(DOC)

Figure S1 Distribution of participant's reaction times (blue dots) across the 12 movie segments. Reaction times for the different actions were pooled across subjects. Red squares: mean reaction times across participants for each of the 12 duration ranges.
(TIF)

Figure S2 BASIC experiment: psychometric curve fit to the cumulative distribution of participant's correct responses (red dots). Responses for the different actions were pooled across. The blue dot refers to the inflexion point of the sigmoid curve. In each experiment, the inflexion point occurs at the following duration: **A**. BASIC: 1576 ms. **B**. SUPERORD.: 1558 ms. **C**. SOCIAL BASIC: 1546 ms. **D**. SOCIAL SUPERORD. 1550 ms.
(TIF)

Acknowledgments

We are grateful to Mathilde Vernet, Juliette Sablier, and Mariia Kaliuzhna for their help in preparing the stimuli. We also wish to thank Karen Reilly, Coralie Chevallier, Hugo Mercier, Nicolas Baumard, and Guillaume Barbalat for their helpful comments and suggestions on an earlier draft of this article.

Author Contributions

Conceived and designed the experiments: VC PD EP EK CF. Performed the experiments: VC. Analyzed the data: VC PB CF. Wrote the manuscript: VC PD EP CF.

References

1. Kilner JM, Friston KJ, Frith CD (2007a) Predictive coding: an account of the mirror neuron system. Cogn Process 8: 159–66.
2. Kilner JM, Friston KJ, Frith CD (2007b) The mirror-neuron system: a Bayesian perspective. Neuroreport 18: 619–23.
3. Csibra G, Gergely G (2007) 'Obsessed with goals': functions and mechanisms of teleological interpretation of actions in humans. Acta Psychol 124: 60–78.
4. Sebanz N, Shiffrar M (2009) Detecting deception in a bluffing body: the role of expertise. Psycho Bull Rev 16: 70–5.
5. Aglioti SM, Cesari P, Romani M, Urgesi C (2008) Action anticipation and motor resonance in elite basketball players. Nature Neuroscience 11: 1109–16.
6. Gold JI, Shadlen MN (2002) Banburismus and the brain: decoding the relationship between sensory stimuli, decisions, and reward. Neuron 36: 299–308.
7. Carey S (1985) Conceptual Change in Childhood. Cambridge, MA: MIT Press.
8. Gopnik A, Wellman H (1994) The theory theory. In: Hirschfeld L, Gelman S, eds. Mapping the Mind: Domain Specificity in Cognition and Culture. Cambridge: Cambridge University Press.
9. Singer T, Seymour B, O'Doherty JP, Stephan KE, Dolan RJ, Frith CD (2006) Empathic neural responses are modulated by the perceived fairness of others. Nature 439: 466–9.
10. King-Casas B, Tomlin D, Anen C, Camerer CF, Quartz SR, et al. (2005) Getting to know you: reputation and trust in a two-person economic exchange. Science 308: 78–83.
11. Sebanz N, Bekkering H, Knoblich G (2006) Joint action: bodies and minds moving together. Trends Cogn Sci 10: 70–6.
12. Frith CD, Frith U (2006) How we predict what other people are going to do. Brain Research 1079: 36–46.
13. Baker CL, Tenenbaum JB, Saxe RR (2006) Bayesian models of human action Understanding. In: Weiss Y, Scholkopf B, Platt J, eds. Advances in Neural Information Processing Systems: MIT Press. pp 99–106.
14. Baker CL, Tenenbaum JB, Saxe RR (2007) Goal inference as inverse planning. Proceedings of the Twenty-Ninth Annual Conference of the Cognitive Science Society. pp 779–784.
15. Griffiths TL, Kemp C, Tenenbaum JB (2008) Bayesian models of cognition. In: Sun R, ed. The Cambridge handbook of computational cognitive modelling. Cambridge: Cambridge University Press.

16. Gallese V, Keysers C, Rizzolatti G (2004) A unifying view of the basis of social cognition. Trends Cogn Sci 8: 396–403.
17. Jacob P, Jeannerod M (2005) The motor theory of social cognition: a critique. Trends Cogn Sci 9: 21–25.
18. Saxe R (2005) Against simulation: the argument from error. Trends Cogn Sci 9: 174–9.
19. Goldman AI, Sebanz N (2005) Simulation, mirroring, and a different argument from error. Trends Cogn Sci 9: 320.
20. Mitchell JP (2005) The false dichotomy between simulation and theory-theory: the argument's error. Trends Cogn Sci 9: 363–364.
21. Nichols S, Stich S (2003) Mindreading: an integrated account of pretence, self-awareness, and understanding other minds. Oxford University Press.
22. Keysers C, Gazzola V (2007) Integrating simulation and theory of mind: from self to social cognition. Trends Cogn Sci 11: 194–6.
23. de Lange FP, Spronk M, Willems RM, Toni I, Bekkering H (2008) Complementary systems for understanding action intentions. Current Biology 25: 454–7.
24. Searle J (1983) Intentionality: An Essay in the Philosophy of Mind. Cambridge University Press.
25. Bratman ME (1987) Intention, Plans, and Practical Reason. Cambridge, MA: Harvard University Press.
26. Mele A (1992) Springs of Action: Understanding Intentional Behavior. Oxford University Press.
27. Pacherie E (2000) The content of intentions. Mind and Language 15: 400–432.
28. Pacherie E (2008) The phenomenology of action: a conceptual framework. Cognition 107: 179–217.
29. Jeannerod M, Pacherie E (2004) Agency, simulation, and self-identification. Mind and Language 19: 113–146.
30. Searle J (1995) The Construction of Social Reality. New York: The Free Press.
31. Blakemore SJ, Frith U (2004) How does the brain deal with the social world? Neuroreport 19: 119–28.
32. Frith CD, Frith U (2007) Social cognition in humans. Current Biology 17: 724–32.
33. Ciaramidaro A, Adenzato M, Enrici I, Erk S, Pia L, et al. (2007) The intentional network: how the brain reads varieties of intentions. Neuropsychologia 45: 3105–13.
34. Körding KP, Wolpert DM (2006) Bayesian decision theory in sensorimotor control. Trends Cogn Sci 10: 319–26.
35. Rizzolatti G, Craighero L (2004) The mirror-neuron system. Annu Rev Neurosci 27: 169–92.
36. Jacob P (2009) The tuning-fork model of human social cognition: a critique. Consciousness and Cognition 18: 229–43.
37. Fu G, Lee K (2007) Social grooming in the kindergarten: the emergence of flattery behavior. Developmental Science 10: 255–265.
38. Oldfield RC (1971) The assessment and analysis of handedness: the Edinburgh inventory. Neuropsychologia 9: 97–113.
39. Georgiou I, Becchio C, Glover S, Castiello U (2007) Different action patterns for cooperative and competitive behaviour. Cognition 102: 415–433.
40. Rapoport A (1967) Optimal policies for the Prisoner's Dilemma. Psychol Rev 74: 136–48.
41. André JB, Day T (2007) Perfect reciprocity is the only evolutionarily stable strategy in the continuous iterated prisoner's dilemma. J Theor Biol 247: 11–22.
42. Axelrod R (1997) The Complexity of Cooperation: Agent-Based Models of Competition and Collaboration. PrincetonNew Jersey: Princeton University Press.
43. Mamassian P, Goutcher R (2001) Prior knowledge on the illumination position. Cognition 81: B1–9.
44. Csibra G, Gergely G, Biró S, Koós O, Brockbank M (1999) Goal attribution without agency cues: the perception of 'pure reason' in infancy. Cognition 26: 237–67.
45. Onishi KH, Baillargeon R, Leslie AM (2007) 15-month-old infants detect violations in pretend scenarios. Acta Psychol 124: 106–28.
46. Umiltà MA, Kohler E, Gallese V, Fogassi L, Fagiga L, et al. (2001) I know what you are doing. A neurophsyiological study. Neuron 31: 155–65.
47. Gallese V (2007) Before and below 'theory of mind': embodied simulation and the neural correlates of social cognition. Philosophical Transactions of the Royal Society 362: 659–669.
48. Heider F, Simmel M (1944) An experimental study of apparent behaviour. American Journal of Psychology 57: 243–259.
49. Castelli F, Happé F, Frith U, Frith CD (2000) Movement and mind: a functional imaging study of perception and interpretation of complex intentional movement patterns. Neuroimage 12: 314–325.
50. Scholl BJ, Tremoulet PD (2000) Perceptual causality and animacy. Trends Cogn Sci 4: 299–309.
51. Kourtis D, Sebanz N, Knoblich G (2010) Favouritism in the motor system: social interaction modulates action simulation. Biol Lett 6: 758–61.
52. Fiske ST, Cuddy AJ, Glick P, Xu J (2002) A model of (often mixed) stereotype content: competence and warmth respectively follow from perceived status and competition. J Pers Soc Psychol 82: 878–902.
53. Ybarra O (2002) Naive causal understanding of valenced behaviors and its implications for social information processing. Pychol Bull 128: 421–41.
54. Leslie AM (1987) Pretense and representation: the origins of "theory of mind". Psychological Review 94: 412–42.
55. Gopnik A, Wellman H (1992) Why the child's theory of mind really is a theory. Mind and Language 7: 145–71.
56. Brass M, Schmitt RM, Spengler S, Gergely G (2007) Investigating action understanding: inferential processes vs. action simulation. Current Biology 17: 2117–2121.
57. Grafton ST, Hamilton AF (2007) Evidence for a distributed hierarchy of action representation in the brain. Hum Mov Sci 26: 590–616.
58. Nachmias J (1981) On the psychometric function for contrast detection. Vision Research 21: 215–223.
59. Wichmann FA, Hill NJ (2001) The psychometric function: I. Fitting, sampling, and goodness of fit. Perception & Psychophysics 63: 1293–1313.

Article 4 : Impaired hierarchical control within the lateral prefrontal cortex in schizophrenia

Guillaume Barbalat, Philippe Domenech*, Valérian Chambon*, Chystèle Ody, Etienne Koechlin, Nicolas Frack and Chlöé Farrer

Publié dans Biological Psychiatry (2011) ahead of print

ARCHIVAL REPORT

Impaired Hierarchical Control Within the Lateral Prefrontal Cortex in Schizophrenia

Guillaume Barbalat, Valerian Chambon, Philippe J.D. Domenech, Chrystèle Ody, Etienne Koechlin, Nicolas Franck, and Chlöé Farrer

Background: In schizophrenia, disturbances of cognitive control have been associated with impaired functional specialization within the lateral prefrontal cortex (LPFC), but little is known about the functional interactions between specialized LPFC subregions. Here, we addressed this question with a recent model that describes the LPFC functioning as a cascade of control processes along a rostrocaudal axis, whereby anterior frontal regions influence the processing in posterior frontal regions to guide action selection on the basis of the temporal structure of information.

Methods: We assessed effective connectivity within the rostrocaudal axis of the LPFC by means of functional magnetic resonance imaging in 15 schizophrenic patients and 14 matched healthy control subjects with structural equation modeling and psychophysiological interactions.

Results: In healthy subjects, activity in the left caudal LPFC regions was under the influence of left rostral LPFC regions when controlling information conveyed by past events. By contrast, schizophrenic patients failed to demonstrate significant effective connectivity from rostral to caudal LPFC regions in both hemispheres.

Conclusions: The hierarchical control along the rostrocaudal axis of the LPFC is impaired in schizophrenia. This provides the first evidence of a top-down functional disconnection within the LPFC in this disorder. This disruption of top-down connectivity from rostral to caudal LPFC regions observed in patients might affect their ability to select the appropriate sets of stimulus-response associations in the caudal LPFC on the basis of information conveyed by past events. This impaired hierarchical control within the LPFC could result from poorly encoded contextual information due to abnormal computations in the caudal LPFC.

Key Words: Effective connectivity, functional magnetic resonance imaging, hierarchical control, lateral prefrontal cortex, rostrocaudal axis, schizophrenia

In schizophrenia, disturbances of cognitive control, the ability to coordinate thoughts and actions in relation to internal goals, have been robustly associated with impaired functional specialization within the lateral prefrontal cortex (LPFC) (1–6). Recent models suggest that cognitive control is constructed as a set of hierarchical modules that involve selecting and maintaining goals at multiple levels of abstraction, from general task goals at higher levels (such as watching a movie in the cinema) to concrete motor responses at the lowest levels (such as taking transport to go to the cinema, buying a ticket at the box office, or sitting comfortably in front of the screen) (7). Such a behavioral hierarchy has been shown to be subserved by a hierarchical organization along the rostrocaudal axis of the LPFC, where more anterior regions are associated with progressively more abstract action control, whereas more posterior regions process more concrete information about action (i.e., action that is closer to the actual motor output) (8). Furthermore, there seems to be a dominance relationship whereby more anterior regions that process abstract, superordinate, domain-general rules, modulate domain-specific, subordinate, posterior regions (9).

From the Centre de Neuroscience Cognitive, (GB, VC, PD, NF), UMR 5229 CNRS, Université Claude Bernard Lyon1, Lyon, France; Centre Hospitalier le Vinatier (NF), Lyon; Institut National de la Sante Et de la Recherche Medicale (CO, EK), Université Pierre et Marie Curie and École Normale Supérieure, Paris; and Université de Toulouse (CF), CerCo, UPS and UMR5549 CNRS, Faculté de Médecine de Rangueil, Toulouse, France.

Authors VC and PJDD contributed equally to this work.

Address correspondence to Guillaume Barbalat, M.D., Ph.D. Centre deNeuroscience Cognitive Universite Claude Bernard Lyon, 67, bd Pinel, 69 675 BRON, Cedex, France; E-mail: gbarbalat@isc.cnrs.fr.

Received Dec 30, 2009; revised Jan 31, 2011; accepted Feb 1, 2011.

We previously investigated the overall organization of cognitive control within the LPFC in schizophrenia with an influential model (10) that describes the architecture of cognitive control as a cascade of executive modules ranging from premotor to more anterior LPFC regions (3,11). This model includes a sensory control level involved in selecting the motor responses that are the most appropriate to stimuli that occur and subserved by the lateral premotor regions (typically, Brodmann Area [BA] 6). A contextual control level is then involved in selecting premotor representations (i.e., stimulus-response associations) according to contextual signals that accompany the occurrence of stimuli. This control is subserved by the caudal part of the LPFC (typically, BAs 9/44/45). Finally, the episodic control level is involved in selecting caudal LPFC representations (task-sets or consistent sets of stimulus-response associations evoked in the same immediate, perceptual context) according to the temporal episode in which stimuli occur. This control is subserved by the rostral part of the LPFC (typically, BAs 46/10).

We demonstrated that, although the lower-order, less abstract, sensory level of cognitive control was spared in schizophrenia, contextual control was significantly impaired (11), which was related to hypoactivation in the caudal LPFC regions (3). With regard to episodic control, we found mixed but consistent findings. When no contextual signals were involved in the task, there was no behavioral disturbance of episodic control in schizophrenia (11). By contrast, adding contextual signals in the task reduced this level of cognitive control. In other words, this impaired episodic control process refers in fact to a dysfunctional interaction between the "episodic" and the "contextual" modules (3,11).

At the neural level, this disturbed episodic control process in schizophrenic patients was not reflected by any hypoactivation in the rostral LPFC. By contrast, we found a hyperactivation in this region, which we interpreted as a consequence of the added effort that patients might expend to retrieve the poorly integrated contextual information (2,3,12,13). However, the neural substrates underlying this dysfunctional control of episodic signals remain unknown.

0006-3223/$36.00
doi:10.1016/j.biopsych.2011.02.009

According to the functional disconnection hypothesis proposed by Friston (14), such a dysfunctional interaction between two cognitive processes should result from dysfunctional interaction in the dynamics of the brain regions subserving these processes rather than dysfunctional specialization within a specific region. The framing of the cascade model further predicts that this impairment in episodic control would depend on the way rostral LPFC exerts its influence on the caudal LPFC regions (9). However, until now, studies that have investigated the interaction between specialized neural systems related to executive dysfunctions in schizophrenia have demonstrated altered LPFC connectivity with other cortical structures such as the inferior parietal lobule (5), the hippocampus (15), or the anterior cingulate cortex (16) but have not directly studied the functional integration of the different cognitive control modules within the LPFC itself.

The goal of this follow-up study was to test whether the perturbed control of temporal episodic signals in patients reflects a dysfunction in the top-down selection of caudal LPFC representations by rostral LPFC. For this purpose, we based our analysis on data collected in our previously published study (3) and measured effective connectivity between LPFC regions involved in controlling episodic and contextual signals in both groups with structural equation modeling (SEM) and psychophysiological interactions (PPIs).

Methods and Materials

Subjects

This analysis initially involved 15 schizophrenic patients ($n = 15$) and 15 matched healthy control subjects, 1 of whom was excluded because of excessive motion in the scanner ($n = 14$) (3). For more details about the description of the participants, please refer to Supplement 1 (see also Table 1).

Experimental Paradigm

The experiment included eight scanning sessions, each consisting of eight separate blocks presented in a counterbalanced order. Each block comprised a series of 12 successive stimuli (colored letters; duration: 500 msec; onset asynchrony: 3500 msec) preceded by an instruction cue lasting 4200 msec (Figure 1). Each instruction informed the subjects to make speeded responses to stimuli by pressing left or right hand-held response buttons or to withhold a response to a no-go stimulus. Instructions were prelearned by the subjects before running the experiment to avoid possible biases due to learning effects during the test session.

In each scanning session, the eight blocks formed four distinct experimental conditions crossing the demands of contextual and episodic control varied by manipulating the context (I_{con}) and the episode (I_{epi}) factors, respectively. These variations were quantified according to the computational model from Koechlin *et al.* (10), on the basis of Shannon's information theory (17).

The color of the letter was the contextual signal within each block. According to the contextual signal, subjects had to perform one of three tasks: 1) ignore the letters; 2) a vowel/consonant discrimination task (T1: if the letter is a vowel, press the right response button; if the letter is a consonant, press left); or 3) a lower/uppercase discrimination task (T2: if the letter is uppercase, press right; if the letter is lowercase, press left). Where contextual control was low, the task remained the same across the entire block (T1 or T2, single-task-set blocks, $I_{con} = 0$ bit; block no. 1,2,5,6 in Figure 1). In high contextual control blocks, the task changed from trial to trial (T1 and T2, dual task-set blocks, $I_{con} = 1$ bit; blocks no. 3,4,7,8 in Figure 1).

The episodic signal was by definition the instruction cue preceding each block. Episodic signals conveyed information about the contingencies linking contextual signals (i.e., the color of the letter) and task-sets (i.e., T1 or T2) that occurred in the proceeding sequence of letters and were chosen to parametrically vary the amount of episodic information across blocks. Therefore, the episode factor was the covariate of interest that contrasted episodes according to the episodic information I_{epi} conveyed by instruction cues that were required for subsequently selecting appropriate task-sets with respect to contextual signals ($I_{epi} = 0$ to 1 and 2 bits). For example, in Block No. 1, the instruction cue indicated that, if the letter is white, no response should be given, whereas if the letter is green, the subjects should perform task T1 (Figure 1). Then, with information theory, we computed different values for the episodic control demand, such that the more frequent the crosstemporal

Table 1. Clinical and Demographic Characteristics

Characteristic	Patients ($n = 15$)	Comparison Subjects ($n = 14$)	p
Male Gender, *n* (%)	8 (53)	8 (57)	.68
Age, yrs	35 (10.5)	36 (10.6)	.79
Education, yrs	11 (1.3)	11 (1.9)	.82
Handedness	.86 (.09)	.84 (.11)	.50
Duration of Illness, yrs	10 (9)	—	—
SANS Score	43 (19)	—	—
SAPS Score	23 (21)	—	—
Reality Distortion Score[a]	8 (10)	—	—
Poverty Score[b]	34 (18)	—	—
Disorganization Score[c]	23 (13)	—	—
Chlorpromazine-Equivalent[d], mg/day	247 (190)	—	—

Values are mean ± SD, unless otherwise indicated.

SANS, Scale for the Assessment for Negative Symptoms (50). SAPS, Scale for the Assessment of Positive Symptoms (51).

[a]Sum of the scores for hallucinations and delusions from the SAPS.

[b]Sum of the scores for poverty of speech, flat affect, anhedonia/asociality, and amotivation from the SANS.

[c]Sum of the scores for formal thought disorder and bizarre behavior from the SAPS and the score for attention from the SANS.

[d]Depot doses of and daily-oral atypical antipsychotics at the time of the examination (risperidone in 6 patients, olanzapine in 3 patients, amilsupride in 3 patients, and aripiprazole in 2 patients) were converted to average daily chlorpromazine-equivalent doses. None of the patients received a concurrent typical antipsychotic, anticholinergic agent, sedative treatment, mood stabilizer, antidepressant, or other psychotropic agent.

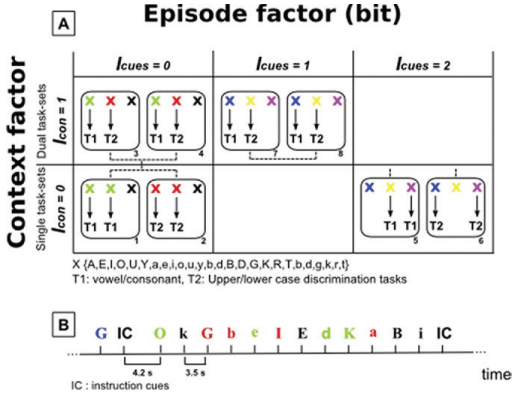

Figure 1. Experimental design. **(A)** Rounded boxes represent behavioral episodes (numbered from no. 1 to no. 8) with related stimuli (letters) and instructions. Episodes formed four distinct experimental conditions crossing the episodic factor with the context factor. According to the color of the letter (contextual signal), subjects either ignored the letter or performed a vowel/consonant (T1) or lower/uppercase (T2) discrimination task on the letters. Block no. 1: contextual signals were either green or white. White signals indicated that subjects should ignore the letter. Green signals indicated that subjects should perform task T1 (single task-set episode). Block no. 2: contextual signals were either red or white. White signals indicated that subjects should ignore the letter. Red signals indicated that subjects should perform task T2 (single task-set episode). Blocks no. 3 and no. 4: contextual signals were green, red, or white. Subjects responded to letters as described for blocks no. 1 and no. 2 (dual task-set episode). Blocks no. 5: contextual signals were yellow, blue, or purple. Blue signals instructed subjects to ignore the letters. Yellow and purple signals instructed subjects to perform task T1 (single task-set episode). Block no. 6: contextual signals were yellow, blue, or purple. Yellow signals instructed subjects to ignore the letters. Blue and purple signals instructed subjects to perform task T2 (single task-set episode). Blocks no. 7 and no. 8: contextual signals were yellow, blue, or purple. Purple signals instructed subjects to ignore the letters. Blue and yellow signals instructed subjects to perform tasks T1 and T2, respectively (dual task-set episode). Dashed lines connect episodes involving congruent associations between contextual signals and task-sets. **(B)** Typical episode.

contingencies between contextual signals and task-sets, the lower the amount of episodic information—thus the lower the demand of episodic control. More specifically, the episodic control demand depended on the proportion *f* of episodes involving congruent associations between contextual signals and task-sets over the whole experiment. When this proportion was maximal ($f = 1$, such as in blocks no. 1,2,3,4 where green always denoted "T1," red always denoted "T2," and white was always "no-go"), the demand of episodic control was low ($I_{epi} = 0$ bit). By contrast, the decrease of this frequency ($f < 1$, such as in blocks no. 5,6,7,8 where blue, purple, and yellow could all denote "T1," "T2," or "no-go") led to an increase in the episodic control demand ($I_{epi} > 0$ bit). Because the same crosstemporal contingencies were involved in blocks no.7 and no. 8, these two blocks had a lower episodic control demand ($I_{epi} = 1$ bit) than that in blocks no. 5 or no. 6, which contained different crosstemporal contingencies ($I_{epi} = 2$ bits).

In each block, the proportion of letters to be ignored was 33%. In dual task-set blocks, the ratio of trials associated with task-set T1 versus task-set T2 was equal to 1. Finally, in each block, the ratio of left versus right responses was equal to 1, and the ratio of congruent versus incongruent letters (same vs. different responses for T1 and T2) was equal to 1. Accordingly, sensorimotor control was constant across the experiment.

The methods for the behavioral analyses, magnetic resonance imaging (MRI) procedures and preprocessing, delimitation of the regions of interest, and regions of interest analyses are reported in Supplement 1.

Effective Connectivity Analyses

We investigated, on the basis of anatomical and functional connections in the frontal lobes described previously (10,18), the existence of a top-down control system from rostral to caudal LPFC regions (identified by the exploratory analyses in each of the two groups, see Supplement 1).

Structural Equation Modeling

The structural equation model included top-down paths from rostral to caudal regions as well as additional reciprocal paths linking the same regions located in the left and right hemispheres to account for callosal interhemispheric connections. The functional model was therefore reformulated as a model of structural linear equations with path coefficients quantifying effective connectivity as partial temporal correlations between related regional activations.

We sought to test the prediction of the cascade model that path coefficients from rostral to caudal LPFC regions significantly increase with the demand of episodic control rather than contextual control (10). Subject-specific time series of functional MRI signals were obtained at activation peaks, averaged over subjects, and standardized in each condition (mean and variance were equated across conditions). The resulting time series were then used for structural model estimation and statistical inference on the basis of maximum-likelihood statistics. We assessed significant variations of path coefficients within each group with a nested model approach (19) (see also Supplement 1). Variations of path coefficients related to the episode and context factors were estimated from variations in interregional correlation matrices observed between all episodes with $I_{epi} = 0$ versus $I_{epi} > 0$ and $I_{con} = 0$ versus $I_{con} = 1$, respectively.

PPIs

To account for between-subject variability and to make a statistical inference about group differences in effective connectivity within the LPFC, we computed pair-wise PPI between LPFC regions (20).

Here, we specifically sought to test whether substantial variations from rostral to caudal LPFC activity resulted from underlying neuronal interactions with the episodic factor in both hemispheres (i.e., from the condition where the episodic control demand was low—$I_{epi} = 0$ bit—to the condition where the episodic control demand was high—$I_{epi} = 2$ bits—with $I_{con} = 0$ bit). For each of the regions identified by the exploratory voxel-wise contrasts, individual time-series were extracted at the peak voxel and standardized in each condition. Then, treating intersubject variability as a random factor, we tested whether the slopes (β) of the regression of caudal LPFC activity against rostral LPFC activity significantly increased as a function of the episodic factor within each group and between groups (from β_{low}, the slope when $I_{epi} = 0$, to β_{high}, the slope when $I_{epi} = 2$ bits) (see Supplement 1 for more details). Note that these PPI analyses are orthogonal with the ones issued from our previous report (3).

Results

Patients made significantly more errors than control subjects with regard to both the context and the episode factors (Figure 2). Because this poor performance in patients might confound

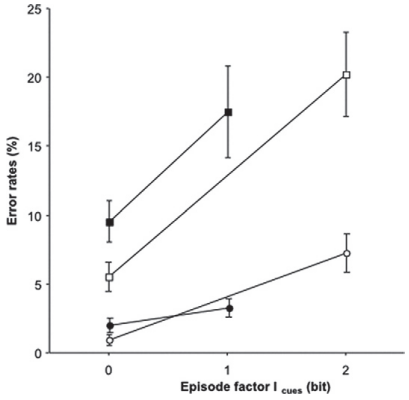

Figure 2. Behavioral results. Error rates (%, mean ± SE across participants) across experimental conditions. Open circles and squares indicate single task-set episodes in control subjects and schizophrenic patients, respectively. Solid circles and squares indicate dual task-sets episodes in control subjects and schizophrenic patients, respectively.

changes in functional brain activation, we matched groups for accuracy by removing from the analyses blocks in which performance was unsatisfactory (i.e., accuracy < .65) (see Tan *et al.* [4] for the use of a similar threshold) (see also Supplement 1 for more details). After applying this criterion, there were no behavioral differences between the two groups with regard to both the episode and the context factors [$F(1,81) < .21$, $p > .05$].

In each of the two groups, we first identified rostral and caudal LPFC as the LPFC regions involved in controlling episodic and contextual signals, respectively (Table 2). Caudal LPFC regions demonstrated a group × context interaction [$F(1,81) = 3.76$, $p = .05$], with patients showing no modulation of activation related to the contextual factor in these regions (Figure S1 in Supplement 1). By contrast, caudal LPFC regions demonstrated neither a main effect of group nor an interaction between group and episode [$F(1,81) < 1.15$, $p > .05$]. Finally, we found a group effect in rostral LPFC regions [$F(1,81) = 6.97$, $p < .05$], with patients activating this region more than control subjects.

Structural Equation Modeling Analyses

The cascade model predicts that contextual control involves no top-down control from anterior to more posterior LPFC regions (10,18). Indeed, when the demand of contextual control increased, no path coefficients were found to significantly increase from rostral to caudal LPFC regions with the context factor in both groups [all $\chi^2(1) < 3.36$, $p > .05$; Figure 3].

By contrast, the model predicts that path coefficients from rostral to caudal LPFC regions will significantly increase with the demand of episodic control (10,18). Indeed, when the demand of episodic control increased, a significant increase of path coefficients was found in healthy subjects from rostral to caudal left LPFC regions [$\chi^2(1) = 4.44$, $p < .05$; in the right hemisphere: $\chi^2(1) = .23$, $p > .05$; Figure 3]. This left lateralization might result from the exclusive use of verbal material (letter stimuli), which is preferentially processed in the left hemisphere (21). In patients, however, no path coefficients significantly increased with the episodic factor from rostral to caudal LPFC regions in either hemisphere [$\chi^2(1) < 1.96$, $p > .05$; Figure 3].

PPI Analyses

In control subjects, the significant variations of path coefficients from rostral to caudal LPFC regions reported in the SEM analysis corresponded to a significant PPI between activity in rostral and caudal LPFC regions related to the episodic factor (Figure 4). In other words, the strength of the regression between activity in caudal and rostral LPFC regions depended on the episodic factor (from $I_{epi} = 0$ to $I_{epi} = 2$ bits). Indeed, we found a significant increase in the regression slopes (β) of left caudal LPFC activity against left rostral LPFC activity as a function of the episodic factor [$F(1,459) = 8.9$, $p < .005$; $\beta_{low} = -.04$; $\beta_{high} = .43$; Figure 4A]. In patients,

Table 2. Within-Group Localization of the LPFC Regions Displaying Episode and Context Effects Used for the Effective Connectivity Analyses

Group, Effect, and Lateral Frontal Cortex Region	Estimated BA	Coordinates[a] x	y	z	Analysis t[b]	Volume[c]	FDR p
Healthy Subjects							
Context effect[d]							
Left middle frontal gyrus, caudal PFC	BA 9	−42	39	36	6.27	37,084	.038
Right middle frontal gyrus, caudal PFC	BA 9	42	33	39	5.21	8277	.038
Episode effect (excluding context effect)							
Left superior frontal gyrus, rostral PFC	BA 10	−27	54	−3	4.23	185	.037
Right middle frontal gyrus, rostral PFC	BA 10	33	63	9	3.49	139	.037
Schizophrenia Patients							
Context effect[d]							
Left middle frontal gyrus, caudal PFC	BA 9	−33	42	12	4.92	2867	.087
Right middle frontal gyrus, caudal PFC	BA 9	33	36	27	4.41	786	.087
Episode effect (excluding context effect)							
Right middle frontal gyrus, rostral cortex	BA 10	27	51	0	4.77	8046	.026
Left middle frontal gyrus, rostral cortex	BA 46	−36	48	9	4.02	1295	.026

LPFC, lateral prefrontal cortex; BA, Brodmann's Area; FDR, false discovery rate; PFC, prefrontal cortex.
[a]Coordinates from the stereotaxic atlas of Talairach and Tournoux (52).
[b]Regional peak activation representing blood oxygen-level dependent signal change that reached a threshold of $p < .05$ (corrected for the false discovery rate) in a random-effect analysis.
[c]Values are mm^3.
[d]These peaks are nonsignificant but are reported because we do not want to give the impression that the activations are absent in schizophrenia patients regarding the context effect.

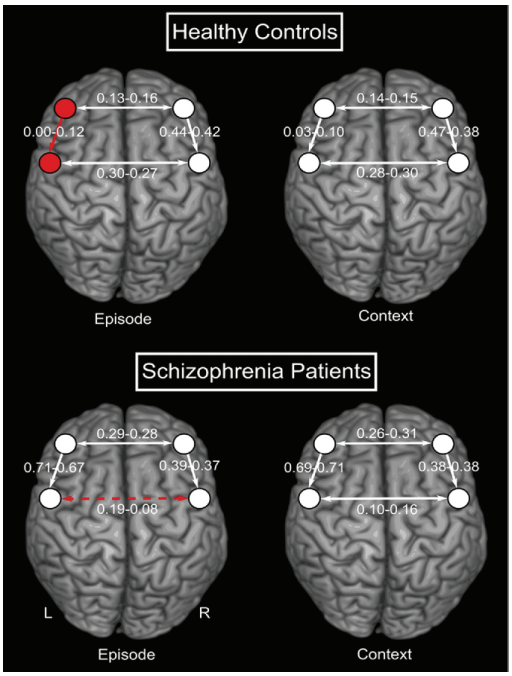

Figure 3. Diagram of path coefficients between lateral prefrontal regions involved in episodic and contextual control subjects for healthy subjects and schizophrenic patients. The structural equation model included the paths (lines, arrows indicate oriented structural paths) connecting prefrontal regions described in the text (circles, neurological convention, approximate locations). Variations of path coefficients in healthy subjects (upper panels) and in schizophrenic patients (lower panels) are shown. (**Left**) Path coefficients in episodes associated with $I_{epi} = 0$ (left number) and $I_{epi} > 0$ (right number). (**Right**) Path coefficients in single-task-set (left number) and dual-task-sets (right number) episodes. Path coefficients that significantly increased with the episodic factor are shown in red. No path coefficients were found to significantly increase with the context factor. The red dashed arrow in the left lower panel indicates a path coefficient that significantly decreased with the episode factor in patients [$\chi^2(1) = 15.78$, $p < .001$].

however, we found a significant decrease in the regression slopes of left caudal LPFC activity against left rostral LPFC activity as a function of the episodic factor [$F(1,492) = 8.9$, $p < .01$; $\beta_{low} = .60$; $\beta_{high} = .42$; Figure 4B]. We observed no significant PPI between rostral and caudal LPFC regions related to the episodic factor in the right hemisphere in either group ($F < 1.8$, $p > .05$; Figures 4C and 4D). Finally, we observed no significant PPI between rostral and caudal LPFC regions related to the contextual factor in both hemispheres, in either group ($F < 3.0$, $p > .05$), which confirmed the results of our SEM analysis.

We observed stronger effective connectivity from rostral to caudal LPFC regions related to the episodic factor in control subjects than in patients in the left hemisphere [left hemisphere: interaction among rostral LPFC activity, the episodic factor and the group factor: $F(1,951) = 16.6$, $p < .001$; right hemisphere: no interaction, $F(1,951) = .8$, $p > .05$]. The β value was significantly greater in the low-episodic control condition in patients than in control subjects [interaction between rostral LPFC activity and the group factor: $F(1,462) = 14$, $p < .001$]. In contrast, the β values were nonsignificantly different between the two groups in the high-episodic control condition [rostral LPFC activity × Group interaction: $F(1,462) = .01$, $p > .05$].

Finally, one could argue that the reduced rostrocaudal connectivity in patients could result from a bias in the analyses, because we excluded blocks in which accuracy was < .65 to prevent a performance bias. This manipulation could indeed have reduced the power of the analysis of the schizophrenia dataset relative to the control subjects. However, when rerunning the analysis with the whole dataset in both groups, we still found significantly less modulation of the caudal LPFC by the rostral LPFC in patients relative to control subjects with regard to the episodic factor in the left hemisphere [left hemisphere: interaction among rostral LPFC activity, the episodic factor, and the group factor, $F(1,951) = 10$, $p < .005$; right hemisphere: no interaction, $F(1,951) = .04$, $p > .05$].

Discussion

Our analyses support the idea that, in healthy subjects, the LPFC is hierarchically organized from rostral to caudal LPFC regions, where anterior regions integrate temporally dispersed information for selecting the appropriate action at each time from posterior LPFC regions (8–10,18,22). By contrast, we found impaired hierarchical control along the rostrocaudal axis of the LPFC in individuals with schizophrenia.

It is worth noting that our sample of patients was treated with atypical antipsychotics, which could potentially perturb the effective connectivity through the frontal cortex in schizophrenic patients. However, impaired effective connectivity within the frontal lobes has been observed in drug-naive as well as in medicated patients, making this potential confound a less likely explanation of our findings (23,24). Another potential limitation of our findings pertains to the difficulty of the task itself. Because the task was relatively complicated, it is likely that the patients who participated in the study performed much better than other patients with lower levels of education or more florid positive or negative symptoms would. That being said, we are quite confident that our results are reproducible, provided that they involve clinically stable patients with a minimum level of education, as in the current experiment. Indeed, a previous study from our group found the same pattern of behavioral results (i.e., contextual and episodic control impairments in patients) with a different sample of subjects (11). Moreover, although our functional MRI findings are novel, they support other studies showing hypoactivation in the caudal LPFC in schizophrenia (1,2,4,5,13,25–27) and are consistent with our initial hypotheses.

According to the cascade model, rostral LPFC regions are involved in selecting caudal LPFC representations to monitor the appropriate selection of task-sets evoked in the same context, a process referred to as episodic control (10). More specifically, the episodic control demand depends on the proportion *f* of episodes involving congruent associations between contextual signals and task-sets. When this proportion is maximal ($f = 1$, such as in blocks no. 1, 2, 3, and 4 in our task), the demands on episodic control are low, which is paralleled by a decrease in top-down connectivity from rostral to caudal LPFC regions. By contrast, the decrease in this frequency ($f < 1$, such as in blocks no. 5, 6, 7, and 8) leads to an increase in episodic control demands and in rostrocaudal connectivity within the LPFC. In the current study, we demonstrated that this modulation of top-down LPFC connectivity by the demands of episodic control was impaired in schizophrenia. Crucially, this might have affected the ability of patients to select the appropriate

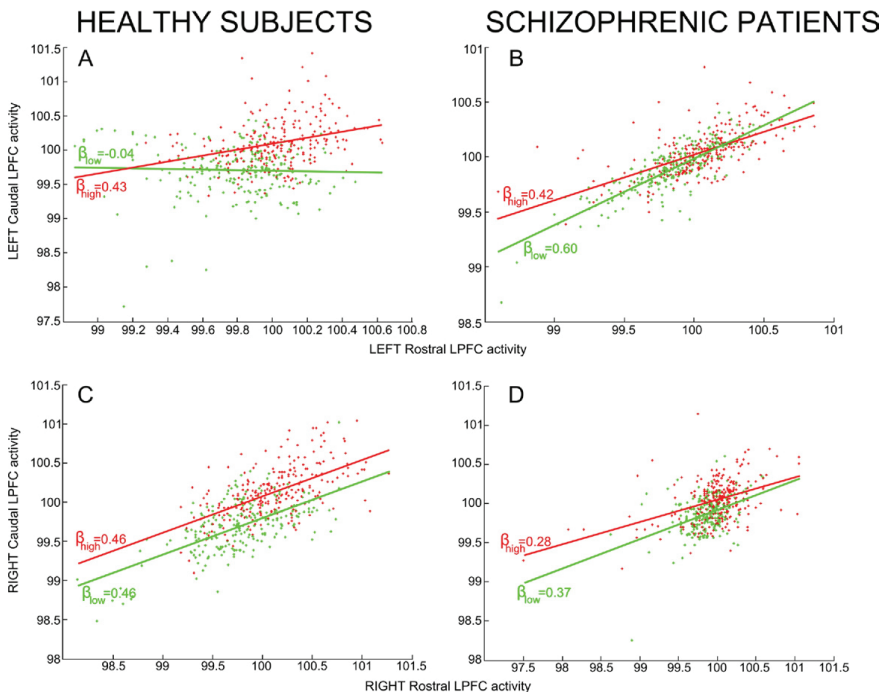

Figure 4. Psychophysiological interaction (PPI) between rostral and caudal lateral prefrontal cortex (LPFC) in healthy subjects and schizophrenic patients. Measurements when the demand of episodic control is low (I_{epi} = 0 bit), green crosses; measurements when the demand of episodic control is high (I_{epi} = 2 bits), red crosses. Condition-specific regression slopes, β_{low} (i.e., when I_{epi} = 0 bit) and β_{high} (i.e., when I_{epi} = 2 bits). All subjects are plotted together. The difference between regression slopes constitutes the PPIs. (**A** and **B**) Mean-corrected blood oxygen-level dependent (BOLD) activity (in arbitrary units) in left caudal LPFC is displayed as a function of the mean-corrected BOLD activity in left rostral LPFC. (**C** and **D**) Mean-corrected BOLD activity in the right caudal LPFC is displayed as a function of mean-corrected BOLD activity in right rostral LPFC.

sets of stimulus-response associations in the caudal LPFC on the basis of the information conveyed by past events.

Previous findings from our group demonstrated that this impaired episodic control process was specifically observed when patients had to control information conveyed by episodic and contextual (vs. sensory) signals (11). This result suggests that episodic control disturbances could arise from inappropriate contextual control, which is itself related to abnormal activation of the caudal LPFC (3). Other findings from the schizophrenia literature have also proposed that a context processing impairment could be at the core of the cognitive control disturbances in schizophrenic patients, related to specific disturbances in the dorso-caudal LPFC (1,2,26–30). In other terms, the disruption of top-down connectivity from rostral to caudal LPFC regions in patients could primarily be the consequence of poorly encoded contextual information, which might be due to abnormal computations in the caudal LPFC. In turn, hyperactivation in rostral LPFC regions might serve as a compensatory function to maintain a minimum level of performance during episodic control (i.e., to retrieve the poorly integrated contextual information) (12,13).

At a more distal level, our results suggest that this impaired effective connectivity within the LPFC in patients is related to abnormally high levels of connectivity between rostral and caudal LPFC regions in the low-episodic control condition (the regression coefficient between rostral and caudal LPFC activities was significantly greater in patients than in control subjects in the low-episodic control condition, whereas the groups did not significantly differ in the high-episodic control condition). It is interesting to note that such an increase in connectivity in low-level conditions, together with a relative decrease in higher-level conditions of cognitive control, is conceptually analogous to findings from previous studies that also investigated cognitive control in schizophrenia, with computational models of context processing (31). Specifically, it was suggested that increased noise in the subcortical dopamine system at rest (32,33) leads to abnormal "gating" of context information into prefrontal cortex (34–35). Although these findings deal with distinct types of information (contextual vs. episodic signals), one cannot exclude that these two phenomena both rely on the same neurobiological mechanism responsible for "gating" different classes of information into specialized subregions within the prefrontal cortex.

Other hypotheses closely related to the concept of episodic control have been proposed to better characterize the impaired processes involved in episodic task performances in schizophrenia. One hypothesis highlights the importance of cognitive control and related LPFC functioning in episodic memory disturbances in schizophrenia (25,36). The cascade model claims that episodic control monitors the flexible and temporary reinstantiation of episodic

information (e.g., past events, rules, or task instructions) to modulate action selection across a behavioral episode (9). As such, episodic control can be understood as the process that supervises the retrieval of information from episodic memory (37–39). Consistently, other studies have found that rostral LPFC activations were observed in episodic memory paradigms in retrieval phases, when subjects selected actions on the basis of the occurrence of previous events (40–43). Therefore, our finding of an impaired episodic control process related to a perturbed rostrocaudal hierarchy within the LPFC could represent a potential cause for the episodic memory retrieval disturbances in schizophrenia—a hypothesis that should be further investigated in the future.

Another well-known concept intimately related to episodic control, as defined by the cascade model, is the so-called "episodic buffer," a new component included in the former working memory model (44). Indeed, the cascade model generalizes the classical theory of executive control on the basis of a central executive system controlling multiple slave systems, inspired from the working memory framework (45). In those two models, each stage maintains active representations that are controlled by higher stages and that exert control on representations at lower stages. Recently, the episodic buffer has been defined as a new temporary system, thought to be biologically implemented by the frontal areas (44). Crucially, the episodic buffer is important for integrating representations of information bound in a multimodal code being entered into or retrieved from long-term episodic memory (44). Executive processes engaged in the episodic domain (i.e., episodic control) could thus be conceptualized as mechanisms that monitor the binding between different temporal features of information into a temporary, unitary, and coherent representation of events (i.e., within the episodic buffer). Our findings therefore suggest a core impairment in control processes devoted to building a new, consistent, multi-featured representation of temporally dispersed contextual signals, which might account for the perturbations of the episodic buffer observed by others in schizophrenia (46,47).

This impaired functional connectivity between rostral and caudal LPFC regions supports the functional disconnection hypothesis in schizophrenia initially proposed by Friston (14). We also provide, to the best of our knowledge, the first evidence of a top-down disconnection within the LPFC in this disorder. Because the anatomical connectivity within the LPFC was not found to be disrupted in schizophrenia (48,49), we suggest that our result reflects something more dynamic in the way those areas function as a whole to produce cognitive control (e.g., via impaired synaptic transmission) (14).

Finally, in addition to its clinical implications with regard to the pathophysiology of cognitive disturbances of schizophrenic patients, we believe that this result has more general theoretical implications. Indeed, there has recently been a growing interest in the study of the hierarchical organization of cognitive control within the rostrocaudal axis of the frontal lobes, either in healthy subjects (18) or in patients with frontal lobe damage (22). The present study provides additional support confirming that this hierarchy might be a fruitful framework in which to investigate frontal lobe architecture and its pathology.

This research was supported by a grant of the Conseil Scientifique de la Recherche, Le Vinatier (CSRA 05). The author GB was supported by a grant from the Fondation pour la Recherche Médicale (DEA20050904971). We wish to thank S.J. Blakemore and S. White for their assistance in proofreading this report.

The authors report no biomedical financial interests or potential conflicts of interest.

Supplementary material cited in this article is available online.

1. Barch DM, Carter CS, Braver TS, Sabb FW, MacDonald A III, Noll DC, Cohen JD (2001): Selective deficits in prefrontal cortex function in medication-naive patients with schizophrenia. *Arch Gen Psychiatry* 58:280–288.
2. MacDonald AW III, Carter CS, Kerns JG, Ursu S, Barch DM, Holmes AJ, *et al.* (2005): Specificity of prefrontal dysfunction and context processing deficits to schizophrenia in never-medicated patients with first-episode psychosis. *Am J Psychiatry* 162:475–484.
3. Barbalat G, Chambon V, Franck N, Koechlin E, Farrer C (2009): Organization of cognitive control within the lateral prefrontal cortex in schizophrenia. *Arch Gen Psychiatry* 66:377–386.
4. Tan H, Choo W, Fones CSL, Chee MWL (2005): fMRI study of maintenance and manipulation processes within working memory in first-episode schizophrenia. *Am J Psychiatry* 162:1849–1858.
5. Tan H, Sust S, Buckholtz JW, Mattay VS, Meyer-Lindenberg A, Egan MF, *et al.* (2006): Dysfunctional prefrontal regional specialization and compensation in schizophrenia. *Am J Psychiatry* 163:1969–1977.
6. Cannon TD, Glahn DC, Kim J, Van Erp TGM, Karlsgodt K, Cohen MS, *et al.* (2005): Dorsolateral prefrontal cortex activity during maintenance and manipulation of information in working memory in patients with schizophrenia. *Arch Gen Psychiatry* 62:1071–1080.
7. Badre D (2008): Cognitive control, hierarchy, and the rostro-caudal organization of the frontal lobes. *Trends Cogn Sci* 12:193–200.
8. Badre D, D'Esposito M (2009): Is the rostro-caudal axis of the frontal lobe hierarchical? *Nat Rev Neurosci* 10:659–669.
9. Koechlin E, Summerfield C (2007): An information theoretical approach to prefrontal executive function. *Trends Cogn Sci* 11:229–235.
10. Koechlin E, Ody C, Kouneiher F (2003): The architecture of cognitive control in the human prefrontal cortex. *Science* 302:1181–1185.
11. Chambon V, Franck N, Koechlin E, Fakra E, Ciuperca G, Azorin J, Farrer C (2008): The architecture of cognitive control in schizophrenia. *Brain* 131:962–970.
12. Weiss AP, Schacter DL, Goff DC, Rauch SL, Alpert NM, Fischman AJ, Heckers S (2003): Impaired hippocampal recruitment during normal modulation of memory performance in schizophrenia. *Biol Psychiatry* 53:48–55.
13. Heckers S, Rauch SL, Goff D, Savage CR, Schacter DL, Fischman AJ, Alpert NM (1998): Impaired recruitment of the hippocampus during conscious recollection in schizophrenia. *Nat Neurosci* 1:318–323.
14. Friston KJ (1998): The disconnection hypothesis. *Schizophr Res* 30:115–125.
15. Meyer-Lindenberg AS, Olsen RK, Kohn PD, Brown T, Egan MF, Weinberger DR, Berman KF (2005): Regionally specific disturbance of dorsolateral prefrontal-hippocampal functional connectivity in schizophrenia. *Arch Gen Psychiatry* 62:379–386.
16. Honey GD, Pomarol-Clotet E, Corlett PR, Honey RAE, McKenna PJ, Bullmore ET, Fletcher PC (2005): Functional dysconnectivity in schizophrenia associated with attentional modulation of motor function. *Brain* 128:2597–2611.
17. Shannon C (1948): A mathematical theory of communication. *Bell Syst Tech J* 27:379–423,623–656.
18. Kouneiher F, Charron S, Koechlin E (2009): Motivation and cognitive control in the human prefrontal cortex. *Nat Neurosci* 12:939–945.
19. Mueller RO (1996): *Basic Principles of Structural Equation Modeling*. New York: Springer Texts in Statistics, Springer-Verlag.
20. Gitelman DR, Penny WD, Ashburner J, Friston KJ (2003): Modeling regional and psychophysiologic interactions in fMRI: The importance of hemodynamic deconvolution. *Neuroimage* 19:200–207.
21. Stephan KE, Marshall JC, Friston KJ, Rowe JB, Ritzl A, Zilles K, Fink GR (2003): Lateralized cognitive processes and lateralized task control in the human brain. *Science* 301:384–386.
22. Badre D, Hoffman J, Cooney JW, D'Esposito M (2009): Hierarchical cognitive control deficits following damage to the human frontal lobe. *Nat Neurosci* 12:515–522.
23. Schlösser R, Gesierich T, Kaufmann B, Vucurevic G, Hunsche S, Gawehn J, Stoeter P (2003): Altered effective connectivity during working memory performance in schizophrenia: A study with fMRI and structural equation modeling. *Neuroimage* 19:751–763.
24. Schlösser R, Gesierich T, Kaufmann B, Vucurevic G, Stoeter P (2003): Altered effective connectivity in drug free schizophrenic patients. *Neuroreport* 14:2233–2237.

25. Ragland JD, Laird AR, Ranganath C, Blumenfeld RS, Gonzales SM, Glahn DC (2009): Prefrontal activation deficits during episodic memory in schizophrenia. *Am J Psychiatry* 166:863–874.
26. MacDonald AW III, Carter CS (2003): Event-related FMRI study of context processing in dorsolateral prefrontal cortex of patients with schizophrenia. *J Abnorm Psychol* 112:689–697.
27. Barch DM (2005): The cognitive neuroscience of schizophrenia. *Annu Rev Clin Psychol* 1:321–353.
28. Holmes AJ, MacDonald A III, Carter CS, Barch DM, Andrew Stenger V, Cohen JD (2005): Prefrontal functioning during context processing in schizophrenia and major depression: An event-related fMRI study. *Schizophr Res* 76:199–206.
29. MacDonald AW III, Pogue-Geile MF, Johnson MK, Carter CS (2003): A specific deficit in context processing in the unaffected siblings of patients with schizophrenia. *Arch Gen Psychiatry* 60:57–65.
30. Delawalla Z, Csernansky JG, Barch DM (2008): Prefrontal cortex function in nonpsychotic siblings of individuals with schizophrenia. *Biol Psychiatry* 63:490–497.
31. Braver TS, Barch DM, Cohen JD (1999): Cognition and control in schizophrenia: A computational model of dopamine and prefrontal function. *Biol Psychiatry* 46:312–328.
32. Meyer-Lindenberg A, Miletich RS, Kohn PD, Esposito G, Carson RE, Quarantelli M, *et al.* (2002): Reduced prefrontal activity predicts exaggerated striatal dopaminergic function in schizophrenia. *Nat Neurosci* 5:267–271.
33. Abi-Dargham A, Mawlawi O, Lombardo I, Gil R, Martinez D, Huang Y, *et al.* (2002): Prefrontal dopamine D1 receptors and working memory in schizophrenia. *J Neurosci* 22:3708–3719.
34. Braver TS, Cohen JD (1999): Dopamine, cognitive control, and schizophrenia: The gating model. *Prog Brain Res* 121:327–349.
35. Swerdlow NR, Geyer MA (1998): Using an animal model of deficient sensorimotor gating to study the pathophysiology and new treatments of schizophrenia. *Schizophr Bull* 24:285–301.
36. Ranganath C, Minzenberg MJ, Ragland JD (2008): The cognitive neuroscience of memory function and dysfunction in schizophrenia. *Biol Psychiatry* 64:18–25.
37. Henson RN, Rugg MD, Shallice T, Josephs O, Dolan RJ (1999): Recollection and familiarity in recognition memory: An event-related functional magnetic resonance imaging study. *J Neurosci* 19:3962–3972.
38. Henson RN, Rugg MD, Shallice T, Dolan RJ (2000): Confidence in recognition memory for words: Dissociating right prefrontal roles in episodic retrieval. *J Cogn Neurosci* 12:913–923.
39. Bunge SA, Burrows B, Wagner AD (2004): Prefrontal and hippocampal contributions to visual associative recognition: Interactions between cognitive control and episodic retrieval. *Brain Cogn* 56:141–152.
40. Velanova K, Jacoby LL, Wheeler ME, McAvoy MP, Petersen SE, Buckner RL (2003): Functional-anatomic correlates of sustained and transient processing components engaged during controlled retrieval. *J Neurosci* 23:8460–8470.
41. Sakai K, Passingham RE (2003): Prefrontal interactions reflect future task operations. *Nat Neurosci* 6:75–81.
42. Sakai K, Rowe JB, Passingham RE (2002): Active maintenance in prefrontal area 46 creates distractor-resistant memory. *Nat Neurosci* 5:479–484.
43. Fletcher PC, Henson RN (2001): Frontal lobes and human memory: Insights from functional neuroimaging. *Brain* 124:849–881.
44. Baddeley A (2000): The episodic buffer: A new component of working memory? *Trends Cogn Sci* 4:417–423.
45. Baddeley A, Della Sala S (1996): Working memory and executive control. *Philos Trans R Soc Lond B Biol Sci* 351:1397–1403; discussion:1403–1404.
46. Burglen F, Marczewski P, Mitchell KJ, van der Linden M, Johnson MK, Danion J, Salamé P (2004): Impaired performance in a working memory binding task in patients with schizophrenia. *Psychiatry Res* 125:247–255.
47. Rizzo L, Danion JM, van der Linden M, Grangé D (1996): Patients with schizophrenia remember that an event has occurred, but not when. *Br J Psychiatry* 168:427–431.
48. Jensen JE, Miller J, Williamson PC, Neufeld RWJ, Menon RS, Malla A, *et al.* (2006): Grey and white matter differences in brain energy metabolism in first episode schizophrenia: 31P-MRS chemical shift imaging at 4 Tesla. *Psychiatry Res* 146:127–135.
49. Highley JR, Walker MA, Esiri MM, McDonald B, Harrison PJ, Crow TJ (2001): Schizophrenia and the frontal lobes: Post-mortem stereological study of tissue volume. *Br J Psychiatry* 178:337–343.
50. Andreasen NC (1984): *The Scale for the Assessment of Positive Symptoms (SAPS)*. Iowa City, Iowa: University of Iowa Press.
51. Andreasen NC (1983): *The Scale for the Assessment of Negative Symptoms (SANS)*. Iowa City, Iowa: University of Iowa Press.
52. Talairach J, Tournoux P (1988): *Co-Planar Stereotaxic Atlas of the Human Brain*. New York, New York: Thieme Medical Publishers.

Supplemental Information

Subjects

Fifteen schizophrenic patients and 15 healthy controls, who were all right-handed (Edinburgh Handedness Survey (1)) and matched for age, sex, and years of education, were recruited to participate in the fMRI experiment (see the Clinical and Demographic Characteristics of the participants in Table 1 from the main article). Other results from this sample have been published elsewhere (2). After the study was completely described to the participants, written informed consent was obtained, as approved by the local ethics committee. All of the participants were paid for their time. Diagnosis was confirmed for each patient by an MD- and PhD-level clinical psychiatrist (masked to task performance) based on the Structured Clinical Interview of the DSM-IV-TR (3).

None of the participants had a history of brain trauma, seizure disorder, electroconvulsive therapy, mental retardation, affective disorder, substance abuse, or substance dependence within the past 6 months. In addition to these exclusion criteria, special exclusion criteria for the controls included having a history of an Axis I disorder, having a first-degree relative with a psychotic disorder, and receiving treatment with any psychotropic medication within the past 6 months. One control participant was excluded because of motion artifact in the scanner (> 2 voxels translation, > 2 degrees rotation) (4). No patients were excluded.

Training was done outside the scanner, in the three days preceding the scanning session. On average, healthy participants were trained one hour and schizophrenic patients, two hours. This procedure was critical to ensure that subjects correctly understood the task and to prevent any learning effects in the scanner (which might have recruited extra brain regions). In line with this point, we chose not to recruit participants who were clinically unstable or below a minimum level of education (8 years of education), because they would probably not have been able to perform the task properly. It is noteworthy that no patients from our sample were excluded because of not being able to follow the task rules.

Behavioral Analyses

Error rates and reaction times for correct trials acquired during scanning were analyzed using analyses of covariance with subject as a random factor, group as a between-subject factor,

context as a within-subject factor, and episode as a within-subject covariate. When significant, interactions were decomposed using *t* tests.

The analysis of covariance performed on reaction times showed significant effects of episode ($F(1,81) = 100.16$, $P < .001$) and context ($F(1,81) = 197.89$, $P < .001$), revealing slower reaction times as the demands of cognitive controls increased. Patients' reaction times, however, did not deteriorate in a manner that was distinct from the controls' as the demands of contextual and episodic controls increased (all interactions with group factor: $F(1,81) < 0.67$, $P > .05$), indicating that varying the amount of information conveyed by contextual and episodic signals did not increase patients' reaction times more than it did in the control group.

Participants' error percentages were found to significantly increase with the contextual ($F(1,81) = 4.16$, $P < .05$) and episodic ($F(1,81) = 66.23$, $P < .001$) factors. Significant interactions between group and cognitive factors were observed in both the contextual ($F(1,81) = 4.58$, $P < .05$) and the episodic ($F(1,81) = 13.26$, $P < .001$) factors. These effects were due to a greater decrement in performance among patients than controls regarding both the episodic and contextual factors. Patients performed worse than controls for I_{con}=0 and 1 bit and for I_{epi}=0, 1, and 2 bits (all $t > 3.50$, $P < .002$) (Figure 2 from the main article).

MRI Procedures and Preprocessing

Images were collected using the 1.5T MRI system (Siemens Sonata Maestro Class; Siemens, Erlangen, Germany) of the CERMEP Imagerie du vivant in Lyon, France. The fMRI blood oxygenation level dependent (BOLD) signal was measured using a T2*-weighted echo-planar sequence (TR = 2500 msec, flip angle = 90°, TE = 60 msec). Twenty-six axial slices (thickness: 4 mm, gap: 0.4 mm, field of view: 220 mm, matrix size: 64 x 64, in-plane resolution: 3.4 x 3.4 mm^2) were acquired per volume. Following functional image acquisition, a high-resolution T1-weighted anatomical image (TR = 1970 msec, TE = 3.93 msec, 256 x 256 matrix, resolution: 1 x 1 x 1 mm^3) was collected for each subject.

Image preprocessing was performed using SPM5 (Wellcome Department of Imaging Neuroscience, University College London, UK, http://www.fil.ion.ucl.ac.uk/spm/). For each subject, each of the eight scanning sessions contained 155 functional volumes after the first five scans were rejected to eliminate the nonequilibrium effects of magnetization. All functional volumes were realigned to the first volume to correct for inter-scan movement. Functional and

structural images were coregistered and transformed into a standardized, stereotaxic space (MNI template) (5). Functional data were then smoothed with a 10 mm FWHM, isotropic Gaussian kernel and temporally high-pass filtered with a frequency cutoff period of 128 s. Serial correlations were accounted for by use of an autoregressive model of the first order. To control for possible noise artifacts in the data, we used a weighted least-squares approach, in which we down-weighted images with high noise variance (6).

A potential criticism of fMRI studies in schizophrenia is that increased movement among patients creates artifacts that impair detection of cortical activation. We evaluated this possibility by analyzing each of the 6 estimated movement measures in scan-to-scan incremental movements and in absolute movement from the reference scan, collapsed across conditions. Results of the *t* tests indicate no significant group differences for any of the parameters (all $t(27) < 1.18$, $P > 0.05$), suggesting that group-related activation differences cannot be attributed to differential movement in the scanner.

Delimitation of the Regions of Interest – Exploratory Analyses

For the fMRI data, we first conducted voxel-wise exploratory analyses of frontal regions subserving each level of cognitive control (context and episode), in both the schizophrenia and the healthy groups. As in previous studies based on a similar paradigm, we designed the present study as a block-design experiment and followed identical analysis procedures (7-8).

Using SPM5, statistical parametric t-maps (SPM{t}) were computed from local fMRI signals using a linear multiple regression analysis with conditions (modeled as box-car functions convolved by the canonical hemodynamic response function) and scanning series as covariates (9). For all conditions, we defined the preparation phase as the time interval between the instruction cue and the presentation of the first stimulus, and the execution phase was defined as the period from the first stimulus until the end of the series of stimuli. In the current study, we analyzed the frontal regions engaged in cognitive control exertion during the execution phase. Specifically, the context effect was computed as larger activations in the dual- (I_{con}=1 bit) than in the single- (I_{con}=0 bit) task-set episodes with I_{epi}=0 bit (contrast weights assigned as follows: [1] for blocks #3,4 i.e. conditions in which I_{con}=1 bit and I_{epi}=0 bit; [-1] for blocks #1,2 i.e. conditions in which I_{con}=0 bit and I_{epi}=0 bit), and the episode effect as activations that

parametrically varied as the episodic factor I_{epi} (i.e. from I_{epi}=0, to I_{epi}=1 and I_{epi}=2 bits). For the episode effect, the contrast weights were assigned as follows:

- [-3] for conditions in which I_{epi}=0 bit (that is, conditions in which I_{epi}=0 & I_{con}=1 and I_{epi}=0 & I_{con}=0 – i.e. 2 different regressors per run);
- [1] for conditions in which I_{epi}=1 bit (that is, conditions in which I_{epi}=1 & I_{con}=1 – i.e. 1 single regressor per run);
- [5] for conditions in which I_{epi}=2 bit (that is, conditions in which I_{epi}=2 & I_{con}=0 – i.e. 1 single regressor per run).

Therefore, the sum of the contrast weights per run was:

Σ = [-3]*2 regressors + [1] + [5] = 0.

In a second level of analysis, contrasts were performed using a random-effect model. According to the cascade model, rostral LPFC regions subserve episodic control, while caudal LPFC regions subserve contextual control. Another important feature of the model is that rostral LPFC regions select caudal LPFC representations according to the temporal episode in which stimuli occur. Consequently, rostral and caudal LPFC regions are both activated in the episodic control condition, whereas only caudal LPFC regions are activated in the contextual control condition. Therefore, we identified caudal and rostral LPFC as the regions showing an effect of context and an effect of episode but no context effect (computed by masking each region related to the episode effect with the context effect, using an uncorrected voxel-wise threshold $p < 0.05$), respectively (7-8). Those regions were localized within each group to avoid localization bias (i.e. the possibility that significant differences in activation result from the delimitations of the regions of interest in only one of the groups).

MNI coordinates were transformed to the standard space of Talairach and Tournoux (10) and reported as T-scores. In accordance with our a priori hypothesis and on the basis of the known distributed functional and structural anatomy of cognitive control (11-12), our analyses were restricted to the lateral prefrontal cortex by masking through use of WFU PickAtlas software (13) (dilatation parameter = 3 voxels, bilateral mask including Brodman areas [BAs] BA8, BA9, BA10, BA44, BA45 & BA46 from the built-in atlas). The significance voxel-wise threshold was chosen at $p < 0.05$ (corrected for the false discovery rate). Note that at this threshold, we did not find any activation in the caudal LPFC in patients, which suggested that caudal LPFC regions were more activated in controls than in patients during contextual control.

However, this region showed activation at a lowered FDR-corrected threshold of $p < 0.09$. We therefore used this more liberal threshold to find caudal LPFC activations in patients because we did not want to make the impression that the caudal LPFC was not activated in schizophrenia.

According to the seminal study of Koechlin et al. (2003), we defined a cluster as being part of the caudal LPFC region if its peak of activation was located in BAs 9/44/45 (posteriorly) while a cluster would belong to the rostral portion of the LPFC if its peak of activation was located in BAs 46/10 (anteriorly) (Table 2 from the main article) (14).

Regions of Interest Analyses

In a second step of analysis, we tested the prediction that caudal LPFC regions would be more activated in controls than in patients during contextual control. However, the caudal LPFC voxels subserving contextual control did not share the same coordinates in healthy subjects and in patients. Therefore, a usual between-group analysis on a voxel-by-voxel basis with SPM would have resulted in a bias towards hypoactivation in caudal LPFC voxels being activated in controls but not in patients. We therefore tested the above-mentioned assumption by running a region of interest analysis on the caudal LPFC activations whose localizations were different in each group (2). That is, peak-voxel activations for each subject in the healthy group were extracted from the caudal LPFC regions that were specifically identified by the contextual contrast in this group. Conversely, peak-voxel activations for each subject in the schizophrenic group were extracted from the caudal LPFC regions that were specifically identified by the contextual contrast in this latter group ($p < .09$, FDR corrected).

Peak voxel activations (i.e. the signal from the voxel that was the most activated at the group level) in the rostral and caudal LPFC regions identified by the exploratory analyses in each of the two groups were then separately entered into univariate repeated-measure analyses of covariance, with subject as a random factor, hemisphere (left vs. right) and number of alternatives (single vs. dual task set) as within-subject factors, episode (I_{epi}=0, 1, or 2 bits) as a within-subject covariate, and group (patients vs. controls) as a between-subject factor. When significant, interactions were further assessed using *t* tests. To conduct these analyses, we used STATISTICA8. Note that to prevent performance bias (i.e. the possibility that the differences in activations arise from patients' poor engagement in the task, rather than from a specific cognitive deficit), we matched groups for accuracy by removing from the analyses blocks in which

performance was unsatisfactory (i.e. accuracy < 0.65, see (15) for the use of a similar threshold). Using this threshold, a mean of 0.75 (SD = 1.06) blocks per run were considered to be performed near chance for the patients, compared to a mean of 0.12 (SD = 0.32) for the comparison participants ($p < 0.05$). Running the analysis considering only blocks where the accuracy was acceptable (i.e. accuracy > 0.65), there were no behavioral differences between the two groups regarding both the episode and the context factors ($F(1,81) < 0.21$ and $p > 0.05$).

We found a group effect in rostral LPFC regions ($F(1,81) = 6.97$, $p < 0.05$), with patients activating more this region than controls. By contrast, caudal LPFC regions demonstrated a group*context interaction ($F(1,81) = 3.76$, $p = 0.05$), with patients showing no modulation of activation related to the context factor in these regions (we provided a proper activation map to illustrate this between-group analysis on contextual control in Figure S1). Caudal LPFC regions did not demonstrate any main effect of group, nor an interaction between group and episode ($F(1,81) < 1.15$, $p > .05$). Note that these caudal LPFC hypoactivation and rostral LPFC hyperactivation in patients persisted after having re-run the analysis with the whole data set in both groups (2).

Effective Connectivity Analyses

The concept of effective connectivity between brain areas involves model-based assumptions about the effect that a defined neural system exerts over another (16). By contrast, functional connectivity is defined as the correlation of regional brain activity over time. Therefore, with effective connectivity, it is possible to detect increases or decreases in the information flow between regional brain activities with a defined direction (causality), whereas functional connectivity does not account for such directional effects or for an underlying structural model. Another important difference is that effective connectivity, rather than depending simply on the correlation of time courses across conditions, provides additional explanatory power by incorporating a psychological context (or experimental condition) in the analyses.

Here, we conducted hypothesis-driven effective connectivity analyses in the different regions identified by the exploratory analyses in each of the two groups (bilateral rostral and caudal LPFC regions). We used structural equation modeling (SEM) and psycho-physiological interaction (PPI) as effective connectivity measures (17).

→ Structural Equation Modeling

We first performed SEM within each group to assess the effective connectivity between LPFC subregions (18). We followed the same procedure as in previous studies that used an identical paradigm (7-8).

The structural equation modeling technique differs from other (parametrical) statistical approaches such as multiple regression or ANOVA because, instead of considering individual observations for the analyses, in SEM, the *covariance structure* between regional activations is emphasized. Indeed, SEM is a multivariate technique used to analyze the covariance of observations between regional activation – i.e. how much the neural activities of the brain regions involved in the model are related to each other (19). The values for effective connectivity between brain areas – i.e. connection strengths – are known as the path coefficients (i.e. similar to partial correlation or regression coefficients).

Our structural equation model included top-down paths from rostral to caudal LPFC regions, as well as additional reciprocal paths linking the same regions located in the left and right hemispheres to account for callosal interhemispheric connections.

We hypothesized that the connection strength from the rostral to the caudal LPFC would increase with the episodic but not the contextual factor, as demonstrated in (7-8). Crucially, to assess changes in connection strength between two conditions (e.g. from $I_{epi}=0$ vs. $I_{epi}>0$), we used the nested (or stacked) model approach (20-21). Specifically, we first defined the restricted null model, in which all of the path coefficients were forced to be equal between conditions. The second set of models comprised the corresponding alternate free models, in which all of the path coefficients were constrained to be equal between conditions except one that was allowed to vary between conditions. We defined as many free models as there were different pathways in the structural model, each different free model being defined as the free model *for that particular pathway* (4 different free models were therefore defined in our structural equation modeling system).

For each model, the path coefficients were estimated by minimizing the difference between the observed covariances between regional activations and the covariances predicted by the anatomical structural model (using a maximum likelihood fit function). A χ^2 test was used to measure the goodness of fit of each model. This χ^2 test summarized the discrepancy between observed values and values expected under the model in question. χ^2 values were computed for

all models (i.e. the null model and the free models) with corresponding degrees of freedom. Then, the χ^2 value for each free model was compared with the χ^2 value for the constrained null model. This was done by simply subtracting those χ^2 values – then this χ^2 difference was tested with degrees of freedom being equal to the difference of the degrees of freedom for the null vs. the free model.

For a particular pathway, if the χ^2 value for the null model was significantly larger than the one for the free model, the null model was refuted and the free model for that particular pathway was assumed to provide a better fit. In other words, for that particular pathway, there was a statistically significant global difference in path coefficients between the conditions (i.e. from $I_{epi}=0$ vs. $I_{epi}>0$). Such a significant difference in the absolute magnitude of the path coefficients was interpreted as a change in the strength of the influences conveyed through that particular pathway, related to that particular factor (i.e. episodic control).

The overall model fit was assessed by computing standard goodness of fit indices, including normed fit, centrality and relative non-centrality indexes (all indexes > 0.9 indicating an appropriate fit) (22).

SEM was processed using the MX software package (http://www.vcu.edu/mx/).

→ Psycho-Physiological Interactions

Here, we specifically sought to test whether substantial variations from rostral to caudal LPFC activity resulted from underlying neuronal interactions with the episodic factor in both hemispheres (i.e. from the condition where the episodic control demand was low – $I_{epi}=0$ bit – to the condition where the episodic control demand was high – $I_{epi}=2$ bits –, with $I_{con}=0$ bit).

PPI can be understood as the influence that one cerebral region exerts over another in a specific experimental condition. In other terms, PPI looks at how brain activity can be explained by the interaction between 2 variables: an experimental variable and activity in another particular brain area. Such a modulation is reflected by the variation in the slopes of the regression of one region's activity (here, caudal LPFC activity) against another's (here, rostral LPFC activity) as a function of an experimental cognitive factor (here, the episodic control demand) (17).

To demonstrate that the slopes were significantly different across conditions, we tested whether caudal LPFC activity was significantly influenced by the interaction between rostral LPFC activity (a continuous variable) and the episodic factor (a discrete factor with two levels).

When significant, we determined the direction of the psycho-physiological interaction (i.e. whether there is an increase or a decrease in connectivity from rostral to caudal LPFC regarding the episodic factor) by comparing the group level slopes between the low and the high levels of the episode factor.

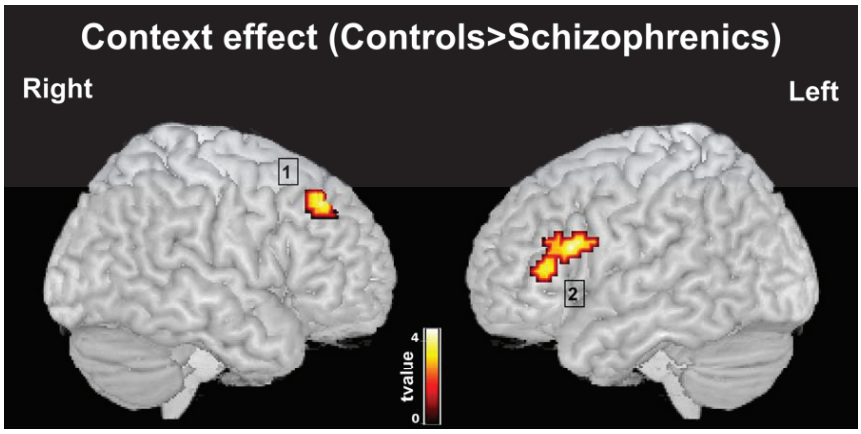

Figure S1. Caudal lateral prefrontal cortex regions demonstrating contextual effects that were significantly greater in healthy control participants than in participants with schizophrenia. 1 indicates dorsocaudal LPFC; 2, ventrocaudal LPFC. For display purposes, the regions of interest have thresholds of $p < .005$ and 15 contiguous voxels.

References

1. Oldfield RC (1971): The assessment and analysis of handedness: the Edinburgh inventory. *Neuropsychologia* 9:97-113.
2. Barbalat G, Chambon V, Franck N, Koechlin E, Farrer C (2009): Organization of cognitive control within the lateral prefrontal cortex in schizophrenia. *Arch Gen Psychiatry* 66:377-386.
3. American Psychiatric Association (2000): *Diagnostic and Statistical Manual of Mental Disorders, Fourth Edition, Text Revision*. Washington, DC: American Psychiatric Press.
4. Cox RW, Jesmanowicz A (1999): Real-time 3D image registration for functional MRI. *Magn Reson Med* 42:1014-1018.
5. Friston KJ, Ashburner J, Frith CD, Poline J, Heather JD, Frackowiak RSJ (1995): Spatial registration and normalization of images. *Hum Brain Mapp* 3:165-189.
6. Diedrichsen J, Shadmehr R (2005): Detecting and adjusting for artifacts in fMRI time series data. *Neuroimage* 27:624-634.
7. Koechlin E, Ody C, Kouneiher F (2003): The architecture of cognitive control in the human prefrontal cortex. *Science* 302:1181-1185.
8. Kouneiher F, Charron S, Koechlin E (2009): Motivation and cognitive control in the human prefrontal cortex. *Nat Neurosci* 12:939-945.
9. Friston KJ, Holmes AP, Worsley KJ, Poline J-B, Frith CD, Frackowiak RSJ (1994): Statistical parametric maps in functional imaging: A general linear approach. *Human Brain Mapp* 2:189-210.
10. Talairach J, Tournoux P (1988): *Co-Planar stereotaxic atlas of the human brain*. New York, NY: Thieme Medical Publishers.
11. Goldman-Rakic PS (1996): The prefrontal landscape: implications of functional architecture for understanding human mentation and the central executive. *Philos Trans R Soc Lond B Biol Sci* 351:1445-1453.
12. Koechlin E, Summerfield C (2007): An information theoretical approach to prefrontal executive function. *Trends Cogn Sci* 11:229-235.
13. Maldjian JA, Laurienti PJ, Kraft RA, Burdette JH (2003): An automated method for neuroanatomic and cytoarchitectonic atlas-based interrogation of fMRI data sets. *Neuroimage* 19:1233-1239.
14. Koechlin E, Summerfield C (2007): An information theoretical approach to prefrontal executive function. *Trends Cogn Sci* 11:229-235.
15. Tan H, Choo W, Fones CSL, Chee MWL (2005): fMRI study of maintenance and manipulation processes within working memory in first-episode schizophrenia. *Am J Psychiatry* 162:1849-1858.
16. Friston KJ (1994): Functional and Effective Connectivity in Neuroimaging: A Synthesis. *Human Brain Mapp* 2:56-78.
17. Friston KJ, Buechel C, Fink GR, Morris J, Rolls E, Dolan RJ (1997): Psychophysiological and modulatory interactions in neuroimaging. *Neuroimage* 6:218-229.
18. Friston KJ, Frith CD, Liddle PF, Frackowiak RS (1991): Comparing functional (PET) images: the assessment of significant change. *J Cereb Blood Flow Metab* 11:690-699.

19. Della-Maggiore V, Sekuler AB, Grady CL, Bennett PJ, Sekuler R, McIntosh AR (2000): Corticolimbic interactions associated with performance on a short-term memory task are modified by age. *J Neurosci* 20:8410-8416.
20. McIntosh AR, Grady CL, Haxby JV, Ungerleider LG, Horwitz B (1996): Changes in limbic and prefrontal functional interactions in a working memory task for faces. *Cereb Cortex* 6:571-584.
21. McIntosh AR (1998): Understanding neural interactions in learning and memory using functional neuroimaging. *Ann N Y Acad Sci* 855:556-571.
22. Mueller RO (1996): *Basic principles of structural equation modeling*. New York: Springer texts in statistics (Springer-Verlag).

limite reflète le degré d'urgence associé à la décision, c'est-à-dire le temps maximum alloué par le sujet à chaque décision. Ce type de phénomène est ubiquitaire dans les tâches de décision simple[5,28,45,62], y compris les choix économiques[30,31].

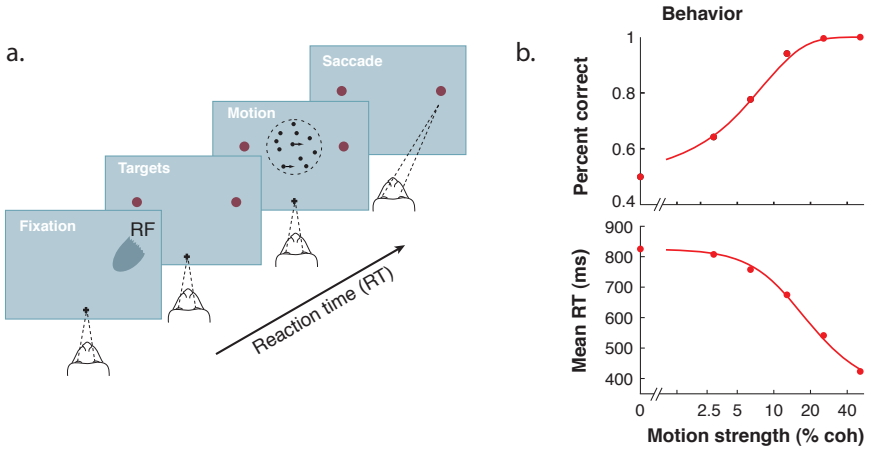

Figure 10 : Exemple de décision perceptuelle binaire. **(A)** le sujet est face à un écran, deux cibles sont affichées de part et d'autre de celui-ci. L'essai débute avec l'affichage d'un nuage de point se déplaçant aléatoirement. Une fraction des points se déplace de manière cohérente en direction d'une des cibles. Le sujet doit indiquer cette direction par une saccade oculaire vers la cible correspondante dès que possible. L'expérimentateur manipule la proportion de points se déplaçant de manière cohérente (% coh), de telle sorte que la décision est d'autant plus dure que cette proportion est faible. **(B) Panel haut :** proportion de choix en fonction du pourcentage de cohérence. **Panel bas :** temps de réaction moyen en fonction du pourcentage de cohérence. D'après Gold et Shadlen[5]

- **Arrêt du processus de décision : Réponses différées**

Dans la tâche présentée précédemment, le moment de la décision perceptuelle coïncide avec celui de la commande motrice. Il est cependant possible de dissocier ces deux phénomènes en donnant l'instruction au sujet d'attendre un signal pour indiquer son choix plutôt que de répondre dès que la décision est prise.

Si l'on continue d'afficher le stimulus et que le signal de réponse est suffisamment retardé, les SSM font alors la prédiction contre-intuitive que la probabilité d'erreur observée correspond à celle déterminée *a priori* par le seuil de décision. En d'autre terme, bien qu'il soit théoriquement possible de poursuivre l'accumulation d'évidence, le processus s'arrête au moment où la variable de décision atteint le seuil de décision indépendamment de la disponibilité d'informations supplémentaires dans

identifiant dans ces trois régions cérébrales des populations de neurones dont l'activité correspondait aux prédictions du modèle proposé par Shadlen.

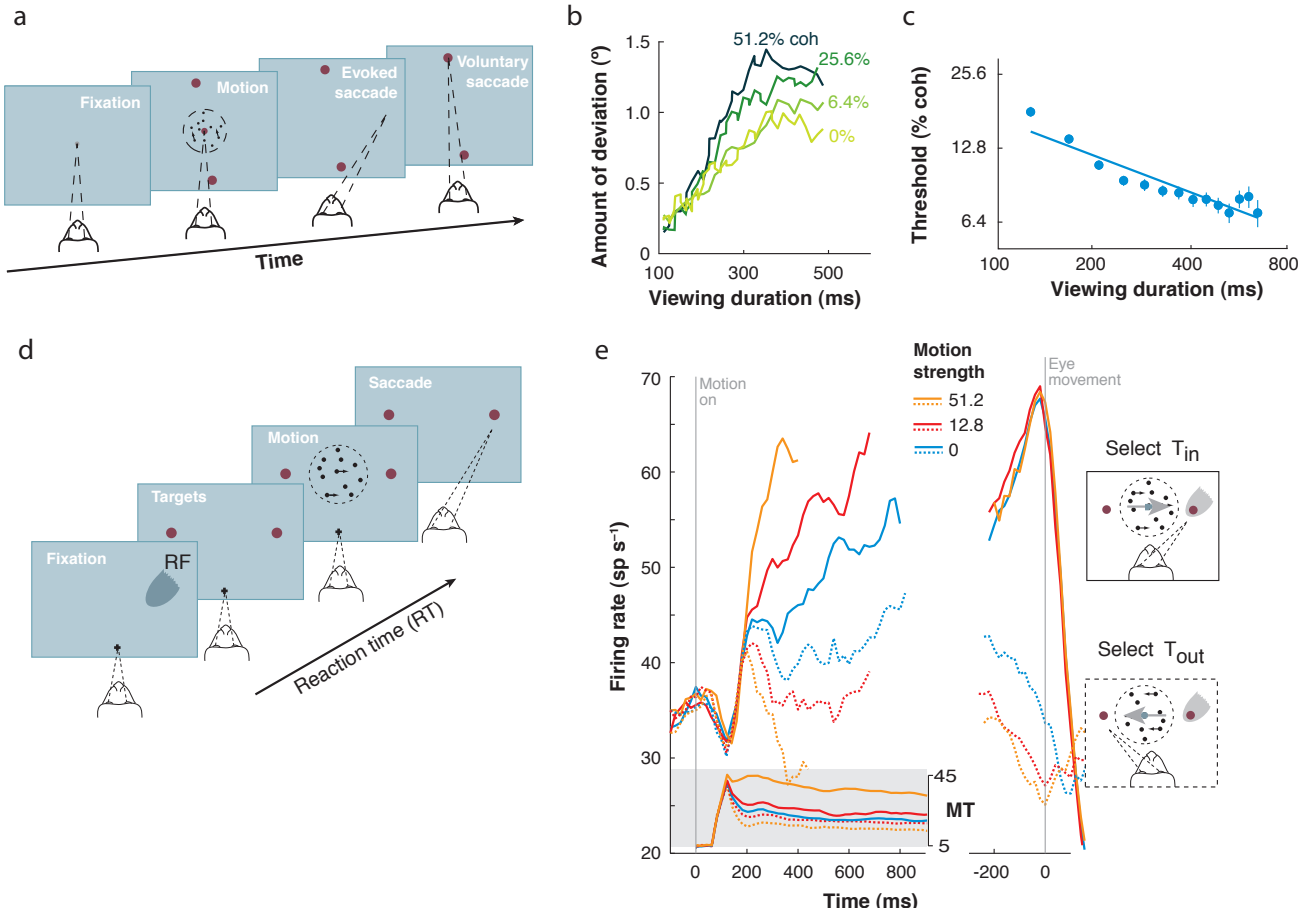

Figure 12 : (A) Le sujet est face à un écran, deux cibles sont affichées de part et d'autre de celui-ci. L'essai débute avec l'affichage d'un nuage de points se déplaçant aléatoirement. La fraction des points se déplaçant de manière cohérente est systématiquement manipulée par l'expérimentateur (% coh). Le processus de décision est interrompu par microstimulation du FEF, ce qui évoque une première saccade, suivie d'une deuxième saccade amenant le regard du singe sur une des cibles et indiquant son choix. **(B)** Déviation moyenne de la saccade évoquée en fonction de délai entre l'affichage du stimulus et la microstimulation pour les 4 niveaux de cohérences étudiés. **(C)** Cohérence évoquant 80% de réponse correcte en fonction de la durée d'affichage du stimulus. **(D)** Version « temps de réaction » du paradigme de Newsome. Le sujet doit indiquer la direction de déplacement du nuage de points par une saccade oculaire vers la cible correspondante le plus rapidement possible. L'expérimentateur manipule la proportion de points se déplaçant de manière cohérente (% coh). **(E)** Activité unitaire enregistrée dans LIP et dans MT centrée sur l'affichage du stimulus (panel gauche) et sur la réponse (panel droit). Les lignes pleines indiquent les essais aboutissant à une saccade dans le champ récepteur du neurone, alors que les lignes en pointillés indiquent les essais aboutissant à une saccade en dehors du champ récepteur. D'après Gold et Shadlen[5].

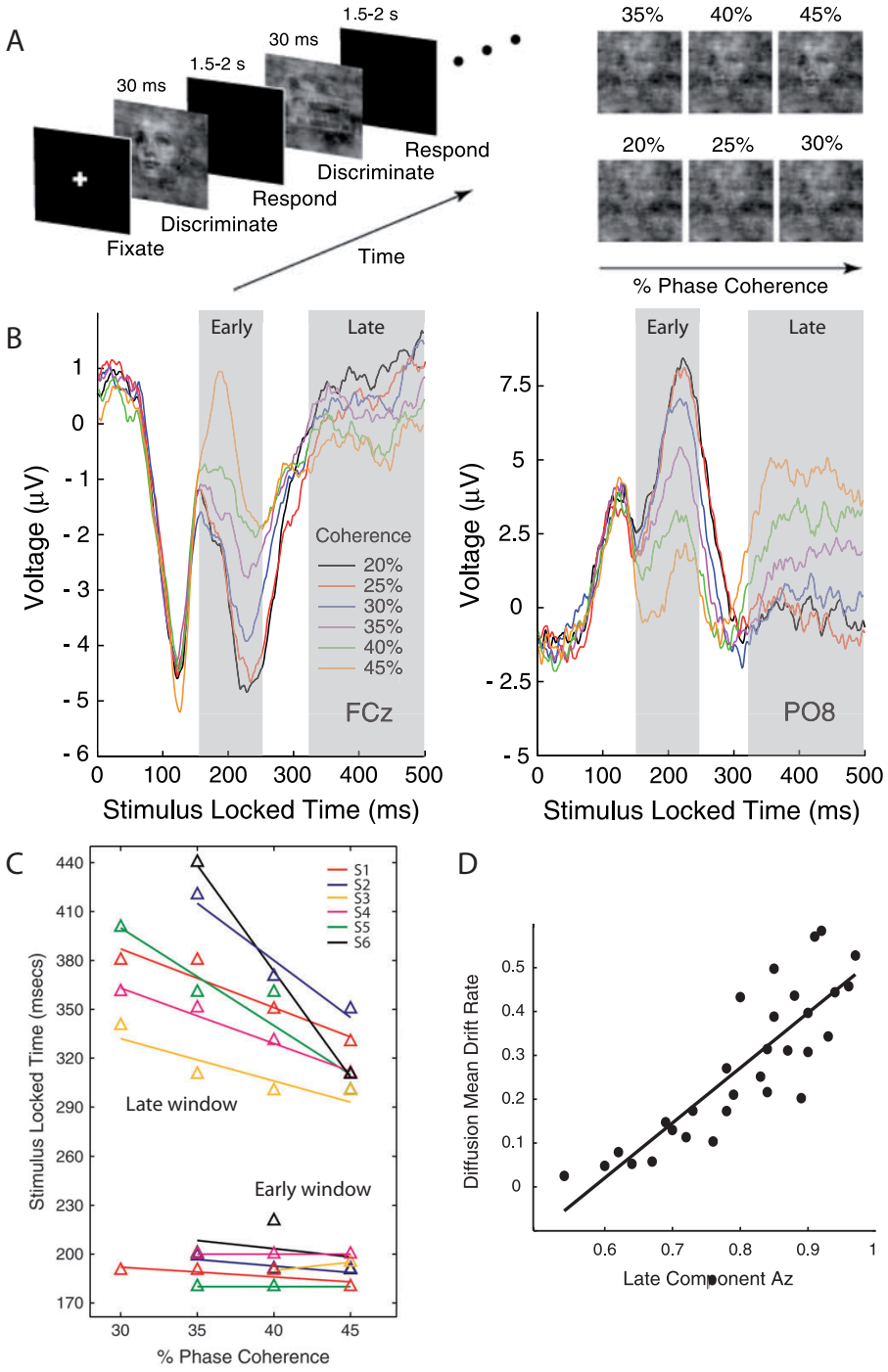

Figure 16 : (A) Paradigme de décision perceptuelle. (Panel Gauche) Une image de visage ou de voiture dont le niveau de bruit est systématiquement manipulé est présentée à un sujet. Celui-ci doit déterminer quel type d'image lui a été présenté en indiquant dès que possible sa réponse à l'aide d'un bouton réponse. **(Panel Droit)** Une image de visage à différent niveau de bruit. **(B) ERP moyen pour les électrodes FCz (Panel Gauche) et PO8 (Panel Droit) pour chaque niveau de cohérence**, indépendamment du type de stimulus ou de réponse. Les fonds grisés indiquent les composantes précoces et tardives. **(C) Latence d'apparition de la composante précoce et tardive en fonction du niveau de bruit. (D) Corrélation entre la proportion d'essais correctement prédits par le classifieur linéaire à partir de la composante tardive et vitesse de dérive du modèle de diffusion.** Chaque point correspond à un sujet et un niveau de cohérence. D'après Philiastides[103,104].

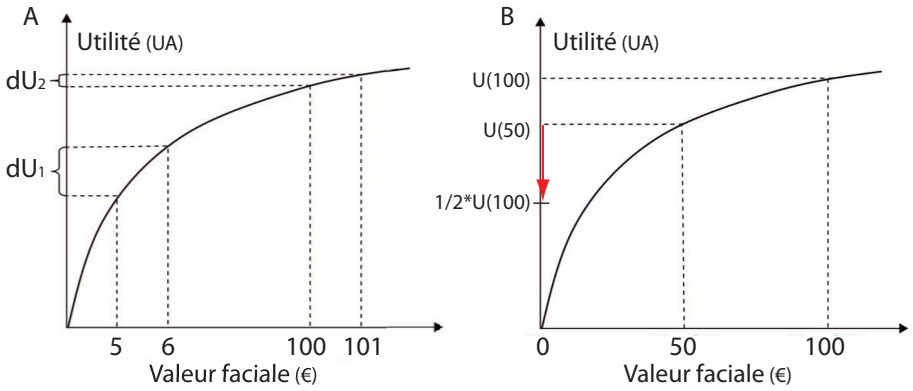

Figure 19 : Utilité en fonction de la valeur faciale du bien attendu. (A) L'utilité du gain décroit à la marge. L'utilité de 1€ est plus grande lorsqu'on a 5€ en poche (dU_1) que lorsqu'on a 100€ (dU_2). **(B) Aversion à l'incertitude.** L'utilité de 50€, U_{50}, est supérieur à l'utilité moyenne de 50% de chance d'obtenir 100€, $½*U_{100}$. En d'autre terme, l'utilité de 50€ qu'on est sûr d'obtenir est supérieure à l'utilité de 50% de chance d'obtenir 100€. Cet effet est d'autant plus prononcé que la fonction d'utilité est concave et déforme la projection des valeurs faciales dans l'espace des utilités, i.e. que son paramètre tend vers 0. D'après Glimcher[115].

Il fallut cependant attendre la première moitié du XX^{ème} siècle pour qu'une méthode de mesure des fonctions d'utilité soit proposée. La théorie de la préférence révélée de Samuelson fait l'hypothèse que, dans la mesure où les choix d'un individu se portent sur les options dont l'utilité est maximale, ceux-ci reflètent ses préférences[116,117]. L'identification de propositions équivalentes, dont les alternatives sont choisies indifféremment par le sujet, permet ainsi de mesurer la valeur relative d'offres comportant des biens de natures différentes, en quantité variable et/ou dont l'obtention est incertaine[117]. Cette approche s'enracine dans la démonstration qu'un individu ayant ordonné l'ensemble des options ouvertes au choix par utilité croissante, c'est-à-dire sur une échelle interne de valeur commune, fait des choix cohérents si ceux-ci maximisent l'utilité espérée[116]. L'articulation par Von Neumann et Morgenstern d'un ensemble d'axiomes (complétude, transitivité, continuité et indépendance des préférences révélées) à la fois nécessaire et suffisant pour que les choix d'un agent économique puissent être prédits par la maximisation de l'utilité espérée marque l'apogée de l'entreprise néoclassique dans le domaine de la théorie de la décision[118], Von Neumann et Morgenstern aboutissant à une définition formelle et normative de la rationalité intégrant les théories de l'utilité attendue et des préférences révélées.

En effet, l'identification de situations décisionnelles durant lesquelles les axiomes de Von Neumann et Morgenstern n'étaient pas respectés amena progressivement

certains économistes à se tourner vers d'autres disciplines, comme la psychologie, pour expliquer ces comportement paradoxaux[115]. Ainsi, la théorie des perspectives (« *prospect theory* ») revisite le concept d'utilité attendue de Von Neumann et Morgenstern pour mieux rendre compte de la construction et de la représentation des valeurs subjectives guidant le choix en introduisant de nombreuses modifications de sa fonction d'utilité[115,119,120] (Fig. 20) : (1) Les enjeux d'une décision risquée sont perçus en termes de gains et de pertes, définis relativement à un cadre de référence subjectif (*status quo*), (2) la fonction de liaison entre les valeurs faciales et les valeurs subjectives (concept se substituant à l'utilité) sont différentes dans le domaine des gains et des pertes. La pente à l'origine de la fonction de valeur subjective est deux fois plus importante en moyenne pour les pertes que pour les gains, induisant une asymétrie dans leurs représentations subjectives qui se traduit comportementalement par une sensibilité accrue aux pertes[119,120]. De plus, la fonction est concave dans le domaine des gains, ce qui induit une aversion au risque, alors qu'elle est convexe dans le domaine des pertes, induisant l'effet inverse, (3) finalement, les probabilités influencent la décision au travers d'une représentation subjective qui surévalue les poids des événements rares et sous-évalue les évènements fréquents.

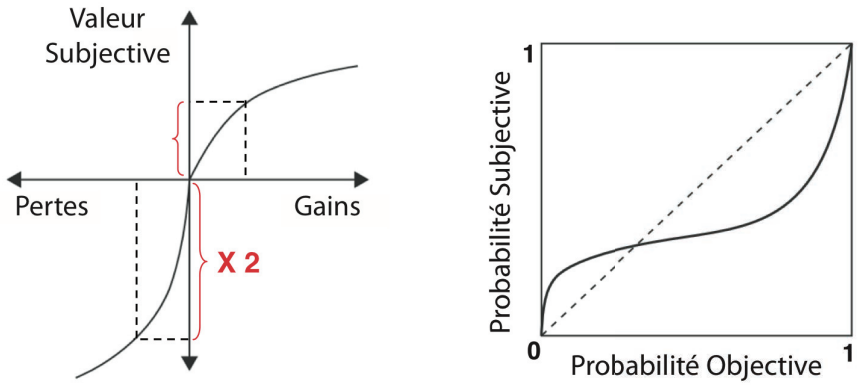

Figure 20 : Représentation des valeurs et des probabilités dans la théorie des perspectives. (Panel gauche) Valeur subjective en fonction de la valeur faciale des gains et pertes potentielles. (Panel droit) Probabilités subjectives en fonction des probabilités objectives. D'après Kahneman et Tversky[120].

La plupart des théories économiques de la décision, de la théorie de l'utilité espérée[118] à la théorie des perspectives[120], au même titre que les théories d'apprentissage par renforcement issues des travaux en intelligence artificielle[121],

Approche neuroéconomique des décisions basées sur les valeurs subjectives en condition d'incertitude.

- **Système dopaminergique : Apprentissage et prédiction de la valeur subjective des choix**

Dans les années 1990, une série d'études électrophysiologiques portant sur le conditionnement opérant montra que l'anticipation ou la réception de récompense était associée à une augmentation phasique de l'activité neurale dans 60 à 80% des neurones dopaminergiques[127-129]. Cette augmentation d'activité était également retrouvée au niveau de leurs cibles ; striatum, amygdale, cortex orbito-frontal et cortex cingulaire antérieur. Ensemble, ces structures constituent le « système de récompense »[127-129].

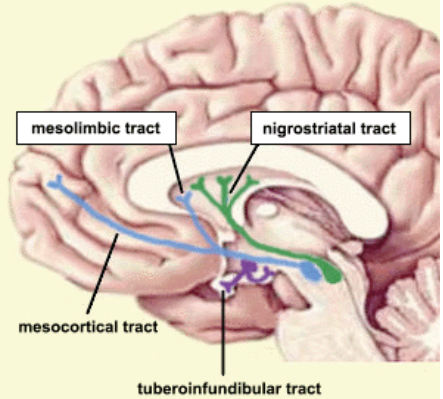

Figure 22 : Principaux faisceaux ascendants de projections des noyaux dopaminergiques mésencéphaliques. Les neurones dopaminergiques sont regroupés au sein de deux noyaux mésencéphaliques : l'aire tégmentale ventrale et la substance noire *pars compacta,* qui constituent les points de départ respectifs des voies ascendantes neuromodulatrices dites méso-cortico-limbique (bleue) et nigro-striée (vert).

Les caractéristiques électrophysiologiques des neurones dopaminergiques suggèrent cependant une fonction plus complexe que la simple détection de stimuli hédoniques. En effet, on observe une augmentation de l'activité phasique dopaminergique lors de l'obtention d'une récompense inattendue (Fig. 23A), une absence de réponse lorsqu'une récompense prédite avec certitude est reçue (Fig. 23B), et une inhibition phasique de leur activité lorsqu'une récompense prédite est omise[130,131] (Fig. 23C). Ce profil de réponse est évocateur d'un signal d'erreur de prédiction (noté δ, Fig. 24 et Eq. 9), c'est à dire d'une représentation de la différence entre ce qui était attendu (V_t) et ce qui est obtenu (Q_t).

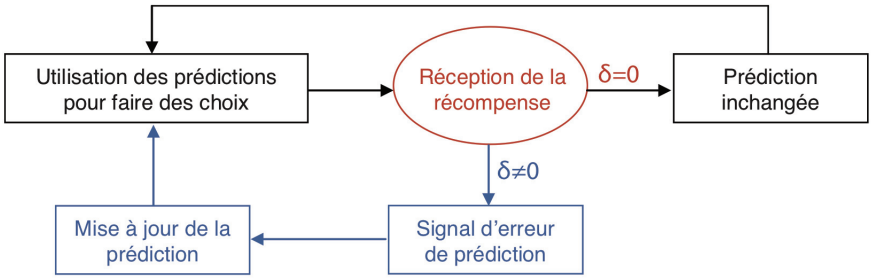

Figure 24 : Algorithme d'apprentissage par renforcement (Eq. 9).

Du point de vue de l'apprentissage par renforcement, l'activité phasique dopaminergique évoquée par l'apparition du stimulus conditionnel prédit la valeur de la récompense à venir, tandis que l'activité au moment de l'obtention de la récompense signale l'erreur de prédiction. Confirmant cette hypothèse, des études électrophysiologiques complémentaires ont montré, qu'après conditionnement, l'activité dopaminergique à l'affichage du stimulus prédictif était proportionnelle à la valeur de la récompense espérée, c'est-à-dire au produit de la quantité et de la probabilité de récompense[133,134] (Fig. 25A). De plus, l'activité phasique à la réception de la récompense est proportionnelle à la quantité de fluide obtenue comme récompense au début de l'apprentissage [134] (Fig. 25B). En revanche, après conditionnement, l'activité phasique suivant la réception d'une récompense diminue linéairement avec la probabilité de récompense reflétant ainsi la différence entre la valeur prédite et la valeur de la récompense reçue[131,133]. L'enregistrement direct de signaux d'erreur de prédiction dans la substance noire par enregistrements cérébraux profonds a récemment confirmé l'existence de ces signaux dopaminergiques d'erreur de prédiction chez l'Homme[135] (Fig. 25C et D).

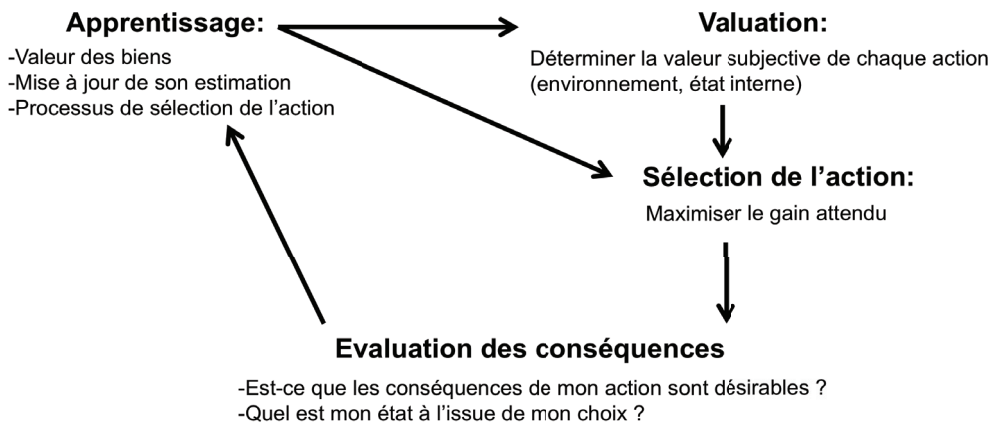

Figure 26 : Représentation schématique des étapes nécessaires à la prise de décision basée sur les valeurs subjectives lorsque les valeurs des options doivent être apprises par renforcement.

- **Le cortex orbito-frontal : Une structure tournée vers les valeurs subjectives**

Depuis le célèbre cas clinique de Phineas Gage (1823-1860), un employé des chemins de fer dont la personnalité s'était radicalement modifiée à la suite d'un accident ayant endommagé son cortex orbito-frontal (OFC), l'étude neuropsychologique de cohortes de patients lésés dans l'OFC a confirmé l'importance de cette région cérébrale dans la formation des choix basés sur les valeurs subjectives[137]. En effet, alors que l'évaluation neuropsychologique de ces patients ne révèle pas d'anomalies (QI, épreuves de Wisconsin et de la tour de Londres), ces patients se comportent de manière inadaptée et irresponsable, persévèrent dans leur échecs jusqu'à la ruine, et échouent à se conformer aux règles sociales, bien qu'ils les connaissent, jusqu'au rejet par leur entourage. Ce profil comportemental est aujourd'hui interprété comme une incapacité à prendre en compte et à réviser la valeur subjective attribuée aux alternatives d'un choix lorsque les règles d'associations entre action et conséquences ne sont pas explicites[137].

En effet, l'OFC est une région multimodale recevant des afférences de l'ensemble des cortex sensoriels[129,137,138], ainsi qu'un grand nombre de terminaisons dopaminergiques par la voie ascendante méso-cortico-limbique. Il est donc idéalement placé pour intégrer les différentes dimensions formant la valeur d'une expérience et les signaux dopaminergiques de prédiction de la valeur et d'erreur de prédiction (Fig. 27).

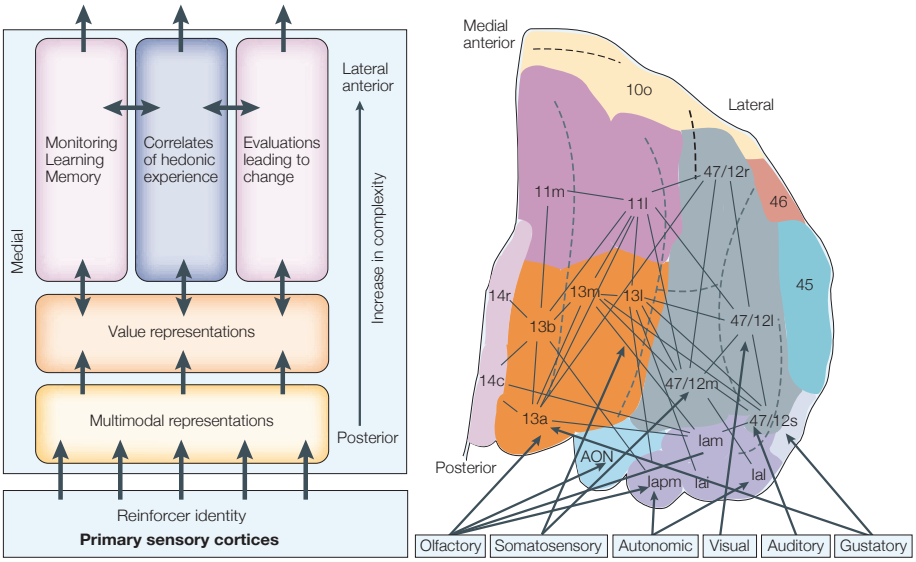

Figure 27 : (A) Modèle d'interactions entre systèmes sensoriels et système de récompense dans l'OFC. (B) Connectivité fonctionnelle au sein de l'OFC : Les informations sensorielles émanant des cortex sensoriels entrent dans l'OFC par sa part caudale. Celle-ci fait l'objet d'une intégration multimodale progressive permettant l'émergence d'une représentation centrée sur la valeur des biens et des expériences. D'après Kringelbach[139].

Chez l'Homme, de nombreuses études en IRMf suggèrent que l'OFC implémente une représentation intégrée et dynamique des valeurs subjectives[137,138]. Ainsi, l'activité cérébrale dans l'OFC corrèle avec la valeur subjective associée à une grande variété d'expériences, tel que le plaisir ressenti lors de la consommation de nourriture dont la texture, la température, l'arôme ou la marque sont manipulés[138,140] (Fig. 28B-C). Cette activité est dynamiquement ajustée : ainsi, plusieurs expériences sur la satiété montrent une extinction graduelle de l'activité cérébrale évoquée dans l'OFC par la consommation de nourriture au fur et à mesure que la faim disparaît[138]. De plus, l'OFC semble représenter sur un axe antéropostérieur les récompenses primaires, dont la valeur hédonique est immédiatement perceptible et les récompenses secondaires, dont le caractère hédonique dérive secondairement des récompenses primaires qu'il permet d'obtenir[141] (Fig. 28A). Lors de tâche de conditionnement, les neurones orbito-frontaux génèrent un signal d'anticipation de la récompense dont l'intensité reflète les préférences révélées par le singe lors de choix libres entre les différents types de récompense possible[142] (Fig. 29). L'activité de ces neurones augmente lorsque l'expérience anticipée est positive, et diminue dans le cas inverse, en fonction de l'intensité de l'expérience anticipée[143].

Behavioral/Systems/Cognitive

Decision Threshold Modulation in the Human Brain

Philippe Domenech and Jean-Claude Dreher
Cognitive Neuroscience Center, Reward and Decision-Making Group, Centre National pour la Recherche Scientifique, Unité Mixte de Recherche 5229, 69675 Bron, France and Université Lyon 1, 69003, Lyon, France

Perceptual decisions are made when sensory evidence accumulated over time reaches a decision threshold. Because decisions are also guided by prior information, one important factor that is likely to shape how a decision is adaptively tuned to its context is the predictability of forthcoming events. However, little is known about the mechanisms underlying this contextual regulation of the perceptual decision-making process. Mathematical models of decision making predict two possible mechanisms supporting this regulation: an adjustment of the distance to the decision threshold, which leads to a change in the amount of accumulated evidence required to make a decision, or a gain control of the sensory evidence, leading to a change in the slope of the sensory evidence accumulation. Here, we show that predictability of the forthcoming event reduces the distance to the threshold of the decision. Then, combining model-driven fMRI and the framework of information theory, we show that the anterior cingulate cortex (ACC) adjusts the distance to the decision threshold in proportion to the current amount of predictive information and that the dorsolateral cortex (DLPFC) codes the accumulation of sensory evidence. Moreover, the information flow from the ACC to the DLPFC region that accumulates sensory evidence increases when optimal adjustment of the distance to the threshold requires more complex computations, reflecting the increased weight of ACC's regulation signals in the decision process. Our results characterize the respective contributions of the ACC and the DLPFC to contextually optimized decision making.

Introduction

Recent advances in neuroscience and mathematical psychology have begun to unravel the neurobiological mechanisms underlying decision making (Gold and Shadlen, 2007). Perceptual decision making, the ability to select a specific action based on our perception, proceeds from the integration of sensory evidence to a categorical choice between alternatives (Smith and Ratcliff, 2004; Lo and Wang, 2006; Bogacz, 2007a). In sequential sampling models, this gradual gathering of sensory information favoring a particular choice is defined as a drift of an abstract decision variable toward a decision threshold. A choice is made when a decision variable is equal to its decision threshold (Carpenter and Williams, 1995; Hanes and Schall, 1996; Usher and McClelland, 2001). These mathematical models of decision making received renewed interest after the demonstration by monkey electrophysiological studies that perceptual choices are made when the ramping activity of neural populations in the dorsolateral prefrontal cortex (DLPFC) and the lateral intraparietal (LIP) area reaches a given threshold (Hanes and Schall, 1996; Kim and Shadlen, 1999; Huk and Shadlen, 2005; Hanks et al., 2006). The ramping rate of this neural activity, which represents the accumulation of sensory evidence, correlates with the decision variable predicted by sequential sampling models. In humans, fMRI studies confirmed the involvement of a similar DLPFC–intraparietal network in coding the decision variable (Heekeren et al., 2004; Forstmann et al., 2008; Ivanoff et al., 2008; Tosoni et al., 2008; van Veen et al., 2008).

One important factor that is likely to shape how a decision is adaptively tuned to its context is the predictability of the forthcoming event (Luce, 1991; Dayan and Abbott, 2001; Harrison et al., 2006; Doya, 2008). However, it remains unclear how decision making is modulated by this predictive information at both the behavioral and the neural levels. Sequential sampling models predict two mechanisms that modulate the decision based on contextual information (Carpenter and Williams, 1995; Reddi et al., 2003): (1) An adjustment of the distance to the decision threshold, which leads to a change in the amount of evidence required to make a decision, but no variation in the slope of the decision variable. According to this mechanism, higher predictability of forthcoming events would reduce the distance to the decision threshold (Fig. 1*a*, top panels). (2) An adjustment of the gain of sensory evidence, leading to a change in the slope of the decision variable, but not in the distance to the threshold. According to this hypothesis, higher predictability would increase the slope of the decision variable (Fig. 1*a*, bottom panels).

Here, we manipulated the amount of contextual information available to predict which stimulus is going to appear next (Fig. 1*b*). This allowed us to distinguish between these two hypotheses by characterizing the computational mechanisms underlying the effect of predictability on decisions. Then, having found that predictability modulates the distance to the threshold of the decision and not the gain control of sensory evidence, we identified the brain regions involved in this reg-

Received May 9, 2010; revised Aug. 15, 2010; accepted Aug. 23, 2010.

This work was funded by a FP6 International reintegration grant and a Fyssen Foundation grant to J.-C.D. P.D. was supported by a French Ministry of Research scholarship and a fellowship from Le Vinatier Hospital (CSRA 05). We thank the CERMEP - Imagerie du Vivant staff for their helpful assistance and Dr. C. Summerfield and E. Koechlin for comments on an early version of the manuscript.

Correspondence should be addressed to Philippe Domenech, Cognitive Neuroscience Center, Reward and Decision-Making Group, 67 Bd Pinel, 69675 Bron, France. E-mail: pdomenech@isc.cnrs.fr.

DOI:10.1523/JNEUROSCI.2371-10.2010

 0270-6474/10/3014305-13$15.00/0

ulation, as well as those coding the decision variable. Finally, we investigated how changes in effective connectivity between these distributed brain regions lead to contextually optimized perceptual decisions.

Materials and Methods

Subjects. Fourteen healthy right-handed subjects [8 males, mean age (±SD): 25.14 ± 3.37 years, mean right-handedness score as estimated by the Edinburgh scale (±SD): 0.86 ± 0.1, mean level of higher education (±SD): 3.6 ± 2.2 years] participated in the study (Oldfield, 1971). None of the participants showed any past or current neurological or psychiatric conditions, as assessed by a medical interview and all had normal or corrected-to-normal visual acuity. None of them was on medication at the time of the study. The experiment was approved by the local ethics committee. Subjects gave their written informed consent and underwent standard medical exams before participation.

Perceptual decision-making paradigm. Participants performed a GO/NO-GO task, in which they had to press a response button for a specific target shape (presented at the beginning of each sequence) among three possible shapes (Fig. 1*b*). Each participant performed the perceptual decision task on 12 randomly ordered unique sequences. All sequences consisted of the successive presentation of blue shapes (circle, square, or triangle) displayed at the center of a screen. At the beginning of each new sequence, the participant was shown one of the three shapes on a yellow background. This shape was the target for the current sequence. After 5 s of target display, the background turned black and the perceptual decision task began. Participants were instructed to press a response button held in their right hand each time they identified the current target, as quickly and as accurately as possible. Each sequence was composed of 400 successive stimuli presented for 300 ms every 400 ms (Fig. 1*b*). A fixation cross was presented for 10 s between two successive sequences. Unbeknownst to participants, there were two types of sequences (Fig. 1*b*): in first-order sequences, the next shape was conditioned on the last shape, whereas in second-order sequences, the next shape was conditioned on the last two shapes. Figure 1*c* shows a set of transition rules for a first-order sequence. Using the framework of Shannon's information theory, we computed for each decision the surprise (Eq. 1), which measures how unlikely an event is, and the predictive information on the forthcoming stimulus (Eq. 2–3), which measures how much the knowledge of the recent history (last shape or penultimate shape) reduces this surprise. Statistical transition rules were held constant within a sequence and varied between sequences. Moreover, both first- and second-order sequences were selected to fall into three categories based on their mutual information (first-order sequences: Eq. 4; second-order sequences: Eq. 5): zero (low), one-third (medium), and two-thirds (high) of the maximum theoretical mutual information (with a tolerance margin of 5%, Eq. 6). This procedure guaranteed a broad range of predictive information values during the experiment.

To minimize potentially confounding effects classically observed during sequential choices, statistical transition rules were constrained to ensure a low repetition probability ($p_{\text{repetition}} < 0.05$) and to minimize tandem repeats in sequences (Kornblum, 1969). Moreover, the pace of perceptual decisions was chosen in accordance with the psychophysical literature, which shows that the behavioral effect of surprise on response time (RT) is minimized when repetition probability is low and the interval between two perceptual decisions is short (Kornblum, 1969) and was further adjusted to guarantee a high level of accuracy (>90%). Sequences were selected to ensure average frequencies in the 0.05–0.45 range for each stimulus, thus controlling for oddball effect (Ranganath and Rainer, 2003) by ensuring that sequences did not contain rare events. All stimuli occurred with the same probability over the whole experiment. Finally, for each sequence, we selected the most sparsely distributed shape in the range 0.25–0.4 as the target. At the end of the scanning session, participants were systematically asked about "their awareness of regularities" as in Harrison et

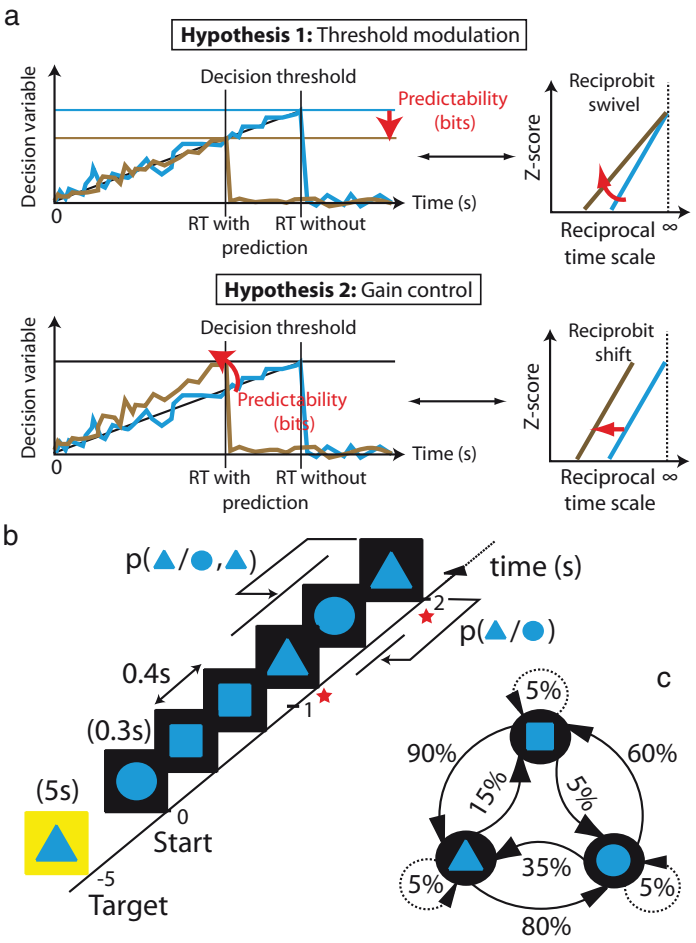

Figure 1. Hypothetical mechanisms by which predictability of forthcoming events modulates the decision-making process. ***a***, Left panels illustrate the progressive drifts of decision variables toward their respective decision threshold. They also correspond to the activity predicted by the decision model for neural populations accumulating sensory evidence. A decision is made when a decision variable equates its threshold. Right panels illustrate how the reciprobit analysis of RT distributions reveals distinct regulatory mechanisms of the decision process. Threshold modulation hypothesis: Reciprobit lines swivel toward lower RT when predictability increases (top right panel), reflecting the lowering of the decision threshold (top left panel). Gain control hypothesis: Reciprobit lines shift toward lower RT when predictability increases (bottom right panel), reflecting the faster rise of the decision variable toward the decision threshold (bottom left panel). ***b***, Task design. Participants had to identify a target shape out of three shapes by pressing a response button (red stars, ISI = 1.35 ± 0.76 s SD). Unbeknownst to the subjects, the next shape could be predicted on the basis of recent history. In first-order sequences, only the last trial had a predictive value on the next shape, whereas in second-order sequences, both the last and the penultimate trials had a predictive value on the next shape. ***c***, Example of a set of transition rules from a first-order sequence. Arrows represent transitions from one shape to the next one and transition probabilities are indicated nearby each arrow.

al. (2006). Only one subject reported he had noticed a pattern, once, during the experiment but could not give a specific example.

Working hypothesis. Bayesian formulations of perceptual decision making distinguish between the prior information (before observing the stimulus) and the accumulation of evidence in term of likelihood (during stimulus observation). In these formulations, the quantity accumulating evidence starts at different levels, according to the prior information. Evidence is then accumulated at a constant rate until the criterion is reached. In the context of our design, before the stimulus arrives, the predictive information (prior beliefs) will reset the level of activity and therefore change the distance to the decision threshold. From this perspective, the predictive information is a prior and the information conveyed by the stimulus represents the evidence entailed by its likelihood. Thus, our hypothesis was that both behavioral and fMRI data would be better explained by an adjustment of the distance to the decision threshold in proportion to the predictive information on the forthcoming stimulus than by a modulation of the slope of the decision variable.

Note that in our paradigm, we kept the level of sensory information constant (by using exactly the same three stimuli across the experiment). This does not mean that what is being integrated in the current paradigm is not sensory evidence. Indeed, perceptual decisions occur even when visual categorization may appear "unambiguous" while monkeys make saccades toward a target. For example, frontal eye field and lateral prefrontal cortex neurons exhibit a ramping activity that decrease after reaching a threshold value (Kim and Shadlen, 1999), both when manipulating the position (Hanes and Schall, 1996) or the color (Stanford et al., 2010) of unambiguous targets.

Thus, although information about local stimulus-response predictability is manipulated in the current study, it is not "integrated" over the decision process (what is being integrated is still sensory evidence). This approach mixing local stimulus-response predictability and perceptual decision making distinguishes our study from the neuroimaging literature investigating which brain regions encode measures of information theory, such as surprise and uncertainty (Huettel et al., 2005; Strange et al., 2005) or their influences on EEG components or corticospinal excitability (Bestmann et al., 2008; Mars et al., 2008).

Estimates of surprise and predictive information. In Shannon's information theory, the surprise of an event is defined by the current estimate of its marginal log-probability (abbreviated as u_t in Eq. 1). This measure has been considered as an instantaneous measure of the level of saliency (Harrison et al., 2006). For each new shape e_t, displayed at time step t, the current estimate of the surprise (u_t) is defined in the following way:

$$u_t(e_t = i) = -\log_2(\text{prob}_t(e_t = i)). \quad (1)$$

The predictive information of the upcoming event is an instantaneous measure of the loss of uncertainty about its occurrence due to the knowledge of the previous event(s) (also called "surprise reduction"). This last measure quantifies the amount of information available at a given time to predict the outcome of the ongoing perceptual decision and is poorly correlated with the surprise (a high level of predictive information does not necessarily mean that surprise is low). We computed both the predictive information conveyed by the last event (abbreviated as $p_{1,t}$ in Eq. 2) and by the last two events (abbreviated as $p_{2,t}$ in Eq. 3). For each new shape e_t, displayed at the time step t, current estimates of the predictive information ($p_{1,t}$ and $p_{2,t}$) are defined in the following way:

$$p_{1,t}(e_t = i, e_{t-1} = j) = \log_2\left(\frac{\text{prob}_t(e_t = i | e_{t-1} = j)}{\text{prob}_t(e_t = i)}\right) \quad (2)$$

$$p_{2,t}(e_t = i, e_{t-1} = j, e_{t-2} = k) = \log_2\left(\frac{\text{prob}_t(e_t = i | e_{t-1} = j, e_{t-2} = k)}{\text{prob}_t(e_t = i)}\right). \quad (3)$$

Supplemental Figure S1 (available at www.jneurosci.org as supplemental material) illustrates the trial-to-trial fluctuations of the predictive information conveyed by the last (Eq. 2) and by the last two (Eq. 3) shapes over the course of two exemplary sequences.

The average predictive information over a whole sequence of events is called the mutual information. By analogy with the predictive information, we computed the mutual information conveyed by the last event (abbreviated as $\text{Im}_{1,t}$ in Eq. 4) and by the last two events for each sequence (abbreviated as $\text{Im}_{2,t}$ in Eq. 5). Mutual information is maximum when a sequence is entirely determined (abbreviated as $\text{Im}_{\max}$ in Eq. 6). It is noteworthy that predictive information is an event-bound measure, whereas mutual information pertains to the average predictability in a sequence without relating to any specific event.

$$\text{Im}_{1,t} = \underset{t,i}{E}(p_{1,i}) \quad (4)$$

$$\text{Im}_{2,t} = \underset{t,i}{E}(p_{2,i}) \quad (5)$$

$$\text{Im}_{\max} = \log_2(k), \quad (6)$$

where k is the number of different shapes in a sequence.

Because participants learned the statistical structure of the sequence as stimuli were presented, we used a simple Bayesian learning scheme (an ideal Bayesian observer), in which all marginal and conditional probability estimates were updated after each new event. Our ideal Bayesian observer was initialized with flat prior distributions and was reset at the beginning of each new sequence to account for the lack of prior knowledge on the upcoming sequence (Harrison et al., 2006). For each new shape e_t, presented at time step t, current values of the marginal probability of the event i (Eq. 7) and of the joint probability of two successive events i and j (Eq. 8) and of three consecutive events i, j, and k (Eq. 9) are defined in the following way:

$$\text{prob}(e_t = i) = \frac{n_i^t + 1}{\sum_i n_i^t + 1} \quad (7)$$

$$\text{prob}(e_t = i, e_{t-1} = j) = \frac{n_{i,j}^t + 1}{\sum_{i,j} n_{i,j}^t + 1} \quad (8)$$

$$\text{prob}(e_t = i, e_{t-1} = j, e_{t-2} = k) = \frac{n_{i,j,k}^t + 1}{\sum_{i,j,k} n_{i,j,k}^t + 1}, \quad (9)$$

where $n_{i,j,k}^t$ is the number of triplets i, j, k at time step t; and $n_{i,j}^t$ is the number of duplets i, j at time step t.

We computed the surprise (Eq. 1) and the predictive information (Eqs. 2, 3) at each time step using the estimates provided by Equations 7–9.

Multilinear model of response times. Behavioral analyses were performed using the software packages R and Statistica (v7.1). We defined the error rate as the number of missed targets divided by the total number of targets over each sequence. Response times were calculated as the time elapsed between the onset of a target and the subject's response.

First, we searched for the best multilinear model of the observed RT using a descending strategy. The error rate, the surprise, the predictive information conveyed by the last shape and by the last two shapes (abbreviated respectively as p_1 and p_2), as well as all the first-order interactions between these explanatory variables were included in the "full" model. Akaike information criterion was minimized after the surprise and all first-order interactions were removed from the "full" model ($\beta_{\text{surprise}} = -0.015$, $p = 0.126$).

$$\text{RT} = \beta_0 + \beta_{p1} \times p1 + \beta_{p2} \times p2 + \beta_{\text{error rate}} \times (1 - \text{error rate}) + \varepsilon. \quad (10)$$

In the reduced behavioral model (Eq. 10), RTs are modeled as a weighted sum of explanatory variables in which the standardized parameter estimates of the model, such as β_{p1} and β_{p2}, are referred to as "behavioral" sensitivity because they represent the slope between response times and the amount of predictive information conveyed by the last and the penultimate shape. So, estimated βs correspond to the independent

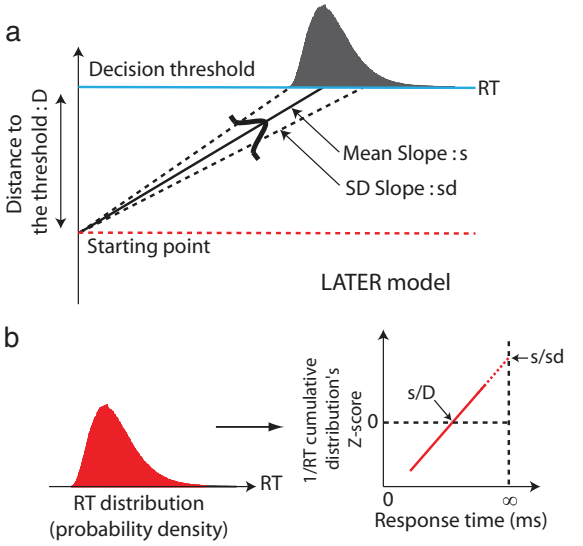

Figure 2. LATER model. ***a***, When a stimulus is presented, a decision signal rises linearly from the starting point (dashed red line) with an average slope *s* and a trial-to-trial standard deviation sd. When the signal reaches the decision threshold, a motor response is initiated. In the model, the amount of sensory evidence needed to reach a decision is represented by the difference between the starting point and the decision threshold, representing the distance to the threshold *D* (Reddi and Carpenter, 2000). ***b***, Relationship between RT distributions, reciprobit plots, and LATER model parameters. The reciprobit plot represents the cumulative 1/RT distribution, linearized by computing *z*-scores (probit transformation), as a function of RT. This graphical representation of RT distribution has two important features: (1) the intercept with the $x = \infty$ line solely depends on the mean slope of the decision process and is equal to *s*/sd; (2) the intercept with the $y = 0$ line is *s*/*D* (which depends on both the slope and the distance to the threshold).

contribution of each explanatory variable to the prediction of RT. This multilinear model is consistent with the relationship predicted by sequential sampling models of decision in which error rate and response times depend on the amount of predictive information available, while keeping the level of sensory information constant across trials. Note that, by construction of our design, there was no predictive information conveyed beyond the penultimate event available to predict the forthcoming event.

LATER model: how RT distributions are used to distinguish between the two modulation mechanisms of the decision process. In the LATER (linear approach to threshold with ergodic rate) model (Carpenter and Williams, 1995; Reddi and Carpenter, 2000; Reddi et al., 2003), the onset of a stimulus (e.g., a shape) is followed by the linear rise of a signal (decision variable) from a starting point (red dashed line) to a decision threshold *D* (Fig. 2*a*, blue line). A response is initiated when the decision signal reaches the threshold. On different trials, the slope of the decision signal varies randomly, but is distributed as a Gaussian probability density function with mean slope *s* and with standard deviation sd (Hanes and Schall, 1996). So, according to the LATER model, the distribution of RT reflects the projection of the decision variable on the decision threshold and depends on three parameters: the distance to the threshold (difference between the starting point and the decision threshold), the mean slope, and its standard deviation (as stated in Eq. 11 and Fig. 2).

Equation 11 simply expresses that, under the LATER model, the main decision process yield 1/RT following a normal distribution, with mean s/D and with standard deviation sd^2/D^2. In addition, fast guesses are modeled as an additional normal distribution, whose mean is equal to zero, and its own standard deviation.

$$1/\mathrm{RT} \rightarrow N\left(\frac{s}{D}, \frac{\mathrm{SD}^2}{D^2}\right). \quad (11)$$

Since 1/RT of the main process is normally distributed (Eq. 11), it is possible to compute *z*-scores that express the divergence of the observed 1/RT from the median 1/RT. Plotting *z*-scores of 1/RT's cumulative distribution against RT plotted on a reciprocal time axis yields a straight line, which is called a reciprobit plot (as illustrated in Fig. 2*b*). This graphical representation is useful because the resulting line intersects *z*-score = 0 at the median latency *s*/*D*, which depends on both the mean slope (*s*) and the distance to the threshold (*D*), whereas it intersects RT = ∞ at a point that does not vary with the distance to the decision threshold (Fig. 2*b*). Importantly, the mathematical properties of the reciprobit transformation provide us with a graphical representation that distinguishes between the two modulation mechanisms in the LATER model (see Fig. 1*a*): (1) if the modulation mechanism is an increase of the slope (sensory evidence gain control), then both intersects will vary in the same proportion and the line will shift (Fig. 1*a*, lower right panel); and (2) if the modulation mechanism is a decrease of the decision threshold, then only the *z*-score = 0 intersect will vary, which will result in a swivel of the reciprobit line around the RT = ∞ intersect (Fig. 1*a*, upper right panel).

To summarize, the reciprobit transformation directly allows us to derive the *z*-scores of 1/RTs cumulative distribution from the RT distribution. From these *z*-scores, it is then possible to estimate the parameters of the LATER model (distance to the decision threshold, mean slope, and sd of the slope) that best fit the data and to perform a Bayesian statistical test to identify the mechanisms of regulation that best explain the changes between conditions (decision threshold modulation or gain control of the sensory evidence).

Psychophysics: LATER model and reciprobit plots. To assess the mechanism underlying the effect of predictive information on decision, we performed a standard reciprobit analysis (Carpenter and Williams, 1995; Reddi et al., 2003).

First, we normalized each participant RT dataset to the population's average and standard deviation. Then, we pooled all the RT datasets together and collapsed the behavioral data from first- and second-order sequences using the optimal amount of predictive information. Next, we discretized each participant RT dataset into equal bins and excluded from further analysis those that did not contain enough data to allow for reliable fits of the decision model. This constraint led us to exclude the 5% lowest predictive information values from further analyses. This is because, in our experiment, the distribution of predictive information had a long tail toward low values. By the end of these preprocessing steps, we had sorted RT data into 6 bins with continuously increasing levels of predictive information ([−0.43, −0.05, 0.25, 0.62, 1, 1.32] bits).

Then, we performed a reciprobit transformation on the resulting RT distributions. This transformation is based on the LATER model and makes testable predictions about how RT distributions should change according to two different modulation mechanisms: distance to the decision threshold or sensory evidence accumulation rate (Carpenter and Williams, 1995; Gold and Shadlen, 2007) (Fig. 1*a*). Plotting the reciprobit lines, which are linearized cumulative RT distributions plotted on a reciprocal time scale, highlights those changes.

In addition to this qualitative assessment of the mechanism regulating the decision process, we used a Bayesian model selection strategy to identify the regulation mechanism that most likely explained the changes observed in RT distributions across levels of predictive information. To do so, we fitted a LATER model using a standard simplex minimization routine and a likelihood-based cost function under the hypotheses that changes in RT distribution either resulted from changes in the sensory evidence accumulation rate or resulted from changes in the distance to the threshold. Model comparison was performed by fitting the LATER model for each experimental condition in such a way that either the slope or the distance to the decision threshold was fixed across condition, depending on the hypothesis tested. Finally, we computed the log likelihood ratio between the two hypotheses ($L_{\mathrm{DT}} - L_{\mathrm{Gain}}$, difference between the log likelihood of the distance to the threshold modulation, L_{DT}, and the log likelihood of the gain control mechanism, L_{Gain}) and used the cutoff value of the Bayesian factor ($L_{\mathrm{DT}} - L_{\mathrm{Gain}} \geq 2.3$) (Jeffrey, 1998) to assess the significance level of our result. For example, a log likelihood ratio equal to 4.6 indicates that a modulation of the distance to the

threshold is 100 times more likely than a gain control of the sensory evidence ($e^{4.6} = 100$).

To assess whether our finding that predictive information modulates the decision threshold depended on some specific aspect of the LATER model, we also fitted a Ratcliff's drift-diffusion model (RDM) to our data using the "D-mat" toolbox (Vandekerckhove and Tuerlinckx, 2008) (http://ppw.kuleuven.be/okp/software/dmat/). However, because the RDM has been specifically formulated for two-alternative choices, it was not possible to use its standard formulation. Because our experiment is a GO/NO-GO task, subjects only responded to one target, which implies that there were no RT distributions for false-negative trials (no response for a GO trial) and for true-negative trials (no response for a NO-GO trial). Therefore, we adapted the D-mat toolbox to fit a GO/NO-GO version of the RDM on our data: first, we modified the loss function to only fit a "hit" RT distribution (Vandekerckhove and Tuerlinckx, 2008); second, we fixed the relative position between the starting point and the boundaries, which means that the changes in the distance from the starting point to the boundary were a priori attributed to the boundary parameter. Overall, our version of the RDM ("single boundary" RDM) retained from the version implemented in the D-mat toolbox the drift-diffusion mechanism, the upper decision boundary, the explicit account of nondecision time (and of its variability), and the variability in the starting point. This version of the RDM was adequate because we only estimated parameters relating to "hit" RT distributions. Note that if we had investigated errors RT distributions and error rates, an implicit lower boundary would also have been necessary (Gomez et al., 2007; Ratcliff and McKoon, 2008).

With these modifications of the D-mat toolbox, it was possible to reliably retrieve the distance to the decision threshold and the slope parameters from synthetic RT datasets. Moreover, we assessed the ability of the "single-boundary" RDM to correctly identify the modulation mechanism underlying changes between conditions using only the hit RT distribution and a Bayesian selection strategy [Bayesian information criterion (BIC); smaller values mean a better model in terms of goodness of fit and parsimony]. In the slope condition (a synthetic RT dataset simulating a change in the slope of the accumulation of evidence), the model in which the drift rate parameter was set free between conditions had the best Bayesian information criterion (BIC drift rate = 41,162, BIC boundary = 55,167). In the threshold condition (a synthetic RT dataset simulating a change in the distance to the threshold), the model in which the boundary parameter was set free between conditions had the best Bayesian information criterion (BIC drift rate = 43,441, BIC boundary = 43,075).

Finally, we performed a Bayesian selection analysis among drift-diffusion models instantiating three alternative mechanisms (distance to the decision threshold, nondecision time, average slope of diffusion process) on our own RT dataset.

fMRI data acquisition. Subjects were scanned at the CERMEP - Imagerie du Vivant using a research dedicated 1.5 T MRI scanner (Siemens Magnetom Sonata with an eight-channel head coil). We acquired 800 echo-planar T2*-weighted functional volumes (200 volumes/run, 4 runs) per experiment. Each volume comprised 28 slices acquired continuously over 2.65 s (TE = 60 ms; interleaved acquisition; slice thickness 4 mm; 0.4 mm noncontiguous; parallel to the subject's Sylvian fissure plane; angle to AC–PC: 20–30°; in-plane resolution: 3.44×3.44 mm^2; matrix size: 64×64), allowing complete brain coverage. Additionally, T1-weighted images were acquired at the end of each experiment (MP-RAGE: TR = 1970 ms; TE = 3.93 ms; T1 = 1100 ms; resolution: $1 \times 1 \times 1$ mm^3; matrix size: 256×256). Head motions were minimized using foam padding and headphones with earplugs were used to dampen the scanner noise.

fMRI data preprocessing. Data preprocessing was performed using the Statistical Parametric Mapping software (SPM2b, Wellcome Department of Imaging Neuroscience, University College London, UK, www.fil.ion.ucl.ac.uk/spm). The first three volumes of each run were removed to allow for T1 equilibrium effects (197 volumes/run). Before statistical analysis, we applied a slice-timing correction using the time center of the volume as reference. Then, head motion correction was applied using rigid-body realignment. We used realignment parameters during the statistical analysis as covariates to model out potential nonlinear head motion artifacts. Functional and morphological images were then normalized into standard MNI space using SPM's default templates. Finally, functional volumes were resampled and smoothed with an 8 mm FWHM Gaussian kernel. A 256 s temporal "high-pass filter" regressor set was included in the design matrix to exclude low-frequency noise and artifacts.

Finally, we explored the data for potential artifacts using tsdiffana, mean and variance images (http://imaging.mrc-cbu.cam.ac.uk/imaging/DataDiagnostics). An artifact is defined as the co-occurrence of a variance spike and a mean intensity drop uncorrelated with experimental design. Only the last two volumes of one participant's session met these criteria and were modeled as confounds in the design matrix. Translational movements estimated during the realignment procedure were small as compared to the voxel size (<1 mm).

General linear model 1: main fMRI data statistical analysis. Whole-brain statistical parametric analyses were performed using a two-stage random-effect approach. We estimated independently the model parameters from each subject's dataset and then made population inferences using the parameter intersubject variance. Regressors of interest were constructed by convolving functions representing the events with the canonical hemodynamic response function. Three event-related categorical regressors ("stimulus regressor," "decision-related regressor," and "motor regressor") and three parametric regressors (surprise, predictive information conveyed by the last shape, and predictive information conveyed by the last two shapes) were used to model the events occurring during the sequences (Fig. 3).

(1) The first regressor modeled the visual stimulation as 0.3-s-long boxcar functions time locked to the onset of visual stimuli (referred to as the "stimulus regressor").

(2) The ongoing processes during perceptual decision formation (referred to as the "decision-related regressor") were modeled as boxcar functions convolved with the response time duration, time locked to each target onset. Because this condition pooled the decision-related activity regardless of the context in which it took place, it modeled the part of the decision-related activity not modulated by its context. Three parametric regressors were added to the decision-related regressor to account for the effect of surprise (Eq. 1) and predictive information (Eqs. 2, 3) on the decision process. These parametric regressors were hierarchically orthogonalized in the following order: surprise, predictive information conveyed by the last shape only, and predictive information conveyed by the last two shapes. This orthogonalization hierarchy naturally emerged from the mathematical definitions of the parameters (Büchel et al., 1998) and unambiguously separated the effect of the information conveyed by the last shape from the information conveyed by the penultimate shape into two parametric regressors. To build these regressors, we weighted each event of the decision-related regressor by the current, and continuously updated, estimates of the parameters, so that each event was characterized by its own set of parameter values.

(3) Finally, the last categorical regressor modeled the motor response associated with the button press, and was modeled as a Dirac function using the timing of the button press as onset. Thus, our model explicitly separated the motor-related activity from the decision-related activity.

Statistical inferences were performed with a threshold of $p < 0.05$ (clusterwise) familywise error (FWE) corrected across the whole brain ($p < 0.001$ voxelwise) (see supplemental Tables S1, S2, available at www.jneurosci.org as supplemental material).

Correlation between "neural" and "behavioral" sensitivity to predictive information. We reasoned that blood oxygenation level-dependent (BOLD) activity in a brain region modulating the distance to the threshold should be predictive of each participant's RT variations (Figs. 4, 5). Thus, we performed a correlation analysis between the sensitivity to predictive information estimated from brain activity and the sensitivity to predictive information estimated from response times for both the information conveyed by the last and the penultimate shape.

To measure the "behavioral" sensitivity to predictive information, we fitted the multilinear model of RT previously identified to each individual RT set, thereby estimating its βs (Eq. 10). Here, the βs are measures of the slope of the decrease in response time with increasing predictive

information conveyed by the last and the penultimate shape, regardless of the current accuracy level. This analysis yielded a behavior-based measure of the individual ability to use the predictive information conveyed by the last shape and the penultimate shape to modulate the distance to the threshold. Then, to measure the "neural" sensitivity to predictive information, we extracted for each participant, and in every brain region found to be sensitive to predictive information in the main fMRI analysis [region of interest (ROI)-based approach using MarsBaR toolbox v0.38, $p < 0.001$ voxelwise; see below, ROI analyses], the β estimates of the parametric regressors, which provided us with measures of the slopes of the decrease between event-related BOLD activity with increasing predictive information conveyed by the last shape and the penultimate shape.

Finally, we performed nonparametric correlation analyses between individual "behavioral" and "neural" sensitivity to identify the brain regions in which the slope of the relationship between predictive information and BOLD activity was predictive of the slope of the relationship between predictive information and RT (Spearman's correlation) (see supplemental Table S1, available at www.jneurosci.org as supplemental material).

General linear model 2: controlling for potential confounding effects in the anterior cingulate cortex. To assess the specificity of our fMRI findings, we performed an additional statistical parametric analysis, in which we added to the general linear model (GLM) 1 (see Figs. 3, 6) three parametric regressors to the "decision-related" regressor, orthogonalized in the following order: the first four parametric regressors controlled for the effects of error likelihood, prediction error, entropy, and surprise, whereas the following two parametric regressors modeled the modulation of BOLD signal by the predictive information conveyed by the last shape and the predictive information conveyed by the penultimate shape. This procedure ensured that any potential confounding effect from the error likelihood, prediction error, entropy, and surprise were removed from the estimation of the effects of the predictive information parametric regressors.

The error likelihood parametric regressor was computed for each sequence from participant error rates during target trials. The error prediction parametric regressor (δ_t) was computed using a standard Rescorla–Wagner algorithm (Dayan and Abbott, 2001), whose learning parameter (α) was adjusted to maximize the correlation between participants RTs and $\mathrm{Prob}_t(e_t = i|e_{t-1} = j)$, the reinforcement learning estimate of the conditional probability of a shape (e_t) at the time step t given the last shape (e_{t-1}) (Eqs. 12, 13). Finally, B_t is a binary function equal to 1 when the expected event actually occurs ($e_t = i$) and to 0 if it does not ($e_t \neq i$) (Eq. 13). The best fit of the Rescorla–Wagner algorithm was obtained for a learning rate $\alpha = 0.08$ (range explored 0.01–0.15).

$$\mathrm{Prob}_{t+1}(e_{t+1} = i|e_t = j) = \mathrm{Prob}_t(e_t = i|e_{t-1} = j) + \alpha \times \delta_t \quad (12)$$

$$\delta_t = B_t(1 - \mathrm{Prob}_t(e_t = i|e_{t-1} = j)). \quad (13)$$

Then, the entropy parametric regressor was computed for each shape from Equation 14. The entropy is classically viewed as an information-theoretic equivalent to the concept of conflict (Berlyne, 1957).

$$H_t = \underset{t,i}{E}(u_{t,i}) \quad (14)$$

General linear model 3: correlation between BOLD activity and LATER model parameters. To assess the correlation between LATER model parameters and BOLD activity, we built and estimated a second variant of GLM 1, in which we sorted the events previously included in the "decision-related" regressor (Fig. 3) into four discrete levels of predictive information ([−0.3, 0.18, 0.72, 1.22] bits), which divided the range of predictive information into bins of equal size (see above, Psychophysics: LATER model and reciprobit plots). Each bin included enough data to reliably perform individual fits of the LATER model.

Then, using these four levels of predictive information, we built four distinct categorical regressors, in which each event was modeled using a Dirac function time locked on the onset of the target. These four categorical regressors replaced the "decision-related" regressor of GLM 1 (Fig. 3). GLM 1 and GLM 3 were otherwise identical.

This procedure allowed us to perform nonparametric correlation analyses (Spearman's correlation) between BOLD activities at the time of decision averaged over the four levels of predictive information for each participant and the corresponding averaged LATER model's parameter estimates (Figs. 5*c*, 7*c*) (see below, ROI analyses).

ROI analyses. We extracted ROI average of estimated βs for the three parametric regressors included in GLM 1 and for the four categorical regressors modeling the levels of predictive information in GLM 3. To do so, ROIs were built from functional clusters from GLM 1 ($p < 0.001$, voxelwise) intersected with a 6-mm-radius sphere centered on the cluster's peak voxel using the MarsBaR toolbox (v0.38, http://marsbar.sourceforge.net).

Conjunction analysis. We performed a conjunction analysis testing the conjunction null (Nichols et al., 2005), using SPM2b to identify clusters that exhibited significant negative parametric effects for predictive information conveyed by the last and the penultimate shape at the onset of decisions. However, because conjunction tests are not as sensitive as single-contrast testing for the average effect over all contrasts and thus underestimate the underlying effect (Friston et al., 2005), and because we had a strong a priori hypothesis regarding the involvement of the DLPFC in implementing the decision variable, here inferences were performed with a level of significance of $p < 10^{-3}$ uncorrected (Fig. 7).

Structural equation modeling. First, to characterize functional subdivisions between the anterior and posterior DLPFC, we built a morphologi-

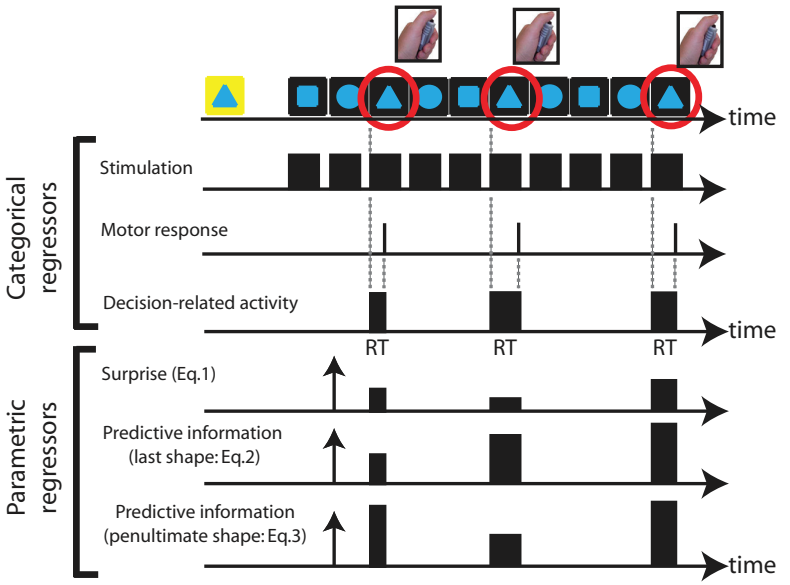

Figure 3. Regressors included in the statistical analysis of fMRI data. The main GLM included three categorical and three parametric regressors (see Materials and Methods, General linear model 1: main fMRI data statistical analysis). The three categorical regressors modeled the main steps of perceptual decision making: sensory processing, decision-related activity and motor response. Three parametric regressors were derived from the decision-related regressors and hierarchically orthogonalized. These parametric regressors modeled the modulation of BOLD activity at the time of decision by the surprise and the predictive information conveyed by the last and the penultimate shape.

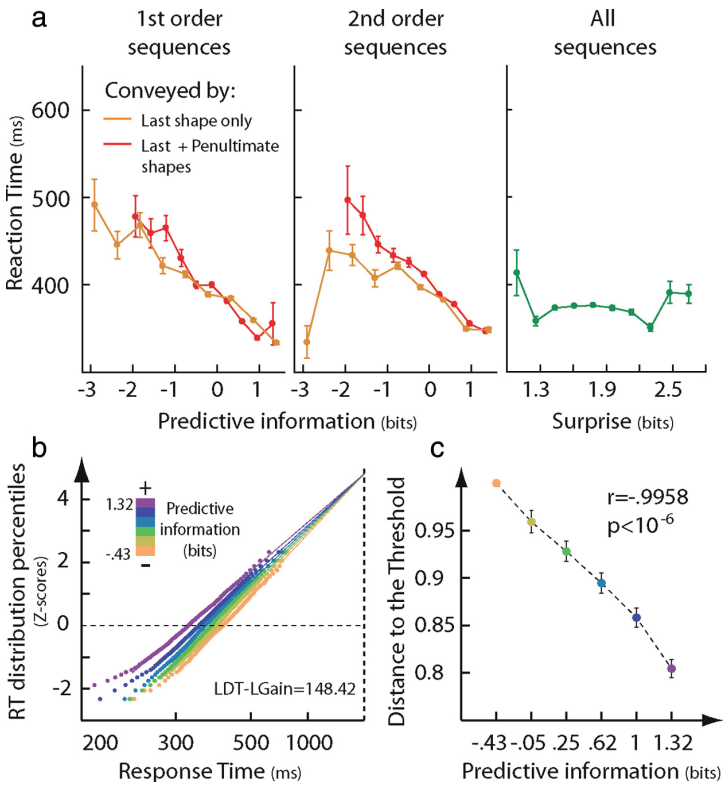

Figure 4. Higher predictive information reduces the distance to the decision threshold. ***a***, RT decreased as predictive information increased in first-order [left panel: $r_{p1} = -0.295$ (orange), $r_{p2} = -0.273$ (red), both $p < 10^{-6}$] and second-order sequences [middle panel: $r_{p1} = -0.235$ (orange), $r_{p2} = -0.292$ (red), both $p < 10^{-6}$]. During second-order sequences (middle panel), RTs were better correlated with the predictive information conveyed by the last two shapes (red) than with the predictive information conveyed by the last shape only (orange) but not during first-order sequences (left panel), indicating that all available predictive information was used in the regulation of the decision process. Finally, there was no effect of surprise (right panel, green) on RT ($r_{surprise} = -0.02$, $p = 0.126$). ***b***, Reciprobit plot based on pooled RT from all participants showing a swivel toward lower RT when predictive information increases, as hypothesized in Figure 1*a* (upper right panel). This aspect is confirmed by the log likelihood ratio ($L_{DT} - L_{Gain}$), in accordance with the hypothesis of the modulation of the distance to the threshold. ***c***, Distance to the decision threshold as a function of the level of predictive information available. Error bars represent 95% confidence intervals of the distance to the threshold. The color code represents the same levels of predictive information in both panels (from −0.43 to 1.32 bits).

cal ROI of the DLPFC (WFU PickAtlas atlas v2.4, http://fmri.wfubmc.edu, dilatation parameter = 2 voxels, bilateral mask including BA9, BA10, and BA46 from WFU PickAtlas built-in atlas, volume = 5994 voxels) and computed statistical maps of the parametric effect of the predictive information conveyed by the last shape and the penultimate shape ($p < 0.001$ voxelwise). From this analysis, we isolated four functional subregions whose activity reflected the amount of predictive information at the moment of the decision ($p < 0.05$ clusterwise, SVC): left anterior DLPFC, right anterior DLPFC, left posterior DLPFC, and right posterior DLPFC.

Then, we extracted ROI-averaged time series during first- and second-order sequences for each participant from 6-mm-radius spheres centered at the peak voxel of the four brain regions identified in the DLPFC (Fig. 8, dashed white circles) and the anterior cingulate cortex (ACC) (Fig. 8, plain white circle) ($N = 5124$ volumes for each brain region and condition, no missing values or deleted data). Structural equation modeling was performed using the Mx software package (v1.65b). Figure 8 represents the path diagram as arrows to indicate directional or symmetric connections between the functional regions included in the model. We performed a maximum-likelihood-based estimation of the model path coefficients on the correlation matrix derived from the two resulting time series and statistical inferences on path coefficient variations between the first- and second-order sequences using a nested model approach (supplemental Table S3, available at www.jneurosci.org as supplemental material) (no convergence problems or inadmissible solutions).

The overall model fit was assessed with standard goodness of fit indices, all indicated a good quality of fit (normed fit indices = 0.91, centrality index = 0.9, and relative noncentrality indices = 0.91; index values above 0.9 indicate a good quality of fit) (Mueller, 1996).

Functional connectivity analysis. To identify brain regions that were functionally coupled with the ACC, we assessed the correlation between BOLD activity in this "seed" region and BOLD activity in each voxel of the brain. To do so, we extracted the cluster-averaged time course from the functional cluster we found in the ACC (Fig. 5*a*) (ROI-based approach using MarsBaR toolbox v0.38, $p < 0.001$ voxelwise; see above, ROI analyses) and included this time course as a regressor not convolved with a hemodynamic response function in a GLM. This GLM also included a 256 s low-pass filter and head motion parameters as regressors of noninterest. We then computed group-level SPM using the standard SPM's RFX approach. Supplemental Figure S6 (available at www.jneurosci.org as supplemental material) shows the main result of this analysis with a threshold of 5% voxelwise, FWE corrected across the whole brain.

Results

Psychophysics: predictive information reduces the distance to the threshold of the decision

RT decreased linearly as predictive information increased (Fig. 4*a*, left and middle panels), showing that participants successfully used the statistical structure of sequences to predict the forthcoming shape. Moreover, participants adjusted to the actual structure of the sequences (first or second order) to exploit all the predictive information available. Indeed, RTs were better correlated with the predictive information conveyed by the last two shapes (last shape and penultimate shape, r_{p2}) (Fig. 4*a*, red line) than with the predictive information conveyed by the last shape only (r_{p1}) (Fig. 4*a*, orange line) during second-order sequences, but not during first-order sequences (Fig. 4*a*) (Hotelling's *t*, first-order sequences, $r_{p1} = r_{p2}$; $p = 0.98$; second-order sequences, $r_{p1} = r_{p2}$; $p < 10^{-6}$). We also assessed the contribution of the source (last or penultimate shape) of predictive information on decision response time by fitting a multilinear model to all participants' RTs (see Materials and Methods, Multilinear model of response times). Predictive information had the same influence on RT whether it was conveyed by the last shape ($\beta_{p1} = -0.148 \pm 10^{-2}$, $p < 10^{-5}$) or by the penultimate shape ($\beta_{p2} = -0.148 \pm 10^{-2}$, $p < 10^{-5}$; $\beta_{p1} = \beta_{p2}$, $t = -3.97 \pm 10^{-4}$, $p = 0.49$), showing that the efficiency of the modulation did not depend on the source of the information. This decrease in RT with increasing predictive information did not occur at the cost of accuracy, as shown by a factorial analysis crossing the type of sequence (first order or second order) and the predictive infor-

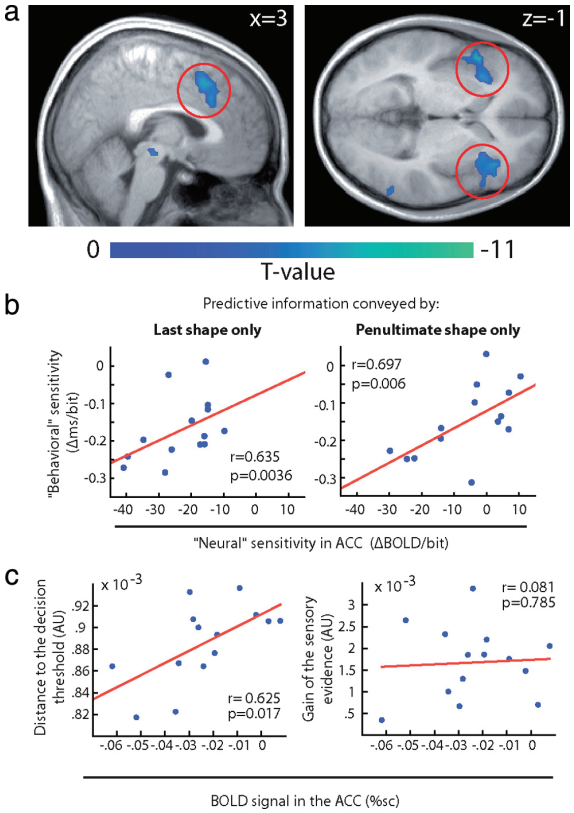

Figure 5. Event-related response in the ACC predicts individual ability to use predictive information to modulate the distance to the threshold. ***a***, Parametric response to the amount of predictive information conveyed by the last shape (rendered with a threshold of $p < 10^{-3}$ uncorrected, activations surviving a threshold of 5% clusterwise corrected across the whole brain are circled in red). The color scale represents the slope of the decrease in activity for an increasing amount of predictive information conveyed by the last shape. Note that it does not reflect deactivation. Also note that additional brain regions (not shown here) also survived the statistical threshold used and are listed in supplemental Table S1 (available at www.jneurosci.org as supplemental material). ***b***, Scatter plots of correspondence between "neural" and "behavioral" sensitivities to predictive information in the ACC ($n = 14$). For each participant, the two sensitivity measures link event-related responses in the ACC and modulation of RTs. (See Materials and Methods, Correlation between "neural" and "behavioral" sensitivity to predictive information.) Individual differences in "behavioral" sensitivity to predictive information conveyed by the last shape (left) and the penultimate shape (right) were predicted by individual differences in "neural" sensitivity in the ACC. Higher "behavioral" sensitivity to predictive information directly reflects the ability to modulate the distance to the threshold. ***c***, Scatter plots of correspondence between BOLD signal change in the ACC and the distance to the decision threshold (left panel) or the gain of the sensory evidence (right panel). Each point represents the BOLD signal change in the ACC plotted against the distance to the decision threshold estimated using the LATER model averaged over the four levels of predictive information (−0.3, 0.18, 0.72, 1.22 bits) for each subject.

mation averaged over each sequence (supplemental Fig. S2, available at www.jneurosci.org as supplemental material; Eqs. 4, 5). Finally, there was no effect of surprise on RT in our experiment, as expected from previous literature (Fig. 4*a*, right panel) (Kornblum, 1969).

Next, to identify which of the two predicted mechanisms—modulation of the distance to the threshold or gain control of the sensory evidence—mediated the effect of predictive information on decision making, we fitted a LATER model to the RT distribution of the subjects' responses and compared the likelihood of the two modulation mechanisms (Carpenter and Williams, 1995; Reddi et al., 2003). The modulation of the distance to the threshold by predictive information was significantly more likely than a gain control of the sensory evidence [log likelihood ratio, defined as the difference between the log likelihood of the distance to the threshold modulation hypothesis (L_{DT}) and the log likelihood of the gain control hypothesis (L_{Gain}), $L_{DT} - L_{Gain} = 148.42$, which is "decisive" according to Bayesian inference theory] (Jeffrey, 1998). Moreover, individual model fits showed that all the participants used predictive information to modulate their distance to the decision threshold, except for two participants for whom data did not allow to conclusively select a mechanism over the other (supplemental Fig. S3, available at www.jneurosci.org as supplemental material). Then, we performed a reciprobit analysis of the population's RT distribution (linearization of RT cumulative distribution resulting in "reciprobit lines") (see Materials and Methods, Psychophysics: LATER model and reciprobit plots, and Fig. 4*b*). This analysis provided us with a graphical representation of the mechanism modulating decision RT based on the variations of the reciprobit line for increasing amounts of predictive information: if the distance to the threshold decreases, then the line swivels around an intercept point toward lower RT (as in Fig. 1*a*, top right panel). By contrast, if the slope of the decision variable increases, then the line shifts toward lower RT (as in Fig. 1*a*, bottom right panel). The swivel of the reciprobit line with increasing levels of predictive information observed in Figure 4*b* further confirmed the reduction of the distance to the threshold by higher predictive information (supplemental Fig. S3, available at www.jneurosci.org as supplemental material). Finally, we observed a strong negative correlation between the distance to the threshold and predictive information ($r = -0.995$, $p < 10^{-6}$) (Fig. 4*c*).

These results did not depend on specific features of the LATER model since fitting a drift-diffusion model to our dataset also led to the conclusion that predictive information modulates the distance to the threshold (log likelihood ratio, $L_{DT} - L_{Gain} = 89.051$). Furthermore, there was an excellent agreement between the distance to the threshold estimated using the LATER and the drift-diffusion models for all levels of predictive information ($r = 0.99$, $p = 10^{-6}$).

Thus, our behavioral results demonstrate that the effect of predictive information on decision RT is mediated by the modulation of the distance to the decision threshold, not by gain control, and uses all the predictive information available to minimize decision RT.

Brain network responding to predictive information

In parallel with our behavioral results showing faster RTs with increasing predictive information (Fig. 4*a*), we investigated the relationship between decision-related brain activity and predictive information (see Materials and Methods, General linear model 1: main fMRI data statistical analysis; and Fig. 3). The results revealed a negative correlation between predictive information conveyed by the last shape and the BOLD activity in the ACC, the inferior frontal gyri bilaterally, the right intraparietal sulcus region (IPS), and the DLPFC bilaterally ($p < 0.05$ clusterwise corrected for multiple comparisons across the whole brain) (see Fig. 5*a* and supplemental Table S1, available at www.jneurosci.org as supplemental material).

These patterns of decision-related activity were preserved when adding prediction errors, error likelihood, entropy (which is a proxy for conflict), and surprise as potential confounds in a new analysis, supporting the specificity of the relationship between BOLD activity in all these brain regions and predictive information (supplemental Table S2, available at www.jneurosci.

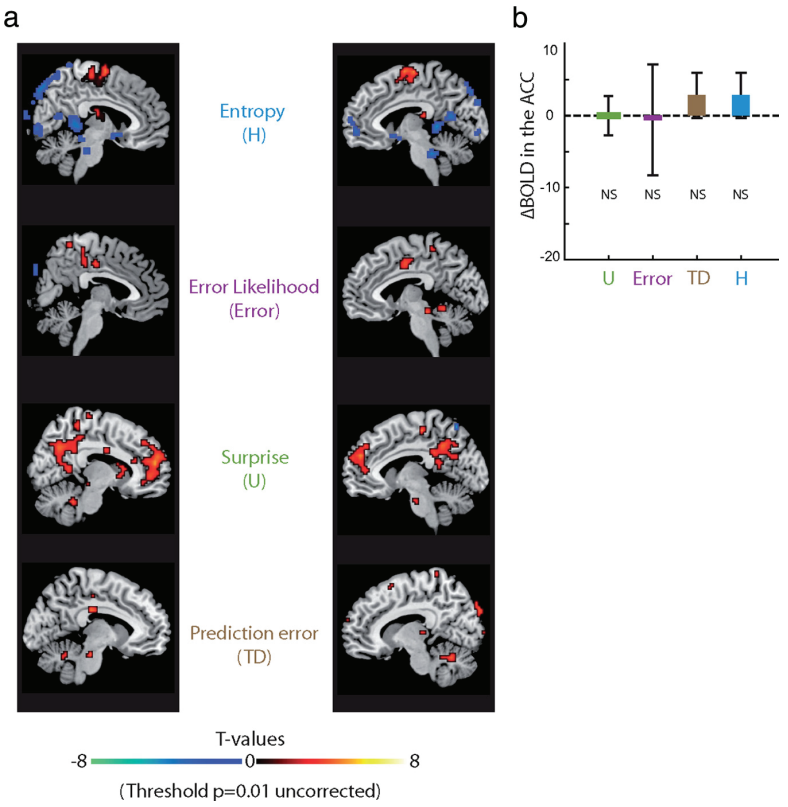

Figure 6. Whole-brain analysis of parametric responses to entropy, surprise, error likelihood and prediction error. ***a***, Statistical maps are rendered with a very lenient uncorrected threshold of $p = 0.01$ to illustrate the absence of effect of these potential confounds in the ACC. Left and right sagittal views are shown in the left and right columns. The cold color scale represents negative correlations and the hot color scale represents positive correlations. ***b***, ROI-average parametric response in the ACC to surprise (*U*), error likelihood (Error), prediction error (TD), and entropy (*H*). None of the four parametric regressors explained a significant portion of the BOLD activity in the ACC (NS, not significant).

org as supplemental material; and see Materials and Methods, General linear model 2: controlling for potential confounding effects in the anterior cingulate cortex). This additional analysis excludes alternative interpretations of the ACC's response in terms of conflict monitoring, postdecisional prediction errors, and error monitoring (Fig. 6; supplemental Fig. S4, available at www.jneurosci.org as supplemental material) (Holroyd and Coles, 2002; Botvinick et al., 2004; Brown and Braver, 2005).

The anterior cingulate cortex modulates the distance to the threshold of the decision

Within the brain regions showing a parametric response to predictive information (supplemental Table S1, available at www.jneurosci.org as supplemental material), we then assessed whether individual differences in brain activity during decision making predicted individual differences in the ability to exploit predictive information to reduce response time (see Materials and Methods, Functional connectivity analysis). From our behavioral analyses showing that the modulation of the distance to the threshold results in a linear decrease of RT with increasing predictive information (Fig. 4), we predicted that in the brain regions modulating the distance to the threshold, individual differences in "neural sensitivity," defined as the slope of the decrease in event-related activity as predictive information increased, should predict "behavioral sensitivity," i.e., the slope of the decrease in RT as predictive information increased. The ACC was the only brain region in which individual differences in event-related response ("neural" sensitivity) predicted each individual's ability to use the information available to modulate the distance to the threshold ("behavioral" sensitivity) (Fig. 5*b*). Moreover, this link between ACC's function and modulation of the distance to the decision threshold was further supported by the positive correlation between ACC's BOLD activity and distance to the decision threshold ($r = 0.625$, $p = 0.017$) (Fig. 5*c*, left panel), but not between ACC's BOLD activity and the slope of the accumulation of sensory evidence ($r = 0.081$, $p = 0.785$) (Fig. 5*c*, right panel). Together, these results demonstrate that the ACC is involved in adjusting the distance to the threshold in proportion to the current amount of predictive information.

The dorsolateral prefrontal cortex codes the decision variable

In a next step, we took advantage of basic properties of sequential sampling models to identify the brain regions computing the decision variable. First, assuming a coupling between neuronal firing rates and BOLD activity, we predicted that the BOLD response in the brain regions coding the decision variable should increase with slower decision RT and decrease when predictive information increases (i.e., when the distance to the threshold decreases). This hypothesis is based on the observation that the duration of the ramping neuronal activity coding the decision variable predicts RT and that its height correlates with the distance to the threshold (as illustrated in Fig. 1*a*, top left panel) (Hanes and Schall, 1996; Huk and Shadlen, 2005). Second, paralleling our behavioral results on RTs, the influence of predictive information on the BOLD response should not depend on the information source (last or penultimate shape) and there should be no influence of surprise on the BOLD response. Finally, BOLD response in brain regions coding the decision variable should reflect the slope of sensory evidence accumulation.

A conjunction analysis between brain regions showing decision-related activity decreasing with higher predictive information conveyed by both the last and the penultimate shapes isolated the anterior part of the right DLPFC and the right IPS ($p < 0.001$ uncorrected) (Fig. 7*a*). As expected, BOLD activity in these brain regions was identically modulated by the predictive information conveyed by the last and by the penultimate shape (Fig. 7*b*) (paired *t* test, $p_1 = p_2$, orange and red bars; right IPS: $p = 0.43$; right DLPFC: $p = 0.34$), and there was no influence of surprise on neural activity in these brain regions (Fig. 7*b*) (*t* test, $u = 0$, green bars; rIPS: $p = 0.29$; rDLPFC: $p = 0.8$).

Among these two brain regions, we assessed the correlation between BOLD response and the slope of sensory evidence accumulation (see Materials and Methods, General linear model 3: correlation between BOLD activity and LATER model parame-

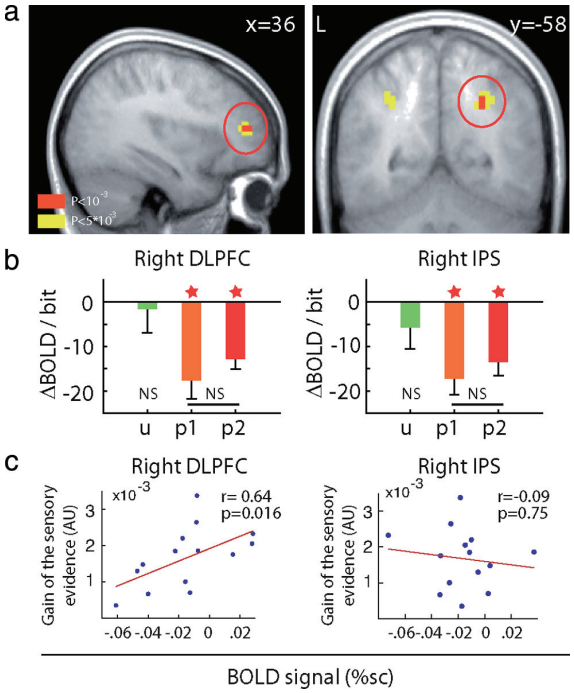

Figure 7. Brain regions coding the decision variable. ***a***, Conjunction map showing the brain regions activated during perceptual decision making in which BOLD activity is negatively modulated by the amount of predictive information conveyed by the last and the penultimate shape. We rendered our map using an uncorrected threshold of $p < 0.001$ (level of significance used for inference, red voxels) and a threshold of $p < 0.005$ to show the full extent of the activations (yellow voxels). ***b***, Average parametric response to surprise (u) and predictive information (p_1 and p_2) in these brain regions. The parametric response to the predictive information conveyed by the last shape (p_1) and the penultimate shape (p_2) was not significantly different (NS) in any of the regions identified ($p_1 = p_2$, orange and red bars; rIPS: $p = 0.43$; rDLPFC: $p = 0.34$). There was no parametric response to surprise ($u = 0$, green bars; rIPS: $p = 0.29$; rDLPFC: $p = 0.8$). ***c***, Scatter plots of correspondence between BOLD signal change in the ACC and accumulation's slope average, for each of the brain regions shown in Figure 7*a* (circled in red; see Materials and Methods, General linear model 3: correlation between BOLD activity and LATER model parameters). Each point represents the BOLD signal change in the ACC and the slope of sensory evidence accumulation estimated using the LATER model averaged over the four levels of predictive information (−0.3, 0.18, 0.72, 1.22 bits) for each subject (see supplemental Fig. S3, available at www.jneurosci.org as supplemental material).

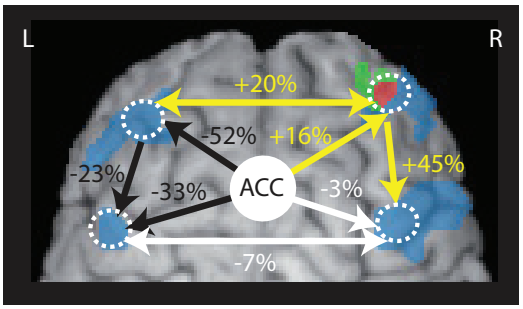

Figure 8. Diagram of effective connectivity between ACC and DLPFC. DLPFC subregions in which BOLD signal decreased as the predictive information conveyed by the last shape increased are rendered in blue, DLPFC subregions in which BOLD signal decreased as the predictive information conveyed by the penultimate shape increased are rendered in green and DLPFC subregions in which both effects were present are rendered in red ($p < 0.005$ uncorrected, for display). Red cluster corresponds to the DLPFC subregion coding the decision variable shown in Figure 7. The plain white circle represents the ACC, which is buried within the medial wall of the frontal cortex. The structural equation model included oriented path (arrows) connecting the ACC and the four functional subregions found in the DLPFC. Dashed circles white indicate the location and the extent of the spheres used for time series extraction. A yellow arrow indicates a significant increase of the path coefficient between first-order and second-order sequences, whereas a black arrow indicates a significant decrease of the path coefficient (all $p < 10^{-2}$). Finally, white arrows indicate path coefficient variations that are not significant. Variations of effective connectivity from first-order sequences to second-order sequences are indicated as relative variations next to each path (supplemental Table S3, available at www.jneurosci.org as supplemental material, indicates absolute values and statistical significance).

ters). Indeed, although the strength of sensory evidence was kept constant throughout the experiment, there were fluctuations of the slope of sensory evidence accumulation between subjects, as can be seen in supplemental Figure S3 (available at www.jneurosci.org as supplemental material). These individual fluctuations of the slope of sensory evidence accumulation correlated with BOLD activity in the right DLPFC ($r = 0.64$, $p = 0.016$), but not in the right IPS ($r = 0.09$, $p = 0.75$), thereby strongly supporting the involvement of the DLPFC in coding the decision variable (Fig. 7*c*).

Effective connectivity between the anterior cingulate cortex and the dorsolateral prefrontal cortex

Finally, having characterized the complementary computations performed in the ACC (Figs. 4, 5), which modulates the distance to the threshold, and the DLPFC region coding the decision variable (Fig. 7), we investigated whether the effective connectivity from the ACC to this DLPFC region increased when optimal regulation of the distance to the threshold required more complex computations. We formalized our hypothesis as a structural equation model (path diagram represented with arrows connecting the ACC to the DLPFC in Fig. 8), based on known anatomical pathways between the ACC and the DLPFC (Beckmann et al., 2009) and an ROI analysis of the parametric effect of predictive information in the DLPFC (Fig. 8). When comparing first-order to second-order sequences, a situation in which computation of the optimal threshold adjustment increases in complexity, the path coefficient from the ACC to the region of the DLPFC that codes the decision variable (Fig. 8, right anterior DLPFC's activation, x, y, z: 45, 45, 12) increased significantly, which was not the case for path coefficients along the other paths originating from the ACC (Fig. 8; supplemental Table S3, available at www.jneurosci.org as supplemental material). Interestingly, this effect was paralleled by an increase in the information flow from right anterior to posterior DLPFC region (right posterior DLPFC activations, x, y, z: 39, 6, 27).

Discussion

The accuracy of a perceptual decision depends on the amount of sensory evidence accumulated (Gold and Shadlen, 2007). However, gathering evidence takes time, which results in a tradeoff between a decision's speed and the accuracy achieved. Thus, optimal decision making should exploit all sources of information available, taking advantage of both the sensory evidence extracted from the environment and the knowledge of contingencies built upon past experiences (Bogacz, 2007b; Gold and Shadlen, 2007). Here, we showed that humans effectively use the predictability of forthcoming events to modulate the distance to the threshold of their decisions, substituting predictive information for sensory information in the decision process to speed up action selection without loss of accuracy (Fig. 4; supplemental Fig. S2, available at www.jneurosci.org as supplemental material). Remarkably, people both estimate and use predictive informa-

tion optimally, adjusting to environmental dynamics of varying complexity.

The key novel finding reported in this study is the coding in the ACC of a signal reflecting the adjustments of the distance to the threshold in proportion to the current amount of predictive information. This pivotal role of the ACC in the contextual guidance of the decision process is supported by two lines of evidence: (1) neural sensitivity to predictive information in the ACC accurately predicts individual fluctuations in the ability to use predictive information to modulate the distance to the threshold of the decision (Fig. 5); and (2) effective connectivity from the ACC to the DLPFC region accumulating sensory evidence increases when optimal adjustment of the distance to the threshold requires more complex computations, reflecting the increased weight of ACC's regulation signals in the decision process (Fig. 8). Overall, our results strongly support the idea that contextually optimized decisions arise from the integration of complementary computations performed in a network of specialized brain regions. In this conceptual framework, the ACC's main function is the computation of regulation signals that optimally adjust the distance to the threshold to the context.

The involvement of the DLPFC in the accumulation of sensory evidence is supported by the fact that BOLD activity observed in this brain region (1) increased with slower decision response times, (2) was negatively modulated by the amount of predictive information conveyed by the last and the penultimate shape, (3) did not depend on the source of predictive information (last or penultimate shape), and (4) is correlated with the slope of the decision variable (Fig. 7). This finding extends previous reports that the DLPFC accumulates sensory evidence related to the correct choice (Kim and Shadlen, 1999; Heekeren et al., 2004; Philiastides and Sajda, 2006; Philiastides and Heekeren, 2009). Note that we implicitly referred to sensory evidence accumulation as the computational mechanism by which a decision variable is implemented, but we acknowledge that other mechanisms have been proposed and are also possible (Ditterich, 2006; Cisek et al., 2009). Finally, the DLPFC activity we observed cannot be attributed to higher attention at the time of target appearance because this would have predicted increased BOLD response with higher predictive information (the latter being associated with faster RTs in our task). By contrast, we observed a negative correlation between predictive information and BOLD signal in this brain region (Fig. 7).

Previous fMRI studies reported a relationship between choice uncertainty and activity in the medial prefrontal cortex when subjects learn through trials and errors the probability of making a correct choice (Volz et al., 2003; Huettel et al., 2005; Volz et al., 2005; Grinband et al., 2006; Huettel, 2006; Platt and Huettel, 2008). These findings parallel studies using fMRI in humans or brain lesions in monkeys showing that one of ACC's critical functions is to build and update an extended action/reward history to guide future decisions optimally (Hampton et al., 2006; Kennerley et al., 2006; Behrens et al., 2007). Our results draw an important link between these two fields of research by showing that the ACC is involved in the regulation of the decision-making process using predictive information (a measure of the reduction of uncertainty estimated on the basis of the history of associations between successive events) and suggests that adjustment signals of the distance to the threshold in the ACC may be a general computational mechanism for the contextual guidance of decisions. Interestingly, theoretical insights into representational learning suggest that a learning signal is needed to support such a function (Williams and Goldman-Rakic, 1998; Holroyd and Coles, 2002; Friston, 2003; Dreher et al., 2006; D'Ardenne et al., 2008). The midbrain activation we observed concomitant with the ACC activation could serve such a functional role since prediction error signal has previously been found in the midbrain (although this cluster did not survive correction for multiple comparison, $p < 0.001$ uncorrected) (see Fig. 5*a*) (Dreher et al., 2006; Behrens et al., 2007; D'Ardenne et al., 2008).

Previous accounts of the ACC's function have stressed factors other than the contextual regulation of the decision-making process, such as the monitoring of errors and conflicts (Carter et al., 1998; Botvinick et al., 2004; Ridderinkhof et al., 2004), the likelihood of errors (Brown and Braver, 2005), and the role of postdecisional prediction-error signals (Holroyd and Coles, 2002). However, none of these alternative functions could account for the relationship observed here between ACC activity and predictive information. Indeed, additional fMRI analyses of our data showed that both the likelihood of error and the prediction error failed to explain our BOLD activity in the ACC at the time of decision formation (Fig. 6). Moreover, once controlled for the level of predictive information, BOLD activity in the ACC did not significantly differ between slow and fast responses, which rules out interpretations of our ACC activity in terms of conflict monitoring or spurious correlation with RT, which would have predicted that decisions with longer RTs are associated with greater levels of conflict and with higher level of ACC activity (supplemental Fig. S5, available at www.jneurosci.org as supplemental material). Moreover, in our experiment, the entropy, which has been proposed as a direct measure of conflict (Berlyne, 1957) did not account for a significant part of BOLD activity in the ACC (supplemental Table S2, available at www.jneurosci.org as supplemental material; Fig. 6).

It should be noted that ACC's regulatory function of the distance to the threshold does not necessarily imply that this brain region directly implements the threshold of the decision. In fact, a number of theoretical accounts propose that the basal ganglia implement a gating mechanism that signals, by a phasic increase of activity in the direct pathway, the moment when the activity of cortical neurons coding the decision variable crosses the decision threshold (Lo and Wang, 2006; Bogacz, 2007a, 2009; Frank et al., 2007). This phasic increase of activity would cancel the tonic inhibition exerted by the basal ganglia's output nuclei on motor command centers (Redgrave et al., 1999). Despite a current lack of direct evidence, this proposal emphasizes the potentially central role of cingulostriatal projections in conveying contextual regulation signals from the ACC to the main input structure of the basal ganglia (Kunishio and Haber, 1994; Lo and Wang, 2006). Supporting this hypothesis, we observed a strong correlation between BOLD activity in the ACC and in the striatum, showing that these two brain regions are functionally coupled when making simple decisions (supplemental Fig. S6, available at www.jneurosci.org as supplemental material; Materials and Methods, Functional connectivity analysis).

Moreover, a recent fMRI study comparing perceptual decisions with cues emphasizing speed or accuracy reported a negative correlation between individual variations of a measure for response caution (ratio between the starting point and the decision threshold) and BOLD activity at the time of the cue in both the pre-SMA and the striatum (Forstmann et al., 2008). Thus, the pre-SMA and the striatum may be involved in motor preparation of fast action when explicitly cued for speed and may implement the global slowing down observed when cueing for higher accuracy. Other recent fMRI studies also explicitly emphasized the speed of the perceptual decision at the expense of its accuracy

(Ivanoff et al., 2008; van Veen et al., 2008). By contrast, in our study, the modulation of the decision process relied upon predictive information (conveyed by recent history) on the forthcoming stimulus, a quantity that participants implicitly tracked and updated online. Our findings highlight the role of the ACC in keeping track of past events to build an inner model of contingencies and in adjusting the distance to the decision threshold and address a more general contextwise modulation of the decision process, which did not result in a simple global inhibition or facilitation of action preparation, but in a weighting of each possible outcome of the decision based on its likeliness. Consistent with our proposal, a recent fMRI study showed that individual differences in perceptual decision criterion shifts induced by expected losses correlates with BOLD activity in the ACC. Although the authors did not analyze their data within the framework of sensory evidence accumulation models, their findings indicate that asymmetric category costs may affect perceptual decision making in a similar way to changes in category expectations (Fleming et al., 2010).

In conclusion, combining psychophysics, model-driven fMRI and the framework of information theory, we characterized the influence of predictive information on two basic elements underlying the formation of human perceptual decision (distance to the threshold and decision variable). Our results reveal how these elements are coded in the human brain and shed a new light on the respective functions played by the DLPFC and the ACC in perceptual decision making. They also suggest new architectural principles governing the organization of the human frontal lobe and how the interactions between the DLPFC and the ACC are required for optimal decision making.

References

Beckmann M, Johansen-Berg H, Rushworth MF (2009) Connectivity-based parcellation of human cingulate cortex and its relation to functional specialization. J Neurosci 29:1175–1190.

Behrens TE, Woolrich MW, Walton ME, Rushworth MF (2007) Learning the value of information in an uncertain world. Nat Neurosci 10:1214–1221.

Berlyne DE (1957) Uncertainty and conflict: a point of contact between information-theory and behavior-theory concepts. Psychol Rev 64:329–339.

Bestmann S, Harrison LM, Blankenburg F, Mars RB, Haggard P, Friston KJ, Rothwell JC (2008) Influence of uncertainty and surprise on human corticospinal excitability during preparation for action. Curr Biol 18:775–780.

Bogacz R (2007a) Optimal decision network with distributed representation. Neural Netw 20:564–576.

Bogacz R (2007b) Optimal decision-making theories: linking neurobiology with behaviour. Trends Cogn Sci 11:118–125.

Bogacz R (2009) Optimal decision-making theories. In: Handbook of reward and decision making (Dreher JC, Tremblay L, eds), pp 367–389. Oxford: Academic.

Botvinick MM, Cohen JD, Carter CS (2004) Conflict monitoring and anterior cingulate cortex: an update. Trends Cogn Sci 8:539–546.

Brown JW, Braver TS (2005) Learned predictions of error likelihood in the anterior cingulate cortex. Science 307:1118–1121.

Büchel C, Holmes AP, Rees G, Friston KJ (1998) Characterizing stimulus-response functions using nonlinear regressors in parametric fMRI experiments. Neuroimage 8:140–148.

Carpenter RH, Williams ML (1995) Neural computation of log likelihood in control of saccadic eye movements. Nature 377:59–62.

Carter CS, Braver TS, Barch DM, Botvinick MM, Noll D, Cohen JD (1998) Anterior cingulate cortex, error detection, and the online monitoring of performance. Science 280:747–749.

Cisek P, Puskas GA, El-Murr S (2009) Decisions in changing conditions: the urgency-gating model. J Neurosci 29:11560–11571.

D'Ardenne K, McClure SM, Nystrom LE, Cohen JD (2008) BOLD responses reflecting dopaminergic signals in the human ventral tegmental area. Science 319:1264–1267.

Dayan P, Abbott LF (2001) Computational and mathematical modeling of neural systems, Ed 1. Cambridge, MA: MIT Press.

Ditterich J (2006) Stochastic models of decisions about motion direction: behavior and physiology. Neural Netw 19:981–1012.

Doya K (2008) Modulators of decision making. Nat Neurosci 11:410–416.

Dreher JC, Kohn P, Berman KF (2006) Neural coding of distinct statistical properties of reward information in humans. Cereb Cortex 16:561–573.

Fleming SM, Whiteley L, Hulme OJ, Sahani M, Dolan RJ (2010) Effects of category-specific costs on neural systems for perceptual decision-making. J Neurophysiol 103:3238–3247.

Forstmann BU, Dutilh G, Brown S, Neumann J, von Cramon DY, Ridderinkhof KR, Wagenmakers EJ (2008) Striatum and pre-SMA facilitate decision-making under time pressure. Proc Natl Acad Sci U S A 105:17538–17542.

Frank MJ, Samanta J, Moustafa AA, Sherman SJ (2007) Hold your horses: impulsivity, deep brain stimulation, and medication in parkinsonism. Science 318:1309–1312.

Friston K (2003) Learning and inference in the brain. Neural Netw 16: 1325–1352.

Friston KJ, Penny WD, Glaser DE (2005) Conjunction revisited. Neuroimage 25:661–667.

Gold JI, Shadlen MN (2007) The neural basis of decision making. Annu Rev Neurosci 30:535–574.

Gomez P, Ratcliff R, Perea M (2007) A model of the go/no-go task. J Exp Psychol Gen 136:389–413.

Grinband J, Hirsch J, Ferrera VP (2006) A neural representation of categorization uncertainty in the human brain. Neuron 49:757–763.

Hampton AN, Bossaerts P, O'Doherty JP (2006) The role of the ventromedial prefrontal cortex in abstract state-based inference during decision making in humans. J Neurosci 26:8360–8367.

Hanes DP, Schall JD (1996) Neural control of voluntary movement initiation. Science 274:427–430.

Hanks TD, Ditterich J, Shadlen MN (2006) Microstimulation of macaque area LIP affects decision-making in a motion discrimination task. Nat Neurosci 9:682–689.

Harrison LM, Duggins A, Friston KJ (2006) Encoding uncertainty in the hippocampus. Neural Netw 19:535–546.

Heekeren HR, Marrett S, Bandettini PA, Ungerleider LG (2004) A general mechanism for perceptual decision-making in the human brain. Nature 431:859–862.

Holroyd CB, Coles MG (2002) The neural basis of human error processing: reinforcement learning, dopamine, and the error-related negativity. Psychol Rev 109:679–709.

Huettel SA (2006) Behavioral, but not reward, risk modulates activation of prefrontal, parietal, and insular cortices. Cogn Affect Behav Neurosci 6:141–151.

Huettel SA, Song AW, McCarthy G (2005) Decisions under uncertainty: probabilistic context influences activation of prefrontal and parietal cortices. J Neurosci 25:3304–3311.

Huk AC, Shadlen MN (2005) Neural activity in macaque parietal cortex reflects temporal integration of visual motion signals during perceptual decision making. J Neurosci 25:10420–10436.

Ivanoff J, Branning P, Marois R (2008) fMRI evidence for a dual process account of the speed-accuracy tradeoff in decision-making. PLoS One 3:e2635.

Jeffrey H (1998) Theory of probability. Ed 3. Oxford: Oxford UP.

Kennerley SW, Walton ME, Behrens TE, Buckley MJ, Rushworth MF (2006) Optimal decision making and the anterior cingulate cortex. Nat Neurosci 9:940–947.

Kim JN, Shadlen MN (1999) Neural correlates of a decision in the dorsolateral prefrontal cortex of the macaque. Nat Neurosci 2:176–185.

Kornblum S (1969) Sequential determinants of information processing in serial and discrete choice reaction time. Psychol Rev 76:113–131.

Kunishio K, Haber SN (1994) Primate cingulostriatal projection: limbic striatal versus sensorimotor striatal input. J Comp Neurol 350:337–356.

Lo CC, Wang XJ (2006) Cortico-basal ganglia circuit mechanism for a decision threshold in reaction time tasks. Nat Neurosci 9:956–963.

Luce R (1991) Response times: their role in inferring elementary mental organization. Oxford: Oxford UP.

Mars RB, Debener S, Gladwin TE, Harrison LM, Haggard P, Rothwell JC, Bestmann S (2008) Trial-by-trial fluctuations in the event-related electroencephalogram reflect dynamic changes in the degree of surprise. J Neurosci 28:12539–12545.

Mueller R (1996) Basic principle of structural equation modeling. New York: Springer.
Nichols T, Brett M, Andersson J, Wager T, Poline JB (2005) Valid conjunction inference with the minimum statistic. Neuroimage 25:653–660.
Oldfield RC (1971) The assessment and analysis of handedness: the Edinburgh inventory. Neuropsychologia 9:97–113.
Philiastides MG, Heekeren HR (2009) Spatiotemporal characteristics of perceptual decision making in the human brain? In: Handbook of reward and decision making (Dreher JC, Tremblay L, eds), pp 185–212. Oxford: Academic.
Philiastides MG, Sajda P (2006) Temporal characterization of the neural correlates of perceptual decision making in the human brain. Cereb Cortex 16:509–518.
Platt ML, Huettel SA (2008) Risky business: the neuroeconomics of decision making under uncertainty. Nat Neurosci 11:398–403.
Ranganath C, Rainer G (2003) Neural mechanisms for detecting and remembering novel events. Nat Rev Neurosci 4:193–202.
Ratcliff R, McKoon G (2008) The diffusion decision model: theory and data for two-choice decision tasks. Neural Comput 20:873–922.
Reddi BA, Carpenter RH (2000) The influence of urgency on decision time. Nat Neurosci 3:827–830.
Reddi BA, Asrress KN, Carpenter RH (2003) Accuracy, information, and response time in a saccadic decision task. J Neurophysiol 90:3538–3546.
Redgrave P, Prescott TJ, Gurney K (1999) The basal ganglia: a vertebrate solution to the selection problem? Neuroscience 89:1009–1023.
Ridderinkhof KR, Ullsperger M, Crone EA, Nieuwenhuis S (2004) The role of the medial frontal cortex in cognitive control. Science 306:443–447.
Smith PL, Ratcliff R (2004) Psychology and neurobiology of simple decisions. Trends Neurosci 27:161–168.
Stanford TR, Shankar S, Massoglia DP, Costello MG, Salinas E (2010) Perceptual decision making in less than 30 milliseconds. Nat Neurosci 13:379–385.
Strange BA, Duggins A, Penny W, Dolan RJ, Friston KJ (2005) Information theory, novelty and hippocampal responses: unpredicted or unpredictable? Neural Netw 18:225–230.
Tosoni A, Galati G, Romani GL, Corbetta M (2008) Sensory-motor mechanisms in human parietal cortex underlie arbitrary visual decisions. Nat Neurosci 11:1446–1453.
Usher M, McClelland JL (2001) The time course of perceptual choice: the leaky, competing accumulator model. Psychol Rev 108:550–592.
Vandekerckhove J, Tuerlinckx F (2008) Diffusion model analysis with MATLAB: a DMAT primer. Behav Res Methods 40:61–72.
van Veen V, Krug MK, Carter CS (2008) The neural and computational basis of controlled speed-accuracy tradeoff during task performance. J Cogn Neurosci 20:1952–1965.
Volz KG, Schubotz RI, von Cramon DY (2003) Predicting events of varying probability: uncertainty investigated by fMRI. Neuroimage 19:271–280.
Volz KG, Schubotz RI, von Cramon DY (2005) Variants of uncertainty in decision-making and their neural correlates. Brain Res Bull 67:403–412.
Williams SM, Goldman-Rakic PS (1998) Widespread origin of the primate mesofrontal dopamine system. Cereb Cortex 8:321–345.

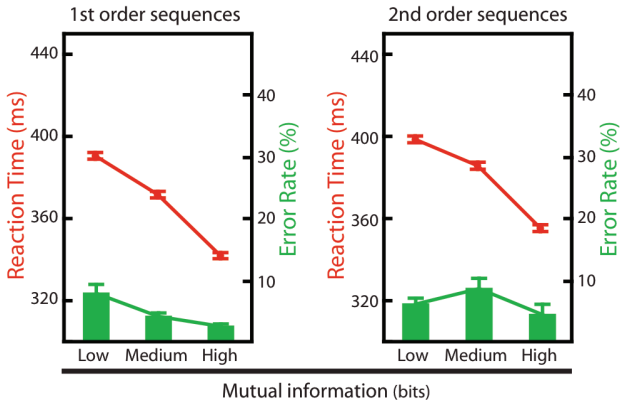

Figure S2. Relationship between increasing mutual information in first and second-order sequences and RT (red circles) and error rates (green bars). RT decreased monotonically as the mutual information of sequences increased ($F=404.1$, $p<10^{-7}$). However, this decrease in RT was not paralleled by increased error rates (Mutual information, $F=4.23$, $p=0.016$; No effect of sequence order, $F=2.79$, $p=0.096$; No interactions, $F=2.99$, $p=0.053$). RTs were on average 14.11 ms longer for second-order sequences compared to first-order sequences ($F=79$, $p<10^{-7}$, no interaction, $F=2.1$, $p=0.118$).

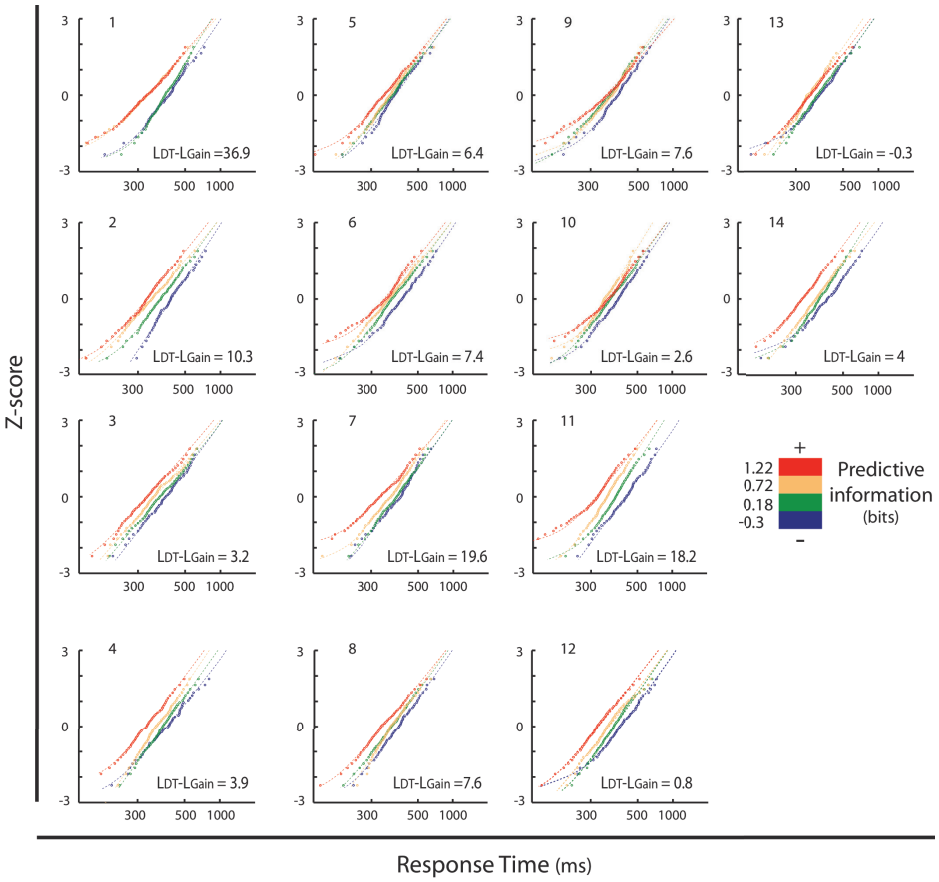

Figure S3: Reciprobit plots for each participant. Most of the individual reciprobit plots shows a clear swivel toward lower RT when predictive information increases, as hypothesized in Figure 1a (upper right panel). The values of each individual's log likelihood ratio (L_{DT}-L_{Gain}) are displayed on each reciprobit plot, favoring the distance to the threshold hypothesis in all but 2 subjects (subjects 12 and 13). For these two subjects, evidence did not allow to conclusively choose one mechanism over the other.

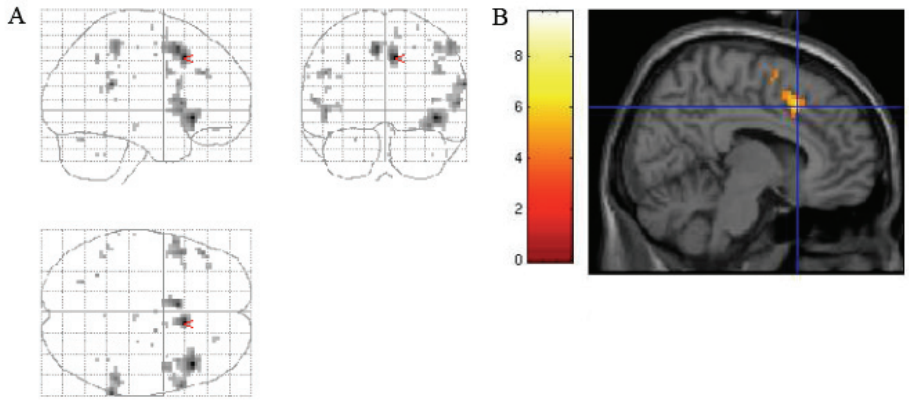

Figure S4: Whole-brain analysis of parametric responses to the amount of predictive information conveyed by the last shape when accounting for the error likelihood, the prediction error, the uncertainty and the surprise (threshold of p<0.001, see methods GLM2)**.** (A) Statistical map is rendered on a glass brain. (B) The crosshair indicates the coordinate of ACC's peak activity (x,y,z=9,18,42, Zmax=5.04).

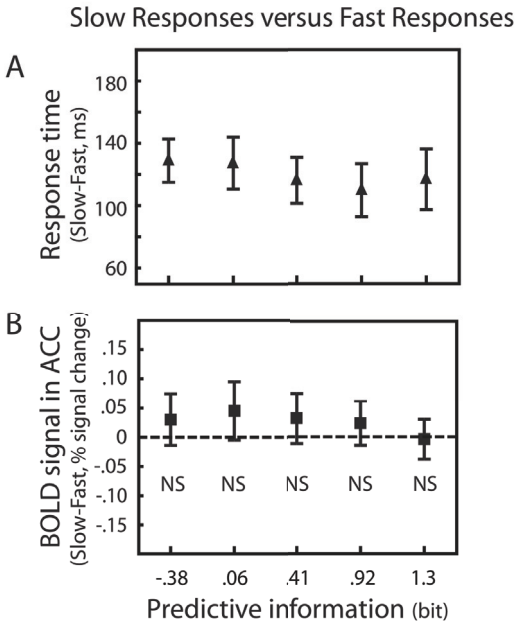

Figure S5: (A) Paired difference in RT between fast and slow responses as a function of the level of predictive information. Correct target trials were binned according to the level of predictive information ([-.43,-.05,.25,.62,1,1.32] bits) and to the response speed (fast and slow responses, according to each subject's median RT). No effect of the level of predictive information was observed on the paired difference in RT between fast and slow responses (effect of predictive information on the paired difference in RT between slow and fast responses: $F_{4,65}$=1.1242, p=0.3529). **(B) Paired difference in ACC's BOLD signal between slow and fast responses as a function of the level of predictive information.** There was no difference in ACC BOLD activity between slow and fast responses for any of the 5 levels of predictive information (T-test, -0.38 bits: p= 0.1643, .06 bits: p=0.0731, .41 bits: p=0.1353, .92 bits: p=0.2040, 1.3 bits: p=0.8053). No effect of predictive information on the paired difference in ACC BOLD activity was observed between slow and fast responses ($F_{4,65}$= 0.86, p=0.4937). Error bars in panels A and B represent 95% confidence intervals.

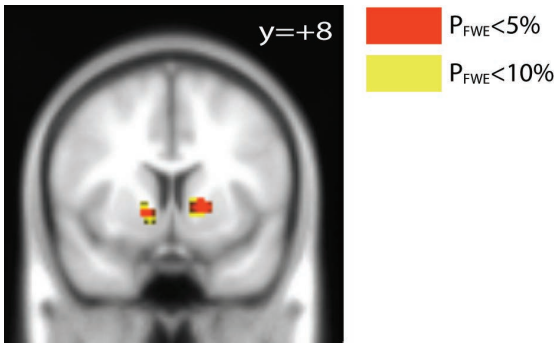

Figure S6: Group-level map of functional connectivity using the ACC as seed region. Red pixels indicate brain regions showing a significant correlation with BOLD activity in the ACC (threshold of 5% FWE whole-brain corrected).

Table S1: Whole brain analysis of parametric response to predictive information.

Location	MNI (x,y,z ;mm)	Zmax	Cluster extent (voxel)	Significance (whole-brain cluster-wise corrected)	Correlation coefficient (BOLD, sr1)	Correlation coefficient (BOLD, sr2)	Correlation coefficient (BOLD,Gain)
Predictive information conveyed by the last shape : negative parametric effect							
Anterior Cingulate Cortex	9 18 42	5.55	233	$\leq 10^{-4}$	.635-0.0036	.697-0.006	.081-NS
L IFG / Anterior Insula	-48 18 -3	5.28	184	$\leq 10^{-4}$	.393-NS	.112-NS	.103-NS
R IFG / Anterior Insula	42 24 -6	5.10	402	$\leq 10^{-4}$	.125-NS	.424-NS	.006-NS
R Intra Parietal Sulcus	36 -48 45	4.87	120	$\leq 10^{-4}$	.204-NS	.428-NS	.195-NS
R DLPFC	12 3 60	4.44	36	$\leq 10^{-4}$	.397-NS	.477-NS	.367-NS
R Superior Temporal Gyrus	63 -42 21	4.05	95	$\leq 10^{-4}$	.226-NS	.323-NS	.336-NS
L DLPFC	-42 39 33	3.67	31	0.018	.182-NS	.195-NS	-.037-NS
Predictive information conveyed by the last shape : positive parametric effect							
Posterior Cingulate Cortex	-12 -54 24	3.74	86	$\leq 10^{-4}$	N/A	N/A	N/A

Table S2: Whole brain analysis of parametric response to predictive information, including the error likelihood the prediction error and the entropy as nuisance regressors.

Location	MNI (x,y,z ;mm)	Zmax	Cluster extent (voxel)	Significance (Whole-brain cluster-wise corrected)
Predictive information conveyed by the last shape : negative parametric effect				
R Anterior Cingulate Cortex	9 18 42	5.04	50	$\leq 10^{-3}$
L Anterior Cingulate Cortex	-6 12 51	4.51	44	2.10^{-3}
L IFG / Anterior Insula	-48 15 0	4.02	50	10^{-3}
R Anterior Insula	42 24 -6	4.86	105	$\leq 10^{-4}$
R IFG	60 15 6	4.22	42	3.10^{-3}
R Intra-Parietal Sulcus	54 -39 51	3.97	40	4.10^{-3}
Predictive information conveyed by the last shape : positive parametric effect				
Posterior Cingulate Cortex	-12 -51 27	3.90	47	0.002
Middle Temporal Cortex	57 -12 -27	3.79	33	0.012

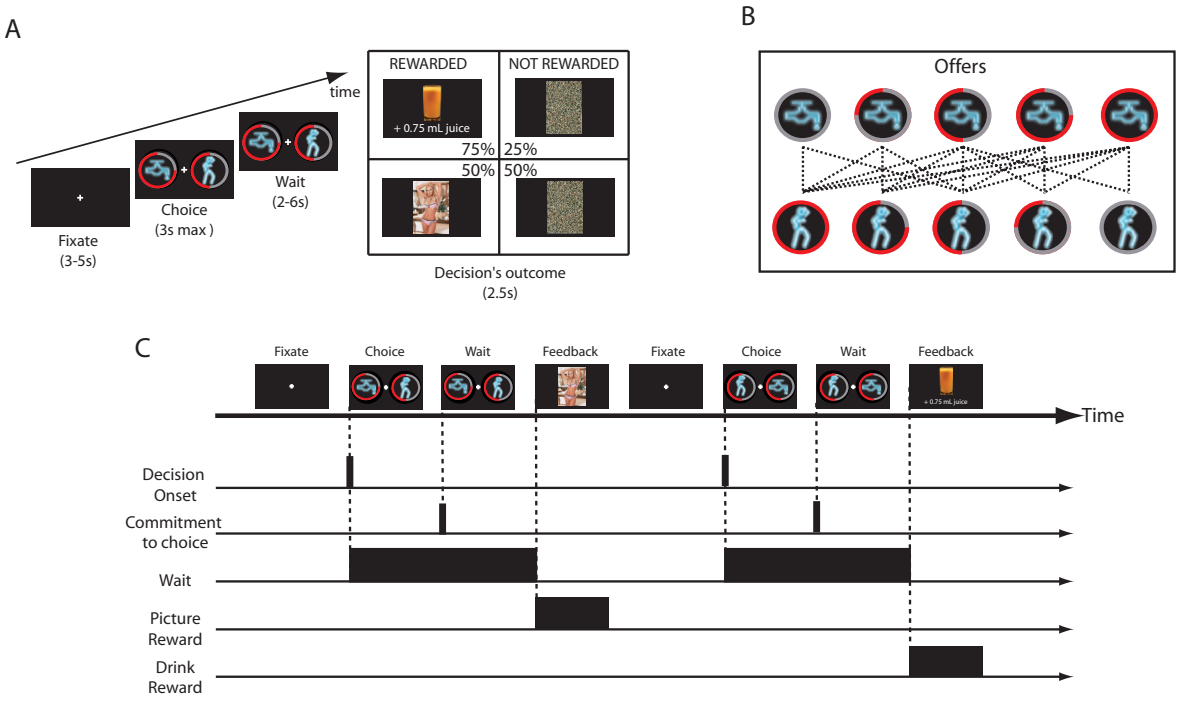

Figure 1: Experimental paradigm. (A) Participants were asked to choose between two options, one of which was probabilistically rewarded by an erotic picture and the other one by a fixed amount of fruit juice delivered to the subject mouth by a computer-driven pump. Here, the participant could choose between 75% chances of drinking 0.75 mL juice or 50% chances of viewing an erotic picture by pressing one of two responses button according to the position of the chosen option relative to the central fixation cross. After a random delay, the participant received the chosen goods according to his choice and the probability of reward associated ("rewarded" choice trials). A scrambled picture was displayed when the choice did not yield the expected good ("not rewarded" choice trials). **(B)** Thirty-nine different offers were built by systematically varying the reward probabilities (p=[0.25, 0.5, 0.75, 1]) associated with the drink and the picture options. **(C)** The main GLM included five event-related categorical regressors to model choice trials: Decision onset, Commitment to choice, Wait, Picture reward and Drink reward. In accordance with drift diffusion model accounts of decision-making, ongoing processes during value-based decision formation were modeled as Dirac functions time locked to each decision onset (Decision onset) and the processes associated with decision threshold crossing or motor responses were modeled as a Dirac function time locked to the response button press. Parametric regressors associated with each categorical regressor modeled events all the variables events and quantities relating to the decision process.

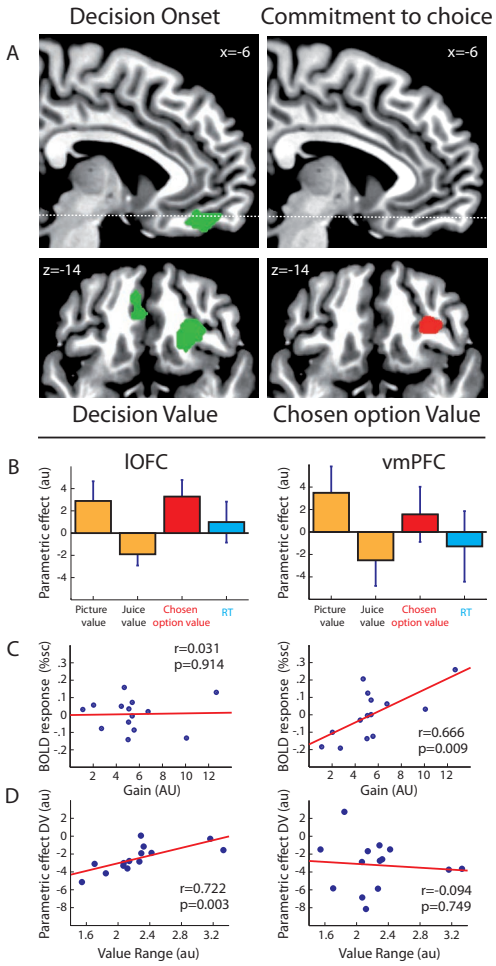

Figure 4: Mediolateral functional specialization in the OFC. (A) Parametric response to subjective values in the OFC (threshold of $p<10^{-3}$ voxelwise for display). OFC clusters showing a significant parametric response to the offer's decision value at decision onset are rendered in green (left column) and those showing a parametric response to the expected value of the chosen option at the time of commitment to choice are rendered in red (right column). (B) Bar graphs reporting the slope of the regression line between BOLD activity and the picture and juice expected value (yellow bars), the expected value of the chosen option (red bars) and response time (blue bars), in the lOFC (left graph) and the vmPFC (right graph). Error bars indicate 95% confidence intervals. In the lOFC, there was a significant parametric effect of the picture (T-test, p=0.0043), of the drink (T-test, p=0.0014) and of the chosen option (T-test, p=0.0013) expected values. In the vmPFC, there was a significant parametric effect of the picture (T-test, p=0.0124), of the drink (T-test, p=0.0384) and of the chosen option (T-test, p=0.252) expected values. By contrast, there was no parametric effect of RTs in both the vmPFC (T-test, p=0.5043) and the lOFC (T-test, p=0.3835). (C) Scatterplots of correspondence between mean BOLD activity at decision onset and the gain parameter estimated using the mEZ2 drift-diffusion model in the lOFC (left graph) and the vmPFC (right graph). (D) Scatterplots of correspondence between the slope of the regression line between BOLD activity at decision onset and the decision value (parametric effect of DV) and the value range (the difference between the maximal and the minimal subjective value in the experiment) in the lOFC (left graph) and the vmPFC (right graph). Please note that the significances of the linear relationship between parametric effect of decision value and value range observed were only marginally affected when removing the two most extremes subjects (value range > 2.5).

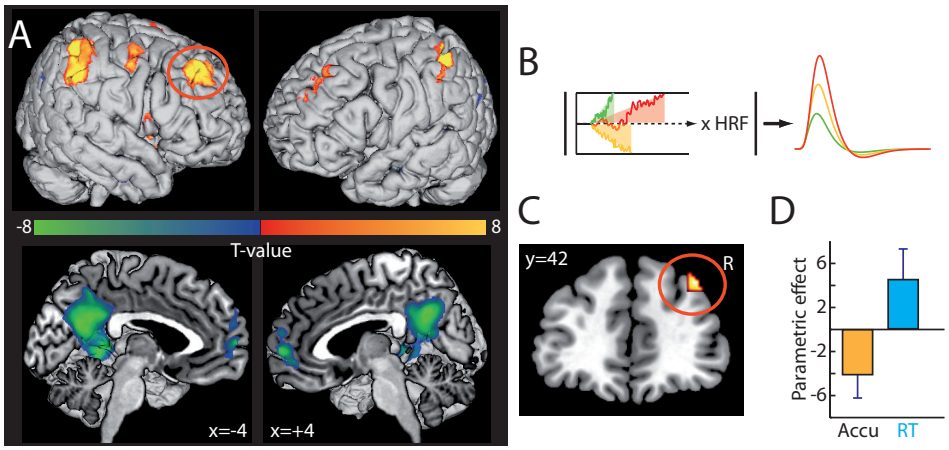

Figure 5: Brain region implementing a drift-diffusion decision process. (A) Psycho-physiological interaction whole-brain analysis between vmPFC and other brain areas during economic choices formation (PPI). Positive PPIs are rendered using a hot scale and negative PPIs are rendered using a cold scale (threshold for display, $p<10^{-3}$ voxelwise). (B) mEZ2 drift-diffusion model predictions on BOLD activity of brain region implementing this process: convolving predicted neural activity with the hemodynamic response function predicted lower BOLD activity for steeper accumulations of the decision value (green) and higher BOLD activity for longer RT (red). (C) Brain regions whose BOLD activity correlates negatively with the absolute value of the drift-diffusion process accumulation slope (MNI, xyz: 38, 42,42, 10^{-3} voxelwise, p=0.03 FWE cluster corrected) among the brain regions exhibiting a positive PPI with the vmPFC during decision formation. (D) Bar graphs reporting the slope of the regression line between BOLD activity and the absolute value of the drift-diffusion process accumulation slope (yellow bars, T-test, p=0.0029) and response times (blue bars, T-test, p= 0.02). Error bars represent 95% confidence intervals.

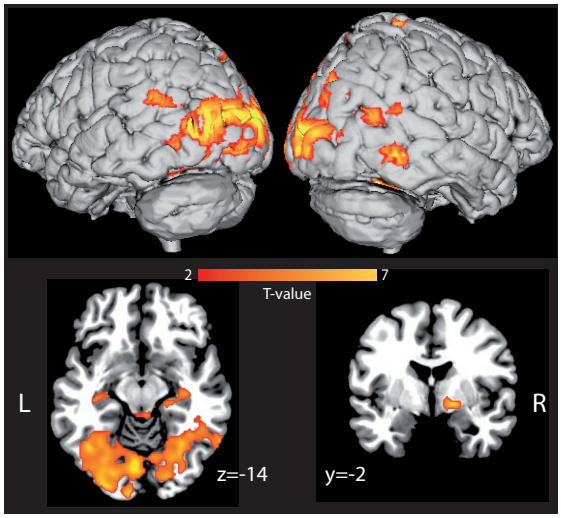

Figure 6: vmPFC input brain regions associated with optimal economic choices. We performed a psycho-physiological whole-brain analysis of vmPFC effective connectivity during economic choice formation by contrasting optimal and suboptimal choices. Positive PPIs are rendered using a hot scale and negative PPIs are rendered using a cold scale (threshold for display, $p<10^{-3}$ voxelwise).

ARCHIVAL REPORT

Impaired Hierarchical Control Within the Lateral Prefrontal Cortex in Schizophrenia

Guillaume Barbalat, Valerian Chambon, Philippe J.D. Domenech, Chrystèle Ody, Etienne Koechlin, Nicolas Franck, and Chlöé Farrer

Background: In schizophrenia, disturbances of cognitive control have been associated with impaired functional specialization within the lateral prefrontal cortex (LPFC), but little is known about the functional interactions between specialized LPFC subregions. Here, we addressed this question with a recent model that describes the LPFC functioning as a cascade of control processes along a rostrocaudal axis, whereby anterior frontal regions influence the processing in posterior frontal regions to guide action selection on the basis of the temporal structure of information.

Methods: We assessed effective connectivity within the rostrocaudal axis of the LPFC by means of functional magnetic resonance imaging in 15 schizophrenic patients and 14 matched healthy control subjects with structural equation modeling and psychophysiological interactions.

Results: In healthy subjects, activity in the left caudal LPFC regions was under the influence of left rostral LPFC regions when controlling information conveyed by past events. By contrast, schizophrenic patients failed to demonstrate significant effective connectivity from rostral to caudal LPFC regions in both hemispheres.

Conclusions: The hierarchical control along the rostrocaudal axis of the LPFC is impaired in schizophrenia. This provides the first evidence of a top-down functional disconnection within the LPFC in this disorder. This disruption of top-down connectivity from rostral to caudal LPFC regions observed in patients might affect their ability to select the appropriate sets of stimulus-response associations in the caudal LPFC on the basis of information conveyed by past events. This impaired hierarchical control within the LPFC could result from poorly encoded contextual information due to abnormal computations in the caudal LPFC.

Key Words: Effective connectivity, functional magnetic resonance imaging, hierarchical control, lateral prefrontal cortex, rostrocaudal axis, schizophrenia

In schizophrenia, disturbances of cognitive control, the ability to coordinate thoughts and actions in relation to internal goals, have been robustly associated with impaired functional specialization within the lateral prefrontal cortex (LPFC) (1–6). Recent models suggest that cognitive control is constructed as a set of hierarchical modules that involve selecting and maintaining goals at multiple levels of abstraction, from general task goals at higher levels (such as watching a movie in the cinema) to concrete motor responses at the lowest levels (such as taking transport to go to the cinema, buying a ticket at the box office, or sitting comfortably in front of the screen) (7). Such a behavioral hierarchy has been shown to be subserved by a hierarchical organization along the rostrocaudal axis of the LPFC, where more anterior regions are associated with progressively more abstract action control, whereas more posterior regions process more concrete information about action (i.e., action that is closer to the actual motor output) (8). Furthermore, there seems to be a dominance relationship whereby more anterior regions that process abstract, superordinate, domain-general rules, modulate domain-specific, subordinate, posterior regions (9).

From the Centre de Neuroscience Cognitive, (GB, VC, PD, NF), UMR 5229 CNRS, Université Claude Bernard Lyon1, Lyon, France; Centre Hospitalier le Vinatier (NF), Lyon; Institut National de la Sante Et de la Recherche Medicale (CO, EK), Université Pierre et Marie Curie and École Normale Supérieure, Paris; and Université de Toulouse (CF), CerCo, UPS and UMR5549 CNRS, Faculté de Médecine de Rangueil, Toulouse, France.

Authors VC and PJDD contributed equally to this work.

Address correspondence to Guillaume Barbalat, M.D., Ph.D. Centre deNeuroscience Cognitive Universite Claude Bernard Lyon, 67, bd Pinel, 69 675 BRON, Cedex, France; E-mail: gbarbalat@isc.cnrs.fr.

Received Dec 30, 2009; revised Jan 31, 2011; accepted Feb 1, 2011.

We previously investigated the overall organization of cognitive control within the LPFC in schizophrenia with an influential model (10) that describes the architecture of cognitive control as a cascade of executive modules ranging from premotor to more anterior LPFC regions (3,11). This model includes a sensory control level involved in selecting the motor responses that are the most appropriate to stimuli that occur and subserved by the lateral premotor regions (typically, Brodmann Area [BA] 6). A contextual control level is then involved in selecting premotor representations (i.e., stimulus-response associations) according to contextual signals that accompany the occurrence of stimuli. This control is subserved by the caudal part of the LPFC (typically, BAs 9/44/45). Finally, the episodic control level is involved in selecting caudal LPFC representations (task-sets or consistent sets of stimulus-response associations evoked in the same immediate, perceptual context) according to the temporal episode in which stimuli occur. This control is subserved by the rostral part of the LPFC (typically, BAs 46/10).

We demonstrated that, although the lower-order, less abstract, sensory level of cognitive control was spared in schizophrenia, contextual control was significantly impaired (11), which was related to hypoactivation in the caudal LPFC regions (3). With regard to episodic control, we found mixed but consistent findings. When no contextual signals were involved in the task, there was no behavioral disturbance of episodic control in schizophrenia (11). By contrast, adding contextual signals in the task reduced this level of cognitive control. In other words, this impaired episodic control process refers in fact to a dysfunctional interaction between the "episodic" and the "contextual" modules (3,11).

At the neural level, this disturbed episodic control process in schizophrenic patients was not reflected by any hypoactivation in the rostral LPFC. By contrast, we found a hyperactivation in this region, which we interpreted as a consequence of the added effort that patients might expend to retrieve the poorly integrated contextual information (2,3,12,13). However, the neural substrates underlying this dysfunctional control of episodic signals remain unknown.

0006-3223/$36.00
doi:10.1016/j.biopsych.2011.02.009

According to the functional disconnection hypothesis proposed by Friston (14), such a dysfunctional interaction between two cognitive processes should result from dysfunctional interaction in the dynamics of the brain regions subserving these processes rather than dysfunctional specialization within a specific region. The framing of the cascade model further predicts that this impairment in episodic control would depend on the way rostral LPFC exerts its influence on the caudal LPFC regions (9). However, until now, studies that have investigated the interaction between specialized neural systems related to executive dysfunctions in schizophrenia have demonstrated altered LPFC connectivity with other cortical structures such as the inferior parietal lobule (5), the hippocampus (15), or the anterior cingulate cortex (16) but have not directly studied the functional integration of the different cognitive control modules within the LPFC itself.

The goal of this follow-up study was to test whether the perturbed control of temporal episodic signals in patients reflects a dysfunction in the top-down selection of caudal LPFC representations by rostral LPFC. For this purpose, we based our analysis on data collected in our previously published study (3) and measured effective connectivity between LPFC regions involved in controlling episodic and contextual signals in both groups with structural equation modeling (SEM) and psychophysiological interactions (PPIs).

Methods and Materials

Subjects

This analysis initially involved 15 schizophrenic patients ($n = 15$) and 15 matched healthy control subjects, 1 of whom was excluded because of excessive motion in the scanner ($n = 14$) (3). For more details about the description of the participants, please refer to Supplement 1 (see also Table 1).

Experimental Paradigm

The experiment included eight scanning sessions, each consisting of eight separate blocks presented in a counterbalanced order. Each block comprised a series of 12 successive stimuli (colored letters; duration: 500 msec; onset asynchrony: 3500 msec) preceded by an instruction cue lasting 4200 msec (Figure 1). Each instruction informed the subjects to make speeded responses to stimuli by pressing left or right hand-held response buttons or to withhold a response to a no-go stimulus. Instructions were prelearned by the subjects before running the experiment to avoid possible biases due to learning effects during the test session.

In each scanning session, the eight blocks formed four distinct experimental conditions crossing the demands of contextual and episodic control varied by manipulating the context (I_{con}) and the episode (I_{epi}) factors, respectively. These variations were quantified according to the computational model from Koechlin *et al.* (10), on the basis of Shannon's information theory (17).

The color of the letter was the contextual signal within each block. According to the contextual signal, subjects had to perform one of three tasks: 1) ignore the letters; 2) a vowel/consonant discrimination task (T1: if the letter is a vowel, press the right response button; if the letter is a consonant, press left); or 3) a lower/uppercase discrimination task (T2: if the letter is uppercase, press right; if the letter is lowercase, press left). Where contextual control was low, the task remained the same across the entire block (T1 or T2, single-task-set blocks, $I_{con} = 0$ bit; block no. 1,2,5,6 in Figure 1). In high contextual control blocks, the task changed from trial to trial (T1 and T2, dual task-set blocks, $I_{con} = 1$ bit; blocks no. 3,4,7,8 in Figure 1).

The episodic signal was by definition the instruction cue preceding each block. Episodic signals conveyed information about the contingencies linking contextual signals (i.e., the color of the letter) and task-sets (i.e., T1 or T2) that occurred in the proceeding sequence of letters and were chosen to parametrically vary the amount of episodic information across blocks. Therefore, the episode factor was the covariate of interest that contrasted episodes according to the episodic information I_{epi} conveyed by instruction cues that were required for subsequently selecting appropriate task-sets with respect to contextual signals ($I_{epi} = 0$ to 1 and 2 bits). For example, in Block No. 1, the instruction cue indicated that, if the letter is white, no response should be given, whereas if the letter is green, the subjects should perform task T1 (Figure 1). Then, with information theory, we computed different values for the episodic control demand, such that the more frequent the crosstemporal

Table 1. Clinical and Demographic Characteristics

Characteristic	Patients ($n = 15$)	Comparison Subjects ($n = 14$)	p
Male Gender, *n* (%)	8 (53)	8 (57)	.68
Age, yrs	35 (10.5)	36 (10.6)	.79
Education, yrs	11 (1.3)	11 (1.9)	.82
Handedness	.86 (.09)	.84 (.11)	.50
Duration of Illness, yrs	10 (9)	—	—
SANS Score	43 (19)	—	—
SAPS Score	23 (21)	—	—
Reality Distortion Score[a]	8 (10)	—	—
Poverty Score[b]	34 (18)	—	—
Disorganization Score[c]	23 (13)	—	—
Chlorpromazine-Equivalent[d], mg/day	247 (190)	—	—

Values are mean ± SD, unless otherwise indicated.

SANS, Scale for the Assessment for Negative Symptoms (50). SAPS, Scale for the Assessment of Positive Symptoms (51).

[a]Sum of the scores for hallucinations and delusions from the SAPS.

[b]Sum of the scores for poverty of speech, flat affect, anhedonia/asociality, and amotivation from the SANS.

[c]Sum of the scores for formal thought disorder and bizarre behavior from the SAPS and the score for attention from the SANS.

[d]Depot doses of and daily-oral atypical antipsychotics at the time of the examination (risperidone in 6 patients, olanzapine in 3 patients, amilsupride in 3 patients, and aripiprazole in 2 patients) were converted to average daily chlorpromazine-equivalent doses. None of the patients received a concurrent typical antipsychotic, anticholinergic agent, sedative treatment, mood stabilizer, antidepressant, or other psychotropic agent.

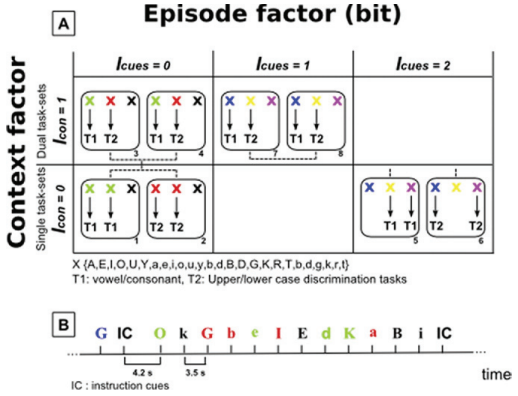

Figure 1. Experimental design. **(A)** Rounded boxes represent behavioral episodes (numbered from no. 1 to no. 8) with related stimuli (letters) and instructions. Episodes formed four distinct experimental conditions crossing the episodic factor with the context factor. According to the color of the letter (contextual signal), subjects either ignored the letter or performed a vowel/consonant (T1) or lower/uppercase (T2) discrimination task on the letters. Block no. 1: contextual signals were either green or white. White signals indicated that subjects should ignore the letter. Green signals indicated that subjects should perform task T1 (single task-set episode). Block no. 2: contextual signals were either red or white. White signals indicated that subjects should ignore the letter. Red signals indicated that subjects should perform task T2 (single task-set episode). Blocks no. 3 and no. 4: contextual signals were green, red, or white. Subjects responded to letters as described for blocks no. 1 and no. 2 (dual task-set episode). Blocks no. 5: contextual signals were yellow, blue, or purple. Blue signals instructed subjects to ignore the letters. Yellow and purple signals instructed subjects to perform task T1 (single task-set episode). Block no. 6: contextual signals were yellow, blue, or purple. Yellow signals instructed subjects to ignore the letters. Blue and purple signals instructed subjects to perform task T2 (single task-set episode). Blocks no. 7 and no. 8: contextual signals were yellow, blue, or purple. Purple signals instructed subjects to ignore the letters. Blue and yellow signals instructed subjects to perform tasks T1 and T2, respectively (dual task-set episode). Dashed lines connect episodes involving congruent associations between contextual signals and task-sets. **(B)** Typical episode.

contingencies between contextual signals and task-sets, the lower the amount of episodic information—thus the lower the demand of episodic control. More specifically, the episodic control demand depended on the proportion *f* of episodes involving congruent associations between contextual signals and task-sets over the whole experiment. When this proportion was maximal ($f = 1$, such as in blocks no. 1,2,3,4 where green always denoted "T1," red always denoted "T2," and white was always "no-go"), the demand of episodic control was low ($I_{epi} = 0$ bit). By contrast, the decrease of this frequency ($f < 1$, such as in blocks no. 5,6,7,8 where blue, purple, and yellow could all denote "T1," "T2," or "no-go") led to an increase in the episodic control demand ($I_{epi} > 0$ bit). Because the same crosstemporal contingencies were involved in blocks no.7 and no. 8, these two blocks had a lower episodic control demand ($I_{epi} = 1$ bit) than that in blocks no. 5 or no. 6, which contained different crosstemporal contingencies ($I_{epi} = 2$ bits).

In each block, the proportion of letters to be ignored was 33%. In dual task-set blocks, the ratio of trials associated with task-set T1 versus task-set T2 was equal to 1. Finally, in each block, the ratio of left versus right responses was equal to 1, and the ratio of congruent versus incongruent letters (same vs. different responses for T1 and T2) was equal to 1. Accordingly, sensorimotor control was constant across the experiment.

The methods for the behavioral analyses, magnetic resonance imaging (MRI) procedures and preprocessing, delimitation of the regions of interest, and regions of interest analyses are reported in Supplement 1.

Effective Connectivity Analyses

We investigated, on the basis of anatomical and functional connections in the frontal lobes described previously (10,18), the existence of a top-down control system from rostral to caudal LPFC regions (identified by the exploratory analyses in each of the two groups, see Supplement 1).

Structural Equation Modeling

The structural equation model included top-down paths from rostral to caudal regions as well as additional reciprocal paths linking the same regions located in the left and right hemispheres to account for callosal interhemispheric connections. The functional model was therefore reformulated as a model of structural linear equations with path coefficients quantifying effective connectivity as partial temporal correlations between related regional activations.

We sought to test the prediction of the cascade model that path coefficients from rostral to caudal LPFC regions significantly increase with the demand of episodic control rather than contextual control (10). Subject-specific time series of functional MRI signals were obtained at activation peaks, averaged over subjects, and standardized in each condition (mean and variance were equated across conditions). The resulting time series were then used for structural model estimation and statistical inference on the basis of maximum-likelihood statistics. We assessed significant variations of path coefficients within each group with a nested model approach (19) (see also Supplement 1). Variations of path coefficients related to the episode and context factors were estimated from variations in interregional correlation matrices observed between all episodes with $I_{epi} = 0$ versus $I_{epi} > 0$ and $I_{con} = 0$ versus $I_{con} = 1$, respectively.

PPIs

To account for between-subject variability and to make a statistical inference about group differences in effective connectivity within the LPFC, we computed pair-wise PPI between LPFC regions (20).

Here, we specifically sought to test whether substantial variations from rostral to caudal LPFC activity resulted from underlying neuronal interactions with the episodic factor in both hemispheres (i.e., from the condition where the episodic control demand was low—$I_{epi} = 0$ bit—to the condition where the episodic control demand was high—$I_{epi} = 2$ bits—with $I_{con} = 0$ bit). For each of the regions identified by the exploratory voxel-wise contrasts, individual time-series were extracted at the peak voxel and standardized in each condition. Then, treating intersubject variability as a random factor, we tested whether the slopes (β) of the regression of caudal LPFC activity against rostral LPFC activity significantly increased as a function of the episodic factor within each group and between groups (from β_{low}, the slope when $I_{epi} = 0$, to β_{high}, the slope when $I_{epi} = 2$ bits) (see Supplement 1 for more details). Note that these PPI analyses are orthogonal with the ones issued from our previous report (3).

Results

Patients made significantly more errors than control subjects with regard to both the context and the episode factors (Figure 2). Because this poor performance in patients might confound

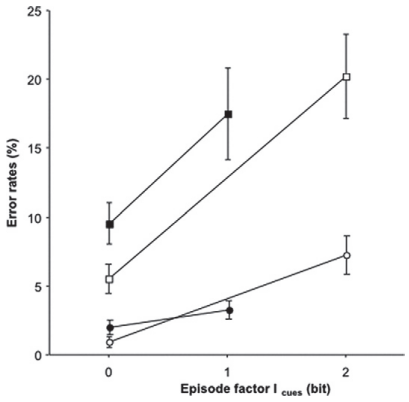

Figure 2. Behavioral results. Error rates (%, mean ± SE across participants) across experimental conditions. Open circles and squares indicate single task-set episodes in control subjects and schizophrenic patients, respectively. Solid circles and squares indicate dual task-sets episodes in control subjects and schizophrenic patients, respectively.

changes in functional brain activation, we matched groups for accuracy by removing from the analyses blocks in which performance was unsatisfactory (i.e., accuracy < .65) (see Tan *et al.* [4] for the use of a similar threshold) (see also Supplement 1 for more details). After applying this criterion, there were no behavioral differences between the two groups with regard to both the episode and the context factors [$F(1,81) < .21$, $p > .05$].

In each of the two groups, we first identified rostral and caudal LPFC as the LPFC regions involved in controlling episodic and contextual signals, respectively (Table 2). Caudal LPFC regions demonstrated a group × context interaction [$F(1,81) = 3.76$, $p = .05$], with patients showing no modulation of activation related to the contextual factor in these regions (Figure S1 in Supplement 1). By contrast, caudal LPFC regions demonstrated neither a main effect of group nor an interaction between group and episode [$F(1,81) < 1.15$, $p > .05$]. Finally, we found a group effect in rostral LPFC regions [$F(1,81) = 6.97$, $p < .05$], with patients activating this region more than control subjects.

Structural Equation Modeling Analyses

The cascade model predicts that contextual control involves no top-down control from anterior to more posterior LPFC regions (10,18). Indeed, when the demand of contextual control increased, no path coefficients were found to significantly increase from rostral to caudal LPFC regions with the context factor in both groups [all $\chi^2(1) < 3.36$, $p > .05$; Figure 3].

By contrast, the model predicts that path coefficients from rostral to caudal LPFC regions will significantly increase with the demand of episodic control (10,18). Indeed, when the demand of episodic control increased, a significant increase of path coefficients was found in healthy subjects from rostral to caudal left LPFC regions [$\chi^2(1) = 4.44$, $p < .05$; in the right hemisphere: $\chi^2(1) = .23$, $p > .05$; Figure 3]. This left lateralization might result from the exclusive use of verbal material (letter stimuli), which is preferentially processed in the left hemisphere (21). In patients, however, no path coefficients significantly increased with the episodic factor from rostral to caudal LPFC regions in either hemisphere [$\chi^2(1) < 1.96$, $p > .05$; Figure 3].

PPI Analyses

In control subjects, the significant variations of path coefficients from rostral to caudal LPFC regions reported in the SEM analysis corresponded to a significant PPI between activity in rostral and caudal LPFC regions related to the episodic factor (Figure 4). In other words, the strength of the regression between activity in caudal and rostral LPFC regions depended on the episodic factor (from $I_{epi} = 0$ to $I_{epi} = 2$ bits). Indeed, we found a significant increase in the regression slopes (β) of left caudal LPFC activity against left rostral LPFC activity as a function of the episodic factor [$F(1,459) = 8.9$, $p < .005$; $\beta_{low} = -.04$; $\beta_{high} = .43$; Figure 4A]. In patients,

Table 2. Within-Group Localization of the LPFC Regions Displaying Episode and Context Effects Used for the Effective Connectivity Analyses

Group, Effect, and Lateral Frontal Cortex Region	Estimated BA	Coordinates[a] x	y	z	Analysis t[b]	Volume[c]	FDR p
Healthy Subjects							
Context effect[d]							
Left middle frontal gyrus, caudal PFC	BA 9	−42	39	36	6.27	37,084	.038
Right middle frontal gyrus, caudal PFC	BA 9	42	33	39	5.21	8277	.038
Episode effect (excluding context effect)							
Left superior frontal gyrus, rostral PFC	BA 10	−27	54	−3	4.23	185	.037
Right middle frontal gyrus, rostral PFC	BA 10	33	63	9	3.49	139	.037
Schizophrenia Patients							
Context effect[d]							
Left middle frontal gyrus, caudal PFC	BA 9	−33	42	12	4.92	2867	.087
Right middle frontal gyrus, caudal PFC	BA 9	33	36	27	4.41	786	.087
Episode effect (excluding context effect)							
Right middle frontal gyrus, rostral cortex	BA 10	27	51	0	4.77	8046	.026
Left middle frontal gyrus, rostral cortex	BA 46	−36	48	9	4.02	1295	.026

LPFC, lateral prefrontal cortex; BA, Brodmann's Area; FDR, false discovery rate; PFC, prefrontal cortex.
[a]Coordinates from the stereotaxic atlas of Talairach and Tournoux (52).
[b]Regional peak activation representing blood oxygen-level dependent signal change that reached a threshold of $p < .05$ (corrected for the false discovery rate) in a random-effect analysis.
[c]Values are mm^3.
[d]These peaks are nonsignificant but are reported because we do not want to give the impression that the activations are absent in schizophrenia patients regarding the context effect.

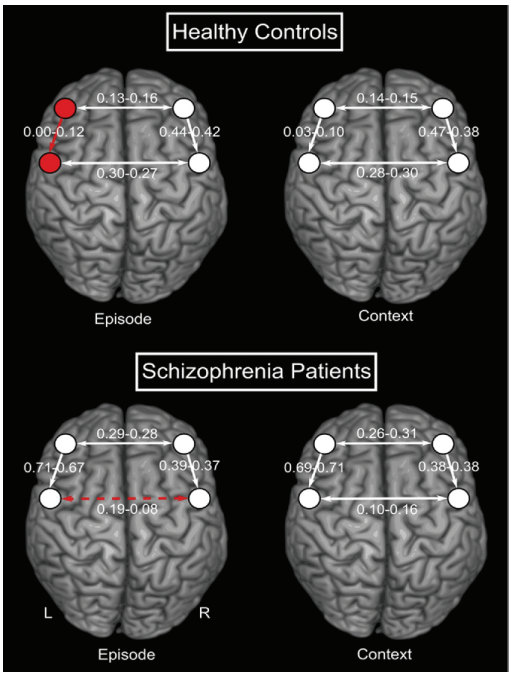

Figure 3. Diagram of path coefficients between lateral prefrontal regions involved in episodic and contextual control subjects for healthy subjects and schizophrenic patients. The structural equation model included the paths (lines, arrows indicate oriented structural paths) connecting prefrontal regions described in the text (circles, neurological convention, approximate locations). Variations of path coefficients in healthy subjects (upper panels) and in schizophrenic patients (lower panels) are shown. (**Left**) Path coefficients in episodes associated with $I_{epi} = 0$ (left number) and $I_{epi} > 0$ (right number). (**Right**) Path coefficients in single-task-set (left number) and dual-task-sets (right number) episodes. Path coefficients that significantly increased with the episodic factor are shown in red. No path coefficients were found to significantly increase with the context factor. The red dashed arrow in the left lower panel indicates a path coefficient that significantly decreased with the episode factor in patients [$\chi^2(1) = 15.78$, $p < .001$].

however, we found a significant decrease in the regression slopes of left caudal LPFC activity against left rostral LPFC activity as a function of the episodic factor [$F(1,492) = 8.9$, $p < .01$; $\beta_{low} = .60$; $\beta_{high} = .42$; Figure 4B]. We observed no significant PPI between rostral and caudal LPFC regions related to the episodic factor in the right hemisphere in either group ($F < 1.8$, $p > .05$; Figures 4C and 4D). Finally, we observed no significant PPI between rostral and caudal LPFC regions related to the contextual factor in both hemispheres, in either group ($F < 3.0$, $p > .05$), which confirmed the results of our SEM analysis.

We observed stronger effective connectivity from rostral to caudal LPFC regions related to the episodic factor in control subjects than in patients in the left hemisphere [left hemisphere: interaction among rostral LPFC activity, the episodic factor and the group factor: $F(1,951) = 16.6$, $p < .001$; right hemisphere: no interaction, $F(1,951) = .8$, $p > .05$]. The β value was significantly greater in the low-episodic control condition in patients than in control subjects [interaction between rostral LPFC activity and the group factor: $F(1,462) = 14$, $p < .001$]. In contrast, the β values were nonsignificantly different between the two groups in the high-episodic control condition [rostral LPFC activity × Group interaction: $F(1,462) = .01$, $p > .05$].

Finally, one could argue that the reduced rostrocaudal connectivity in patients could result from a bias in the analyses, because we excluded blocks in which accuracy was < .65 to prevent a performance bias. This manipulation could indeed have reduced the power of the analysis of the schizophrenia dataset relative to the control subjects. However, when rerunning the analysis with the whole dataset in both groups, we still found significantly less modulation of the caudal LPFC by the rostral LPFC in patients relative to control subjects with regard to the episodic factor in the left hemisphere [left hemisphere: interaction among rostral LPFC activity, the episodic factor, and the group factor, $F(1,951) = 10$, $p < .005$; right hemisphere: no interaction, $F(1,951) = .04$, $p > .05$].

Discussion

Our analyses support the idea that, in healthy subjects, the LPFC is hierarchically organized from rostral to caudal LPFC regions, where anterior regions integrate temporally dispersed information for selecting the appropriate action at each time from posterior LPFC regions (8–10,18,22). By contrast, we found impaired hierarchical control along the rostrocaudal axis of the LPFC in individuals with schizophrenia.

It is worth noting that our sample of patients was treated with atypical antipsychotics, which could potentially perturb the effective connectivity through the frontal cortex in schizophrenic patients. However, impaired effective connectivity within the frontal lobes has been observed in drug-naive as well as in medicated patients, making this potential confound a less likely explanation of our findings (23,24). Another potential limitation of our findings pertains to the difficulty of the task itself. Because the task was relatively complicated, it is likely that the patients who participated in the study performed much better than other patients with lower levels of education or more florid positive or negative symptoms would. That being said, we are quite confident that our results are reproducible, provided that they involve clinically stable patients with a minimum level of education, as in the current experiment. Indeed, a previous study from our group found the same pattern of behavioral results (i.e., contextual and episodic control impairments in patients) with a different sample of subjects (11). Moreover, although our functional MRI findings are novel, they support other studies showing hypoactivation in the caudal LPFC in schizophrenia (1,2,4,5,13,25–27) and are consistent with our initial hypotheses.

According to the cascade model, rostral LPFC regions are involved in selecting caudal LPFC representations to monitor the appropriate selection of task-sets evoked in the same context, a process referred to as episodic control (10). More specifically, the episodic control demand depends on the proportion *f* of episodes involving congruent associations between contextual signals and task-sets. When this proportion is maximal ($f = 1$, such as in blocks no. 1, 2, 3, and 4 in our task), the demands on episodic control are low, which is paralleled by a decrease in top-down connectivity from rostral to caudal LPFC regions. By contrast, the decrease in this frequency ($f < 1$, such as in blocks no. 5, 6, 7, and 8) leads to an increase in episodic control demands and in rostrocaudal connectivity within the LPFC. In the current study, we demonstrated that this modulation of top-down LPFC connectivity by the demands of episodic control was impaired in schizophrenia. Crucially, this might have affected the ability of patients to select the appropriate

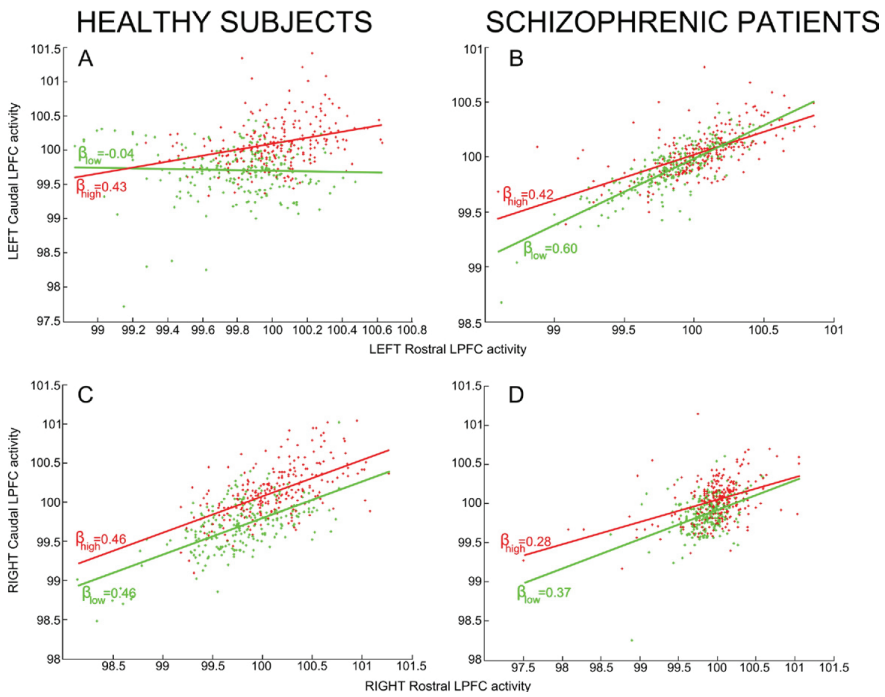

Figure 4. Psychophysiological interaction (PPI) between rostral and caudal lateral prefrontal cortex (LPFC) in healthy subjects and schizophrenic patients. Measurements when the demand of episodic control is low ($I_{epi} = 0$ bit), green crosses; measurements when the demand of episodic control is high ($I_{epi} = 2$ bits), red crosses. Condition-specific regression slopes, β_{low} (i.e., when $I_{epi} = 0$ bit) and β_{high} (i.e., when $I_{epi} = 2$ bits). All subjects are plotted together. The difference between regression slopes constitutes the PPIs. (**A** and **B**) Mean-corrected blood oxygen-level dependent (BOLD) activity (in arbitrary units) in left caudal LPFC is displayed as a function of the mean-corrected BOLD activity in left rostral LPFC. (**C** and **D**) Mean-corrected BOLD activity in the right caudal LPFC is displayed as a function of mean-corrected BOLD activity in right rostral LPFC.

sets of stimulus-response associations in the caudal LPFC on the basis of the information conveyed by past events.

Previous findings from our group demonstrated that this impaired episodic control process was specifically observed when patients had to control information conveyed by episodic and contextual (vs. sensory) signals (11). This result suggests that episodic control disturbances could arise from inappropriate contextual control, which is itself related to abnormal activation of the caudal LPFC (3). Other findings from the schizophrenia literature have also proposed that a context processing impairment could be at the core of the cognitive control disturbances in schizophrenic patients, related to specific disturbances in the dorso-caudal LPFC (1,2,26–30). In other terms, the disruption of top-down connectivity from rostral to caudal LPFC regions in patients could primarily be the consequence of poorly encoded contextual information, which might be due to abnormal computations in the caudal LPFC. In turn, hyperactivation in rostral LPFC regions might serve as a compensatory function to maintain a minimum level of performance during episodic control (i.e., to retrieve the poorly integrated contextual information) (12,13).

At a more distal level, our results suggest that this impaired effective connectivity within the LPFC in patients is related to abnormally high levels of connectivity between rostral and caudal LPFC regions in the low-episodic control condition (the regression coefficient between rostral and caudal LPFC activities was significantly greater in patients than in control subjects in the low-episodic control condition, whereas the groups did not significantly differ in the high-episodic control condition). It is interesting to note that such an increase in connectivity in low-level conditions, together with a relative decrease in higher-level conditions of cognitive control, is conceptually analogous to findings from previous studies that also investigated cognitive control in schizophrenia, with computational models of context processing (31). Specifically, it was suggested that increased noise in the subcortical dopamine system at rest (32,33) leads to abnormal "gating" of context information into prefrontal cortex (34–35). Although these findings deal with distinct types of information (contextual vs. episodic signals), one cannot exclude that these two phenomena both rely on the same neurobiological mechanism responsible for "gating" different classes of information into specialized subregions within the prefrontal cortex.

Other hypotheses closely related to the concept of episodic control have been proposed to better characterize the impaired processes involved in episodic task performances in schizophrenia. One hypothesis highlights the importance of cognitive control and related LPFC functioning in episodic memory disturbances in schizophrenia (25,36). The cascade model claims that episodic control monitors the flexible and temporary reinstantiation of episodic

information (e.g., past events, rules, or task instructions) to modulate action selection across a behavioral episode (9). As such, episodic control can be understood as the process that supervises the retrieval of information from episodic memory (37–39). Consistently, other studies have found that rostral LPFC activations were observed in episodic memory paradigms in retrieval phases, when subjects selected actions on the basis of the occurrence of previous events (40–43). Therefore, our finding of an impaired episodic control process related to a perturbed rostrocaudal hierarchy within the LPFC could represent a potential cause for the episodic memory retrieval disturbances in schizophrenia—a hypothesis that should be further investigated in the future.

Another well-known concept intimately related to episodic control, as defined by the cascade model, is the so-called "episodic buffer," a new component included in the former working memory model (44). Indeed, the cascade model generalizes the classical theory of executive control on the basis of a central executive system controlling multiple slave systems, inspired from the working memory framework (45). In those two models, each stage maintains active representations that are controlled by higher stages and that exert control on representations at lower stages. Recently, the episodic buffer has been defined as a new temporary system, thought to be biologically implemented by the frontal areas (44). Crucially, the episodic buffer is important for integrating representations of information bound in a multimodal code being entered into or retrieved from long-term episodic memory (44). Executive processes engaged in the episodic domain (i.e., episodic control) could thus be conceptualized as mechanisms that monitor the binding between different temporal features of information into a temporary, unitary, and coherent representation of events (i.e., within the episodic buffer). Our findings therefore suggest a core impairment in control processes devoted to building a new, consistent, multi-featured representation of temporally dispersed contextual signals, which might account for the perturbations of the episodic buffer observed by others in schizophrenia (46,47).

This impaired functional connectivity between rostral and caudal LPFC regions supports the functional disconnection hypothesis in schizophrenia initially proposed by Friston (14). We also provide, to the best of our knowledge, the first evidence of a top-down disconnection within the LPFC in this disorder. Because the anatomical connectivity within the LPFC was not found to be disrupted in schizophrenia (48,49), we suggest that our result reflects something more dynamic in the way those areas function as a whole to produce cognitive control (e.g., via impaired synaptic transmission) (14).

Finally, in addition to its clinical implications with regard to the pathophysiology of cognitive disturbances of schizophrenic patients, we believe that this result has more general theoretical implications. Indeed, there has recently been a growing interest in the study of the hierarchical organization of cognitive control within the rostrocaudal axis of the frontal lobes, either in healthy subjects (18) or in patients with frontal lobe damage (22). The present study provides additional support confirming that this hierarchy might be a fruitful framework in which to investigate frontal lobe architecture and its pathology.

This research was supported by a grant of the Conseil Scientifique de la Recherche, Le Vinatier (CSRA 05). The author GB was supported by a grant from the Fondation pour la Recherche Médicale (DEA20050904971). We wish to thank S.J. Blakemore and S. White for their assistance in proofreading this report.

The authors report no biomedical financial interests or potential conflicts of interest.

Supplementary material cited in this article is available online.

1. Barch DM, Carter CS, Braver TS, Sabb FW, MacDonald A III, Noll DC, Cohen JD (2001): Selective deficits in prefrontal cortex function in medication-naive patients with schizophrenia. *Arch Gen Psychiatry* 58:280–288.
2. MacDonald AW III, Carter CS, Kerns JG, Ursu S, Barch DM, Holmes AJ, *et al.* (2005): Specificity of prefrontal dysfunction and context processing deficits to schizophrenia in never-medicated patients with first-episode psychosis. *Am J Psychiatry* 162:475–484.
3. Barbalat G, Chambon V, Franck N, Koechlin E, Farrer C (2009): Organization of cognitive control within the lateral prefrontal cortex in schizophrenia. *Arch Gen Psychiatry* 66:377–386.
4. Tan H, Choo W, Fones CSL, Chee MWL (2005): fMRI study of maintenance and manipulation processes within working memory in first-episode schizophrenia. *Am J Psychiatry* 162:1849–1858.
5. Tan H, Sust S, Buckholtz JW, Mattay VS, Meyer-Lindenberg A, Egan MF, *et al.* (2006): Dysfunctional prefrontal regional specialization and compensation in schizophrenia. *Am J Psychiatry* 163:1969–1977.
6. Cannon TD, Glahn DC, Kim J, Van Erp TGM, Karlsgodt K, Cohen MS, *et al.* (2005): Dorsolateral prefrontal cortex activity during maintenance and manipulation of information in working memory in patients with schizophrenia. *Arch Gen Psychiatry* 62:1071–1080.
7. Badre D (2008): Cognitive control, hierarchy, and the rostro-caudal organization of the frontal lobes. *Trends Cogn Sci* 12:193–200.
8. Badre D, D'Esposito M (2009): Is the rostro-caudal axis of the frontal lobe hierarchical? *Nat Rev Neurosci* 10:659–669.
9. Koechlin E, Summerfield C (2007): An information theoretical approach to prefrontal executive function. *Trends Cogn Sci* 11:229–235.
10. Koechlin E, Ody C, Kouneiher F (2003): The architecture of cognitive control in the human prefrontal cortex. *Science* 302:1181–1185.
11. Chambon V, Franck N, Koechlin E, Fakra E, Ciuperca G, Azorin J, Farrer C (2008): The architecture of cognitive control in schizophrenia. *Brain* 131:962–970.
12. Weiss AP, Schacter DL, Goff DC, Rauch SL, Alpert NM, Fischman AJ, Heckers S (2003): Impaired hippocampal recruitment during normal modulation of memory performance in schizophrenia. *Biol Psychiatry* 53:48–55.
13. Heckers S, Rauch SL, Goff D, Savage CR, Schacter DL, Fischman AJ, Alpert NM (1998): Impaired recruitment of the hippocampus during conscious recollection in schizophrenia. *Nat Neurosci* 1:318–323.
14. Friston KJ (1998): The disconnection hypothesis. *Schizophr Res* 30:115–125.
15. Meyer-Lindenberg AS, Olsen RK, Kohn PD, Brown T, Egan MF, Weinberger DR, Berman KF (2005): Regionally specific disturbance of dorsolateral prefrontal-hippocampal functional connectivity in schizophrenia. *Arch Gen Psychiatry* 62:379–386.
16. Honey GD, Pomarol-Clotet E, Corlett PR, Honey RAE, McKenna PJ, Bullmore ET, Fletcher PC (2005): Functional dysconnectivity in schizophrenia associated with attentional modulation of motor function. *Brain* 128:2597–2611.
17. Shannon C (1948): A mathematical theory of communication. *Bell Syst Tech J* 27:379–423,623–656.
18. Kouneiher F, Charron S, Koechlin E (2009): Motivation and cognitive control in the human prefrontal cortex. *Nat Neurosci* 12:939–945.
19. Mueller RO (1996): *Basic Principles of Structural Equation Modeling*. New York: Springer Texts in Statistics, Springer-Verlag.
20. Gitelman DR, Penny WD, Ashburner J, Friston KJ (2003): Modeling regional and psychophysiologic interactions in fMRI: The importance of hemodynamic deconvolution. *Neuroimage* 19:200–207.
21. Stephan KE, Marshall JC, Friston KJ, Rowe JB, Ritzl A, Zilles K, Fink GR (2003): Lateralized cognitive processes and lateralized task control in the human brain. *Science* 301:384–386.
22. Badre D, Hoffman J, Cooney JW, D'Esposito M (2009): Hierarchical cognitive control deficits following damage to the human frontal lobe. *Nat Neurosci* 12:515–522.
23. Schlösser R, Gesierich T, Kaufmann B, Vucurevic G, Hunsche S, Gawehn J, Stoeter P (2003): Altered effective connectivity during working memory performance in schizophrenia: A study with fMRI and structural equation modeling. *Neuroimage* 19:751–763.
24. Schlösser R, Gesierich T, Kaufmann B, Vucurevic G, Stoeter P (2003): Altered effective connectivity in drug free schizophrenic patients. *Neuroreport* 14:2233–2237.

25. Ragland JD, Laird AR, Ranganath C, Blumenfeld RS, Gonzales SM, Glahn DC (2009): Prefrontal activation deficits during episodic memory in schizophrenia. *Am J Psychiatry* 166:863–874.
26. MacDonald AW III, Carter CS (2003): Event-related FMRI study of context processing in dorsolateral prefrontal cortex of patients with schizophrenia. *J Abnorm Psychol* 112:689–697.
27. Barch DM (2005): The cognitive neuroscience of schizophrenia. *Annu Rev Clin Psychol* 1:321–353.
28. Holmes AJ, MacDonald A III, Carter CS, Barch DM, Andrew Stenger V, Cohen JD (2005): Prefrontal functioning during context processing in schizophrenia and major depression: An event-related fMRI study. *Schizophr Res* 76:199–206.
29. MacDonald AW III, Pogue-Geile MF, Johnson MK, Carter CS (2003): A specific deficit in context processing in the unaffected siblings of patients with schizophrenia. *Arch Gen Psychiatry* 60:57–65.
30. Delawalla Z, Csernansky JG, Barch DM (2008): Prefrontal cortex function in nonpsychotic siblings of individuals with schizophrenia. *Biol Psychiatry* 63:490–497.
31. Braver TS, Barch DM, Cohen JD (1999): Cognition and control in schizophrenia: A computational model of dopamine and prefrontal function. *Biol Psychiatry* 46:312–328.
32. Meyer-Lindenberg A, Miletich RS, Kohn PD, Esposito G, Carson RE, Quarantelli M, *et al.* (2002): Reduced prefrontal activity predicts exaggerated striatal dopaminergic function in schizophrenia. *Nat Neurosci* 5:267–271.
33. Abi-Dargham A, Mawlawi O, Lombardo I, Gil R, Martinez D, Huang Y, *et al.* (2002): Prefrontal dopamine D1 receptors and working memory in schizophrenia. *J Neurosci* 22:3708–3719.
34. Braver TS, Cohen JD (1999): Dopamine, cognitive control, and schizophrenia: The gating model. *Prog Brain Res* 121:327–349.
35. Swerdlow NR, Geyer MA (1998): Using an animal model of deficient sensorimotor gating to study the pathophysiology and new treatments of schizophrenia. *Schizophr Bull* 24:285–301.
36. Ranganath C, Minzenberg MJ, Ragland JD (2008): The cognitive neuroscience of memory function and dysfunction in schizophrenia. *Biol Psychiatry* 64:18–25.
37. Henson RN, Rugg MD, Shallice T, Josephs O, Dolan RJ (1999): Recollection and familiarity in recognition memory: An event-related functional magnetic resonance imaging study. *J Neurosci* 19:3962–3972.
38. Henson RN, Rugg MD, Shallice T, Dolan RJ (2000): Confidence in recognition memory for words: Dissociating right prefrontal roles in episodic retrieval. *J Cogn Neurosci* 12:913–923.
39. Bunge SA, Burrows B, Wagner AD (2004): Prefrontal and hippocampal contributions to visual associative recognition: Interactions between cognitive control and episodic retrieval. *Brain Cogn* 56:141–152.
40. Velanova K, Jacoby LL, Wheeler ME, McAvoy MP, Petersen SE, Buckner RL (2003): Functional-anatomic correlates of sustained and transient processing components engaged during controlled retrieval. *J Neurosci* 23:8460–8470.
41. Sakai K, Passingham RE (2003): Prefrontal interactions reflect future task operations. *Nat Neurosci* 6:75–81.
42. Sakai K, Rowe JB, Passingham RE (2002): Active maintenance in prefrontal area 46 creates distractor-resistant memory. *Nat Neurosci* 5:479–484.
43. Fletcher PC, Henson RN (2001): Frontal lobes and human memory: Insights from functional neuroimaging. *Brain* 124:849–881.
44. Baddeley A (2000): The episodic buffer: A new component of working memory? *Trends Cogn Sci* 4:417–423.
45. Baddeley A, Della Sala S (1996): Working memory and executive control. *Philos Trans R Soc Lond B Biol Sci* 351:1397–1403; discussion:1403–1404.
46. Burglen F, Marczewski P, Mitchell KJ, van der Linden M, Johnson MK, Danion J, Salamé P (2004): Impaired performance in a working memory binding task in patients with schizophrenia. *Psychiatry Res* 125:247–255.
47. Rizzo L, Danion JM, van der Linden M, Grangé D (1996): Patients with schizophrenia remember that an event has occurred, but not when. *Br J Psychiatry* 168:427–431.
48. Jensen JE, Miller J, Williamson PC, Neufeld RWJ, Menon RS, Malla A, *et al.* (2006): Grey and white matter differences in brain energy metabolism in first episode schizophrenia: 31P-MRS chemical shift imaging at 4 Tesla. *Psychiatry Res* 146:127–135.
49. Highley JR, Walker MA, Esiri MM, McDonald B, Harrison PJ, Crow TJ (2001): Schizophrenia and the frontal lobes: Post-mortem stereological study of tissue volume. *Br J Psychiatry* 178:337–343.
50. Andreasen NC (1984): *The Scale for the Assessment of Positive Symptoms (SAPS)*. Iowa City, Iowa: University of Iowa Press.
51. Andreasen NC (1983): *The Scale for the Assessment of Negative Symptoms (SANS)*. Iowa City, Iowa: University of Iowa Press.
52. Talairach J, Tournoux P (1988): *Co-Planar Stereotaxic Atlas of the Human Brain*. New York, New York: Thieme Medical Publishers.